Université d'Ottawa · University of Ottawa

Université d'Ottawa · University of Ottawa

FACULTÉ DE ÉTUDES SUPÉRIEURES ET POSTDOCTORALES

FACULTY OF GRADUATE AND POSTDOCTORAL STUDIES

Jingning SHAN

AUTEUR DE LA THÈSE - AUTHOR OF THESIS

Ph.D. (Chemistry)

GRADE - DEGREE

Department of Chemistry

FACULTÉ, ÉCOLE, DÉPARTEMENT - FACULTY, SCHOOL, DEPARTMENT

TITRE DE LA THÈSE - TITLE OF THE THESIS

Synthesis of Organic and Inorganic Compounds for OLED Application : Physico-chemical Characterization of New Diamines, Heterocyles and Group 13 Compounds

D. Richeson

DIRECTEUR DE LA THÈSE - THESIS SUPERVISOR

CO-DIRECTEUR DE LA THÈSE - THESIS CO-SUPERVISOR

EXAMINATEURS DE LA THÈSE - THESIS EXAMINERS

S. Barry

C. Detellier

S. Gambarotta

S. Wang

J.-M. De Koninck, Ph.D.

LE DOYEN DE LA FACULTÉ DES ÉTUDES SUPÉRIEURES ET POSTDOCTORALES

DEAN OF THE FACULTY OF GRADUATE AND POSTDOCTORAL STUDIES

Synthesis of Organic and Inorganic Compounds for OLED Application: Physico-Chemical Characterization of New Diamines, Heterocycles and Group 13 Compounds

Jingning Shan

Thesis submitted to the
Faculty of Graduate and Postdoctoral Studies
in partial fulfillment of the requirements for the degree of

Doctorate in Philosophy
in Chemistry

Ottawa-Carleton Chemistry Institute
University of Ottawa

Candidate
Jingning Shan

Supervisor
Professor Darrin Richeson

© Jingning Shan, Ottawa, Canada

Library and Archives Canada

Published Heritage Branch

395 Wellington Street
Ottawa ON K1A 0N4
Canada

Bibliothèque et Archives Canada

Direction du Patrimoine de l'édition

395, rue Wellington
Ottawa ON K1A 0N4
Canada

Your file Votre référence
ISBN: 0-494-01759-7
Our file Notre référence
ISBN: 0-494-01759-7

NOTICE:
The author has granted a non-exclusive license allowing Library and Archives Canada to reproduce, publish, archive, preserve, conserve, communicate to the public by telecommunication or on the Internet, loan, distribute and sell theses worldwide, for commercial or non-commercial purposes, in microform, paper, electronic and/or any other formats.

The author retains copyright ownership and moral rights in this thesis. Neither the thesis nor substantial extracts from it may be printed or otherwise reproduced without the author's permission.

AVIS:
L'auteur a accordé une licence non exclusive permettant à la Bibliothèque et Archives Canada de reproduire, publier, archiver, sauvegarder, conserver, transmettre au public par télécommunication ou par l'Internet, prêter, distribuer et vendre des thèses partout dans le monde, à des fins commerciales ou autres, sur support microforme, papier, électronique et/ou autres formats.

L'auteur conserve la propriété du droit d'auteur et des droits moraux qui protège cette thèse. Ni la thèse ni des extraits substantiels de celle-ci ne doivent être imprimés ou autrement reproduits sans son autorisation.

In compliance with the Canadian Privacy Act some supporting forms may have been removed from this thesis.

While these forms may be included in the document page count, their removal does not represent any loss of content from the thesis.

Conformément à la loi canadienne sur la protection de la vie privée, quelques formulaires secondaires ont été enlevés de cette thèse.

Bien que ces formulaires aient inclus dans la pagination, il n'y aura aucun contenu manquant.

Canada

Abstract

This thesis is focused on the synthesis and characterization of organic and inorganic electroluminescent materials for organic light-emitting diodes (OLED). The synthetic work was aimed at several of the key components of multilayer OLEDs and followed the latest developments in this area. Three types of OLED materials, namely hole-transport (HT), electron-transport (ET) and emission (EM) materials in four groups were successfully synthesized. The characterization of these materials focuses on the physical and chemical features that are important in defining performance parameters. This chemist's perspective highlights the potential application of these novel compounds employed in fabricating OLEDs, which is based on the results from thermal, photophysical and electrochemical analysis.

Chapter one outlines the background of OLED, the operation of a double-layer and multilayer OLEDs and the current state of OLED materials. The objectives of this thesis are proposed after describing the general techniques that are important for characterization of the parameters needed for further OLED fabrication.

Chapter two focuses on the synthesis and characterization of HT materials based of aryldiamines with a naphthalene core (bis(N,N-diaryl)-1,5-diaminonaphthalene). Pd-based catalysts have been employed in the C-N bond formation steps of the synthesis of these compounds. The thermal results indicated that these diamines, particularly when they possess bulky aryl groups such as biphenyl and naphthyl, had high glass transition temperatures and thus offer the potential for improving upon OLED stability. The influence of the position of the aryl substituents on the photophysical properties of these compounds is discussed. All of the synthesized diaminonapthalene compounds showed good electrochemical stability as determined by cyclic voltammetry (CV). The highest occupied molecular orbital (HOMO) and lowest occupied molecular orbital (LUMO) energy levels were calculated from the CV and UV-vis characterization and were compared with the known HT materials such as N,N'-Diphenyl-N,N'-bis(3-methylphenyl)benzidine (TPD). This data provided important performance indicators and a reference for the future application.

Chapter three is concerned with developing C-4 substituted tris(8-hydroxyquinoline) aluminum (Alq_3) derivatives. Alq_3 is frequently used as both an ET and an EM material in OLEDs. The modification of the C-4 position of Alq_3 and the subsequent influence on the LUMO energy was investigated. Aryl and diarylamine derivatives were selected as substituents aimed at tuning intermolecular interactions and balancing the hole/electron mobility for these molecules. Thermal data from glass transition temperatures and decomposition temperatures suggested that all these C-4 substituted Alq_3 derivatives have improved stability compared to parent Alq_3. Photophysical analysis indicated that the important electronic transitions in C-4 aryl substituted Alq_3 derivatives is a π(phenoxy)$\rightarrow\pi^*$(pyridyl) transition; while C-4 diarylamine substituted Alq_3 derivatives exhibit an $n\rightarrow\pi^*$ transition from the diarylamine nitrogen to the pyridyl ring of the quinoline group. The HOMO/LUMO results also indicated that C-4 diarylamine substituted Alq_3 derivatives could be used in single-layer device structures. The quantum efficiency in this group of compounds was comparable to that of the parent Alq_3. CV measurements showed that oxidation of all these compounds were not irreversible, indicating their cations were not stable; however, the cationic species of these C-4 Alq_3 derivatives are less reactive compared to that of the parent Alq_3.

In **Chapter four,** we investigated EM materials by preparing and characterizing substituted salicylaldimine diphenylboron complexes. Thermal characterization of these compounds indicated that a bulky substituent was needed to improve the thermal stability of these boron complexes. Green-light emission was observed in CH_2Cl_2 from these fluorescent compounds. The HOMO/LUMO energies estimated from CV and UV-vis data suggested that these boron complexes have larger energy gap than that of Alq_3 and relatively high HOMO and LUMO energy levels. This information is helpful for further application.

Chapter five reports our effort to synthesize a novel ET material that was designed as a perimidine-based analogue of 2,2′,2″-(Benzene-1,3,5-triyl)-tris(1-phenyl-1H-benzimidazole) (TPBI). The common feature of these compounds is the presence of 1-aryl-perimidine groups and they include: mono-, di- and tri-perimidene substituted species with phenyl, pyridyl and thiophene cores. Thermal characterization demonstrated that these compounds have excellent stability. Photophysical and electrochemical

characterization suggest that contrary to the original goal of producing an ET material, these compounds appear to be better suited as potential HT materials. Specifically, these perimidine-based compounds possessed low HOMO energy levels, which were similar to HT compounds. As a result these new group compounds are proposed as HT materials or host materials when using fluorescent dopants in HT layer.

In **Chapter six**, a broad summary of these efforts and future prospects are presented.

Acknowledgements

This work would be a mission impossible without the support and encouragement of my supervisor, Dr. Darrin Richeson, under whose supervision I chose these projects and began the thesis. I could not have imagined having a better advisor for my PhD schooling, and without his commonsense, knowledge, perceptiveness and passion, I would never arrive to this page.

I would like to thank Patrick Bazinet, the first guy Darrin introduced to me in this lab. It is really helpful working with such a smart and sometime shy colleague with a Canadian belly; it would be a pleasure memory to go over the numerous talk and argue on research and lives between us. Thanks are also given to my current and former group members, Dr. Tiow-Gan Ong, for being the colleagues in such a long time and Dr. Zhixian Liu, Dr. Sean Barry, and Malcom Downey.

I would like to thank Dr. Min Tian and Dr. Jianjun Niu from Dr. Brian Conway's group, they helped me to conduct electrochemical experiments; Marius Gabriel Ivan from Dr. Tito Scaiano's group, he helped me to collect fluorescence data; Dr. Wenxin Kuang from Dr. Christian Detellier's group, with whom I collaborated to finish thermal analysis; Dr. Louis Barriault's group, where I shot numerous samples in his GC-MS; Dr. Glenn Yap and Dr. Sean Ouyang helped to collect XRD data. Many thanks to my friends and the people we have smiled to each other on/off the campus. The smile makes me forget that Ottawa is the coldest capital in the world.

This thesis is dedicated to my father Yeyu Shan, my mother Cuihua Tang and my big sister Bingbin Shan, for their endless love.

Table of Contents

List of Abbreviations and Symbols Used

Φ_f	Quantum efficiency
Φ_{PL}	Photoluminescence efficiency
A	Absorbance at the excitation wavelength
$AlMq_2OH$	Bis(2-methyl-8-quinolinolato) aluminum hydroxide
Alq_3	Tris(8-hydroxyquinoline) aluminum
$AlPh_3$	Tris(4-phenanthridinolato) aluminum
$Al(QS)_3$	Tris(8-hydroxy-5-peperidinylquinolinesulfonamide) aluminum
$BePP_2$	Bis[2-(2-hydroxyphenyl)pyridine]beryllium
BINAP	*rac*-2,2'-Bis(diphenylphosphino)-1,1'-binaphthy
BPh_2(F-2-PI)	5-Fluoro-2-(2′-pyridyl)indole
Cp_2Fe	Ferrocene
CRT	Cathode ray tube
CV	Cyclic voltammetry
$DAlq_3$	Diarylamine substituted Alq_3 analogues
dba	Dibenzylidineacetone
DME	1,2-Dimethoxyenthane
DSC	Differential scanning calorimetry
EL	Electroluminescence
ET	Electron-transport
EM	Emission

EML	Emission layer
ETL	Electron-transport layer
F	Area under the corrected emission curve
p-FTDAB	1,3,5-Tris(4-fluorophenylphenylamino)benzene
HOMO	Highest occupied molecular orbital
HRMS	High resolution mass spectrometer
HT	Hole-transport
HTL	Hole-transport layer
ITO	Indium-tin-oxide
k_{ec}	External conversion rate constant
k_f	Fluorescence rate constant
k_i	Intersystem crossing rate constant
k_{ic}	Internal conversion rate constant
k_{pd}	Predissociation rate constant
k_d	Dissociation rate constant
LCD	Liquid crystal displays
LUMO	Lowest occupied molecular orbital
n_x, n_s	Index of unknown (x) and standard (s)
4MeAlq$_3$	4-MethylAlq$_3$
NMR	Nuclear magnetic resonance
NND	1,5-bis[*N*-(1-naphthyl)-*N*-phenyl]naphthalene diamine
NPB or α-NPD	N,N'-Diphenyl-N,N'-bis(1-naphthalyl)benzidine
OLED	Organic light-emitting diode

$PAlq_3$	Phenyl substituted Alq_3 analogues
PBD	2-(4-biphenyl)-5-(4-*t*-butylphenyl)1,3,4-oxadiazole
PLED	Polymer light-emitting diode
p-PMTDATA	4,4′,4″-Tris(biphenyl-4-yl(3′-methylphenyl amino) triphenylamine)
PPV	Polyparaphenylenevinylene
RGB	Red-green-blue
spiro-TAD	2,2',7,7'-Tetrakis-(diphenylamino)-9,9'-spirobifluorene
T_m	Melting point
T_c	Crystallization temperature
T_d	Decomposition temperature
T_g	Glass transition temperature
TBAHFP	Tetrabutyl ammonium hexafluorophosphate
TGA	Thermogravimetric analysis
TLC	Thin layer chromatograph
TPA	9,10-Bis(*m*-tolylphenylamino)anthracene
TPAC	1,1-bis(4-di-*p*-tolylaminophenyl)cyclohexane
TPBI	2,2′,2″-(Benzene-1,3,5-triyl)-tris(1-phenyl-1H-benzimidazole)
TPPI	TPBI analogue, 1,3,5-Tri(1-phenyl-2-perimidine)-benzene
TPD	N,N'-Diphenyl-N,N'-bis(3-methylphenyl)benzidine
o-TTA	4,4′,4″ -Tris(*o*-biphenyl)1,3,5-tris(diphenylamine)
XRD	X-Ray Diffraction
$Zn(BIZ)_2$	Bis[2-(2-hydroxyphenyl)-1-phenylbenzimidazolato]zinc

List of Figures

List of Schemes

List of Tables

Chapter 1

General Review of Organic Light-Emitting Diodes (OLED) and OLED Materials

1.1 Introduction to OLEDs

The development and impact of organic electroluminescent (EL) technology is intimately linked to modern silicon-based electronics and photonics. For example, the ability to display and input computer data forms the direct connection and is the key interface between human (consumer) and machine. In addition, displays for mobile phones, TV screens, digital cameras, flat-panel displays and other technologies are everywhere in our modern lives.

The two dominant display technologies in commercial market are cathode ray tubes (CRT) and liquid crystal displays (LCD). Taking the market of personal computers as an example, CRT monitors have dominated this field for more than 20 years, but LCD monitors have begun to share and replace the traditional CRT monitors in recent years due to its smaller size, lighter weight and higher energy efficiency.[1-2] The market for LCDs in the flat-panel screen industry is worth billions of dollars and will be the

dominant technology in the next five years. On the horizon as a challenge to this technology is the development of organic light-emitting diodes (OLEDs).[2]

An OLED is an EL device made by placing organic active materials between two conductors. When a bias or electrical current is applied to the conductors, a bright light is emitted from the device. Organic electroluminescence was first observed in 1963 by Pope *et al.* in single crystal anthracene and in single crystal anthracene doped with approximately 0.1 mole % tetracene.[3] The early attempts to exploit this discovery in the development of organic EL device were not very successful for the following two decades.[4-8] These initial efforts in organic EL devices typically suffered due to the requirement of high drive voltages (~100V) and low power-conversion efficiency. It was not until in the late 1980s when Tang and coworkers in Kodak invented a double layer OLED that a practical organic EL technology appeared.[9,10] In this early work, organic materials or doped host organic materials were demonstrated to be viable candidates as the emitting elements in an optoelectronic device. These devices were constructed from an electron-transport (ET) layer, that was fabricated from tris(8-hydroxyquinoline) aluminum (Alq_3) or doped Alq_3, and a hole-transport (HT) layer, that was formed with a diamine. These two layers were sandwiched between a transparent indium-tin-oxide anode (ITO) and an alloyed Mg:Ag cathode. These double or multilayer EL diodes operated at a low voltage (< 10 V) with high external quantum efficiency, and were shown to be efficient LEDs. Shortly afterwards, Burroughes *et al.* reported an LED that was based on the conjugated polymer polyparaphenylenevinylene (PPV).[11] This subset of OLEDs, polymer light-emitting diodes (PLEDs), have become another non-silicon based technology competing with current display market. Since these pioneering results, a

worldwide interest in such technology has spurred research activities in these organic materials based LEDs and enormous progress has been made.

There are many reasons that OLEDs are superior to LCDs. Compared to LCDs; the main advantage of an OLED is that there is no need for a backlight or external light source. As a result, there is less heat produced and less power consumed. Another important advantage is OLEDs can have much faster response time than LCD modules, which will make a better application in spectrum analysis and video. Furthermore, OLEDs have a higher viewing angle, are thinner modules, and have fewer manufacturing steps than LCDs. These advantages, combined with the fact that OLEDs can be constructed from cheap materials and have cheap fabrication cost, suggest that OLEDs are a better fit in the flat display technology than LCDs.[12]

The major advantage of OLED's in comparison with the inorganic LEDs which are made from III-V semiconductor compounds[12-14] is their reduced manufacturing cost. It is important to note that inorganic LEDs generally exhibit better quantum efficiency, lower driving voltages, larger color availability and stability as well as higher operation reliability than OLED's. However, OLEDs can be fabricated under reasonable temperatures by thermal evaporation of organic precursors while inorganic LEDs generally require more sophisticated, high temperature deposition approaches. For example, temperatures in excess of 2000 °C are needed to deposit SiC for a blue light LED[13] while only 200 –300 °C is adequate for an organic based system. These milder conditions open a range of substrates for OLEDs that are not accessible to inorganic LED materials and include the option of many flexible support materials, which could yield light weight flexible devices.

With the development of PLED, large-area light-emitting displays have become possible because polymer layers can be spin coated at room temperature.[2,11] There are pros and cons when comparing OLEDs and PLEDs. OLEDs and PLEDs have been developing along two parallel ways, they share the common features of being organic-based materials and their mechanisms of operation are very similar. It is also generally true that whenever one of these areas experiences a breakthrough, this advance will benefit and initiate research of the other field. This thesis focuses on small molecule materials that have potential as components for OLEDs.

Improvements in the device operational lifetime for OLEDs is still needed before these materials can compete with inorganic LEDs and more common display technologies, CRTs and LCDs.[2,14,15] Other areas of improvement that require attention are resistance to color degradation, simplification of manufacturing and the targeted design and synthesis of organic EL materials with specific properties.[15] In the next sections, the mechanism of OLED operation will first be reviewed. This is followed by a brief discussion of current organic EL materials.

1.2 Operation of an OLED

Figure 1.1 shows the basic two-layer OLED configuration and its energy level diagram as reported by Tang.[9]

Application of an electrical potential across such a device causes holes to be injected from the anode to the highest occupied molecular orbital (HOMO) of the hole-transport layer (HTL), while electrons are injected from the cathode to the lowest unoccupied

molecular orbital (LUMO) of the electron-transport layer (ETL). These injected holes and electrons will migrate toward to each other and combine either at the junction of the two layers or within one of the two layers. The energy that is released from electron/hole combination is emitted as light, which can be observed through the transparent ITO anode.

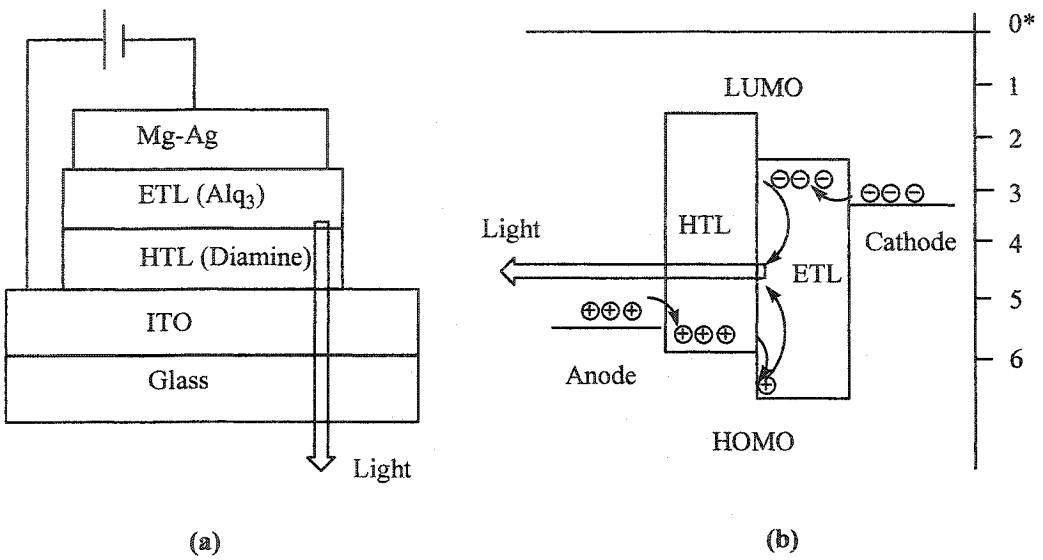

Figure 1.1 Configuration (a) and energy level diagram (b) of a two-layer OLED.
* HOMO/LUMO enery levels are considered as negative with respect to the zero vacuum level and the absolute values are taken into the consideration throughout the thesis.

In the example above, charge (hole) mobility in the HTL exceeds that of electrons in the ETL. As a result, recombination of electrons and holes occurs just within the ETL. Device quenching can arise if, for example, excess holes are injected into the ETL forming the unstable cationic Alq_3 species.[15] The transport of holes across the HTL/ETL interface will depend on the HOMO matching between the layers; a higher HOMO

energy of the ETL relative to that of the HTL leads to a larger barrier to hole transport across the interface. Similarly, a potential barrier can arise for charge injection if the anode energy level does not match well with the HOMO of the HTL. A barrier to transport holes at these junctions will require additional power to inject holes. Such problems will reduce the operational efficiency of an OLED and therefore more elaborate device configurations have been created that can address these problems. For example, Tang *et al* developed three-layer OLEDs in 1989.[10] Since then, multilayer OLED devices have had an increasing profile in both academic research and industrial application.[15] An example of a multilayer OLED structure and its relative HOMO/LUMO energy levels[16] is shown in **Figure 1.2**.

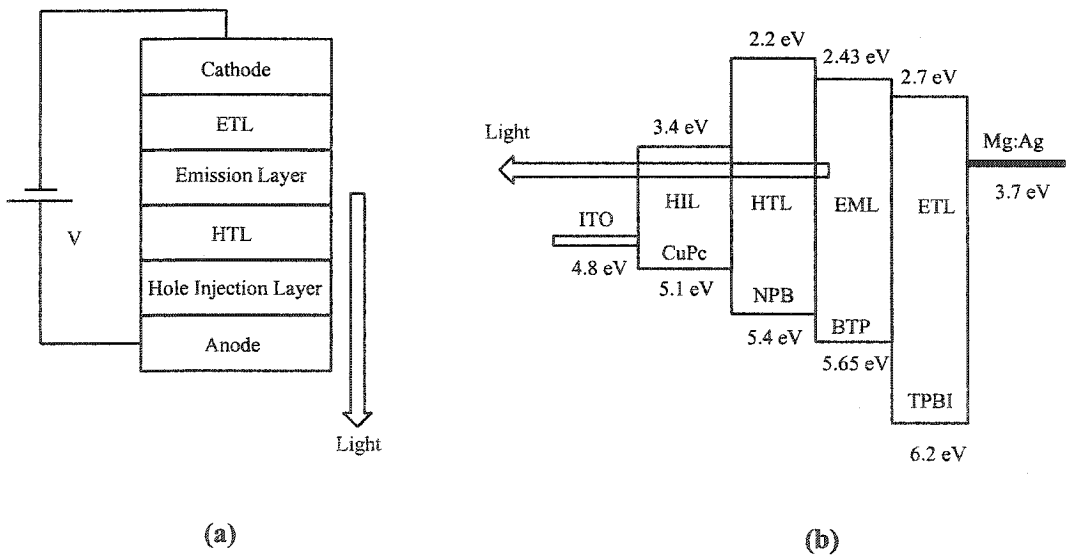

Figure 1.2 Configuration of a multilayer OLED structure (a) and relative HOMO/LUMO energy levels of a corresponding example (b) (redrawn from ref. 16).

In this type of device, the ETL and HTL materials are TPBI and NPB (details for the structure of these materials can be found in the next section of this chapter). The use of

2,2'-bistriphenylenyl (BTP) as the emission layer (EML) has the dual function of providing a location for the combination of holes and electrons that in turn leads to light emission and of preventing the further flow of holes to the cathode. The large HOMO energy difference between TPBI and BTP presents a barrier for hole transport. On the anode side of this OLED is a hole injection layer (HIL), copper phthalocyanine (CuPc), which will modulate the energy barrier between the anode and HTL, thus benefiting the charge injection from the anode.

Since the development of multilayer OLEDs, the materials that are employed in various layers have been classified into groups according to their roles in the device. Therefore in the next section, the general features of HTL, ETL and EML materials, which are the focuses of this thesis, as well some other selected layer materials will be outlined.

1.3 OLED materials

In contrast to crystalline inorganic semiconductor materials, which consist of covalent bonds directed in three dimensions, organic materials are based on molecular entities that aggregate into solids with weaker intermolecular or van der Waals forces. As a result, the description of bonding and charge transition in OLEDs is generally given in the context of molecular orbital theory, while that for inorganic LEDs is presented in the form of band theory.[13] In the past two decades, most of the common molecules for OLED construction exhibit some degree of π–electron delocalization and offer charge transport pathway involving π–electrons.

From the viewpoint of fabricating a high performance OLED, some common requirements of organic EL materials including HT, ET, and EM materials are the following:[15,17,18]

a. Should possess a suitable HOMO and LUMO energy level matching for the injection of charge between the electrodes and the organic materials and for the transport of charge carriers in organic layers;
b. Should form thin films, usually with an amorphous state, in order to simplify manufacture;
c. Should be morphologically and thermally stable under operation (measured by a high glass transition temperature (T_g));
d. Should be electrochemically stable;
e. Should possess high luminescence (high quantum efficiencies).

1.3.1 HT materials

The aromatic diamine TPAC (1,1-bis(4-di-*p*-tolylaminophenyl)cyclohexane) (**Figure 1.3**) was the first HT material that was used by Tang.[9,10] Triarylamine derivatives have remained as the most common synthetic targets due to their high hole mobility, HOMO energy level match with the ITO glass anode (HOMO ~ 4.8 eV), and their ease of thin film formation in OLED manufacture. By far, arylamine derivatives with a "*bi*-phenyl core" such as N,N'-Diphenyl-N,N'-bis(3-methylphenyl)benzidine (TPD) and N,N'-Diphenyl-N,N'-bis(1-naphthalyl)benzidine (NPB or α-NPD) are the most widely used HT materials in OLED research (**Figure 1.3**).[19, 20]

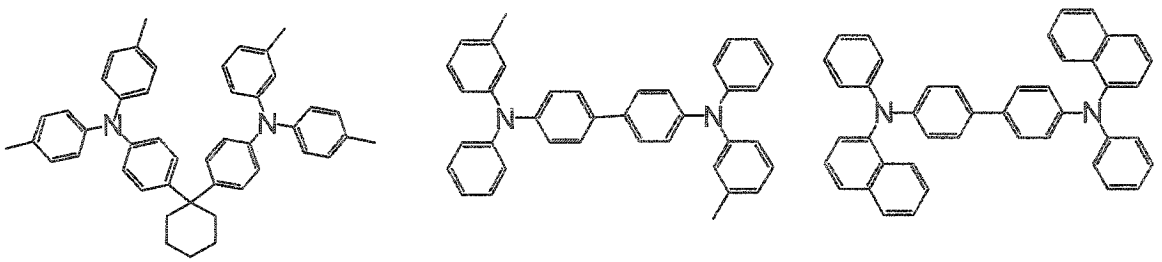

TPAC TPD (T_g 65 °C, T_m 170 °C) NPB (T_g 96 °C, T_m 279 °C)

Figure 1.3 *tri*-arylamine derivatives.

Aside from the common "*bi*-phenyl core" diamine materials, the HT materials that have so far been developed can all be classified as arylamine derivatives with different "core" structures capped by various diarylamines (**Chart 1**). Some examples for this prototype structures like spiro-linked (*spiro*-TAD)[21a] carbazole-linked[21b] and anthracene-linked (TPA)[21c] molecules are shown in **Figure 1.4**.

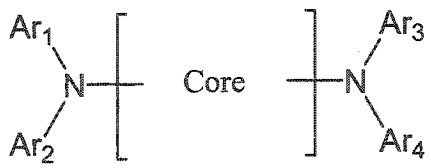

Ar_{1-4} = aromatic groups

Chart 1

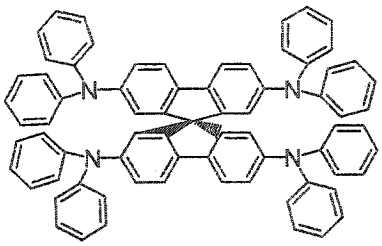

21a

spiro-TAD (T_g 133 °C)

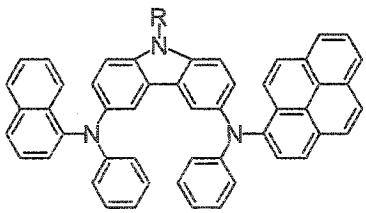

21b

Carbozale core (T_g 174 °C)

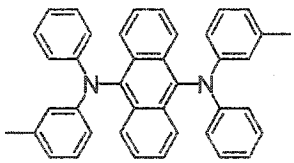

21c

TPA (T_g 103 °C)

Figure 1.4 Examples of HT *tri*-arylamine derivatives with different core structures.

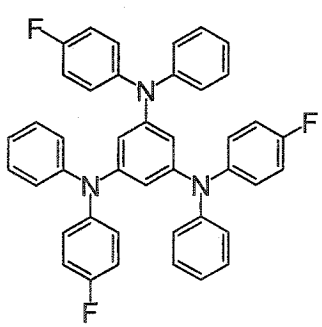

22a

p-FTDAB (T_g 54 °C)

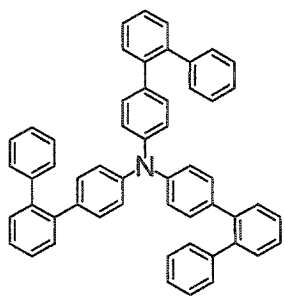

22b

o-TTA (T_g 81 °C)

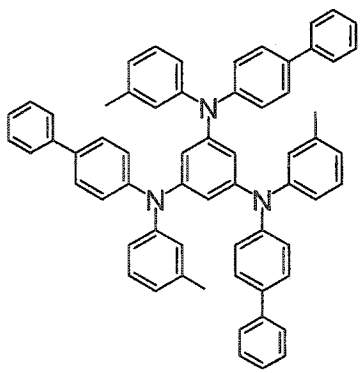

22c

p-PMTDATA (T_g 110 °C)

Figure 1.5 Starburst HT *tri*-arylamine derivatives.

Similar to the arylamine derivatives in **Figure 1.3** and **1.4**, starburst arylamines have also received much attention due to their ability to form pinhole-free thin films with high T_g.[17,22] Some examples include 1,3,5-tris(4-fluorophenylphenylamino)benzene (*p*-FTDAB)[22a] 4,4′,4″-tris(*o*-biphenyl)1,3,5-tris(diphenylamine) (*o*-TTA)[22b] and 4,4′,4″ -tris biphenyl-4-yl (3′-methylphenyl amino triphenylamine (*p*-PMTDATA)[22c] are shown in **Figure 1.5**.

The basic difference between the diamines and starburst amines is in the choice of "core" structure and the way to connect aromatic amines to the core center. They both possess *tri*-arylamine groups and share many of the same physical and chemical properties, which will be further discussed in **Chapter 2**.

1.3.2 ET and EM materials

The materials discussed in this section can be used as either ET or EM materials or both (e.g. Alq_3) in an OLED. The most common ET and EM materials in reported OLEDs can be classified into three broad groups:

I. Alq_3 and Al based chelates (**Figure 1.6**).

II. Non Al metal or metalloid based such as Zn, Be, B etc complexes (**Figure 1.7**).

III. Non-metal containing heterocycles with strong electron-withdrawing groups such as imine (**Figure 1.8**).

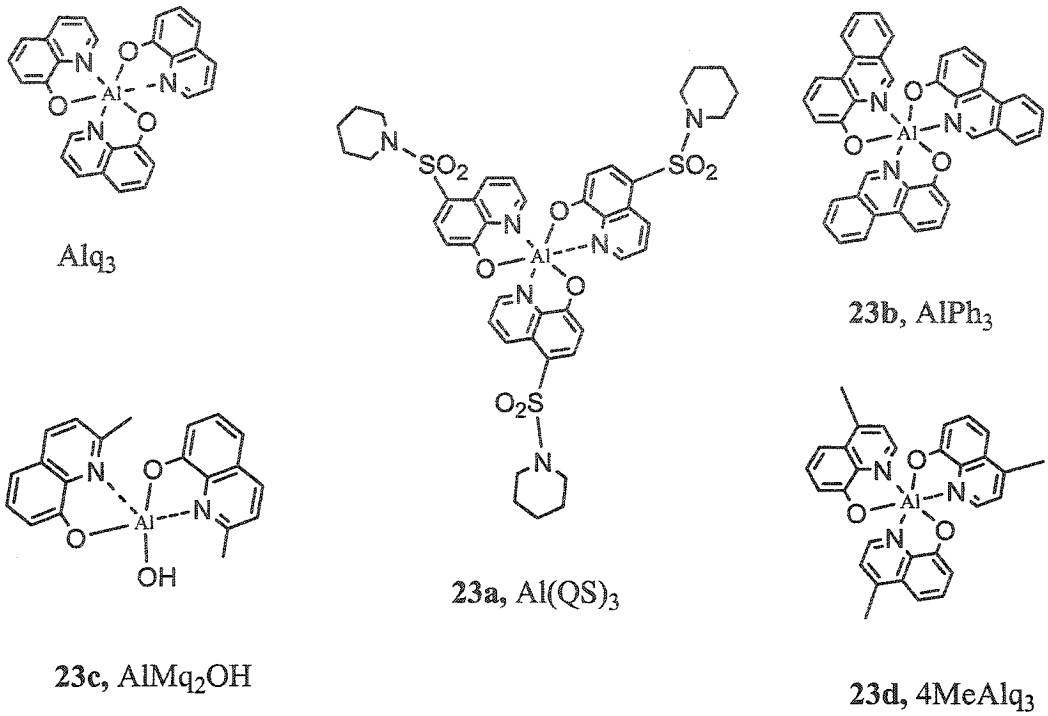

Figure 1.6 Group I, Alq_3 and Al based chelates.

Group I. Since Tang's use of Alq_3 as the ET layer for electron transport and emitting material in 1987,[9,10] it remains one of the most widely employed ET materials. Alq_3 is thermally and morphologically stable and can be evaporated into thin films, easily synthesized and purified, and its ball-shape molecular structure prevents the formation of exciplex. The shortcomings of Alq_3 include low quantum efficiency, charge mobility and ashing problems during sublimation.[15] In order to solve these problems, many Alq_3 analogues have been synthesized and studied.[23] Some examples are shown in **Figure 1.6** and include tris(8-hydroxy-5-peperidinylquinolinesulfonamide) aluminum ($Al(QS)_3$),[23a] $AlPh_3$ having 4-phenanthridinolato as ligand,[23b] bis(2-methyl-8-quinolinolato) aluminum

(III) hydroxide complex ($AlMq_2OH$),[23c] and 4-methylAlq$_3$ (4MeAlq$_3$).[23d] More examples and discussion of this group will be given in **Chapter 3**.

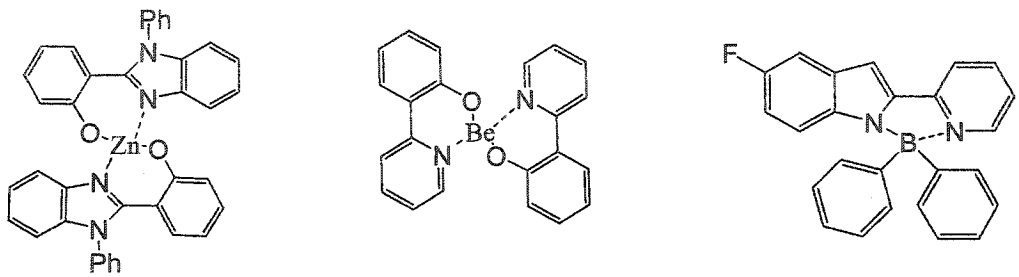

24a **24b** **24c**

$Zn(BIZ)_2$ $BePP_2$ $BPh_2(F\text{-}2\text{-}PI)$

Figure 1.7 Group II, ET and fluorescent Zn, Be and B chelates.

Group II. In addition to aluminum complex, complexes of other metal or metalloid ions, such as Zn, Be, B, Mg, Ca, Sr, Sc, Y, Cu ions have shown ET and fluorescent properties.[15] Among these, Zn, Be and B chelates have received more attention because of the electronegativity or size of the ions. Examples include bis[2-(2-hydroxyphenyl)-1-phenylbenzimidazolato]zinc ($Zn(BIZ)_2$),[24a] bis[2-(2-hydroxyphenyl)pyridine]beryllium ($BePP_2$)[24b] and 5-fluoro-2-(2′-pyridyl)indole ($BPh_2(F\text{-}2\text{-}PI)$)[24c] and are shown in **Figure 1.7**.

Group III. In addition to metal complexes, there are a number of ET heterocyclics that are free of metal atoms. Among them, 2,2′,2″-(benzene-1,3,5-triyl)-tris(1-phenyl-1H-benzimidazole) (TPBI)[25] and 2-(4-biphenyl)-5-(4-*t*-butylphenyl)1,3,4-oxadiazole (PBD)[26] have been widely used in OLEDs as ET and hole-blocking materials (**Figure 1.8**). In general, this group of materials has electron-deficient centers such as oxadiazole (PBD) and imine (TPBI) and is characterized by high HOMO values (or high ionization potential values). They are mainly used as ET, not EM materials in OLEDs. Further examples of this type of materials with electron-deficient centers such as thioxanthene, cyclooctatetraenes, bathophenanthroline *etc.* or substituents such as fluorine can be found in Ref. 15 and 27 and references therein.

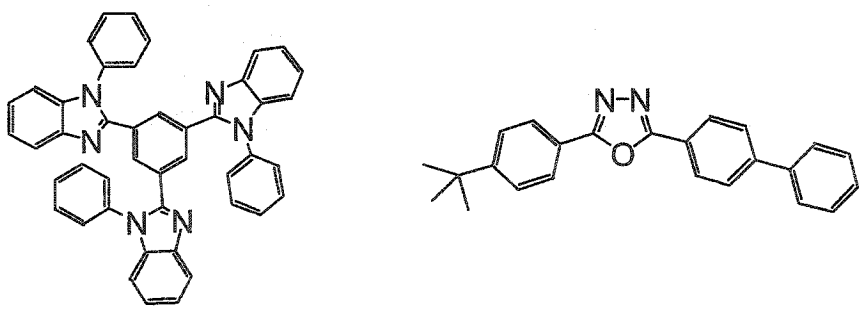

TPBI PBD

Figure 1.8. Group III, ET materials TPBI and PBD

Obviously the complexity of multilayer devices allow for consideration of materials beyond the above HT, ET and EM materials. These three broad classes of target materials form the essential components of an organic EL device and are the focal points of this

thesis. As a result, the other types of materials, which are based on their functions in OLEDs such as HIL materials, fluorescent dopants and triplet emitter materials, while possible the next generation of OLED materials, will be excluded from further consideration in this general introduction. Some of the functions will be mentioned in the later work of this thesis.

1.4 Characterization

The molecular features of the compounds that have been prepared in this thesis are characterized using the standard tools of NMR spectroscopy, mass spectrometry, X-ray analysis and elemental analysis. In addition, the materials-oriented properties have been characterized by thermogravimetric analysis (TGA)/differential scanning calorimetry (DSC), UV-visible absorption and fluorescence emission, and cyclic voltammetry (CV).

DSC has been used to measure the T_gs, the temperature at which glassy amorphous molecules become flexible, of the OLED materials.[19b,28] In fabricating OLEDs, stable amorphous HT and ET materials are needed to preserve the uniformity of the thin films being deposited. If the temperature of the OLED is above the materials' T_gs, grain boundaries will form and damage the electronic properties of the organic layers. Thus, knowledge of the T_g is important information for an OLED material. TGA has been employed in this thesis to assess decomposition temperatures (T_d) of high melting compounds.

UV-visible spectra and fluorescence are useful for probing the HOMO/LUMO energy gap. When combined with electrochemical data, the HOMO/LUMO energies can be estimated.[29] Knowledge of the HOMO/LUMO energy levels gives some information

on suitability of materials for different layers in OLEDs. The quantum efficiency can also be estimated from these data.[30] From quantum efficiency, materials that are potentially useful as emission materials in OLEDs are screened.

1.5 Objectives of this thesis – materials synthesis and characterization

The design and synthesis of EL materials with enhanced operational performance is critical to research and development both in academic and industrial units. The requirements to synthesize OLED materials should be based on the qualifications listed in **section 1.3**. The objectives of this thesis are to synthesize and characterize 1) a group of new diamines and assess their potential as HT materials; 2) potential Al-based ET and EM materials; 3) EM materials derived from boron complexes and 4) a family of perimidine based heterocycles and investigating their potential as EL materials.

The work in **Chapter 2** will report the synthesis of aryldiamines with a naphthalene core. Synthetic routes and choices of catalysts will be discussed in detail. From the characterization results, practical information on thermal, photophysical and electrochemical properties of these compounds will be presented.

In **Chapter 3**, C-4 modified Alq_3 analogues were synthesized. These species possess phenyl or diarylamine groups in C-4 position. The thermal, photophysical and electrochemical properties of these compounds will be compared with Alq_3. One of the targets of this effort was to investigate the effect of C-4 modification on pyridyl ring. Substitutions at this site have very rarely been investigated and may be a way to modify the LUMO of the Alq_3–related materials. Additional aims of this work are to optimize

intermolecular interactions, balance the hole/electron mobility and improve quantum efficiency ultimately improving device performance.

Since boron-based complexes are thought to be promising candidates for EM materials, especially for blue light emission, substituted salicylaldimine (Schiff's Bases) diphenyl boron complexes have been synthesized and characterized in this thesis. The results of this effort are reported in **Chapter 4**,

Finally, **Chapter 5** will present a novel family of perimidine-based compounds that were initially designed as TPBI analogues.[25] In addition to a 1,3,5-substituted phenyl core, pyridine, thiophene, 1,3-substituted and 1,4-substituted phenyl cores were also synthesized and examined as potential EL materials. The properties of thermal, photophysical and electrochemical behaviors will be presented.

Chapter 6 will provide a broad summary of these efforts. Future prospects will also be presented in this chapter.

References for Chapter 1:

(1) Miyata, S.; Sakuratani, Y.; Tao, X. T. *Optical Materials* **2002**, *21*, 99-107.

(2) Tullo, A. H. *C&EN* **2001**, *19*, 49-54.

(3) Pope, M.; Kallmann, H.P.; Magnante, P. *J. Chem. Phys.* **1963**, *38*, 2042-2043.

(4) Helfrich, W.; Schneidere, W. G. *Phys. Rev. Lett.* **1965**, *14*, 229-231.

(5) Williams, D. F.; Schadt, M. *Proc. IEEE* **1970**, *58*, 476.

(6) Vincett, P. S.; Barlow, W. A.; Hann, R. A.; Roberts, G. G. *Thin Solid Films* **1982**, *94*, 171.

(7) Kampas, F. J.; Gouterman, M. *Chem. Phys. Lett.* **1977**, *48*, 233.

(8) Kalinowski, J.; Godlewwski, J.; Dreger, A. *Appl. Phys. A* **1985**, *37*, 179.

(9) Tang, C. W.; VanSlyke, S. A. *Appl. Phys. Lett.* **1987**, *51*, 913-915.

(10) Tang, C. W.; Vanslyke, S. A.; Chen, C. H. *J. Appl. Phys.* **1989**, *83*, 3610-3616.

(11) Burroughes, J. H.; Bradley, D. D. C.; Brown, A. R.; Marks, R. N.; Friend, R. H.; Burn, P. L.; Holmes, A. B. *Nature* **1990**, *347*, 539-541.

(12) Kovax, J.; Peternai, L.; Lengyel, O. *Thin Solid Films* **2003**, *433*, 22-26.

(13) Gillessen, K.; Schairer, W. *Light Emitting Diodes, An Introduction* **1987**, Prince/Hall International.

(14) Sheats, J. R.; Antoniadis, H.; Hueschen, M.; Leonard, W.; Miller, J.; Moon, R.; Roitman, D.; Stocking, A. *Science* **1996**, *273*, 884-888.

(15) Hung, L. S.; Chen, C. H. *Mater. Sci. Engineer.* **2002**, *R 39*, 143-222.

(16) Shih, H. T.; Lin, C. H.; Shih, H. H.; Cheng, C. H. *Adv. Mater.* **2002**, *14*, 1409-1412.

(17) Further examples polyamines can found in: Shirota, Y. *J. Mater. Chem.* **2000**, *10*, 1-25.

(18) Mitschke, U.; Bauerle, P. *J. Mater. Chem.* **2000**, *10*, 1471-1507.

(19) References selected from Thompson's group. (a) Burrows, P. E.; Shen, Z.; Bulovic, V.; McCarty, D. M.; Forrest, S. R.; Cronin, J. A.; Thomposon, M. E. *J. Appl. Phys.* **1996**, *79*, 7991-8006. (b) Koene, B. E.; Loy, D. E.; Thomposon, M. E. *Chem. Mater.* **1998**, *10*, 2235-2250. (c) Lu, P.; Hong, H.; Cal, G.; Djurovich, P.; Weber, W. P.; Thompson, M. E. *J. Am. Chem. Soc.* **2000**, *122*, 7480-7486. (d) Lamansky, S.; Djurovich, P.; Murphy, D. Abdel-Razzaq, F.; Lee, H.; Adachi, C.; Burrows, P. E.; Forrest, S. R.; Thompson, M. E. *J. Am. Chem. Soc.* **2001**, *123*, 4340-4312. (e) Kolosov, D.; Adamovich, V.; Djurovich, P.; Thompson, M. E.; Adachi, C. *J. Am. Chem. Soc.* **2002**, *124*, 9945-9954.

(20) (a) Antoniadis, H.; Inbasekaran, M.; Woo, E. P. *Appl. Phys. Lett.* **1998**, *73*, 3055-3057. (b) Chung, J.; Choi, B. Lee, H. H.; *Appl. Phys. Lett.* **1999**, *74*, 3645-3647. (c) Gao, Z.; Lee, C. S.; Bello, I.; Lee, S. T.; Chem, R.; Luh, T. Y.; Shi, J.; Tang, C. W. *Appl. Phys. Lett.* **1999**, *74*, 865. (d) Ganzorig, C.; Fujihira, M. *Appl. Phys. Lett* **2000**, *77*, 4211-4213. (e) Popovic, Z.; Aziz, H.; Hu, N.; Hor, A.; Xu, G. *Synthetic Metals* **2000**, *111-112*, 229-232. (f) Aziz, H.; Popovic, Z.; Hu, N. *Appl. Phys. Lett* **2002**, *81*, 370-372. (g) Shirota, Y.; Kuwabara, Y.; Inada, H.; Wakimoto, T.; Nakada, H.; Yonemoto, Y.; Kawami, S.; Imai, K. *Appl. Phys. Lett.* **1994**, *65*, 807-809.

(21) (a) Salbeck, J.; Yu, N.; Bauer, J.; Weissortel, F.; Bestgen, H. *Synth. Met.* **1997**, *91*, 209-215. (b) Thomas, K. R.; Lin, J. T.; Tao, Y. T.; Ko, C. W.; *J. Am. Chem. Soc.*

2001, *123*, 9404-9411. (c) Yu, M. X.; Duan, J. P.; Lin, C. H.; Cheng, C. H.; Tao, Y. T. *Chem. Mater.* **2002**, 14, 3958-3963.

(22) (a) Shirota, Y.; Kobata, T.; Noma, N.; *Chem. Lett.* **1989**, 1145-1148. (b) Kageyama, H.; Itano, K.; Ishikawa, W.; Shirota, Y. *J. Mater. Chem.* **1996**, *6*, 675-676. (c) Shirota, Y.; Okumoto, K.; Inada, H. *Synth. Met.* **2000**, *111*, 387-391. (d) Ishikawa, W.; Inada, H.; Nakano, H.; Shirota, Y. *Chem. Lett.* **1991**, 1731-1734. (e) Shirota, Y.; Kuwabara, Y.; Inada, H.; Wakimoto, T.; Nakada, H.; Yonemoto, Y.; Kawami, S.; Imai, K. *Appl. Phys. Lett.* **1994**, *65*, 807-809.

(23) (a) Hopkins, T. A.; Meerholz, K.; Shaheen, S.; Anderson, M. L.; Schmidt, A.; Kippelen, B.; Padias, A. B.; Hall, H. K.; Jr.; Peyghambarian, N.; Armstrong, N. R. *Chem. Mater.* **1996**, *8*, 344-351. (b) Kido, J.; Endo, J. *Chem. Lett.* **1997**, 593-594. (c) Leung, L.; Lo, W. Y.; So, S. K.; Lee, K. M.; Choi, W. K. *J. Am. Chem. Soc.* **2000**, *122*, 5640-5641. (d) Sapochak, L. S.; Padmaperuma, A.; Washton, N.; Endrino, F.; Schmett, G. T.; Marshall, J.; Fogarty, D.; Burrows, P. E.; Forrest, S. R. *J. Am. Chem. Soc.* **2001**, *123*, 6300-6307. (e) Yu, J.; Chen, Z.; Sakuratani, Y.; Suzuki, H.; Tokita, M.; Miyata, S. *Jpn. J. Appl. Phys.* **1999**, *38*, 6762-6763. (f) Shao, Y.; Qiu, Y.; Hu, W.; Hong, X. *Adv. Mater. Opt. Electron.* **2000**, *10*, 285-288. (g) Wang, X.; Chen, Z.; Ogino, K.; Sato, H.; Miyata, S.; Tan, H. *Polymer Journal* **2000**, *32*, 778-783. (h) Chen, Z.; Yu, J.; Sone, M.; Miyata, S.; Lu, Y.; Watanabe, T. *J. Phys. D: Appl. Phys.* **2001**, *34*, 2679-2682. (i) Yu, J.; Chen, Z.; Miyata, S. *Synth. Met.* **2001**, *123*, 239-243. (j) Han, Y. K.; Lee, S. U. *Chem. Phys. Lett.* **2002**, *366*, 9-16. (k) Wang, G.; Liang, F.; Xie, Z.; Su, G.; Wang, L.; Jing, X.; Wang, F. *Synth.*

Met. **2002**, *131*, 1-5. (l) Ghedini, M.; Deda, M. L.; Aiello, I.; Grisolia, A. *Synth. Met.* **2003**, *10327*, 1-4.

(24) (a) Tanaka, H.; Tokito, S.; Taga, Y.; Okada, A. *J. Mater. Chem.* **1998**, *8*, 1999-2003. (b) Liu, Y.; Guo, J.; Feng, J.; Zhang, H.; Li, Y.; Wang, Y. *Appl. Phys. Lett.* **2001**, *78*, 2300. (c) Liu, Q.; Mudadu, M. S.; Schmider, H.; Thummel, R.; Tao, Y.; Wang, S. *Organometallics* **2002**, *21*, 4743-4749.

(25) (a) Shi, J.; Tang, C. W.; Chen, C. H. U.S. *Patent No. 5,646,948*, **1997**. (b) Gao, Z.; Lee, C. S.; Bello, I.; Lee, S. T.; Chen, R.; Luh, T.; Shi, J.; Tang, C. W. *Appl. Phys. Lett.* **1999**, *74*, 865-867.

(26) (a) Adachi, C.; Tsutsui, T.; Saito, S. *Appl. Phys. Lett.* **1989**, *55*, 1489-1491. (b) Adachi, C.; Tsutsui, T.; Saito, S. *Appl. Phys. Lett.* **1990**, *56*, 799-801. (c) Adachi, C.; Tsutsui, T.; Saito, S. *Appl. Phys. Lett.* **1990**, *57*, 531-533.

(27) (a) Thelakkat, M.; Schmidt, H. W. *Polym. Adv. Technol.* **1998**, *9*, 429-442. (b) Maindron, T.; Dodelet, J. P.; Lu, J.; Hlil, A. R.; Hay, A. S.; D'Iorio, M. *Synth. Met.* **2002**, *130*, 247-255. And references therein.

(28) Naito, K.; Miura, A. *J. Phys. Chem.* **1993**, *97*, 6240-6248.

(29) (a) Pommerehne, J.; Vestweber, H.; Guss, W.; Mahrt, R. F.; Bassler, H.; Porsch, M.; Daub, J. *Adv. Mater*, **1995**, *7*, 551-554. (b) Thelakkat, M.; Schmidt, H. W. *Adv. Mater.* **1998**, *10*, 219-223.

(30) (a) Stampfl, J.; Tasch, S.; Leising, G.; Scherf, U. *Synth. Met.* **1995**, *71*, 2125-2128. (b) Fery-Forgues, S.; Lavabre, D. *J. Chem. Ed.* **1999**, *76*, 1260-1264.

Chapter 2

Synthesis and Characterization of Naphthalene Core Hole-Transport OLED Materials

2.1 Introduction

2.1.1 Hole-transport (HT) materials

Presently, there are two main types of hole-transport (HT) materials that belong to the class of *tri*-arylamines that have been used for OLED materials. The first are simple diamines and their derivatives, and the other are the so-called starburst amines. Aromatic diamines have been the most commonly used HT materials since Tang employed a diamine in fabricating two-layer and multilayer OLEDs in the late of 1980s.[1,2] Shortly thereafter, starburst amine molecules were synthesized and demonstrated to be candidates for organic device application.[3,4] The advantages of aromatic diamines include high hole mobility, similarity in energy between the amine HOMO energy level and the anode and the ease of thin film formation in OLED manufacture. Starburst amines have received much attention due to their improved ability to form pinhole-free thin films. These features have made *tri*-arylamines the prototype for synthetic chemists to design new HT materials and the benchmark choices to fabricate OLEDs in recent years.[5-12] The basic

difference of the diamines and starburst amines is in the choice of "core" structure and the way that the aromatic amines are connected to the molecular core. The diamine compounds typically have more variability in the aromatic cores and they are generally capped at the *para*-position with different diarylamines, while starburst amines generally have a phenyl core center branched at the 1, 3, 5 positions with aromatic amines or have nitrogen as the core center bonded with three other functional aromatic groups (see **Figure 1.5**).[4]

The work in this chapter will be focused on materials of the diamine class. The prototype structure for aromatic diamines and their derivatives can be summarized in **Chart 1** from **Chapter 1** and redrawn below.

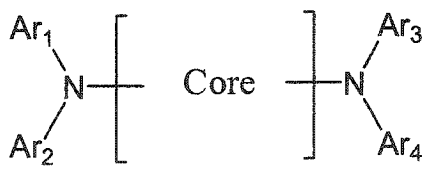

Ar = aromatic groups

Chart 1

Benchmark compounds in this field possessing a biphenyl core structure and are represented by N,N'-diphenyl-N,N'-di(*m*-tolyl)benzidine (TPD) and N,N'-bis(1-naphthyl)-N,N'-diphenyl-benzidine (NPB) (**Figure 1.3**).[5,13] In addition to these biphenyl core diamines, other fused aromatic cores including spiro-linked center,[7] carbazole,[9] anthracene,[10] and other miscellaneous aromatic centers[5] have also been actively synthesized and studied in recent years for the purpose of improving the performance of

HT materials. After the core centers are chosen, diarylamines with various functional groups can be added to them by one pot synthesis to make symmetric compounds in which $Ar_1 = Ar_4$ and $Ar_2 = Ar_3$ or through a two step process to make asymmetric compounds.[8,9] Overall, the synthetic effects to make diamines by choosing a suitable core center capped by various diarylamines have been the focus attempts to obtain compounds that will present improved thermal, photophysical and electrochemical performance in relation to potential applications in an OLED. New HT materials based on diamine structures will continue to be developed and employed in the fabrication of OLEDs.

2.1.2 Synthesis and mechanism

The key step in the synthesis of HT *tri*-arylamines is the aromatic C-N bond formation. The classical method to form such linkages was to apply the Ullmann condensation for N-arylation as depicted in **Scheme 2.1**.[14]

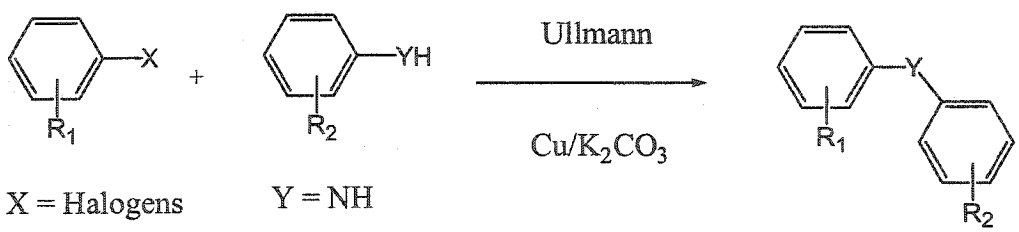

Scheme 2.1 Ullmann reaction

The Ullmann reaction is a process that involves replacing a carbon-iodine or carbon-bromine bond on an aromatic ring between two aromatic nuclei with activated copper. The example of Cu-catalyzed aryl C-N bond formation reaction which employs aryl halide and aryl amine as reagents (**Scheme 2.1**). The role of the Cu catalyst is to polarize C-halogen bond and facilitate further nucleophilic attack for the transformation.[14] This has been the method of choice to synthesize HT *tri*-arylamines. Taking TPD for example, the compound was prepared by the Cu-bronze catalyzed reaction between N,N'-di-phenyl- [1,1'-biphenyl]-4,4'-diamine and *m*-iodotoluene.[15,16]

One of the biggest advantages of Cu catalysts lies in their ready availability, which has made them still one of the candidates to catalyze aryl C-N transformation to synthesize diamines such as naphthalene core diamine[11] and starburst amines.[4,17] However, the harsh reaction conditions of the copper-mediated transformations require high temperatures, strong bases, stoichiometric amounts of copper or copper salts and long reaction times, and usually give low or moderate yield.[3,14] Furthermore, Ullmann reactions are generally limited to aryl iodides as the choice of aryl halide. The formation of C-C and other C-heteroatoms such as aryl C-O and aryl C-S bond formations have also suffered similar problems when using copper as the catalyst. During the last 10 years, much more efficient catalysts using Pd-based catalyst systems that have been developed by Buchwald,[18] Hartwig[19] and their co-workers have gradually replaced copper for the general amination reactions in a wide variety of substrates including aryl C-N formation to synthesize the potential HT OLED materials.[8-10,12, 20-22]

The commonly used Pd-based catalysts are generally prepared by mixing Pd (0) ($Pd(dba)_2$ or $Pd_2(dba)_3$) or $Pd(OAc)_2$ with bulky, electron-rich, phosphine ligands (**Figure**

2.1). The commonly employed bases used in the Pd-catalyzed reactions are NaO-*t*-Bu/ KO-*t*-Bu. When these strong bases cannot tolerate the functional groups of the substrates, the weaker bases such as Cs_2CO_3 or K_3PO_4 can be employed. Furthermore, in Pd-catalyzed reactions, aryl bromides are the most frequently used substrates and in many cases, even aryl chlorides have been applied in cross coupling reactions with amines. The reaction time and temperatures have been also largely reduced at the catalytic Pd loading level (~ 1% Pd), and many coupling reactions will finish within one hour under room temperature if a suitable Pd/L complex were chosen.

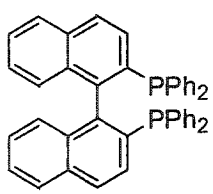

BINAP

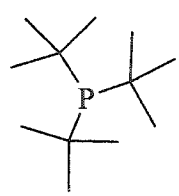

P(*t*-Bu)$_3$

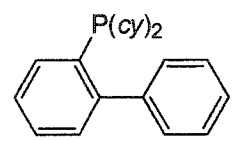

o-biphenylPCy$_2$

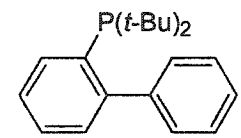

o-biphenylP(*t*-Bu)$_2$

Figure 2.1 Phosphine ligands for Pd-based catalyst system

The catalytic mechanism for the C-N formation has been proposed by Buchwald and Hartwig, and one of the catalytic cycles is redrawn in **Figure 2.2.**[18e] The processes generally start from the dissociation of a dba ligand followed by oxidative addition of the aryl bromide. Amine can then coordinate to the halo aryl complex. Deprotonation of the coordinated ammine function forms an amido complex. The amido complex will then undergo reductive elimination to form the desired product and regenerate Pd(0) catalyst.

When $Pd(OAc)_2$ is employed, the catalytic processes will start from an *in situ* reduction and addition of ligand to Pd[18e] and will then follow similar steps to those outlined in **Figure 2.2**.

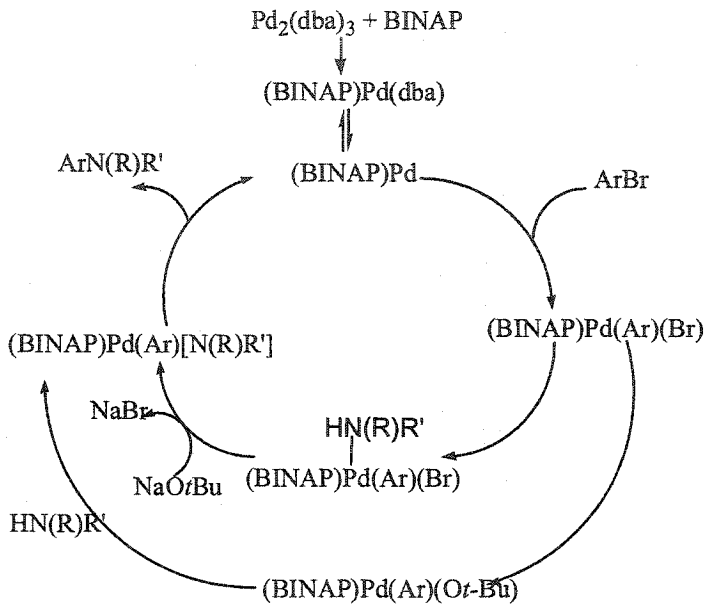

Figure 2.2 Catalytic cycle for Pd-catalyzed reaction

Several Pd/L catalyst systems has been developed and demonstrated to be highly effectively for the aryl C-N bond formation between aryl halide and aryl amine substrates. The choice of a particular Pd/L combination will dictate the efficiency of the C-N bond formation process. One feature of the work presented in this chapter will be an investigation of the appropriate Pd/L combination that will be needed for formation of the targeted compounds.

2.1.3 Objectives of the chapter

Although there are many diamines with various core centers having been developed in recent years, TPD and NPB remain the most widely employed diamines for the fabrication of OLEDs and for the testing and characterization of new transport materials and new device designs.[5] The design and synthesis of a diamine compound used as the HT material in OLEDs is also a comprehensive decision. The basic criteria to be considered should include the thermal, photophysical, electrochemical, film formation and luminescent properties of a new compound. Among these, a high thermal stability is a key requirement that should be met for successful application of a new amine in OLED formation. In other words, one would seek a material that exhibited a higher glass transition temperature (T_g) than those of TPD and NPB, which have values of 65 °C and 98 °C respectively. When deciding on a strategy for increasing T_g, it might be useful to begin with a comparison of the molecular structures of TPD and NPB. Most notable is the fact that replacing a phenyl group on each of the N centers in TPD with a naphthyl group leads to NPB and to an enhancement of the T_g by more than 30 °C. This observation provided one stimulus for replacing the biphenyl core of TPD and NPB with the naphthalene core. The idea here was that this simple modification would achieve one of the objectives of this chapter, which was to obtain high T_g HT materials.

Another aim of the work in this chapter is to apply and optimize Pd-based catalyst system to synthesize naphthalene core diamines. During the progress of the work, Qiu *et al* reported the naphthalene core diamine 1,5-bis[*N*-(1-naphthyl)-*N*-phenyl]naphthalene diamine (NND) and employed it as an HT emitter layer in an OLED.[11] The synthetic

method they used for the synthesis of this species was the Ullmann condensation using 1,5-diiodidenaphthalene as the aryl halide substrate. In the work reported in this chapter, 1,5-dibromonaphthalene has been chosen as the aryl halide substrate and the more efficient Pd-based catalyst systems were chosen for the synthetic work. First, a variety of substituted diarylamines were synthesized using the Pd catalyst system. Next, these amines were coupled with dibromonaphthalene to obtain the targeted products. Various ligands and bases have been tried in order to find the best components (Pd/L) for the aryl C-N bond formation. Meanwhile, some alternative routes using different substrates such as 1,5-diaminonaphthalene and 1,5-dihydroxynaphthalene were attempted for the synthesis of naphthalene core diamines. These results will be briefly discussed in the results and discussion section.

With the naphthalene core diamines in hands, the second set of broad objective of this chapter was to characterize these compounds by investigating their thermal, photophysical and electrochemical properties. These measurements will allow an assessment of the potential of these materials as HT candidates for OLEDs. Furthermore, these properties will direct us in the future design and synthetic efforts to continue to tune the materials properties of these compounds. Special attention has been paid on the effects of substituents that are attached at *para* or *meta*- position of the diarylamines. The relationship between the substituents and material properties will be discussed.

2.2 Experimental

General Information. All reactions were carried out under a nitrogen atmosphere in a sealed Schlenk flask. When required, reactions were heated in an oil bath. All amines, aryl halides, tris(dibenzylidineacetone)dipalladium ($Pd_2(dba)_3$), *rac*-2,2'-Bis(diphenylphosphino)-1,1'-binaphthy (BINAP), sodium *tert*-butoxide, were purchased from Aldrich Chemical Co. and used without further purification. Tri-*t*-butylphosphine, *o*-biphenylPCy_2, *o*-biphenylP(t-Bu)$_2$ were purchased from Strem Chemicals. 1,5 dibromonaphthalene was synthesized from 1,5-diaminonaphthalene according to the literature.[23] Toluene was purified by passage through a column of activated alumina using an apparatus purchased from Anhydrous Engineering. Dichloromethane was freshly distilled over CaH_2 under nitrogen.

All reactions were monitored using Silica Gel 60 F_{254} TLC aluminum sheets by UV lamp and/or GC/MS using a Mass Selective Detector from Agilent GC systems 6890 series with HP-5 capillary column (crosslinked 5% PH ME Siloxane).

^1H and ^{13}C-NMR spectra were run on a Varian Gemini-200 or a Bruker 300 MHz spectrometer using the residual protons of the deuterated solvent for reference. The overlapping ^{13}C peaks were identified through 1D_^{13}C_DEPT and $^1H^{13}C$ HMQC analysis on a Bruker 300 MHz spectrometer. Electron impact mass spectra EI (MS) were recorded on a Kratos Concept IIH instrument using electron ionization at 70 eV. High resolution mass spectrometer (HRMS) was performed at the University of Ottawa on Kratos Concept IIH instrument using electron ionization at 70 eV, acceleration 8 KV, resolution 7000 – 10,000. Single crystals were mounted on thin glass fibers using viscous oil and

then cooled to the data collection temperature. Data were collected on a Bruker AX SMART 1k CCD diffractometer using 0.3° ω-scans at 0, 90, and 180° in ϕ. Unit cell parameters were determined from 60 data frames collected at different sections of the Ewald sphere. Semiempirical absorption corrections based on equivalent reflections were applied. The glass transition temperatures and melting points were measured using a TA 2010 differential scanning calorimeter (DSC) instruments using Indium metal as the reference. The samples were heated at rates ranging from 5 °C/min to 20 °C/min as needed. UV spectra were recorded in CH_2Cl_2 on a Varian Cary spectrophotometer. Steady-state fluorescence spectroscopy was carried out using a Photon Technology International version 1.2 X luminescence spectrometer with the same cuvette used for UV-vis measurements. The quantum efficiency (Φ_f) of the compounds was determined by comparing with that of Coumarine-102. Cyclic voltamograms (CV) were conducted using a Hokuto DenkoHA501 potentiostat connected to a Hokuto Denko HB105 programmable function generator. A Nicolet 310 Oscilloscope was used to follow the *in-situ* CV scans. A fresh polished Pt wire and Pt plate were used as working and counter electrode respectively. A silver wire was employed as a pseudoreference electrode. All solutions were prepared in millimolar concentrations in dry CH_2CL_2, which was freshly distilled over CaH_2. Tetrabutyl ammonium hexafluorophosphate (TBAHFP) was used as supporting electrolyte at a concentration of 0.1 M. The electrochemical cell was degassed with nitrogen prior to analysis and the samples were kept under a nitrogen atmosphere during electrochemical measurements. At the end of each set of CV scans, ferrocene (Cp_2Fe) was added to the solution and another potential scan was performed to provide redox potential for the Cp_2Fe/Cp_2Fe^+ couple as a reference. The HOMO energy levels of

all the compounds were calculated by comparing the oxidation potential for the particular compound with that of the ferrocene reference. The energy of the HOMO of Cp_2Fe that was used in the calculations was 4.80 eV.[24] LUMO energy levels were then obtained by subtracting the HOMO/LUMO energy gap for a particular compound that was obtained from the absorption and emission spectra, from the electrochemically derived HOMO energy.

General procedure for the synthesis of diarylamines

All reactions were processed in 0.1 mol scale if not specified. Yields are presented in **Table 2.1,** in **section 2.3.2** on page 42. Compounds **1a-i** were prepared via Pd-catalyzed coupling of arylbromides and arylamines according to **Scheme 2.3**. The general procedure for the synthesis of diarylamines followed that reported in the literature.[18e] In a Schlenk flask, the appropriate arylbromide and arylamines (1:1.2 molar ratio) were dissolved in toluene and the reaction mixture was placed under an N_2 atmosphere. Solid $Pd_2(dba)_3$ and BINAP (ligand/Pd = 1.5) were weighed out as solids to achieve a catalyst loading of 1-2% relative to ArBr. These solids were added to the reaction mixture under counterflow of N_2. To this mixture, 1.4 equiv (based on ArBr) of NaO*t*Bu was added all at once as a solid under N_2 counterflow. The reaction mixture changed from orange to dark black over the first few seconds. The mixture was then heated to 120 °C and left to stir overnight. The reaction was then cooled to room temperature, filtered and the residue was washed with ethylacetate and combined with the toluene. The solvents were then removed by vacuum evaporation and the residue was dissolved in $CHCl_3$. Column

chromatography was used to purify the product using a $CHCl_3$/hexane mixture as the eluent. Collection of the product was monitored by TLC and all fractions were combined at the end of the separation procedure. The solvents were removed under vacuum to yield pure compounds **1a-j**.

Di-*p*-methoxyphenylamine (1a).

1a was synthesized from 4-bromoanisole and *p*-anisidine. ^1H NMR ($CDCl_3$, δ): 3.77 (s, 6H), 5.27 (s, 1H), 6.80 (d, 4H), 6.83 (d, 4H); ^{13}C NMR ($CDCl_3$, δ): 55.59, 114.48, 114.70, 119.28, 153.09. m/z, 229 (M^+). HRMS (m/z): Calcd for $C_{14}H_{15}N_1O_2$ 229.1103, found 229.1113.

***p*-Methoxyphenylphenylamine (1b)**

1b was synthesized from 4-bromoanisole and aniline. ^1H NMR ($CDCl_3$, δ): 3.79 (s, 3H), 5.29 (s, 1H), 6.8-6.9 (m, 6H), 7.13 (d, 1H), 7.23 (d, 2H); ^{13}C NMR ($CDCl_3$, δ): 55.55, 114.42 (2C, one C hidden), 115.65 (2C, one C hidden), 119.60, 122.20, 129.29 (2C, one C hidden). m/z, 199 (M^+). HRMS (m/z): Calcd for $C_{13}H_{13}N_1O_1$ 199.0997, found 199.0998.

***p*-Methoxyphenyltolylamine (1c)**

1c was synthesized from 4-bromoanisole and *p*-toluidine. ^1H NMR ($CDCl_3$, δ): 2.16 (s, 3H), 3.78 (s, 3H), 5.39 (s, 1H), 6.80-6.85 (m, 4H), 6.90-7.04 (m, 4H). ^{13}C NMR ($CDCl_3$, δ): 20.53, 55.56, 114.61, 116.49, 121.05, 129.28, 129.76, 136.57, 142.33, 154.71. m/z, 213 (M^+). HRMS (m/z): Calcd for $C_{14}H_{15}N_1O_1$ 213.1154, found 213.1155.

_p_-Methoxyphenyl-_p_-fluorophenylamine (1d)

1d was synthesized from 1-fluoro-4-bromobenzene and _p_-anisidine. ^{1}H NMR ($CDCl_3$, δ): 3.78 (s, 3H), 5.32 (s, 1H), 6.8-7.3 (m, 8H). ^{13}C NMR ($CDCl_3$, δ): 55.55, 114.69, 115.76 (J_{C-F} = 22.4 Hz), 117.70 (J_{C-F} = 7.6 Hz), 121.16, 136.43, 141.04, 154.97, 157.11 (J_{C-F} = 236.5 Hz) m/z, 217 (M^+). HRMS (m/z): Calcd for $C_{13}H_{12}F_1N_1O_1$ 217.0903, found 217.0901.

_p_-Methoxyphenyl-_p_-propylphenylamine (1e)

1e was synthesized from 1-propyl-4-bromobenzene and _p_-anisidine.^{1}H NMR ($CDCl_3$, δ): 1.03-1.12 (m, 3H), 1.68-1.79 (m, 2H), 2.63 (t, 2H), 3.86 (s, 3H), 5.48 (s, 1H), 6.88-7.02 (m, 4H), 7.02-7.20 (m, 4H). ^{13}C NMR ($CDCl_3$, δ): 13.71, 24.64, 37.15, 55.35, 114.50, 116.20, 121.02, 129.07, 134.03, 136.44, 142.54, 154.63. m/z, 241 (M^+). HRMS (m/z): Calcd for $C_{16}H_{19}N_1O_1$ 241.1467, found 241.1441.

_p_-Methoxyphenyl-p-biphenylamine (1f)

1f was synthesized from 4-bromobiphenyl and _p_-anisidine.^{1}H NMR ($CDCl_3$, δ): 3.81 (s, 3H), 5.37 (s, 1H), 6.80-7.60 (m, 13H). ^{13}C NMR ($CDCl_3$, δ): 55.53, 114.66, 115.71, 122,41, 126.33, 126.37, 127.91, 128.66, 132.35, 135.24, 140.92, 144.52, 155.33. m/z 275 (M^+). HRMS (m/z): Calcd for $C_{19}H_{17}N_1O_1$ 275.1310, found 275.1325.

_p_-Methoxyphenyl-1-naphthylamine (1g)

1g was synthesized from 1-bromonaphthalene and _p_-anisidine.^{1}H NMR (C_6D_6, δ): 3.79 (s, 3H), 5.89 (s, 1H), 6.86 (d, 1H), 6.89 (d, 1H), 7.03-7.12 (m, 3H), 7.33 (t, 1H), 7.43-7.52 (m, 3H), 7.83-7.87(m, 1H), 7.98-8.01 (m, 1H). ^{13}C NMR ($CDCl_3$, δ): 56.00, 112.09, 115.15, 121.33, 121.47, 122.25, 125.76, 126.32, 126.42, 126.57, 128.99, 135.01, 137.23,

141.25, 155.48. m/z 249 (M^+). HRMS (m/z): Calcd for $C_{17}H_{15}N_1O_1$ 249.1154, found 249.1147.

_m_-Methoxyphenylamine (1h)

1h was synthesized from 3-bromoanisole and *m*-anisidine.^{1}H NMR ($CDCl_3$, δ): 3.77 (s, 6H), 5.72 (s, 1H), 6.2-6.8 (m, 6H), 7.0-7.20(m, 2H). ^{13}C NMR ($CDCl_3$, δ): 55.13, 103.72, 106.41, 110.56, 130.03, 144.22, 160.62. m/z 229 (M^+). HRMS (m/z): Calcd for $C_{14}H_{15}N_1O_2$ 229.1103, found 229.1062.

_p_-Methoxyphenyl-_p_-cyanophenylamine (1i)

1i was synthesized from 4-bromobenzonitrile and *p*-anisidine. ^{1}H NMR ($CDCl_3$, δ): 3.80 (s, 6H), 5.96 (s, 1H), 6.77 (d, 2H), 6.89 (d, 2H), 7.10 (d, 2H), 7.39 (d, 2H). ^{13}C NMR ($CDCl_3$, δ): 55.48, 100.15, 113.66, 114.80, 120.16, 125.00, 132.43, 133.69, 149.59, 156.94. m/z 224.0950 (M^+). HRMS (m/z): Calcd for $C_{14}H_{12}N_2O_1$ 224.0950, found 224.0929.

General procedure for the synthesis of naphthalene core diamines

The general procedure for the synthesis of naphthalene core diamine derivatives and their structures were shown in **Scheme 2.4** and was modified from the literature.[19f] All chemicals and solvent were weighted and added in a Schlenk flask in a drybox. The appropriate arylamines (**1a-j**) and 1,5-dibromonaphthalene (2.2:1 molar ratio) were dissolved in toluene. $Pd(OAc)_2$/P(*t*-Bu)$_3$ (ligand/Pd = 1) were weighed out as solids to achieve a catalyst loading of 1-2% relative to 1,5-dibromonaphthalene and added to the reaction mixture. To this mixture, 2.8 equiv (based on 1,5-dibromonaphthalene) of

NaO*t*Bu was added all at once as a solid. The reaction mixture changed from orange to dark black over the first few seconds. The mixture was then removed from the drybox, heated to 120 °C over oil bath and left to stir overnight. The reaction was then cooled to room temperature, filtered and the residue was washed with ethylacetate and combined with the toluene. The solvents were then removed by vacuum evaporation and the residue was dissolved in $CHCl_3$. Column chromatography was used to purify the product using $CHCl_3$ as the eluent. Collection of the product was monitored by TLC and all fractions were combined at the end of the separation procedure. The solvents were removed under vacuum to yield pure compounds **II 1-9**.

1,5- Bis(di-*p*-methoxyphenylamino)naphthalene (II-1)

Yellow-greenish **II-1** was synthesized from **1a** and 1,5-dibromonaphthalene. Yield: 50%. ^{1}H NMR ($CDCl_3$, δ): 3.79 (s, 12H), 6.64-6.80 (m, 8H), 6.91 (d, 8H), 7.08-7.30 (m, 4H), 7.84 (d, 2H); ^{13}C NMR ($CDCl_3$, δ): 55.48, 114.41, 121.98, 123.44, 126.12, 126.25, 132.82, 142.98, 144.92, 154.54. m/z, 582 (M^+). HRMS (m/z): Calcd for $C_{38}H_{34}N_2O_4$ 582.2519, found 582.2530.

1,5- Bis(*p*-methoxyphenylphenylamino)naphthalene (II-2)

Pale yellow **II-2** was synthesized from **1b** and 1,5-dibromonaphthalene. Yield: 75%. ^{1}H NMR ($CDCl_3$, δ): 3.76 (s, 6H), 6.7-6.9 (m, 9H), 7.0-7.4 (m, 13H), 7.87 (d, 2H); ^{13}C NMR ($CDCl_3$, δ): 55.46, 114.55, 119.84, 120.26, 122.43, 125.38, 126.56, 126.95, 128.93, 133.06, 141.55, 144.30, 149.5, 155.49. m/z, 522 (M^+). HRMS (m/z): Calcd for $C_{36}H_{30}N_2O_2$ 522.2307, found 522.2328.

1,5- Bis(*p*-methoxyphenyltolylamino)naphthalene (II-3)

Yellowish **II-3** was synthesized from **1c** and 1,5-dibromonaphthalene. Yield: 80%. ^{1}H NMR ($CDCl_3$, δ): 2.28 (s, 6H), 3.77 (s, 6H), 6.81 (t, 8H), 7.02 (t, 8H), 7.16-7.34 (m, 4H), 7.88 (d, 2H); ^{13}C NMR ($CDCl_3$, δ): 20.62, 55.46, 114.45, 120.77, 122.20, 124.59, 126.39, 126.58, 129.55, 130.11, 33.00, 142.18, 144.61, 147.05, 155.03. m/z, 550 (M^+). HRMS (m/z): Calcd for $C_{38}H_{34}N_2O_2$ 550.2620, found 550.2642.

1,5- Bis(*p*-methoxyphenyl-*p*-fluorophenylamino)naphthalene (II-4)

White **II-4** was synthesized from **1d** and 1,5-dibromonaphthalene. Yield: 78%. ^{1}H NMR ($CDCl_3$, δ): 3.76 (s, 6H), 6.72-7.32 (m, 20H), 7.82 (d, 2H); ^{13}C NMR ($CDCl_3$, δ): 55.48, 114.64, 115.63 (J_{C-F} = 22.6 Hz), 122.15 (J_{C-F} = 5.0 Hz), 122.22, 124.60, 124.59, 126.49, 126.54, 132.84, 142.11, 144.59, 145.70, 155.33, 157.58 (J_{C-F} = 240.2 Hz) m/z, 558 (M^+). HRMS (m/z): Calcd for $C_{36}H_{28}F_2N_2O_2$ 558.2119, found 558.2101.

1,5- Bis(*p*-methoxyphenyl-*p*-propylphenylamino)naphthalene (II-5)

Yellow-greenish **II-5** was synthesized from **1e** and 1,5-dibromonaphthalene. Yield: 66%. ^{1}H NMR ($CDCl_3$, δ): 0.92 (t, 6H), 1.53-1.63 (m, 4H), 2.49 (t, 4H), 3.76 (s, 6H), 6.75-6.83 (m, 8H), 6.95-7.04 (m, 8H), 7.19-7.30 (m, 4H), 7.86 (d, 2H); ^{13}C NMR ($CDCl_3$, δ): 13.91, 24.62, 37.30, 55.45, 114.45, 120.50, 122.27, 124.65 (2C, one C hidden), 126.40, 126.68, 128.89, 133.07, 134.99, 142.12, 144.59, 147.21, 155.03. m/z, 606 (M^+). HRMS (m/z): Calcd for $C_{42}H_{42}N_2O_2$ 606.3246, found 606.3229.

1,5- Bis(*p*-methoxyphenyl-p-biphenylamino)naphthalene (II-6)

Yellowish **II-6** was synthesized from **1f** and 1,5-dibromonaphthalene. Yield: 50%. ^{1}H NMR ($CDCl_3$, δ): 3.78 (s, 6H), 6.78-7.58 (m, 30H), 7.92 (d, 2H); ^{13}C NMR ($CDCl_3$, δ):

55.47, 114.64, 119.74, 122.58, 125.64, 126.45 (2C, one C hidden), 126.70, 127.08, 127.55, 128.66, 132.82, 133.07, 140.79, 141.25, 144.14, 148.81, 155.51. m/z 674 (M^+). HRMS (m/z): Calcd for $C_{48}H_{38}N_2O_2$ 674.2933, found 674.2908.

1,5- Bis(*p*-methoxyphenyl-1-naphthylamino)naphthalene (II-7)

Orange-yellowish **II-7** was synthesized from **1g** and 1,5-dibromonaphthalene. Yield: 80%. ^{1}H NMR (C_6D_6, δ): 3.20 (s, 6H), 6.54 (d, 4H), 6.72-7.22 (m, 16H), 7.44 (d, 2H), 7.63 (d, 2H), 8.25 (d, 2H), 8.41 (d, 2H); ^{13}C NMR ($CDCl_3$, δ): 54.82, 114.88, 121.75, 123.85, 124.51, 124.92, 125.04, 125.16, 126.24, 126.43, 126.59, 127.12, 128.80, 130.35, 132.50, 135.83, 144.88, 146.34, 147.13, 155.29. m/z 622 (M^+). HRMS (m/z): Calcd for $C_{44}H_{34}N_2O_2$ 622.2620, found 622.2647.

1,5- Bis(di-*m*-methoxyphenylamino)naphthalene (II-8)

White **II-8** was synthesized from **1h** and 1,5-dibromonaphthalene. Yield: 50%. ^{1}H NMR ($CDCl_3$, δ): 3.61 (s, 3H), 3.68 (s, 3H), 6.15 (t, 1H), 6.18 (d, 1H), 6.33 (d, 1H), 6.82-7.33 (m, 14H), 7.96 (d, 2H). ^{13}C NMR ($CDCl_3$, δ): 54.99, 55.61, 103.82, 104.02, 110.55, 112.79, 121.26, 122.81, 125.99, 126.13, 126.26, 128.76, 129.10, 132.86, 135.95, 143.78, 150.78, 155.31, 160.12. m/z 582 (M^+). HRMS (m/z): Calcd for $C_{38}H_{34}N_2O_4$ 582.2519, found 582.2509.

1,5- Bis(diphenylamino)naphthalene (II-9)

White **II-9** was synthesized from diphenylamine and 1,5-dibromonaphthalene. Yield: 52%. ^{1}H NMR ($CDCl_3$, δ): 6.90-7.31 (m, 24H), 7.88 (d, 2H). ^{13}C NMR ($CDCl_3$, δ): 121.71, 121.95, 122.69, 126.73, 127.52, 129.09, 133.24, 144.00, 148.50. m/z 462 (M^+). HRMS (m/z): Calcd for $C_{34}H_{26}N_2$ 462.2096, found 462.2109.

2.3 Results and discussions

2.3.1 Synthetic efforts to obtain naphthalene core diamines

In an effort to synthesize naphthalene core diamines, four synthetic routes were examined from three starting materials, 1,5-diaminonaphthalene, 1,5-dihydroxynaphthalene and 1,5-didromonaphthalene. These efforts are summarized in **Scheme 2.2**.

Route one targets symmetric diaryldiamines. Two catalyst systems were examined, a Cu-based system and the $Pd_2(dba)_3$/BINAP system. The Cu-based catalysts consisted of $Cu/K_2CO_3/I_2$ (trace) and did not yield any products. Some mixed results were obtained in the case of the Pd catalyst system. The reaction when R = H did proceed with an isolated yield of approximately 40%. However, attempts use starting materials with R = OCH_3 gave only trace amounts of product (from TLC).

Both **Routes 2** and **3** are proposed to obtain asymmetric diaryldiamines. **Route 2** is a two-step process. Some success was achieved in the first step where the expected reddish intermediate (R = H) was obtained using the $Pd_2(dba)_3$/BINAP catalysts and the N,N'-diaryl product was obtained in a yield of 50%. However, the second step required the $Pd(OAc)_2/P(t\text{-}Bu)_3$ catalyst system and it only gave a very low yield of product. **Route 3** was based on the coupling reaction between phenol and aniline reported by Thelakkat.[24b] The catalyst for this process was a mixture of Cu/K_2CO_3 in the presence of catalytic amounts of iodine. Two attempts were made at this reaction and even when the reaction mixtures were heated above 200 °C for two days, no products were observed.

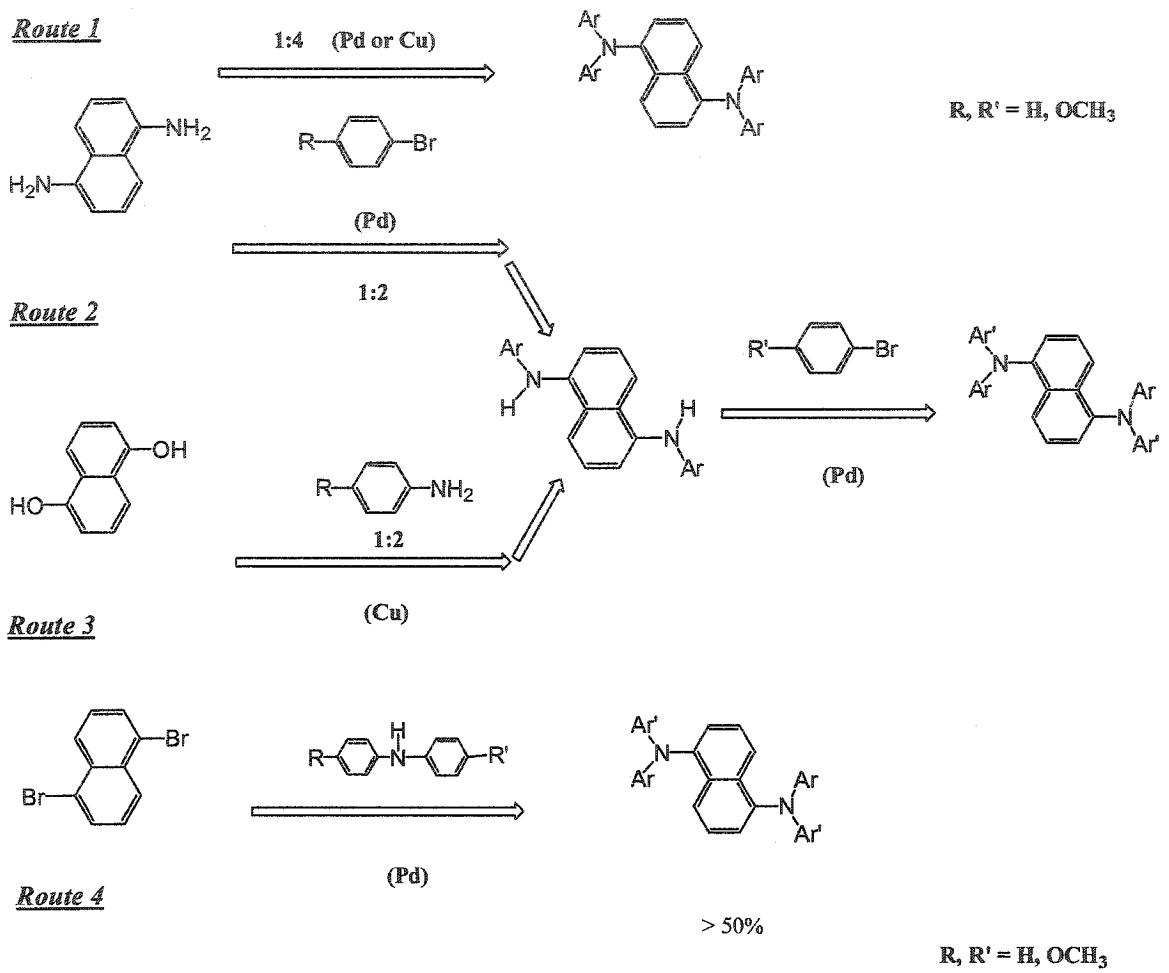

Scheme 2.2 Synthetic efforts toward naphthalene core diamines from different starting materials

In **Route** 4, dibromonaphthalene was synthesized from diaminonaphthalene following the reported procedures.[23] The $Pd(OAc)_2/P(t\text{-}Bu)_3$ catalyst system[19e] was successfully employed to prepare naphthalene core diamines with R = H and OCH_3. Thus, **Route** 4 was applied to catalyze the coupling reactions between dibromonaphthalene and different substituted diarylamines.

2.3.2 Synthesis of substituted diarylamine derivatives

Substituted diarylamines (**1a-i**) were prepared via Pd-catalyzed coupling of arylbromides and arylamines as shown in **Scheme 2.3** and a summary of results is presented in **Table 2.1**. Through variation of the substituents on these diarylamines, it was anticipated that HT efficiency and emission properties could be tuned for future applications.

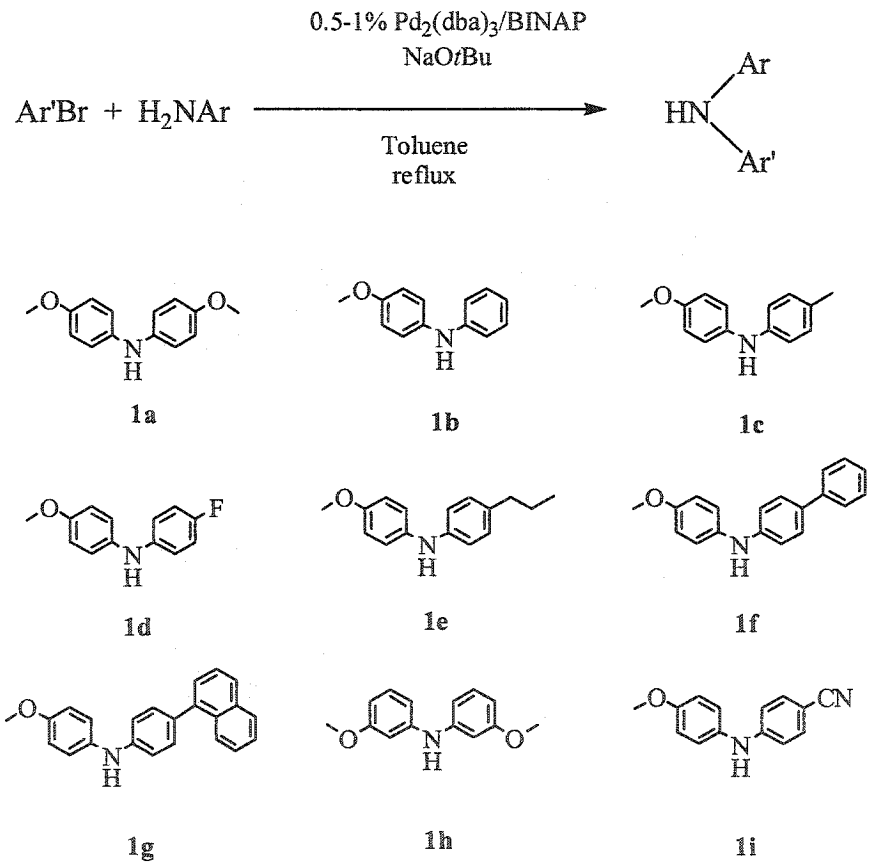

Scheme 2.3 Synthesis of diarylamines and their structures

Table 2.1. Summary of synthesis of HN(Ar)Ar' and 1,5-bis(diarylamino)naphthalenes

Entry	Ar'Br	$ArNH_2$	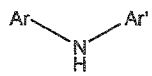 (% yield)	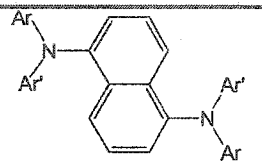 (% yield, $T_g/T_m/T_c$.)
1	p-$MeOC_6H_4Br$	p-$MeOC_6H_4NH_2$	$HN(C_6H_4OMe)_2$ **1a** (78)	**II-1** (50, 76/216/143°C)
2	C_6H_5Br	p-$MeOC_6H_4NH_2$	$HN(C_6H_4OMe)(C_6H_5)$ **1b** (80)	**II-2** (75, 70/230/145°C)
3	p-MeC_6H_4Br	p-$MeOC_6H_4NH_2$	$HN(C_6H_4OMe)(C_6H_4Me)$ **1c** (70)	**II-3** (80, 82/249/103°C)
4	p-FC_6H_4Br	p-$MeOC_6H_4NH_2$	$HN(C_6H_4OMe)(C_6H_4F)$ **1d** (84)	**II-4** (78, 73/192/138°C)
5	p-PrC_6H_4Br	p-$MeOC_6H_4NH_2$	$HN(C_6H_4OMe)(C_6H_4Pr)$ **1e** (86)	**II-5** (66, 51/187/126°C)
6	p-$(C_6H_5)C_6H_4Br$	p-$MeOC_6H_4NH_2$	HN(C_6H_4OMe)(4,4'-biphenyl) **1f** (50)	**II-6** (50, 116/283/200°C)
7	p-$MeOC_6H_4Br$	(1-naphthyl)NH_2	$HN(C_6H_4OMe)$(1-naphthyl) **1g** (50)	**II-7** (80, 131/220/NA°C)
8	m-$MeOC_6H_4Br$	m-$MeOC_6H_4NH_2$	$HN(m\text{-}MeOC_6H_4)_2$ **1h** (40)	**II-8** (50, 72/220/NA°C)
9	p-CNC_6H_4Br	p-$MeOC_6H_4NH_2$	$HN(C_6H_4OMe)(C_6H_4CN)$ **1i** (70)	No reaction
10	-	-	$HN(C_6H_5)_2$ **1j**	**II-9** (52, 83/244/NA°C)
TPD	-	-	-	(85, 66/167°C)

NA, not detected.

A general feature of these coupling reactions was that they proceeded efficiently when the arylbromide substrates bore either an electron donating (methoxyl, methyl and propyl) or withdrawing substituents (fluoro and cyano). However, the coupling reaction would not proceed if arylamine substrate possessed a cyano group. For example, diarylamine **1i** could not be obtained when phenylbromide and 4-aminobenzonitrile were used as reagents in this work. This is a common feature for Pd-catalyzed coupling reaction when an electron-poor arylamine is employed.[18e,20] One possible reason could be in that the cyano group is not tolerated with NaO^tBu as the base for the coupling reaction with primary amines.[18e]

2.3.3 Synthesis of naphthalene core diamines

The general procedure for the synthesis of naphthalene core diamine derivatives was modified from the literature.[19f] and their structures were shown in **Scheme 2.4.** A summary of the results is presented in **Table 2.1** and these demonstrate the efficiency (yields are generally over 50%) of these coupling reactions. There was no product observed in the reaction of dibromonaphthalene with HN(*p*-C_6H_4OMe)(*p*-C_6H_4CN) (entry **9** in **Table 2.1**), which was a further example showing that the amine substrate bearing electron-withdrawing cyano group could not undergo C-N coupling under Pd-catalyzed reactions.

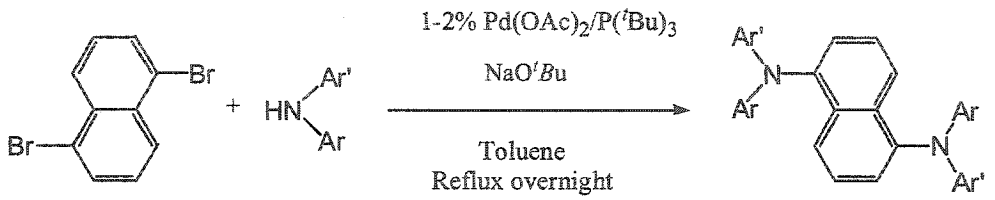

1a-j

II 1-9

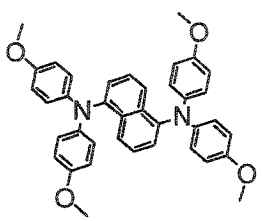

II-1

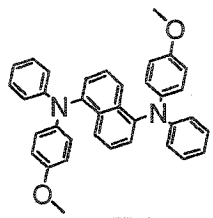

II-2

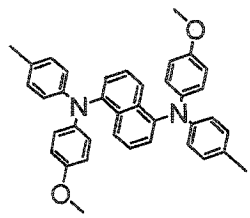

II-3

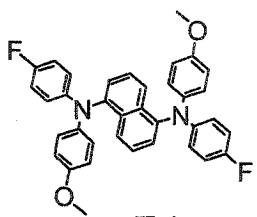

II-4

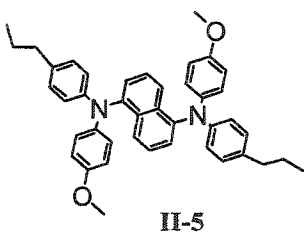

II-5

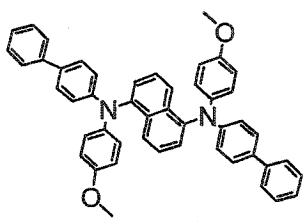

II-6

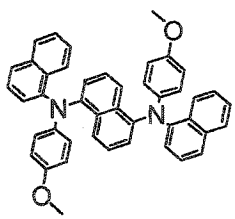

II-7

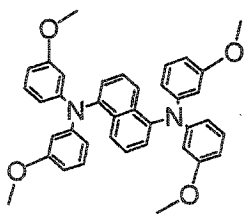

II-8

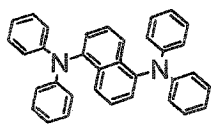

II-9

Scheme 2.4 Synthesis of naphthalene core diamines and their structures

Worth noting in this data is the fact that compounds possessing *m*-methoxy substituents (**1h** and **II-8**) gave relatively low product yields (**1h**, 40%; **II-8** 50%). In addition, compound **II-8** has shown two different methoxy substituents in its ^{1}H NMR (3.61, 3.68 ppm) and ^{13}C NMR (54.99, 55.61 ppm) spectra. This contrasts with the single methoxy signals in **1h**. Since ^{1}H NMR shows 1:1 ratio of methoxy protons, ^{13}C NMR presents 19 C peaks, and HRMS only shows one pure species, the observation of two different methoxy groups was ascribed to a hindered rotation arising from the *meta*-methoxy group. As a result, the two methoxy groups were in different steric positions in **II-8**. The *meta*-substituted compounds also gave different photophysical and electrochemical properties from those of the *para*-substituted compounds, and these will be further discussed in the characterization section.

2.3.4 Molecular structures and XRD data

Crystals of these compounds were grown by slowly evaporating the solvent in a test tube in which the compounds were dissolved in chloroform. Molecular structures of **II-3** and **9** are presented in **Figure 2.3** and **2.4** respectively; selected XRD data of these two compounds are presented in following tables (**Table 2.2-5**). The results further demonstrate the molecular structures of these compounds.

Figure 2.3. Molecular structure and atom numbering scheme for II-3.

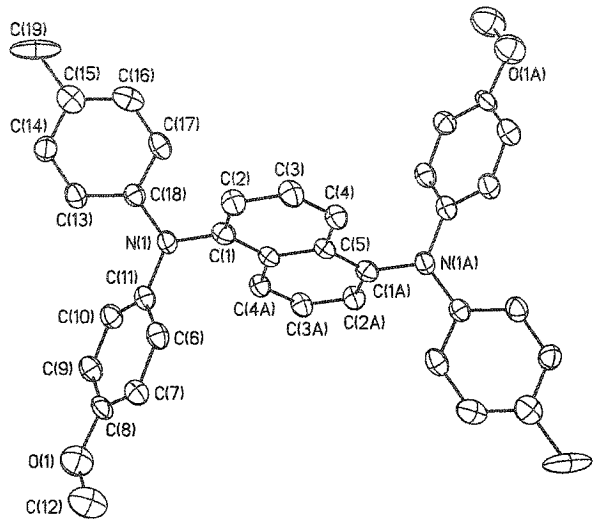

Table 2.2 Selected crystal data and data collection parameters for II-3	
Empirical formula	$C_{38}H_{34}N_2O_2$
formula weight	550.67
T (K)	203(2)
Wavelength (Å)	0.71073
Crystal system	Monoclinic
Space group	P2(1)/c
a (Å)	8.114(2)
b (Å)	16.800(5)
c (Å)	11.090(3)
α (deg)	90
β (deg)	95.361(5)
γ (deg)	90
V (Å^3)	1505.1(7)
Z, Calculated density mg m^{-3}	1.215
abs coeff (mm^{-1})	0.075
Final R indices	R1 = 0.0858, wR2 = 0.1970

Table 2.3. Selected bond distances and angles for II-3.

Bond Distances (Å)		Bond Angles (deg)	
N(1)-C(18)	1.416(6)	C(18)-N(1)-C(11)	123.3(4)
N(1)-C(11)	1.449(6)	C(18)-N(1)-C(1)	118.5(4)
N(1)-C(1)	1.462(3)	C(11)-N(1)-C(1)	116.5(4)

Figure 2.4. Molecular structure and atom numbering scheme for II-9.

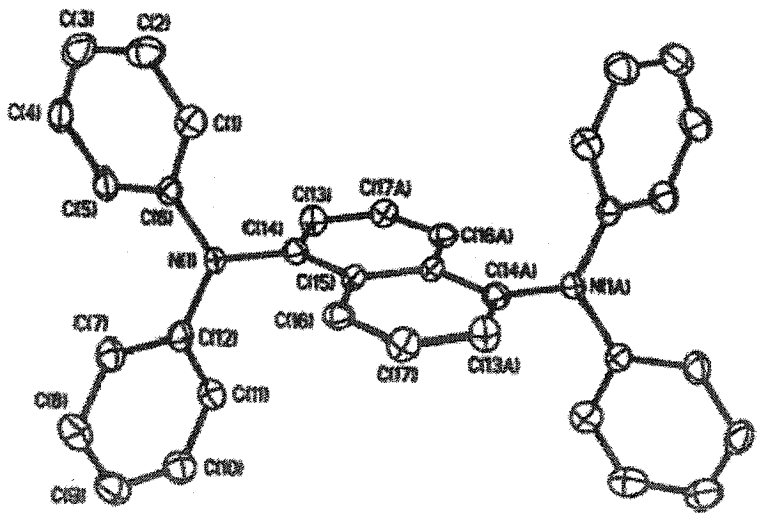

Table 2.4 Selected crystal data and data collection parameters for II-9

Empirical formula	$C_{34}H_{26}N_2$
formula weight	462.57
T (K)	203(2)
Wavelength (Å)	0.71073
Crystal system	Triclinic
Space group	P-1
a (Å)	7.999(3)
b (Å)	9.166(4)
c (Å)	9.511(7)
α (deg)	80.080 (7)
β (deg)	71.614 (7)
γ (deg)	90.933 (7)
V ($Å^3$)	623.6 (5)
Z, Calculated density mg m^{-3}	1.232
abs coeff (mm^{-1})	0.072
Final R indices	R1 = 0.0381, wR2 = 0.0869

Table 2.5. Selected bond distances and angles for II-9.

Bond Distances (Å)		Bond Angles (deg)	
N(1)-C(12)	1.406(3)	C(12)-N(1)-C(6)	121.2(2)
N(1)-C(6)	1.410(3)	C(12)-N(1)-C(14)	119.8(2)
N(1)-C(14)	1.447(3)	C(6)-N(1)-C(14)	116.9(2)

2.3.5 Thermal properties

In order to be of practical consideration for OLED fabrication, the diamines **II 1-9** should form stable glasses. This general feature of materials for OLED construction avoids problems associated with grain boundaries in polycrystalline materials and provides for a high degree of uniformity within thin films. Associated with this amorphous state is the glass transition temperature (T_g), where the glassy and amorphous state of a material begins to soften and flow as the temperature of the sample is increased. Since T_g involves change in heat capacity, not a latent heat, it is characterized by a small slope in a DSC graph. The determination of T_g is further clarified in the next two paragraphs. Above T_g, materials tend to crystallize and produce crystallites that will create grain boundaries and cause nonuniform thin films.[8,25] Generally, a highly symmetric, globular, rigid and dense molecules[25] or asymmetric molecules with reasonably high molecular masses and without stong intermolecular forces[8] have high T_g. These features lead to a high energy for the reorganization/molecular reorientation of the amorphous phase into a crystalline material. In contrast, smaller and more symmetrical molecules have lower reorganization energy with a corresponding lower T_g. Strong intermolecular forces may favor organization of the molecules as they cool below their melting points. This, in turn, encourages crystallization at the expense of glass formation.

A typical DSC for the naphthalene diamines is shown in **Figure 2.5**. The initial scan of compound **II-3** shows a crystal-crystal transition (T_{tr}, 200 °C) and melting point (T_m, 249 °C). After cooling to room temperature the sample was heated a second time. The T_g is observed at 82 °C. Continuing to heat this sample allows observation of an exotherm at 103 °C associated with crystallization (T_c). The melting of **II-3** is again observed at 249

°C. The small peaks after T_c is probably due to the formation of another polymorphism crystalline structures.

A more detailed procedure to measure T_g and more complex phase transitions is shown in **Figure 2.6** for compound **II-6**. In the first run, compound **II-6** shows a coupled endothermic and exothermic phase transition prior to melting at 283 °C. This type of transition has been attributed to polymorphism of the crystalline materials.[26] After the compound was cooled in the liquid nitrogen to form the glassy state the sample was subjected to a second heating cycle which allowed observation of the T_g (116 °C) and T_c (185 °C). Following this second run, the compound was allowed to cool to RT, and a third heating cycle was initiated. This run was stopped prior to melting. The purpose of this heating cycle was to anneal the sample into a crystalline phase. The fourth heating cycle confirmed that **II-6** was again a crystalline sample in that no T_g is observed but T_m is clearly seen. In the fifth run (e), the melted sample was cooled under RT. The data presented in **Figure 2.6** demonstrates that the rate of sample cooling (at RT or liquid nitrogen) has very small effect on the T_g values, but it will affect T_c. For example, T_c is observed at 185 °C for the compound cooled in the liquid nitrogen, while is around 200 °C for the compound cooled under RT (fifth run in **Figure 2.6**).

The T_g, T_m and T_c values of all synthesized naphthalene core diamines were measured by DSC and the results are presented in **Table 2.1**. For comparison, the corresponding values of TPD are listed as the last entry in this table.

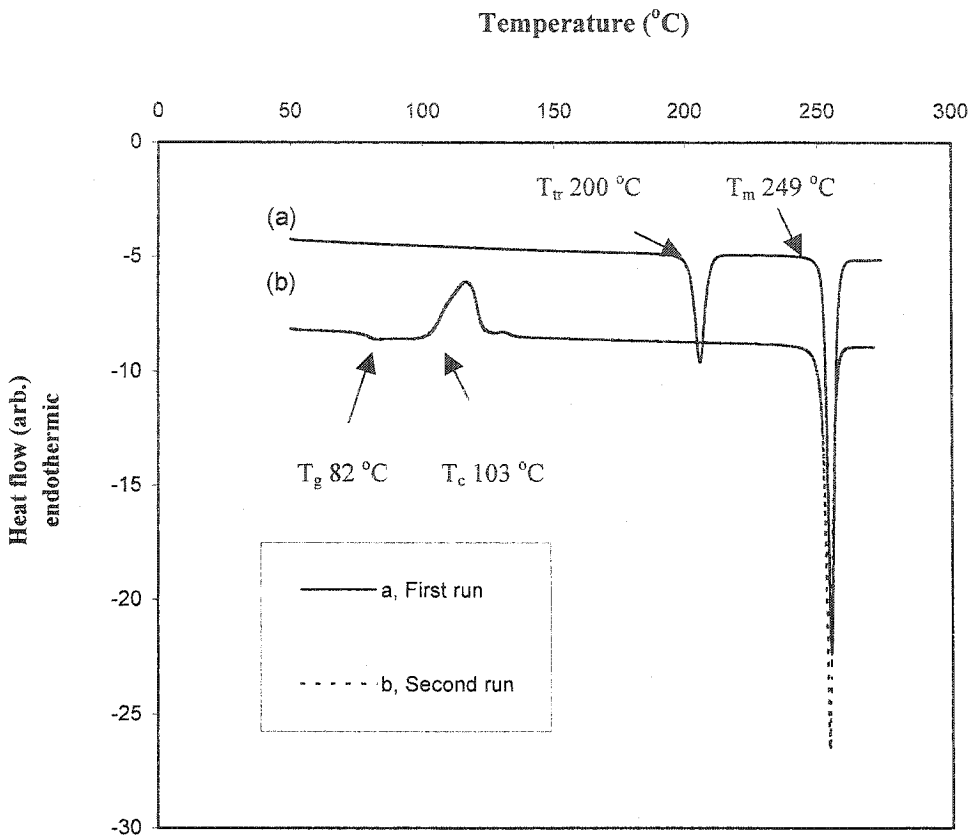

Figure 2.5 DSC curves for compound II-3 at scan rate of 20 °C/min. (a) First run (b) Upon cooling at RT and reheating.

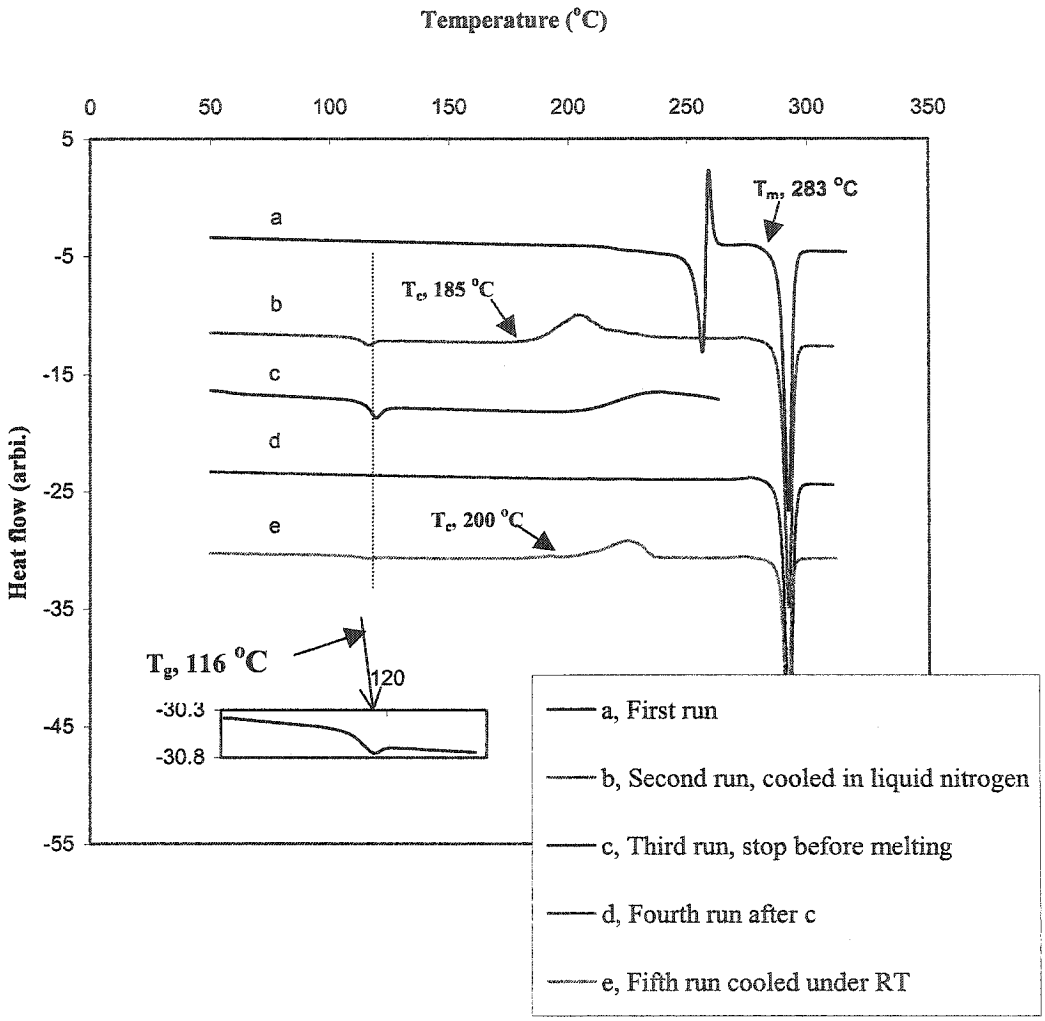

Figure 2.6 DSC curves for compound II-6 at scan rate of 20 °C/min. Inside graph shows the temperature range around T_g of curve e.

As seen in **Table 2.1**, all of the naphthalene core diamines possess melting points from 187-283 °C and these values exceed that of TPD (175 °C). With the exception of **II-5**, all diamines have higher T_g values than TPD and in two cases surpass this value by more than 50 °C. The lowest T_g was observed for **II-5** which can be attributed to the fact that it has a *n*-propyl substituent, a feature that makes it unique among these compounds and likely reduces the overall rigidity of this compound. The highest T_g values were observed for compounds **II-6** and **II-7** which have the extended aromatic subtituents biphenyl and naphthyl respectively. These groups increase the molecular weight and rigidity of **II-6** and **II-7**. The remaining compounds have T_g values that fall within the narrow range of 70 – 83 °C. Compound **II-9**, is unique among this group in that the N-substituents are simple phenyl rings and it exhibited a slightly higher T_g (83 °C) than the substituted-aromatic analogues. This suggests that there is little if any gain in thermal properties by using simple methoxy, methyl or fluoro groups on the aromatic substituents in these systems.

2.3.6 Electronic properties

The naphthalene core diamines **II 1-9** are white, yellow, yellow-greenish or pale orange solids that exhibit absorption maxima (λ_{max}) between 360-380 nm. A summary of their optical absorption data can be found in **Table 2.6**. In addition, all of these diamines exhibited photoluminescence with their emission maxima (λ_{emi}) in the 440-500 nm range and this data is also presented in **Table 2.6**. Specific absorption and emission spectra for **II-1, II-6, II-8** and **II-9** are shown in **Figure 2.7**.

Entry	Absorption λ_{max} (nm) in CH_2CL_2	Emission λ_{emi} (nm)) in CH_2CL_2	Energy gap[a] (nm)	Stokes shift ($\Delta\lambda_{max}$)	(Φ_f) (Relative to Coumarin 102)	ΔEp^b (V)	HOMO[c] (eV)	LUMO[c] (eV)
II-1	375	500	433	125	0.18	0.081	5.10	2.24
II-2	372	475	421	103	0.19	0.160	5.11	2.16
II-3	376	480	425	104	0.22	0.091	5.14	2.22
II-4	370	476	420	106	0.20	0.135	5.15	2.20
II-5	379	480	429	101	0.20	0.123	5.09	2.20
II-6	375	475	425	100	0.19	0.106	5.16	2.24
II-7	375	465	410	90	0.08	0.125	5.14	2.11
II-8	361	441	395	80	0.46	0.202	5.24	2.10
II-9	362	441	401	79	0.48	0.210	5.31	2.22
TPD	350	404	385	54	NA	0.127	5.08	1.86

[a] Estimated from the intersection of normalized absorption and emission graph.
[b] Measured in CH_2Cl_2. All ΔEp are reported relative to Cp_2Fe (ferrocene).
[c] HOMO = (4.8 + ΔEp) eV; LUMO = HOMO – energy gap (eV).
NA, not available
Stokes shift = the difference between absorption and emission peaks.

Table 2.6. Spectroscopic and electrochemical data for naphthalene core diamines.

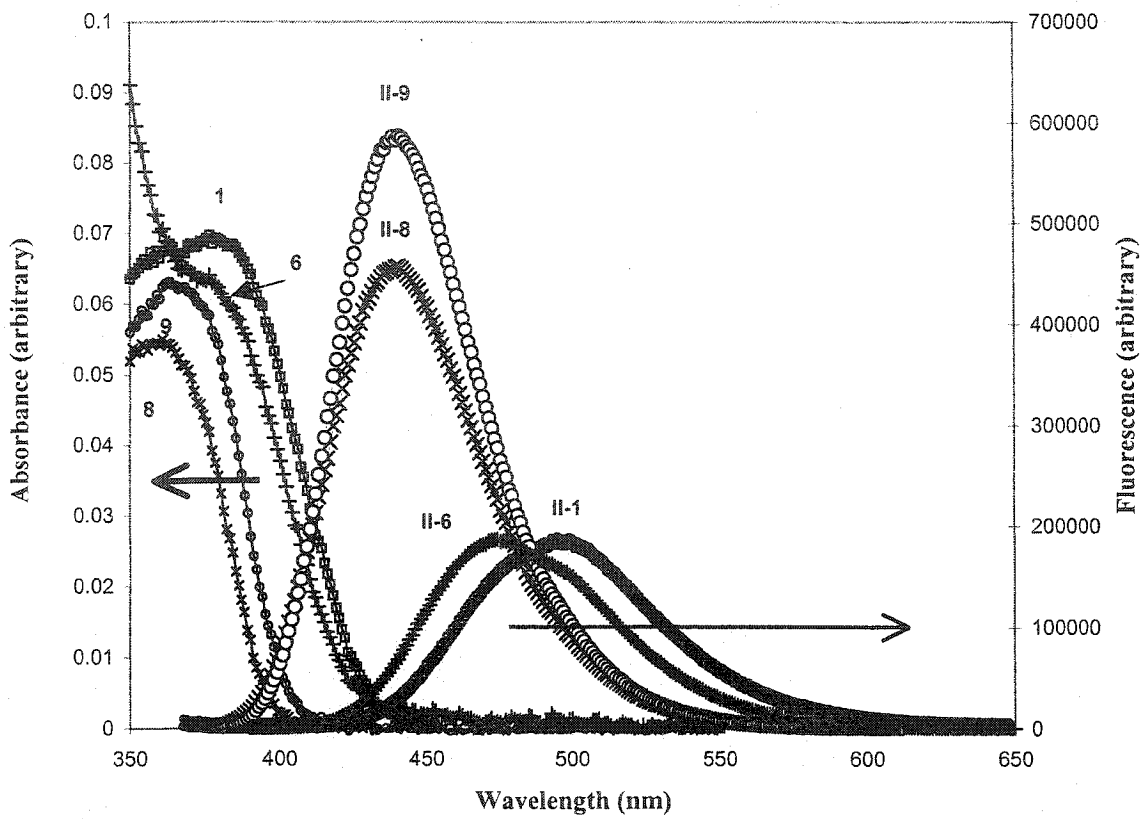

Figure 2.7 UV-vis absorption (left) and emission (right) spectra in CH_2Cl_2 solutions for compounds II-1, II-6, II-8 and II-9.

These spectra are typical for all of the diamines and possess well-separated absorption and emission maxima with the later appearing in the blue to green region of the spectrum and having full width at half maxima in the range 58-77 nm. The HOMO/LUMO gap energy were estimated from these spectra as the intersection between the normalized spectra[9,10] and this data is included in **Table 2.6.**

Except for compound **II-6**, all the diamines exhibit a single λ_{max} in their absorption spectra. In the case of **II-6,** there is an absorption with an approximate λ_{max} of 375 nm with an increasing absorption at shorter wavelength. The absorption maximum for TPD at 350 nm has been assigned to an electronic transition that is due to electron transfer from a nitrogen lone-pair to the π^* orbital of the biphenyl group.[8] Therefore, the λ_{max} absorption values for compounds **II 1-9** was assigned to a similar n-π^* electron transition with the π^* orbital residing on the naphthalene core. The rising absorption of **II-6** below 375 nm is likely a result of another n-π^* electron transition involving the nitrogen lone-pair and the π^* orbital of the biphenyl ring.

The unsubstitued phenyl compound **II-9** can be used as a comparison with the *p*-substituted phenyl compounds (**II 1-7**) to examine the effect of substituents on the phenyl ring. Compounds **II 1-7** exhibit a bathochromic shift in both absorption and emission which was ascribed to the electron donating properties of the aromatic substituents. The electron donating properties of the methoxy substituents appear to overwhelm the electron-withdrawing effects of fluoro (**II-4**), phenyl (**II-6**) and naphthyl groups (**II-7**). As a result, compound **II-1,** for which both N-phenyl groups possess electron donating OMe groups, displays the largest red-shift for emission.

Generally, the HT materials in an OLED are not used as the source of emission. Since the hole mobility is much faster than electron mobility, the charge recombination usually occurs in the ET layer and this is where the emission arises. However, if the difference of HOMO energy levels between HT and ET is big enough, meanwhile the difference in LUMO energy levels is small, holes will be blocked within the HT layer. As a result emission could arise in the HT layer. Diamine based HT materials as the emitter host[10] and emission sources[11,12] have been reported recently. As a result, the emission properties of HT materials, both λ_{emi} and quantum efficiency (Φ_f) provide as important performance criteria as thermal properties and suitable energy (HOMO/LUMO) levels for charge transport to meet requirements for various OLED fabrication. The values of Φ_f for the naphthalene core diamines **II 1-9** were determined. Furthermore, an analysis of the relationship between the Φ_f and molecular structures can be conducted with diamines **II 1-9**. A qualitative interpretation of the structural and environmental factors that influence Φ_f is shown in **Equation 2.1.**[27]

$$\Phi_f = [k_f/(k_f + k_i + k_{ec} + k_{ic} + k_{pd} + k_d)] \qquad \textbf{(Eq. 2.1)}$$

Where k is the relative rate constants for the processes by which the lowest excited singlet state (π^* in this work) is deactivated. They represent fluorescence (k_f), intersystem crossing (k_i), external conversion (k_{ec}), internal conversion (k_{ic}), predissociation (k_{pd}), and dissociation (k_d), respectively. In this work, where the entire naphthalene core diamines have similar structures and measurement conditions, k_i is the most important factor to influence Φ_f values.

To measure Φ_f of the compounds, Coumarin 102 (Φ_f = 93% in ethanol) has been used as the standard.[28] All measurements were conducted in CH_2Cl_2 solution and Φ_f for diamines were compared with Coumarin 102 and calculated by the following equation.[29]

$$\Phi_{f(x)} = (A_s/A_x)(F_x/F_s)(n_x/n_s)^2\Phi_{f(s)} \qquad \textbf{(Eq. 2.2)}$$

where A is the absorbance at the excitation wavelength, F is the area under the corrected emission curve, and n is the refractive index of solvents used. Subscripts s and x refer to the standard and to the unknown that is being measured. In this work, $n_x = n_s$. Thus, Φ_f for all the diamines has been measured by comparing their absorbance and emission area with that of Coumarin 102, and the results are presented **Table 2.6**.

As seen in **Table 2.6**, one of the obvious trends in Φ_f is that the values for **II-8** and **II-9** are identical and more than twice those of the other diamines. Furthermore **II-8** and **II-9** have identical absorption and emission maxima values. From the thermodynamic considerations, since the lowest energy transition type is $n\rightarrow\pi^*$ in all the diamines, the electron-donating groups at *p*- position will make nitrogen more electron rich and thus reduce the HOMO/LUMO gap and energy difference between the singlet and triplet. As a consequence, k_i is increased which in turn leads to a smaller Φ_f.[27] Apparently, and perhaps not surprisingly, the *meta*-methoxy substituent of **II-8** has little influence compared to the isomeric *para*-substituent and this compound exhibits similar absorption and emission position, and fluorescence properties to the unsubstituted compound **II-9**.

2.3.7 Electrochemistry

In a simple OLED, emission arises from the recombination of electrons originating in the electron-transport (ET) layer with holes that are transported in the HT material.[1,2] This combination can occur in either of the two layers and for charge transfer across the ET/HT interface some degree of HOMO and/or LUMO matching is required as discussed in the previous section. Matching of the HOMO level of the HT layer and that of the anode is also important in EL device engineering. As a result, knowledge of the HOMO level of compunds **II 1-9** is important and an electrochemical method, based on cyclic voltammetry (CV), was chosen to estimate the HOMO energies of diamines. This method has been widely used for HT materials.[9,10,24] These measurements also provide some data on the electrochemical stability of the diamines.

Cyclic voltammetric scans were recorded under an N_2 atmosphere in CH_2Cl_2 solvent against a Ag wire pseudo-reference with tetrabutyl ammonium hexafluorophosphate (TBAHFP) as supporting electrolyte. At the end of each set of scans, ferrocene (Cp_2Fe) was added to the solution and another potential scan was performed which provided a reference potential for the Cp_2Fe/Cp_2Fe^+ couple as a calibration standard. The HOMO energy levels of the diamines were then calculated on the basis of the potential difference between the amine/amine$^+$ couple and the Cp_2Fe/Cp_2Fe^+ couple. A value of 4.80 eV was employed as the reference HOMO level of ferrocene.[24]

Compounds **II 1-9** displayed no reduction peaks at negative scan range (-2 to 0 V). Over the positive potential scan range (0 to +2V), compounds **II 1-7** exhibit two reversible oxidation waves for at least five scan cycles, and an irreversible oxidation

process at more positive potentials. Examples of CV data for **II-1, II-4** and **II-6** are shown in **Figure 2.8.** Compounds **II-8** and **II-9** exhibit different CV behaviors and their CV curves are shown in **Figure 2.9** and **Figure 2.10** respectively.

From the **Figure 2.9**, it can be seen that the CV of compound **II-8** shows two oxidation peaks but they are irreversible when the scan range extends to to +2 V. Compound **II-9** gave CV data shown in **Figure 2.10**. This compound appears to exhibit the same two reversible redox waves for amines **II 1-7,** however, there is a third irreversible oxidation for this compound at higher potential. Scanning through this oxidation on successive cycles leads changes in the CV data that suggest formation of a new and unstable species with two new reversible redox cycles. Reversible behavior for compounds **II-8** and **II-9** can be obtained if the positive potential scan is limited to the potential of the second oxidation as seen in **Figure 2.11**. In this figure, the two reversible redox processes of **II-8** and **II-9** are shown with representative compound **II-6** for comparison. The shifts in both redox waves to higher voltage correlates with the presence and strength of electron donating substituents in the *para*- position of the N-phenyl groups. The irreversible redox CV of **II-8** and **II-9** could be a result of the fact that these two compounds do not possess a substituent in the *para* position of the N-phenyl. The identity of this new species that are produced upon extensive oxidation of **II-8** and **II-9** has not been established but the fact that this observation is associated with the unsubstituted N-phenyl compound suggests that there may be a reaction of the oxidized **II-9** on the N-phenyl ring.

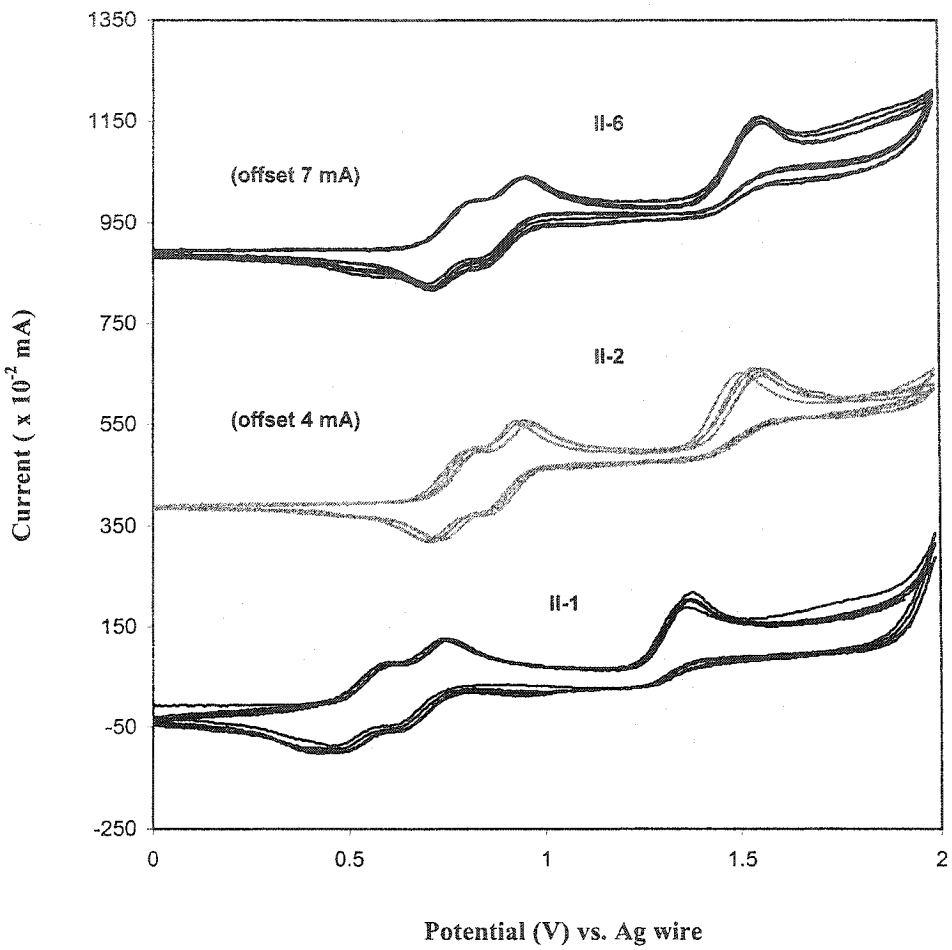

Figure 2.8. CVs at 100 mV/s in CH_2Cl_2 with 0.1 M TBAHP for compounds II-1, II-2 and II-6 under N_2. Five scans recorded.

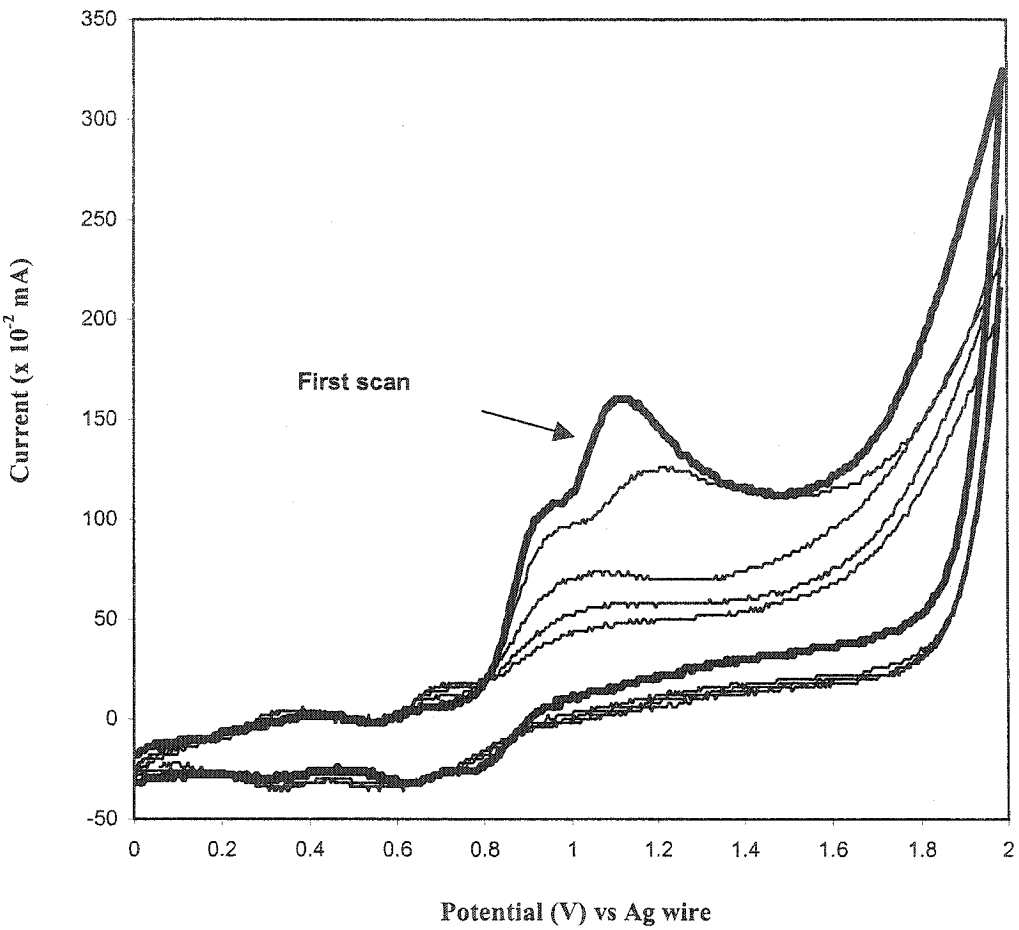

Figure 2.9. CVs at 100 mV/s in CH_2Cl_2 with 0.1 M TBAHP for compound II-8 under N_2. Five scans recorded.

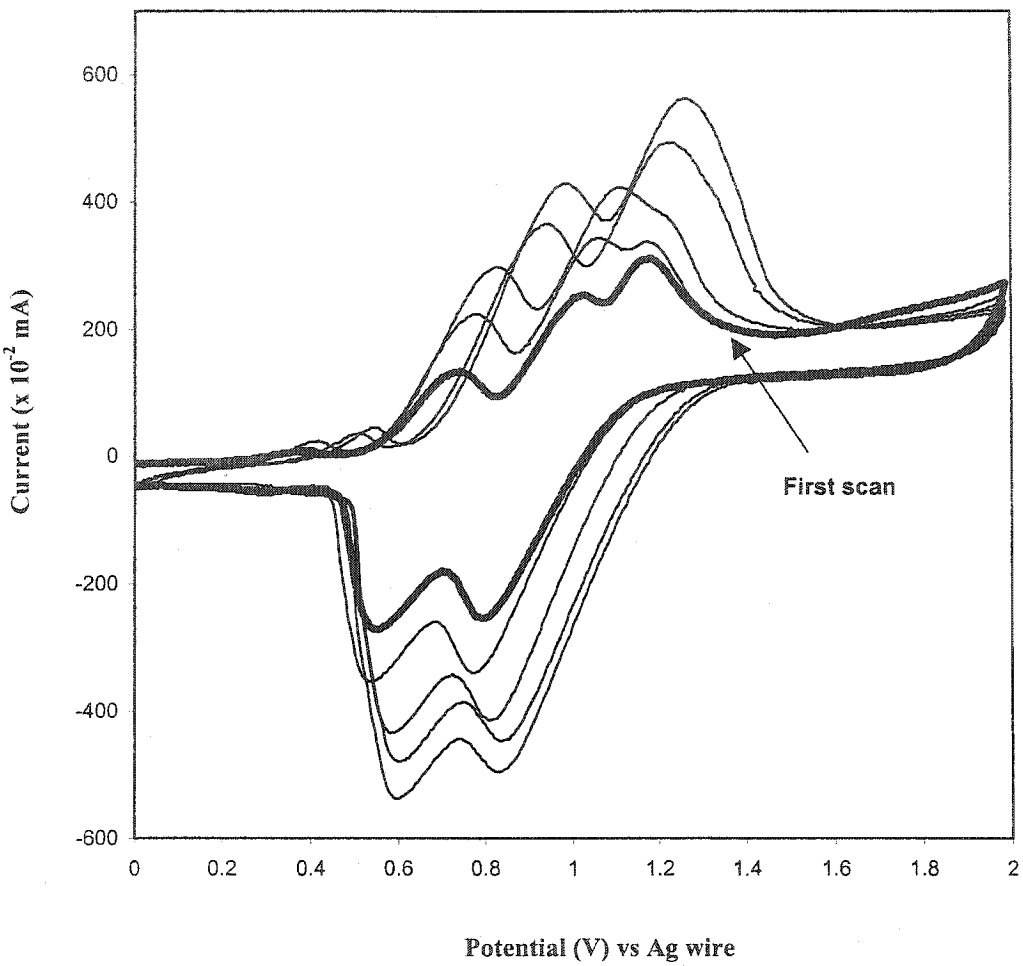

Figure 2.10. CVs at 100 mV/s in CH_2Cl_2 with 0.1 M TBAHP for compound II-9 under N_2. Five scans recorded.

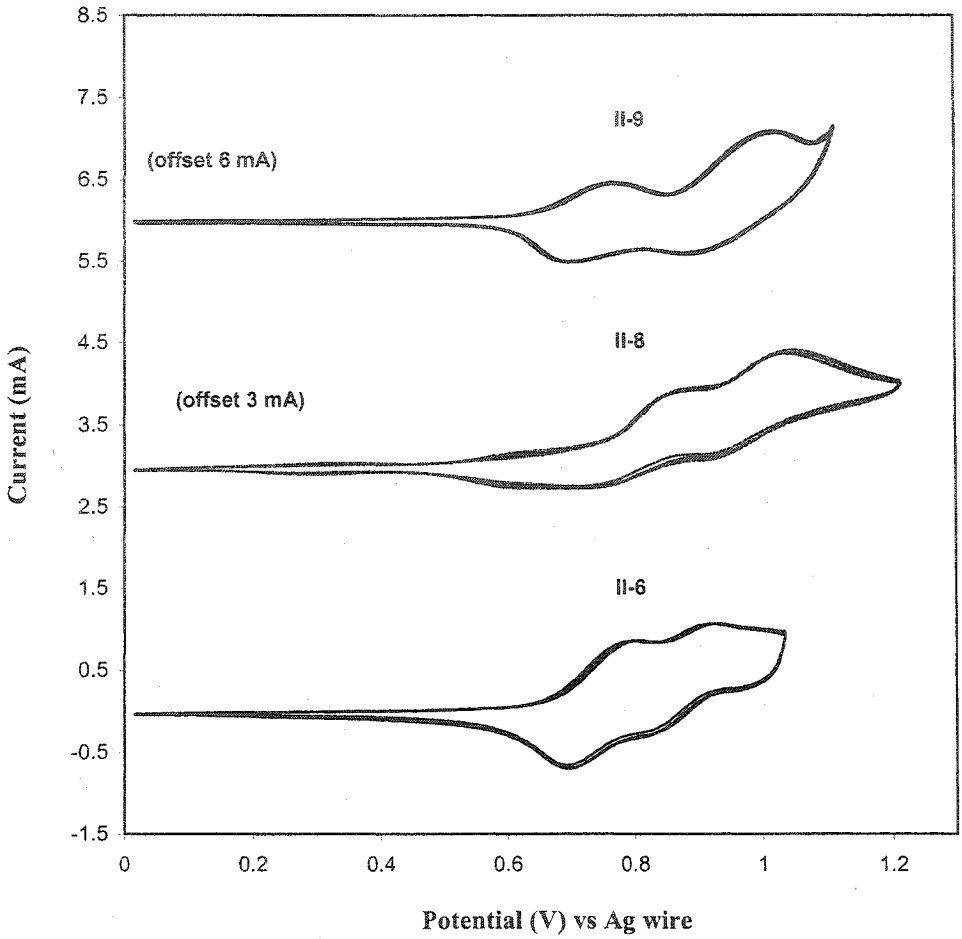

Figure 2.11. CVs at 100 mV/s in CH_2Cl_2 with 0.05 M TBAHP for compounds II-6, II-8 and II-9 under N_2. Five scans recorded.

The first reversible redox potentials of **II 1-9** are reported in **Table 2.6** and were used in the estimation of the energies of the HOMO levels of these species. This was done by taking the difference in potential between this oxidation and that of the Cp_2Fe/Cp_2Fe^+ couple. The relative potential for the ferrocene/ferrocenium couple was obtained by adding a small amount of Cp_2Fe to the CV samples of compounds **II 1-9** and carrying out a subsequent potential scan of both the Cp_2Fe and the diamine. The value of the Cp_2Fe HOMO energy used in these calculations was 4.80 eV.[24] An example of such a measurement on compounds **II-9** and TPD is shown in **Figure 2.12**. Schmidt *et al* used the same method to calculate the HOMO energy levels of some triamines, TPD and some substituted TPD analogues.[24] They measured the HOMO energy level of TPD using this technique as 5.13 eV.[24c] There has been some criticism of this method by Thompson *et al* for measuring the HOMO levels of diphenyl core diamines.[8] These workers observed shifts in the CV oxidation peak potentials before and after adding Cp_2Fe and concluded that this method was not satisfactory for these particular compounds. We also observed a shift in the potential positions of amine oxidation peaks before and after adding Cp_2Fe in the solution. However, the difference between the Cp_2Fe/Cp_2Fe^+ couple and the amine/amine$^+$ couple remained constant. For example, the potential (V) differences for compound **II-9**, three trials were 0.500, 0.510 and 0.505, and similar results were observed for all other diamines. Thus, the method can still be used to estimated HOMO energy levels for the diamine compounds reported in this chapter.

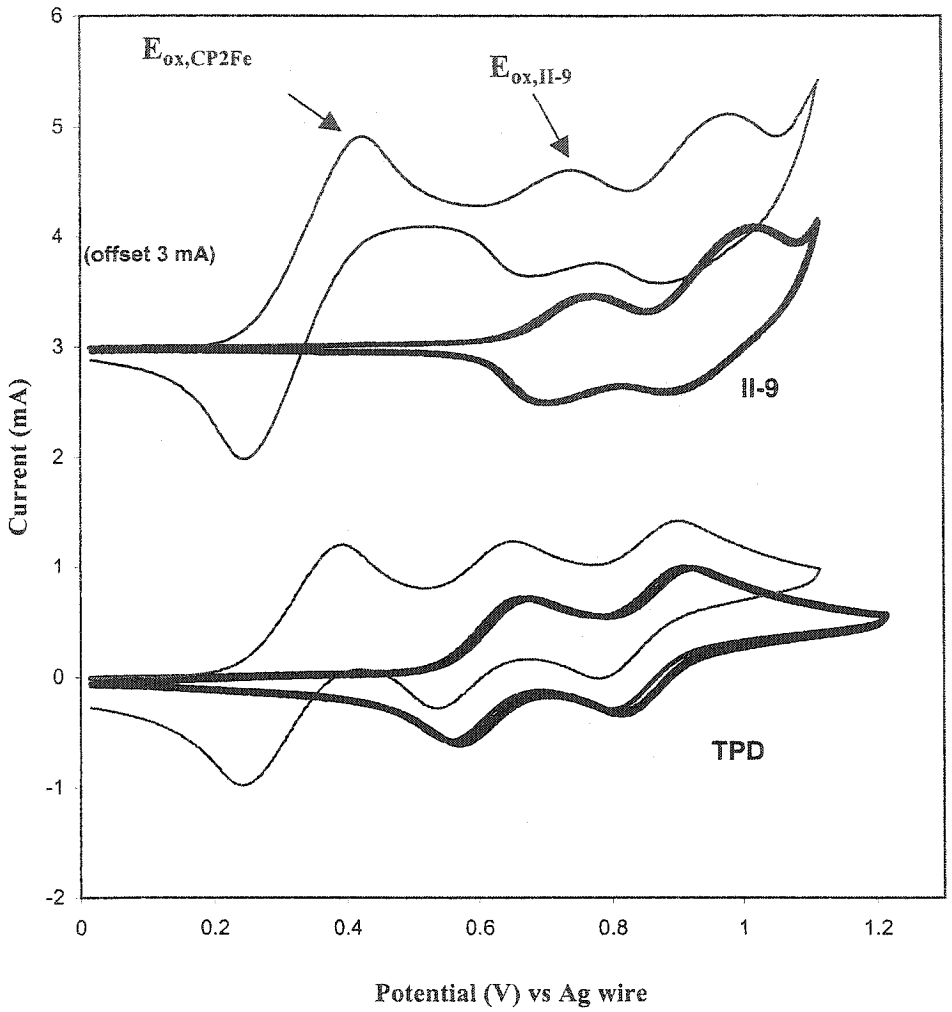

Figure 2.12 CVs at 100 mV/s in CH_2Cl_2 with 0.05 M TBAHP for TPD and compound II-9 under N_2. Bold line, before adding Cp_2Fe, five scan cycles recorded; Light line, after adding Cp_2Fe, first scan was recorded.

The LUMO energies for **II 1-9** could then be estimated by combining the data from the UV-vis measurements (HOMO/LUMO gap) and electrochemistry (HOMO energy). A summary of the data for HOMO and LUMO energy levels of compounds **II 1-9** are represented in **Table 2.6**. As seen in the table, the HOMO energy levels calculated for TPD through the method in this work was 5.08 eV, which is very close to Schmidt's result 5.13 eV.[24c]

From the data, it can be seen that **II-8** and **II-9** have the largest HOMO values. Meanwhile all *p*-substituted compounds have HOMO values varying between 0 – 0.07eV and LUMO values between 0 – 0.12 eV. The *meta*-substituted compound **II-8**, has the lowest LUMO values. The effect of substituents on the HOMO-LUMO energy levels should provide reasonable prediction on what compounds can be fabricated in an OLED to match the energy level requirements for charge transport between electrode and transporting layer or between the transporting layers that were deposited between conductors.

2.4 Conclusions

Routes have been developed to synthesize naphthalene core diamines as potential HT materials for OLEDs. Pd-based catalysts were found to be the most efficient system to faciliate the carbon-nitrogen bond formation. Amine substrates bearing electron withdrawing cyano substituents will not undergo C-N bond formation under Pd-catalyzed reaction.

A full thermal, photophysical and electrochemical characterization of naphthalene core diamines have been conducted in this work. The reported compounds exhibited superior thermal properties (a higher T_g than TPD). Emissions are extended into the blue to green color region for these compounds and the effects of substituents on the chromophores was demonstrated. Electrochemical method (CV) has been shown to be a good method to check the electrochemical stability and HOMO/LUMO energy levels of these naphthalene diamines. The design and synthesis of naphthalene core or other new diamine materials for practical application can be envisaged. Substituting different chromophores on diarylamines to suit the device fabrication requirements offers a possible way to adjust the T_g, HOMO/LUMO energy levels and electrochemical stabilities of these diamines. From the results, **II-6** and **II-7** that have highest T_g, among the new compounds, small HOMO values and reasonalbe electrochemical stability would be better HT material candidates for an OLED fabrication.

References for Chapter 2:

(1) Tang, C. W.; VanSlyke, S. A. *Appl. Phys. Lett.* **1987**, *51*, 913-915.

(2) Tang, C. W.; Vanslyke, S. A.; Chen, C. H. *J. Appl. Phys.* **1989**, *83*, 3610-3616.

(3) Shirota, Y.; Kobata, T.; Noma, N.; *Chem. Lett.* **1989**, 1145-1148.

(4) Shirota, Y. *J. Mater. Chem.* **2000**, *10*, 1-25.

(5) Hung, L. S.; Chen, C. H. *Mater. Sci. Engineer.* **2002**, *R 39*, 143-222.

(6) Adachi, C.; Nagai, K., Tamoto, N. *Appl. Phys. Lett.* **1995**, *66*, 2679-2681.

(7) Salbeck, J.; Yu, N.; Bauer, J.; Weissortel, F.; Bestgen, H. *Synth. Met.* **1997**, *91*, 209-215.

(8) Koene, B. E.; Loy, D. E.; Thompson, M. E. *Chem. Mater.* **1998**, *10*, 2235-2250.

(9) Thomas, K. R.; Lin, J. T.; Tao, Y. T.; Ko, C. W. *J. Am. Chem. Soc.* **2001**, *123*, 9404-9411.

(10) Yu, M. X.; Duan, J. P.; Lin, C. H.; Cheng, C. H.; Tao, Y. T. *Chem. Mater.* **2002**, 14, 3958-3963.

(11) Qiu, Y.; Qiao, J.; Gao, Y.; Zhang, D.; Wang, L. *Synth. Met.* **2002**, *129*, 25-28.

(12) Danel, K.; Huang, T. H.; Lin, J. T.; Tao, Y. T.; Chuen, C. H. *Chem. Mater.* **2002**, *14*, 3860-3865.

(13) Van Slyke, S. A.; Chen, C. H.; Tang, C. W. *Appl. Phys. Lett.* **1996**, *69*, 2160-2162.

(14) Thomas, A. W., Ley, S. V. *Angew. Chem. Int. Ed.* **2003**, *42*, 5400-5449. More references therein.

(15) Nelson, R. F.; Adams, R. N. *J. Am. Chem. Soc.* **1968**, *90*, 3925-3930.

(16) Stolka, M.; Janus, J. F.; Pai, D. M. *J. Phys. Chem.* **1984**, *88*, 4707-4714.

(17) Shirota, Y.; Okumoto, K.; Inada, H. *Synth. Met.* **2000**, *111*, 387-391.

(18) Selected papers from Buchwald's group. (a) Wolfe, J. P.; Wagaw, S.; Buchwald, S. L. *J. Am. Chem. Soc.* **1996**, *118*, 7215-7216. (b) Wagaw, S.; Buchwald, S. L. *J. Org. Chem.* **1996**, *61*, 7240-7241. (c) Old, D. W.; Wolfe, J. P.; Buchwald, S. L. *J. Am. Chem. Soc.* **1998**, *120*, 9722-9723. (d) Wolfe, J. P.; Wagaw, S.; Marcoux, J-F.; Buchwald, S. L. *Acc. Chem. Res.***1998**, *31*, 805-818. (e) Wolfe, J. P.; Buchwald, S. L. *J. Org. Chem.* **2000**, *65*, 1144-1157. (f) Wolfe, J. P.; Tomori, H.; Sadighi, J. P.; Yin, J.; Buchwald, S. L. *J. Org. Chem.* **2000**, *65*, 1158-1174.

(19) Selected papers from Hartwig's group. (a) Louie, J.; Hartwig, J. F. *Tetrahedron Lett.***1995**, *36*, 3609-3612. (b) Paul, F.; Patt, J.; Hartwig, J. F.; *J. Am. Chem. Soc.* **1994**, *116*, 5969-5970. (c) Hartwig, J. F.; Paul, F. *J. Am. Chem. Soc.* **1995**, *117*, 5373-5374. (e) Louie, J.; Hartwig, J. F. *J. Am. Chem. Soc.* **1997**, *119*, 11695-11696. (f) Hartwig, J. F.; Kawatsura, M.; Hauck, S. I.; Shaughnessy, K. H.; Alcazar-Roman, L. M. *J. Org. Chem.* **1999**, *64*, 5575-5580.

(20) Ferreira, I. C. F. R.; Queiroz, M. J. R. P.; Kirsch, G. *Tetrahedron* **2003**, *59*, 975-981.

(21) Bellmann, E.; Shaheen, S. E.; Thayumanavan, S.; Barlow, S.; Grubbs, R. H.; Marder, S. R.; Kippelen, B.; Peyghambarian. *Chem. Mater.* **1998**, *10*, 1668-1676.

(22) Watanabe, M; Yamamoto, T; Nishiyama, M. *Chem. Commun.* **2000**, 133.

(23) House, H. O.; Koepsell, D. G; Campbell, W. J. *J. Org. Chem.* **1972**, *37*, 1003.

(24) (a) Pommerehne, J.; Vestweber, H.; Guss, W.; Mahrt, R. F.; Bassler, H.; Porsch, M.; Daub, J. *Adv. Mater*, **1995**, *7*, 551-554. (b) Thelakkat, M.; Schmidt, H. W. *Adv.*

Mater. **1998**, *10*, 219-223. (c) Thelakkat, M.; Schmidt, H. W. *Polym. Adv. Technol.* **1998**, *9*, 429-442.

(25) Naito, K.; Miura, A. *J. Phys. Chem.* **1993**, *97*, 6240-6248.

(26) Cölle, M.; Gmeiner, J.; Milius, W.; Hillebrecht, H.; Brütting, W. *Adv. Funct. Mater.* **2003**, *13*, 108.

(27) Skoog, D. A.; Holler, F. J.; Nieman, T. A. *Principles of Instrumental Analysis*, Fifth edition, p 361.

(28) Stampfl, J.; Tasch, S.; Leising, G.; Scherf, U. *Synth. Met.* **1995**, *71*, 2125-2128.

(29) Fery-Forgues, S.; Lavabre, D. *J. Chem. Ed.* **1999**, *76*, 1260-1264.

Chapter 3

Synthesis and Characterization of C-4 Aryl and Diarylamine Substituted Tris(8-hydroxyquinoline)aluminum (III) (Alq_3) Derivatives

3.1 Introduction

3.1.1 Electron-transport materials based on Al chelates

Since Tang and VanSlyke first used the metal chelate complex tris(8-hydroxyquinoline)aluminum (III), so-called Alq_3, as an electron transport (ET) and emitting (EM) material to fabricate a double layer organic light-emitting devices (OLED) in 1987,[1] Alq_3 and Alq_3–type complexes have become the most widely used and studied materials for organic electroluminescent (EL) devices.[2] The reasons for the popularity of Alq_3 are due to its ease of synthesis and purification, its high thermal stability, its propensity to form morphologically stable thin film upon vacuum deposition, its high electron mobility, and its high quantum efficiency because of the ball-shape molecular geometry preventing the formation of exciplex. These features have made Alq_3 the benchmark in the field for comparison of other metal chelates.[2-6]

The typical emission wavelength of Alq_3 in CH_2Cl_2 solution is 515 nm, which makes Alq_3 a green emitting material.[2-7] In order to obtain a full color red-green-blue (RGB) display while maintaining the properties of Alq_3, synthetic efforts on Al chelates have been focused on Alq_3 analogues that exhibit bathochromic or hypsochromic shifted emissions.

One direct way to modify Alq_3 is modification of the bidentate 8-quinolinolato ligand (see **Figure 3.1**) of Alq_3 by adding functional groups that will change the electronic properties of the phenoxide or pyridyl ring portions of the ligand.[7] It has been demonstrated that the $\pi \rightarrow \pi^*$ electronic transitions in Alq_3 are localized on the 8-quinolinolato ligand.[3] Of the two rings that make up this ligand, the electron rich side is the phenoxide ring. The highest occupied molecular orbital (HOMO) is localized on this ring. On the other hand, the pyridyl ring portion of the ligand is electron deficient and site of the unfilled π^* lowest occupied molecular orbital (LUMO). There are two methods to obtain a bathochromic shift in Alq_3 analogues. One could prepare complexes with electron donating groups (EDG) on the phenoxide ring. These modifications should increase the HOMO energy. Alternatively, introducing an electron withdrawing groups (EWG) on the pyridyl ring should decrease the LUMO energy. A hypsochromic shift should be observed when the electronic properties of the substituents are reversed. These simple means to tune the emission color of Alq_3 has prompted many workers to prepare 8-quinolinols with different substituents on the two rings in order to obtain Alq_3 analogues. It is also anticipated that modification of the quinolinolate ligand could lead to changes in the thermal, photophysical and electrochemical properties compared to the parent compound.

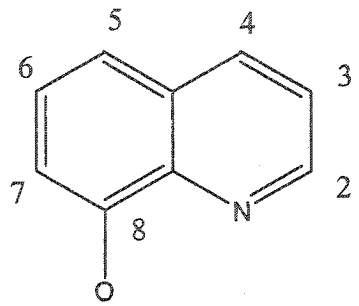

Figure 3.1 The quinolinolate ligand with carbon atom numbering scheme.

Modifications of the phenoxide ring component have been mainly focused on the preparation of C-5 substituted analogues, and examples represented by **3a-3e** are shown in **Figure 3.2**. Complexes with functional groups in the C-5 position include sulfonamide ($Al(qs)_3$) (**3a**),[7a] methyl-malononitrile ($AlCNq_3$) (**3b**),[7f] amidopyridine (**3c**),[7i] phenyl ($AlPq_3$) (**3d**)[7j] species. A more recently series of C-5 arylethynyl substituted Alq_3 (**3e**) analogues with full RGB emission have been reported.[7k]

Examples of Alq_3 analogues that have been modified on the pyridyl group are shown in **Figure 3.3** (**3f-3h**). Some examples such as $Alph_3$ (**3f**),[7b] C-2, 3 methylAlq_3 ($Alm_{23}q_3$) (**3g**),[7d] and C-4 methylAlq_3 (**3h**) (3 or $4Meq_3Al$)[7e] have been reported. It can be seen that complexes which possess C-4 modified ligands are relatively scarce.

Examples of other efforts to obtain Alq_3-type chelates are either to synthesize asymmetric Al chelates[8] by replacing one or two 8-quinolinol with new ligands, such as $AlMq_2OH$ (3i),[8a] monodentate phenolato (**3j**)[8b] or tridentate salicylidene-*o*-aminophenolato (**3k**)[8c] or to synthesize symmetric Al chelates but using new ligands (**3l**).[8d] The examples (**3i-3l**) have been given in **Figure 3.4** and more examples can been seen in reference 3.

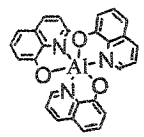

Alq_3

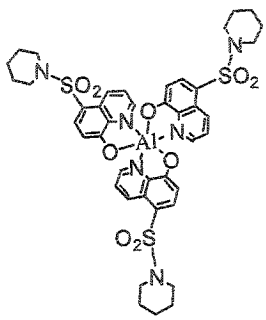

3a, $Al(qs)_3$

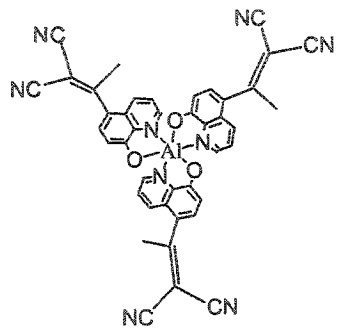

3b, $AlCNq_3$

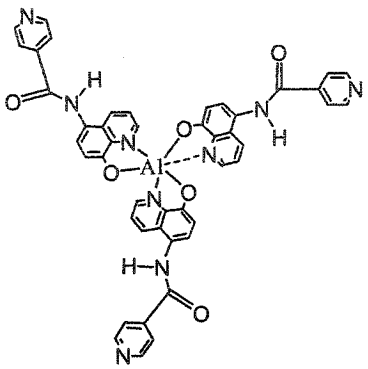

3c

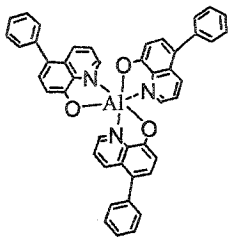

3d, $AlPq_3$

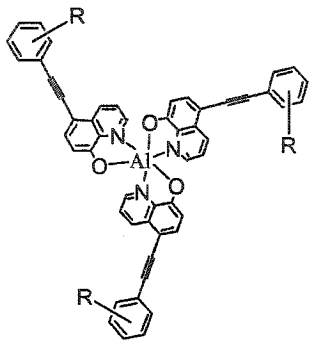

3e, R = EWG or EDG

Figure 3.2 Examples of C-5 substituted Alq_3 analogues.

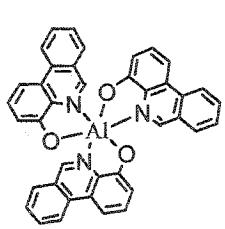

3f, $AlPh_3$

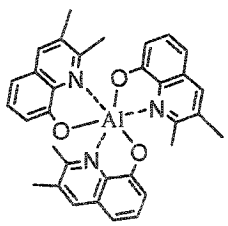

3g, $Alm_{23}q_3$

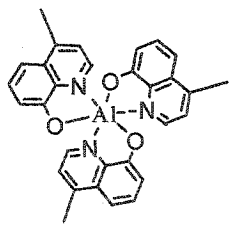

3h, $4MeAlq_3$

Figure 3.3 Examples of Alq_3 analogues modified at pyridyl ring.

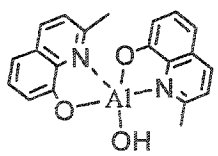

3i, $AlMq_2OH$

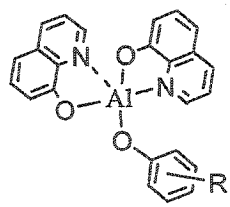

3j, $Alq_{2}p$

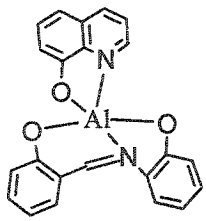

3k, Al(Saph-q)

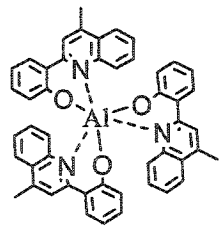

3l, $Al(mqp)_3$

Figure 3.4 Al chelates using ligands other than quinolato.

From the examples given above, it can be seen that although many Alq_3-type chelates have been synthesized and characterized, the basic bonding features of these species are the same. These stable Al chelate complexes exhibit five or six coordinate Al(III) centers with the Al coordination sphere dominated by Al-O and Al-N bonds.

One of the purposes of this chapter is to present our attempts to develop 8-quinolinolato-modified Alq_3 chelates, thus in the next section, a review of the ring modifications of quinolinato ligands and complex synthesis will be discussed.

3.1.2 Modification of 8-quinolinol and synthesis of chelates

Modifications of the 8-quinoline ligand system are generally at the C-5 on the phenoxide ring with a rather limited number of complexes with substituents at the C-4 position on the pyridyl ring. Positioning substituents at C-2 and/or C-7 will result unstable metal chelates due to the steric effects.[3] From the synthetic point of view, the phenoxide ring is an electron rich system, thus it is easier to carry out electrophilic substitution on this ring than on the pyridyl ring. For instance, 8-methoxy-5-quinolinesulfonic acid monohydrate, the key intermediate to synthesize $Al(qs)_3$ (see **3a** in **Figure 3.2)** was obtained through the direct electrophilic sulfonation of 8-methoxyquinoline.[7a] Other routes employed for the synthesis of C-5 modified quinilinolato ligands which were reported recently are presented in **Scheme 3.1**. $AlPq_3$[7j] and other reported C-5 aryl-substituted Alq_3 analogues[7k,7l] were synthesized through Suzuki or Sonogashira-Hagihara coupling reaction of hydroxy group protected 5-bromo-8-(hydroxy)quinoline with corresponding arylboronic acids or arylacetylenes. This starting material was obtained from the direct bromination of protected 8-(hydroxy)quinoline ring.

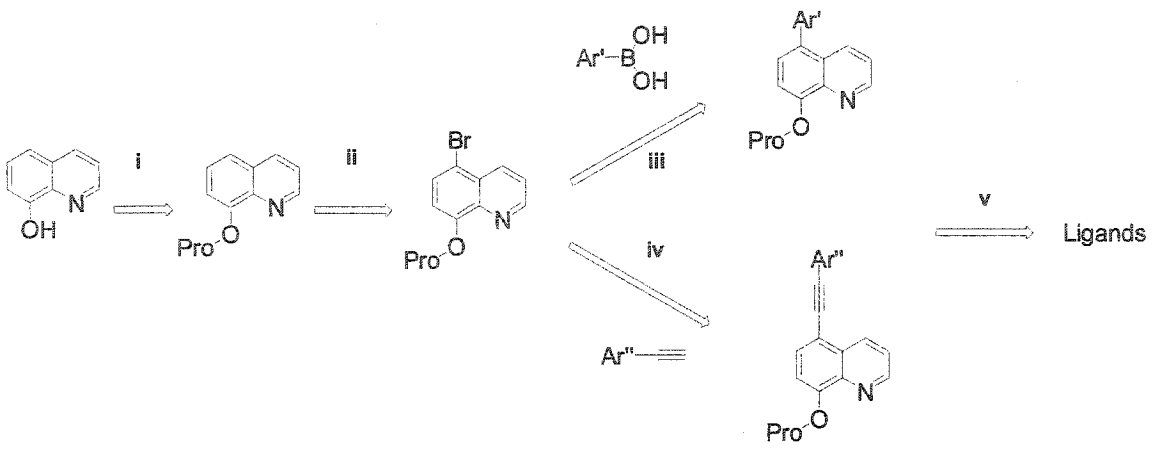

Conditions: (i) Bn-Cl, K_2CO_3, AcCN, reflux; (ii) NBS/CH_3Cl (iii) $Pd(TPP)_4/K_2CO_3$, toluene, TBACl, 90 °C; (iv) $Pd(TPP)_4$/CuI/DIPEA/THF; (v) 1,4-cyclohexadiene/Pd/C/isopropyl alcohol/reflux. Pro = benzyl (Bn) or di-*tert*-butyl dicarbonate (Boc). Simplified from refs 7k and 7l.

Scheme 3.1 Synthesis of C-5 aryl quinolinolate ligands

In comparison with the C-5 modified Alq_3 analogues, C-4 modified Alq_3 chelates are relatively rare. It is not unexpected that the electron-deficient pyridyl ring will be more difficult to modify by electrophilic substitutions such as bromination, and thus the further coupling reactions to add substituents are hard to achieve. The reported C-2,3 methyl substituted quinilinolato ligands was obtained from trans-2-methyl-2-butanol and *o*-aminophenol-hydrochloride,[7d] while methyl substituted quinolinolato ligands at C-3 or C-4 were synthesized through the condensation reactions between *o*-aminophenol and methylated unsaturated aldehyde or ketone.[7e] These methyl substituents cannot be added like C-5 modification and they were generally introduced into the synthetic scheme *en route* to the targeted ligands before the ring formation.

The synthesis of Al chelates such as Alq_3 can be achieved by mixing the 8-quinolinol ligands with $AlCl_3$ or trialkylaluminum such as $Al(Me)_3$ or $Al(CH_3CH_2)_3$[7,8] in 3:1 molar ratio. In some cases, tri(*iso*-propoxide)aluminum ($Al(OPr\text{-}i)_3$) can be employed in the sythesis of Al complexes.[3]

3.1.2 Objectives of this chapter

As the ET and EM materials in OLEDs, Alq_3 and Al-based metal chelates have exhibited many advantages outlined above. However, their properties and performance in quantum efficiency, mobility, bandgap and the ashing problem during vacuum sublimation (compound broken when being heated) offer room for improvement.[6] Scientists in this area have been actively engaged in developing Alq_3 analogues by structural modifications in order to improve their performance in an EL device. Among these Alq_3 analogues, C-5 modified Alq_3 compounds have been successfully synthesized and fabricated into OLEDs. Specifically, a recent paper reports a new class of C-5 aryl-modified Alq_3 with tunable emission from blue to red depending on the electronic properties of the aryl substituents.[71] These results significantly expand the role of Alq_3 based chelates in OLEDs. Based on the current development around Al based complexes, it is reasonable to believe that more work and progress in this area can be envisioned in the coming future.

In order to complement the reported efforts to tune the HOMO of Alq_3 species through C-5 modification of the quinolinolato ring, one of the aims in this chapter is to investigate the ability to tune the LUMO of these species through C-4 modification. The

C-4 methylated version of Alq_3, $(4Meq)_3Al$ (**3h**) has been reported by Forrest *et al* and found to have reduced intermolecular overlap of pyridyl rings, loss of hydrogen-bonding interactions which were attributed to increased steric factors. These changes were responsible for the poorer electron transport, compared to unsubstituted Alq_3, through the metal/organic interface region and resulted a higher operating potential in an OLED device.[7e] Therefore, in this chapter, aryl and diarylamine groups have been selected as the C-4 subsituents to optimize interaction of metal/organic interface region and the molecular packing of π-π systems between pyridyl rings. On the other hand, since the hole mobility in Alq_3 is much slower than electron mobility[6] and excess holes injected at the interface of the Alq_3 layer were demonstrated to be the main factor responsible for the degradation of Alq_3-based deviced.[2c] The C-4 functionalized materials presented herein may address this problem by lending increased stability of these materials to holes/oxidation. Furthermore, the amine functionalized materials will possess both electron and hole conduction sites within the same molecule this may allow better control of the location of electron and hole combination within the device and may also provide efficient electron/hole combination. In addition to the synthetic work, this chapter also reports the characterization of the thermal, photophysical and electrochemical properties of these C-4 modified Alq_3 analogues. A comparison of these important performance parameters with those of Alq_3 is necessary to assess their potential for future electroluminescent device application.

3.2 Experimental

General information. All reagents, *o*-anisidine, ethoxymethylenemalonic ester, diphenyl ether, cyclohexanone, phosphorous oxychloride, phosphorous oxybromide, dichlorobis(triphenylphosphine)palladium ($Pd(PPh_3)_3Cl_2$), diisobutylaluminum hydride, sodium ethoxide, boron tribromide (BBr_3, 1.0 M solution in hexane) and aluminun isopropoxide ($Al(OPr\text{-}i)_3$) were obtained from Aldrich Chemical Company and used without further purification. Tri-*t*-butylphosphine that was purchased from Strem Chemicals. Toluene, THF and Hexane were purified by passage through a column of activated alumina using an apparatus purchased from Anhydrous Engineering. Dichloromethane was freshly distilled over CaH_2 under nitrogen. 1,2-Dimethoxyenthane (DME) was stored in molecular sieves over 24 hours and used directly. Potassium phosphate was heated under vacuum at 150 °C overnight and then was pulverized and stored in drybox. Since sublimation of C-4 substituted Alq_3 analogues provided only trace products (< 5% yield), all compounds were purified by recrystallization from CH_3Cl/Hexane mixture at least five times before being submitted for elemental analysis. Simultaneous TGA (Thermal gravimetric analysis)/DSC of samples was measured using a simultaneous SDT 2960 from TA Instruments. Around 5 mg sample was subjected to heating program (10 °C/min) in an open ceramic pan under nitrogen atmosphere. Differential scanning calorimeter (DSC), UV-vis, steady-state fluorescence spectroscopy, cyclic voltammetry (CV) and other experimental and characterization information are described in **Section 2.2**. The detailed synthetic procedures are described in the following sections.

The Alq_3 used in this work was synthesized by the reaction of commercially available 8-hydroxyquinoline with $Al(OPr\text{-}i)_3$. The following characterization data was obtained for this compound: ^1H NMR ($CDCl_3$), δ (ppm): 6.84-7.51 (m, 13H), 8.17 (d, 2H), 8.26 (d, 1H), 8.79 (d, 1H), 8.83 (d, 1H). m/z 492 (M^+). HRMS (m/z): Calcd for $C_{27}H_{18}AlN_3O_3$ 459.1164, found 459.1149. ^1H NMR data is the same as reported.[2f]

General procedure for the synthesis of 4-halo-8-methoxyquinoline

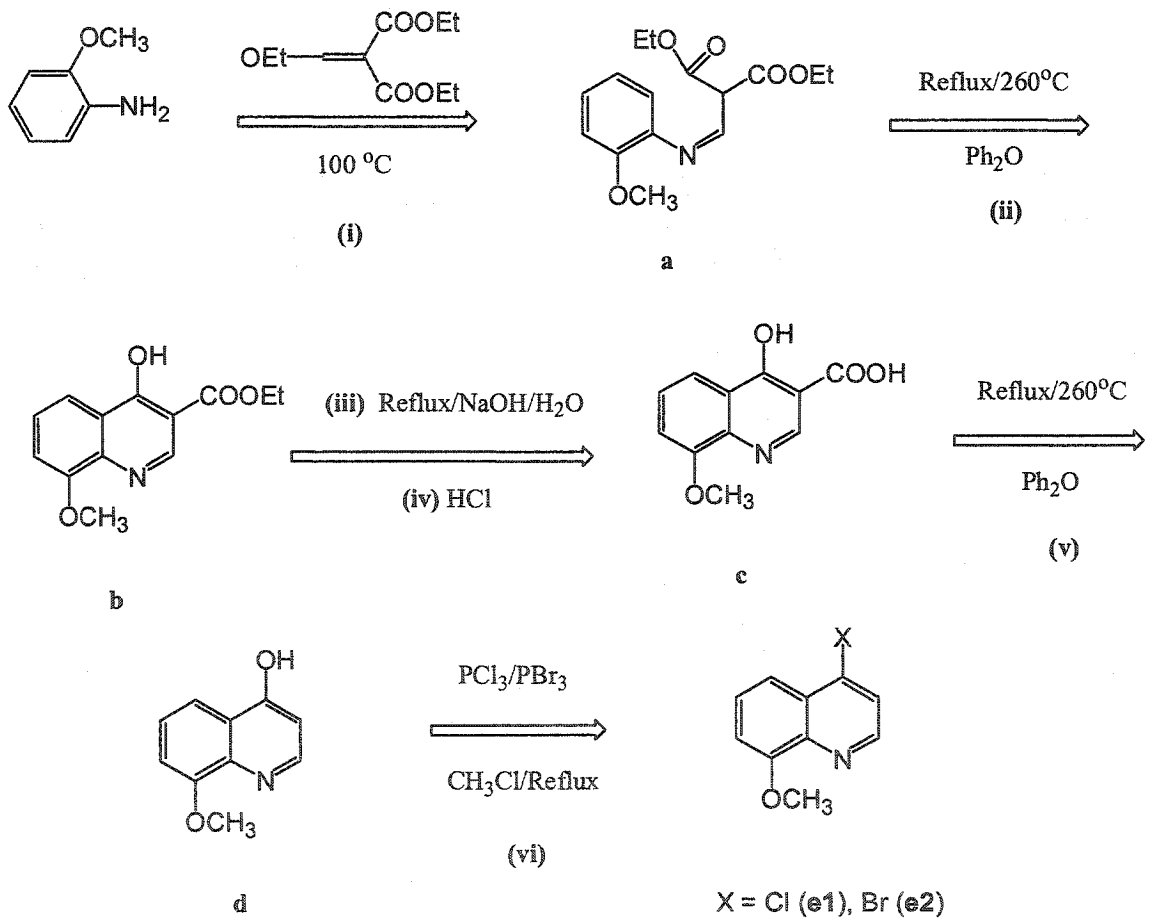

Scheme 3.2 Synthesis of 4-halogen-8-methoxyquinoline

The synthesis of C-4 halogenated 8-quinolinol was modified from two references[9, 10] and is summarized in **Scheme 3.2**. In a 500 ml two neck round-bottom flask fitted with magnetic stirrer, *o*-anisidine (123 g, 1mol) and ethoxymethylenemalonic ester (216 g, 1mol). The mixture was heated at 100°C for two hours during which time nitrogen was bubbled through the mixture to remove the ethanol produced during the reaction. The product **a** (*o*-Methoxyphenylaminomethylenemalonic Ester) was used directly for the step (ii). In another 1000 ml two neck flask fitted with condenser was added 500 ml diphenyl ether and dry nitrogen was passed though the solvent. The hot solution of **a** from step (i) was transferred into boiling diphenyl ether using a pipette. When the transfer was complete, heating was continued for additional one hour. On cooling, the crude product **b** (3-Carbethoxy-4-hydroxy-8-methoxyquinoline) was recrystallized from cyclohexanone. Compound **b** was then refluxed for three hours in 1000 ml sodium hydroxide solution (10%). On cooling, concentrated HCl was added until the solution became acidic to yield **c** (3-Carboxy-4-hydroxy-8-methoxyquinoline). Compound **c** was removed by filtration and dried in the oven at 120 °C for more than 5 hours. The dried **c** was pulverized and was heated at reflux in diphenyl ether for two hours to remove the carboxy group. On cooling, the crude **d** (4-Hydroxy-8-methoxyquinoline) was deposited and separated from diphenyl ether in two layers. Diphenyl ether was removed by pipette as much as possible and crude **d** was crystallized from water to yield a hydrate. The hydrate was heated in the oven between 135 – 140 °C to yield **d**. Compound **d** was dissolved in phosphorous oxychloride and refluxed for 5 hours under nitrogen to produce product **e1** (4-Chloro-8-methoxyquinoline). Alternatively **d** was refluxed with phosphorous oxybromide in chloroform under nitrogen to produce **e2** (4-Bromo-8-

methoxyquinoline). After workup, the crude **e1** and **e2** were purified by recrystallizing from ethanol giving the pure 4-halo-8-methoxyquinoline (halogen = Br or Cl).

General procedure for the synthesis of 4-aryl and diarylamine substituted 8-quinolinol

Scheme 3.3 summarizes the reaction processes employed the substituted 8-quinolinol ligands. Boronic acid, 4-methylboronic acid and 4-fluoroboronic acid were synthesized according to literature procedures.[11] 4-Methyldiphenylamine was obtained through Pd catalyzed coupling reaction between 4-bromotoluene and aniline[12] and the detailed procedure has been discussed in **Section 2.2**.

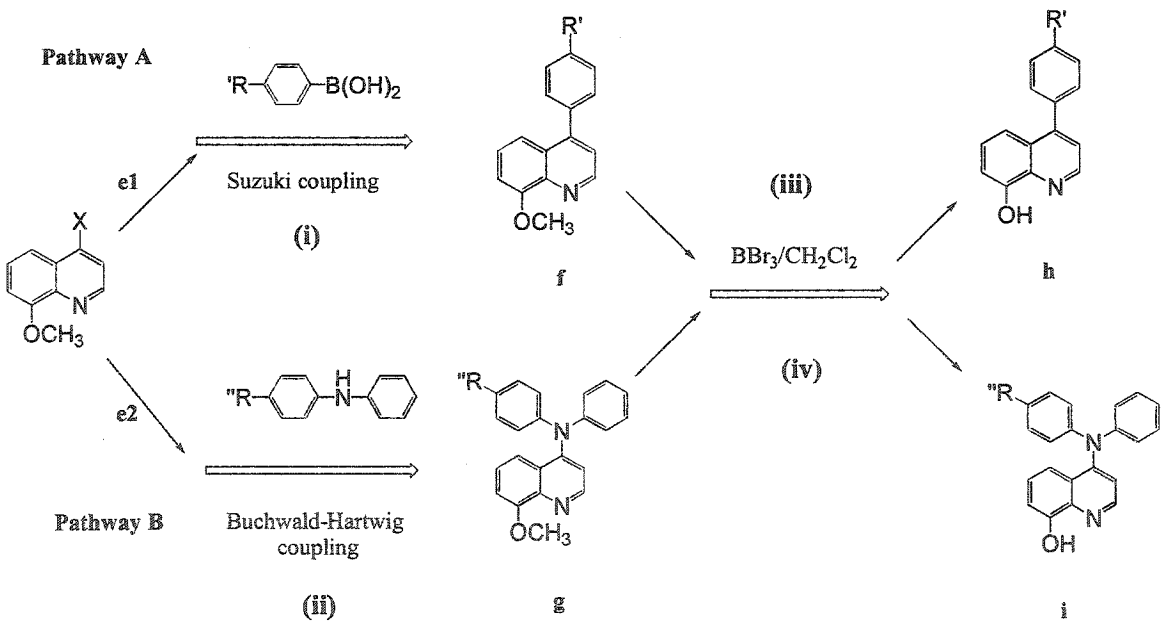

Scheme 3.3 Synthesis of 4-substituted 8-quinolinols

Pathway A

The synthetic procedures were modified from the reference.[8d] An oven-dried Schlenk flask was evacuated and backfilled with dry nitrogen. $Pd(PPh_3)_3Cl_2$ (0.14 g, 0.2mmol), DME (2.5 mL) and diisobutylaluminum hydride (DBA, 1.0 M in hexane, 0.4 mL, 0.4mmol) were added in consecutively. After mixture was stirred for 5 minutes, 4-chloro-8-hydroxyquinoline (**e1**, 0.965 g, 5mmol) in 5 mL DME was added to this mixture and the reaction was stirred for another 20 minutes at room temperature. 5 mmol of the appropriate boronic acid, 10 mmol sodium ethoxide (21 wt. % in denatured ethyl alcohol) were then added in successively and the resulting mixture was heated at reflux overnight under nitrogen. On cooling, the solution was filtered and concentrated by vacuum evaporation to give brown-black crude **f**, which was purified by column chromatography using $CHCl_3$ as the eluent. The products of these reactions (**f**) were obtained as yellow solids. Compounds **f** was dissolved in CH_2Cl_2 solvent and one equivalent of BBr_3 (1.0 M in hexane) solution was added in by syringe at –78 °C under nitrogen. The reaction mixture was then warmed to room temperature and stirred overnight. H_2O and $CHCl_3$ were then added and stirred for 30 minutes. The mixture was then neutralized with saturated $NaHCO_3$ and extracted with $CHCl_3$ for at least three times. The organic phases were combined and washed with brine and dried over magnesium sulfate. After the solvent was removed, the residue was purified by column chromatograph using $CHCl_3$. Yellow products **h** were obtained from these reactions. In Suzuki coupling reaction, if **e2** (4-bromo-8-hydroxyquinoline) was used, the yields are generally higher than using **e1**. For example 88% 8-methoxy-4-(4-fluorolphenyl)quinoline was obtained using **e2** instead of 70% when using **e1**.

8-Methoxy-4-phenylquinoline

Yield: 81%. ^{1}H NMR ($CDCl_3$), δ (ppm): 4.09 (s, 3H), 7.05 (d, 1H), 7.35-7.48 (m, 8H), 8.94 (d, 1H). ^{13}C NMR ($CDCl_3$), δ (ppm): 55.08, 107.44, 117.61, 121.99, 126.65, 127.82, 128.39, 128.49, 129.50, 138.17, 140.28, 148.54, 155.41, 159.03. m/z, 235 (M+). HRMS (m/z): Calcd for $C_{16}H_{13}NO$ 235.0997 found 235.1004.

8-Hydroxy-4-phenylquinoline

Yield: 90%. ^{1}H NMR ($CDCl_3$), δ (ppm): 7.19 (d, 1H), 7.35-7.48 (m, 8H), 8.78 (d, 1H). ^{13}C NMR ($CDCl_3$), δ (ppm): 109.78, 116.10, 122.07, 126.97, 127.66, 128.53, 128.56, 129.43, 137.87, 138.60, 147.23, 148.92, 152.33. m/z, 221 (M+). HRMS (m/z): Calcd for $C_{15}H_{11}NO$ 221.0841 found 221.0841.

8-Methoxy-4-(*p*-tolyl)quinoline

Yield: 88%. ^{1}H NMR ($CDCl_3$), δ (ppm): 2.44 (s, 3H), 4.10 (s, 3H), 7.04 (d, 1H). 7.24-7.50 (m, 7H), 8.92 (d, 1H). ^{13}C NMR ($CDCl_3$), δ (ppm): 20.32, 55.93, 107.30, 108.35, 115.33, 115.49, 117.45, 121.82, 126.47, 127.73, 129.07, 129.25, 129.66, 148.14, 155.23. m/z, 249 (M+). HRMS (m/z): Calcd for $C_{17}H_{15}NO$ 249.1154 found 249.1170.

8-Hydroxy-4-(*p*-tolyl)quinoline

Yield: 93%. ^{1}H NMR ($CDCl_3$), δ (ppm): 2.45 (s, 3H), 7.19 (d, 1H). 7.30-7.44 (m, 7H), 8.78 (d, 1H). ^{13}C NMR ($CDCl_3$), δ (ppm): 21.31, 109.83, 116.18, 122.00, 127.09, 127.60, 129.28, 129.36, 134.91, 138.46, 138.57, 147.12, 149.16, 152.26. m/z, 235 (M+). HRMS (m/z): Calcd for $C_{16}H_{13}NO$ 235.0997 found 235.1022.

8-Methoxy-4-(4-fluorophenyl)quinoline

Yield: 70%. ^{1}H NMR ($CDCl_3$), δ (ppm): 4.10 (s, 3H), 7.07 (d, 1H). 7.15-7.22 (m, 2H), 7.31 (d, 1H), 7.37-7.47 (m, 4H), 8.93 (d, 1H). ^{13}C NMR ($CDCl_3$), δ (ppm): 56.08, 107.43, 115.56 (J_{C-F}, 21.6 Hz), 117.27, 122.03, 126.77, 127.77, 131.21 (J_{C-F}, 8.2 Hz), 134.14, 140.48, 147.33, 148.61, 155.60, 162.82 (J_{C-F}, 247.7 Hz), m/z, 253 (M+). HRMS (m/z): Calcd for $C_{16}H_{12}NOF$ 253.0903 found 253.0911.

8-Hydroxy-4-(4-fluorophenyl)quinoline

Yield: 90%. ^{1}H NMR ($CDCl_3$), δ (ppm): 6.93-7.20 (m, 3H). 7.32-7.59 (m, 5H), 8.78 (d, 1H), ^{13}C NMR ($CDCl_3$), δ (ppm): 109.86, 115.49, 115.78, 122.08, 126.93, 127.80, 131.14 (J_{C-F}, 8.2 Hz), 133.82 (J_{C-F}, 3.3 Hz), 138.68, 147.27, 147.71, 152.44, 162.92 (J_{C-F}, 248.3 Hz), m/z, 39 (M+). HRMS (m/z): Calcd for $C_{15}H_{10}NOF$ 239.0746 found 239.0755.

Pathway B

The synthetic procedures for pathway B were modified from the literature methods.[8, 13] An oven-dried Schlenk flask was evacuated and backfilled with dry nitrogen. 1-2 mol% $Pd(OAc)_2$/P(*t*-Bu)$_3$ (1:1) in toluene was added and stirred at room temperature for approximately 30 min until the red solution became green-yellowish. Then **e2**, diphenylamine (or 4-methyldiphenylamine) and K_3PO_4 in molar ration of 1: 1.2:1.4 were added successively. The resulting mixture was heated at 110°C for two days in a sealed Schlenk flask. On cooling, the mixture was filtered and concentrated, and purified by column chromatography using CH_3Cl as the eluent. Compounds **g** were then obtained. Compounds **i** were obtained by methoxy deprotection as described for **pathway A**. When

using column chromatography to purify the compounds i, 5% triethylamine CH_3Cl was used as the eluent.

8-Methoxy-4-(diphenylamino)quinoline

Yield: 86%. ^1H NMR ($CDCl_3$), δ (ppm): 4.05 (s, 3H), 6.96-7.03 (m, 7H), 7.19-7.27 (m, 7H), 8.75 (d, 1H). ^{13}C NMR ($CDCl_3$), δ (ppm): 55.97, 107.28, 116.56, 119.00, 123.51, 123.88, 125.88, 126.06, 129.36, 142.33, 147.98, 149.65, 152.27, 155.68. m/z, 326 (M+). HRMS (m/z): Calcd for $C_{22}H_{18}N_2O$ 326.1419 found 326.1408.

8-Hydroxy-4-(diphenylamino)quinoline

Yield: 82%. ^1H NMR ($CDCl_3$), δ (ppm): 6.96-7.30 (m, 14H), 8.56 (d, 1H). ^{13}C NMR ($CDCl_3$), δ (ppm): 109.45, 115.30, 118.24, 123.85, 124.29, 124.73, 126.60, 129.42, 140.50, 147.90, 148.13, 152.50, 152.65. m/z, 312 (M+). HRMS (m/z): Calcd for $C_{21}H_{16}N_2O$ 312.1263 found 312.1261.

8-Methoxy-4-(*p*-tolylphenylamino)quinoline

Yield: 88%. ^1H NMR ($CDCl_3$), δ (ppm): 2.29 (s, 3H), 4.05 (s, 3H), 6.88-7.07 (m, 9H), 7.17-7.27 (m, 5H), 8.73 (d, 1H). ^{13}C NMR ($CDCl_3$), δ (ppm): 20.83, 55.98, 107.23, 116.69, 118.56 (one C hidden, seen from $^1H^{13}C$ HMQC), 123.20, 123.53, 124.42, 125.72, 125.92, 129.29, 130.06, 133.57, 145.50, 148.26, 149.58, 152.49, 155.63. m/z, 340 (M+). HRMS (m/z): Calcd for $C_{23}H_{20}N_2O$ 340.1576 found 340.1570.

8-Hydroxy-4-(*p*-tolylphenylamino)quinoline

Yield: 90%. ^{1}H NMR ($CDCl_3$), δ (ppm): 2.31 (s, 3H), 6.88-7.26 (m, 8H), 8.56 (d, 1H). ^{13}C NMR ($CDCl_3$), δ (ppm): 20.08, 109.62, 115.46, 117.56, 123.69, 124.06, 124.79, 126.47, 128.77, 129.37, 130.14, 130.86, 134.02, 145.36, 147.79, 148.08, 152.34, 153.03. m/z, 326 (M+). HRMS (m/z): Calcd for $C_{22}H_{18}N_2O$ 326.1419 found 326.1404.

General procedure for the synthesis Alq_3 analogues

C-4 phenyl substituted Alq_3 derivatives are abbreviated as $PAlq_3$ derivatives while C-4 diarylamine substituted are abbreviated as $DAlq_3$ derivatives. The general procedures for the synthesis of $PAlq_3$ and $DAlq_3$ are similar and are summarized in **Scheme 3.4.** The syntheses of these compounds deviate only in the application of ligands **h** or ligands **i** (**Scheme 3.3**).

In a dried Schlenk flask, ligands of type **h** or **i** and Al(OPr-*i*)$_3$ in a molar ratio of 3:1 were dissolved in THF solvent, and the mixtures were heated at 80 °C under nitrogen for 5 hours. In the first half hour, yellow clear solution became yellow cloudy indicating the formation of Al chelates. The yellow precipitate was filtered and washed with cooled ethyl acetate solvent, and then was recrystallized from CH_3Cl/Hexane.

Aluminum (III) tris(4-phenyl-8-quinolinolate) (III-1)

Yield: 70%. ^{1}H NMR (CDCl3), δ (ppm): 7.03-7.21 (m, 16H), 7.28 (d, 1H), 7.36-7.55 (m, 11H), 8.89 (d, 1H), 8.97 (d, 1H). m/z (ESI), 688 (+ H^+). Anal. Calcd for $C_{45}H_{30}AlN_3O_3$: C, 78.59; H, 4.40; N, 6.11; O, 6.98. Found C, 78.92; H, 3.99; N, 5.83; O, 6.98.

Aluminum (III) tris[4-(4-fluorophenyl)-8-quinolinolate] (III-2)

Yield: 75%. ^{1}H NMR ($CDCl_3$), δ (ppm): 7.08-7.56 (m, 25H), 8.88 (d, 1H), 8.95 (d, 1H). m/z (ESI), 742 (M+ H^+). Anal. Calcd for $C_{45}H_{27}AlF_3N_3O_3$: C, 72.87; H, 3.67; N, 5.67; O, 6.48. Found C, 72.53; H, 3.46; N, 5.40; O, 6.02.

Aluminum (III) tris[4-(*p*-tolyl)-8-quinolinolate] (III-3)

Yield: 65%. ^{1}H NMR ($CDCl_3$), δ (ppm): 2.42 (s, 9H), 7.01-7.59 (m, 25H), 8.85 (d, 1H), 8.93 (d, 1H). m/z (ESI), 730 (+ H^+). Anal. Calcd for $C_{48}H_{36}AlN_3O_3$: C, 79.00; H, 4.97; N, 5.76. Found C, 79.41; H, 4.58; N, 5.35.

Aluminum (III) tris[4-(diphenylamino)-8-quinolinolate] (III-4)

Yield: 60%. ^{1}H NMR ($CDCl_3$), δ (ppm): 6.47-7.33 (m, 43H), 8.55 (d, 1H), 8.58 (d, 1H). m/z (ESI), 961 (M+ H^+). Anal. Calcd for $C_{63}H_{45}AlN_6O_3$: C, 78.73; H, 4.72; N, 8.74; O, 4.99. Found C, 78.75; H, 4.35; N, 8.79; O, 4.12.

Aluminum (III) tris[4-(*p*-tolylphenylamino)-8-quinolinolate] (III-5)

Yield: 70%. ^{1}H NMR ($CDCl_3$), δ (ppm): 2.31 (s, 9H), 6.46-7.28 (m, 40H), 8.51 (d, 1H), 8.55 (d, 1H). m/z (ESI), 1003 (+ H^+). Anal. Calcd for $C_{66}H_{51}AlN_6O_3$: C, 79.02; H, 5.12; N, 8.38; O, 4.78. Found C, 79.16; H, 5.13; N, 8.19; O, 3.85.

3.3 Results and discussion

3.3.1 Synthesis of C-4 Alq_3 derivatives

The synthetic routes for the formation of C-4 substituted 8-hydroxylquinoline ligands is summarized in **Schemes 3.2** and **3.3**. The first step in the synthesis relied on a modification of the literature to generate 4-bromo-8-methoxyquinolines and 4-chloro-8-methoxyquinolines. These two methyl-protected species were then converted to C-4 aryl substituted or C-4 amine substituted 8-quinolinol precursors using Suzuki and Buchwald-Hartwig conditions respectively. Deprotection of these compounds yielded C-4 substituted 8-hydroxyquinolines that have aryl groups (3 compounds symbolized by **h**) or diarlyamine groups (2 compounds symbolized by **i**).

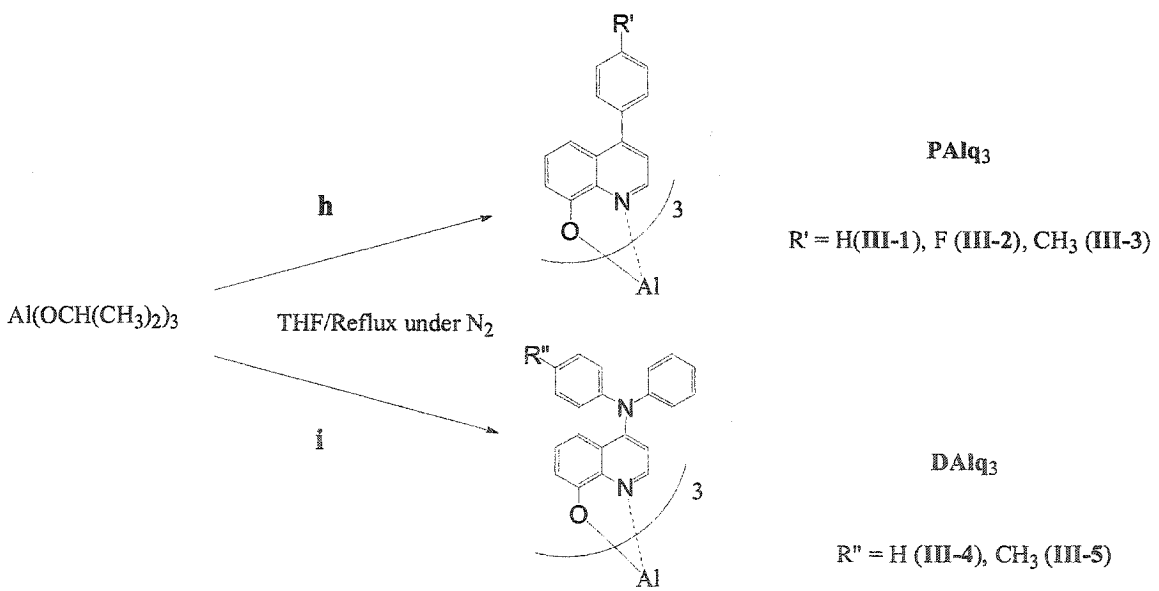

Scheme 3.4 Synthetic routes to Al complexes of the C-4 modified 8-quinolinolato ligands

Formation of the tris(chelate) Al species was readily achieved by reactions of compounds **h** and **i** with Al(OPr-*i*)$_3$ according to the procedure summarized in **Scheme 3.4**. These species were isolated in good yield and fully characterized by ^{1}H and ^{13}C NMR spectroscopy.

3.3.2 Geometric structure of Alq_3 analogues and ^{1}H Spectrum

Two geometric isomers of Alq_3 have been found.[2f] In the facial isomer the three hydroyquinolinato ligands are equivalent by symmetry while the meridianal isomer possesses three distinct ligands. (see **Figure 3.5**). At room temperature, the meridianal isomer is the more stable isomeric form for Alq_3. This leads to a distinct signature in the ^{1}H NMR spectra for Alq_3.[2e] By using a, b and c to represent the three distinct bidentate ligands for mer-Alq_3, one can observe the characteristic H2a, H2b, H4a and H4b,c peaks that appear at high field (>8 ppm) in the ^{1}H NMR spectra. The remaining proton peaks belonging to the quinoline ring (including H2c) appear at lower field (between 7-7.6 ppm) and are well separated from these peaks. In the case of C-5 substituted Alq_3 analogues,[7k, 7l] the ^{1}H NMR spectra display a similar pattern for the H2a, H2b, H4a and H4b,c peaks. The ^{1}H NMR spectra for C-4 substituted Alq_3 analogues obtained in this work no longer possess the H4 protons and, therefore, show only H2a, H2b resonances at higher field. Again the remaining aromatic resonances are overlapped at relative lower field. These results are all consistent with a meridianal structure for all of the C-4 substituted Alq_3 analogues presented in this thesis.

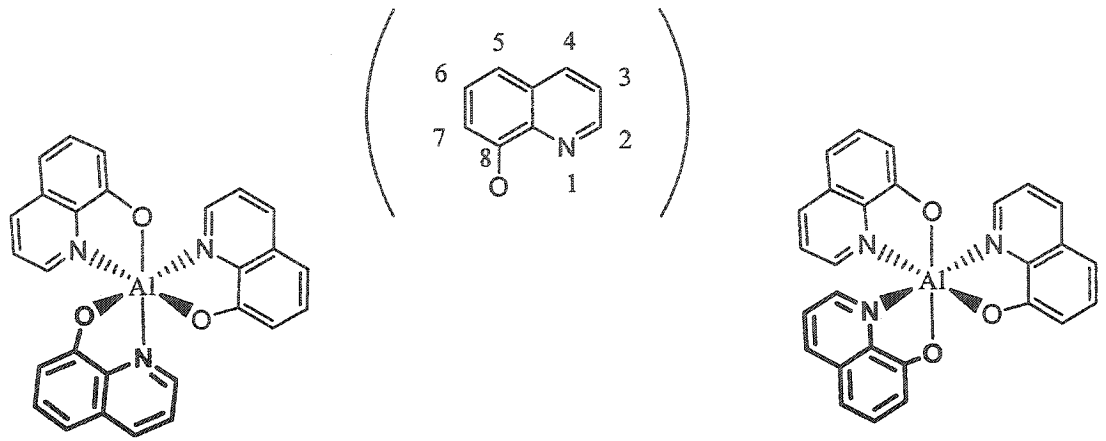

Facial

Meridianal

Figure 3.5 Geometric structure of Alq_3

3.3.3 Thermal properties

The ability to form an amorphous state with high thermal stability is vital for practical application of a compound in fabricating OLEDs was discussed in **section 1.3** and **section 2.4.1**. With these features in mind the thermal analysis, TGA and DSC, of C-4 substituted Alq_3 were examined. The investigation was carried out under the same experimental conditions with Alq_3 in order to make a direct comparison of these new compounds with this benchmark species.

In this work, the thermal information such as melting point (T_m) and gravimetric loss (decomposition temperature (T_d)) as a function of temperature were carried out using simultaneous TGA/DSC measurement at the heating rate of 10°C/min. The thermal properties of these compounds were further examined with DSC measurement in which

the compounds were sealed in aluminum pans, which will avoid the error caused by the weight loss due to sublimation of the samples in an open ceramic pan in simultaneous TGA/DSC measurement and thus provide more accurate T_m values. The type of measurement provides important information on thermal stability and formation of amorphous phases for these C-4 modified Alq_3 analogues and can also shed light on the ability of a material to form a glassy amorphous phase by allowing the observation of T_g and crystallization (T_c) before melting. The results of thermal data for all the new compounds (**III 1-5**) with Alq_3 and $4Meq_3Al$[7e] are presented in **Table 3.1** and shown in **Figures 3.6 - 3.11.**

Entry	C-4 substituted Alq_3 derivatives	T_m (°C)	T_g (°C)	15% wt. loss temp (°C)	Max. wt. loss temp (°C)
1	Alq_3	416	175	402	464
2	$HPAlq_3$, R'=H (**III-1**)	336	207	460	534
3	$FPAlq_3$, R'=F (**III-2**)	NO	206	429	504
4	$MePAlq_3$, R'=CH_3 (**III-3**)	NO	207	472	544
5	$HDAlq_3$, R_1=R_2=H (**III-4**)	NO	210	479	549
6	$MeDAlq_3$, R_1=CH_3, R_2=H (**III-5**)	NO	218	499	525
7*	$4Meq_3Al$	345	194	NA	494

NA, not available. NO, not observed; * from reference [7e].

Table 3.1 Thermal (TGA and DSC) data for $PAlq_3$ and $DAlq_3$ derivatives.

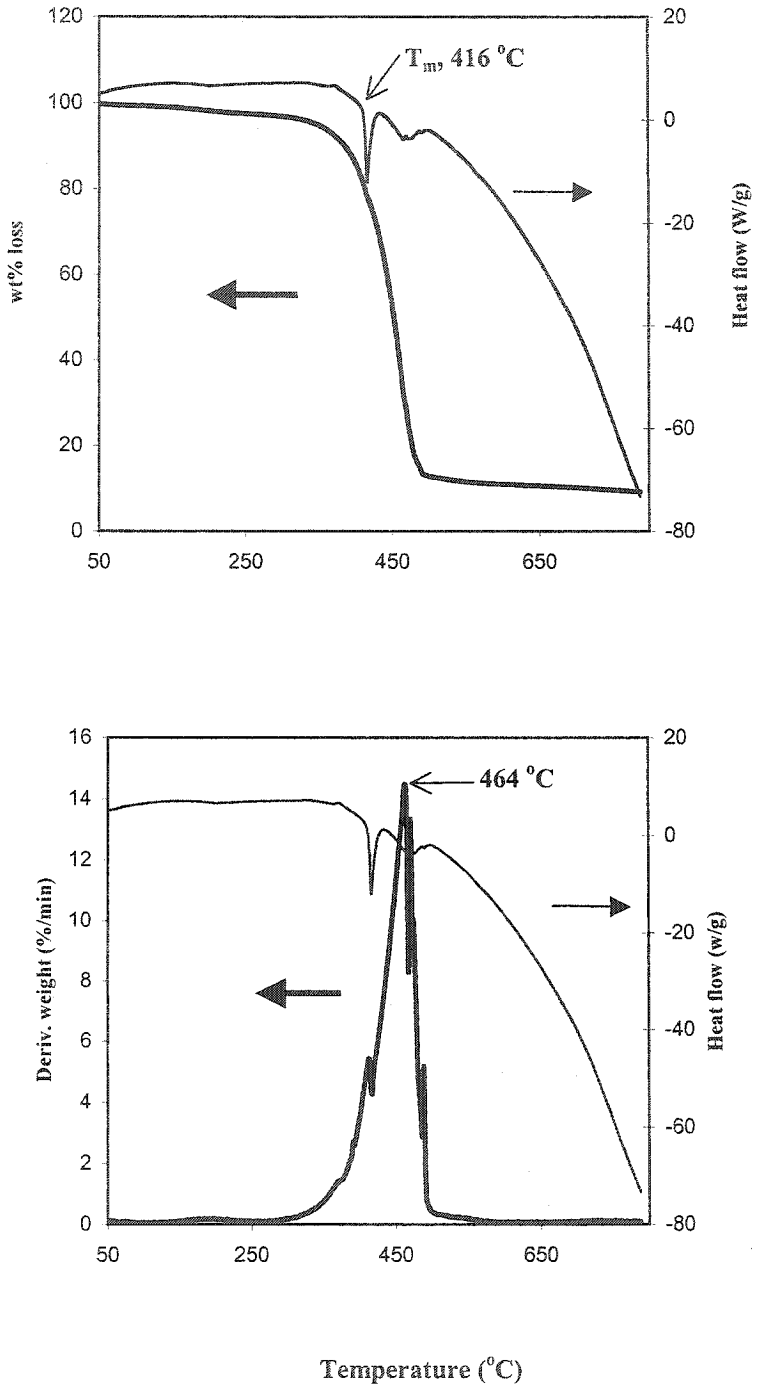

Figure 3.6 TGA and DTA traces of Alq_3 at heating rate of 10 °C/min.

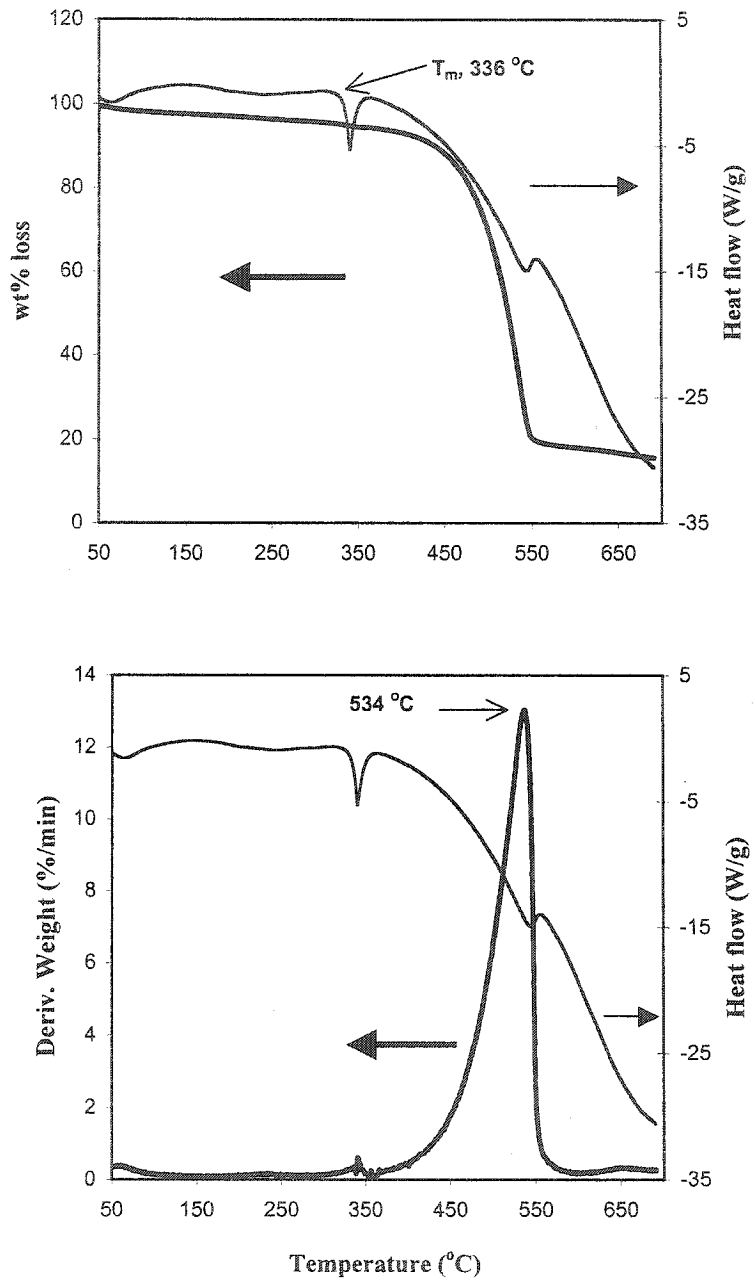

Figure 3.7 TGA and DTA traces of $HPAlq_3$ (III-1) at heating rate of 10 °C/min.

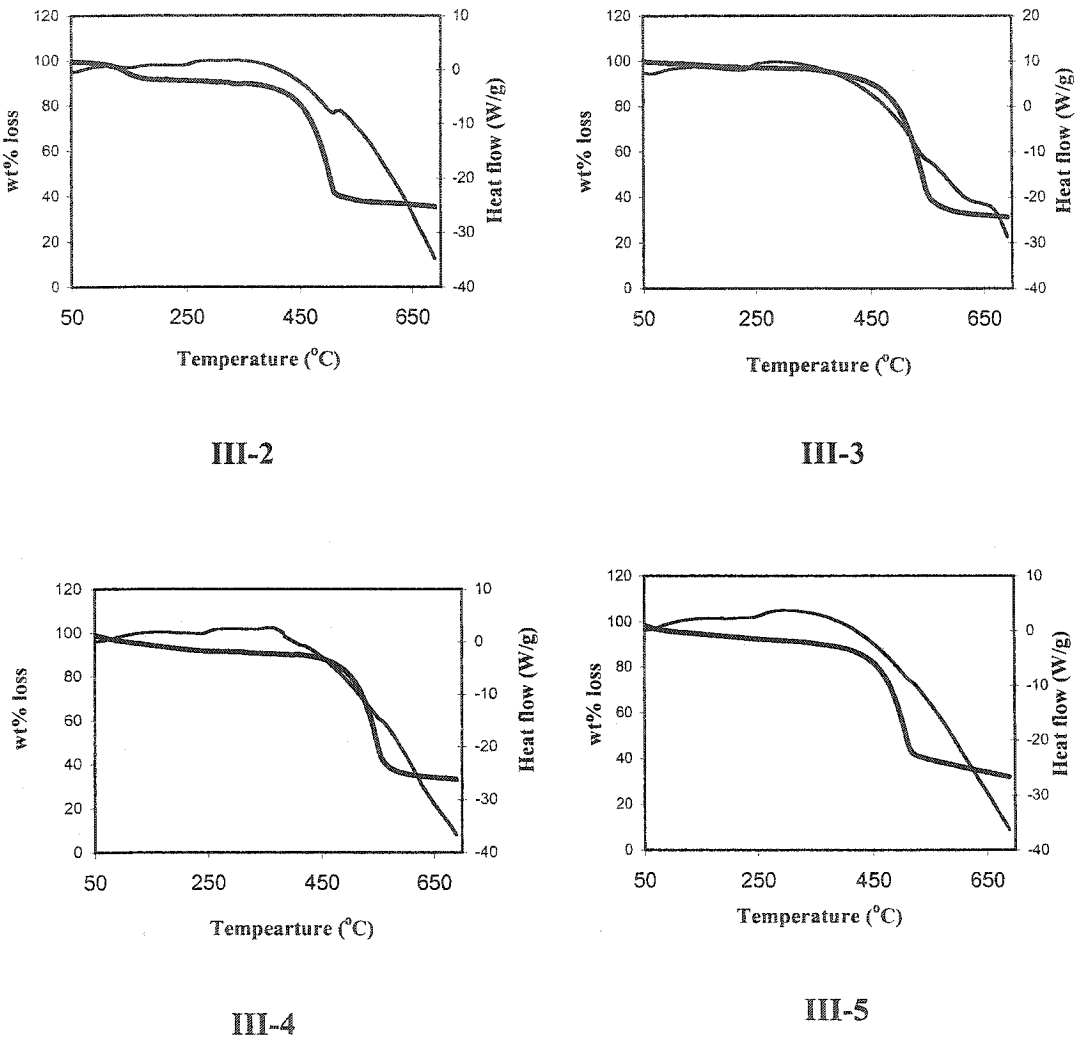

Figure 3.8 TGA traces for compounds III 2-5 at heating rate of 10 °C/min

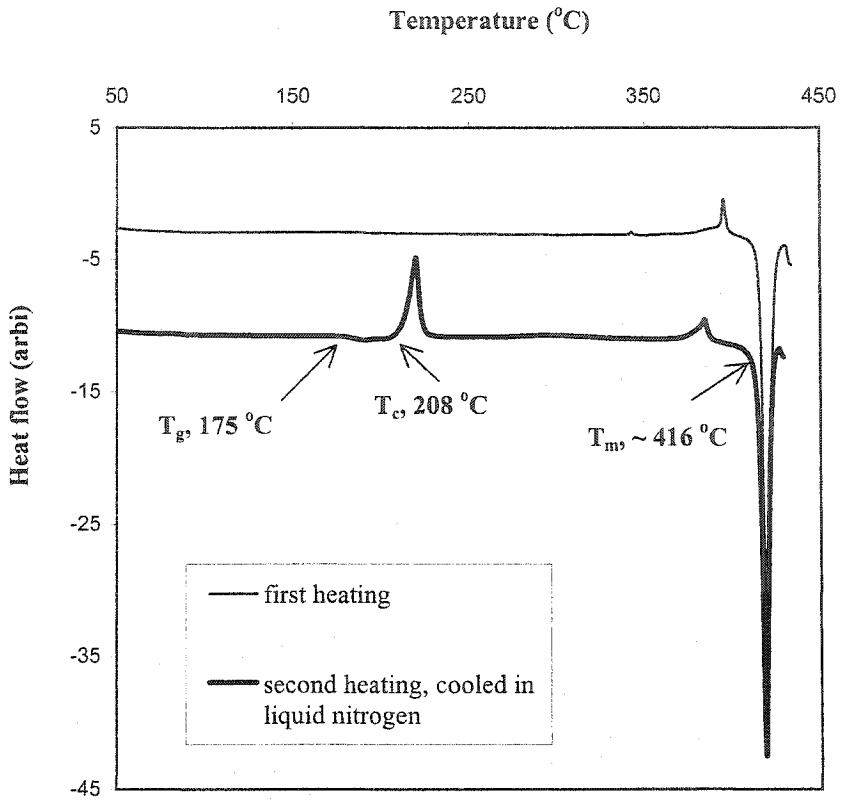

Figure 3.9 DSC traces of Alq_3 at heating rate of 20 °C/min.

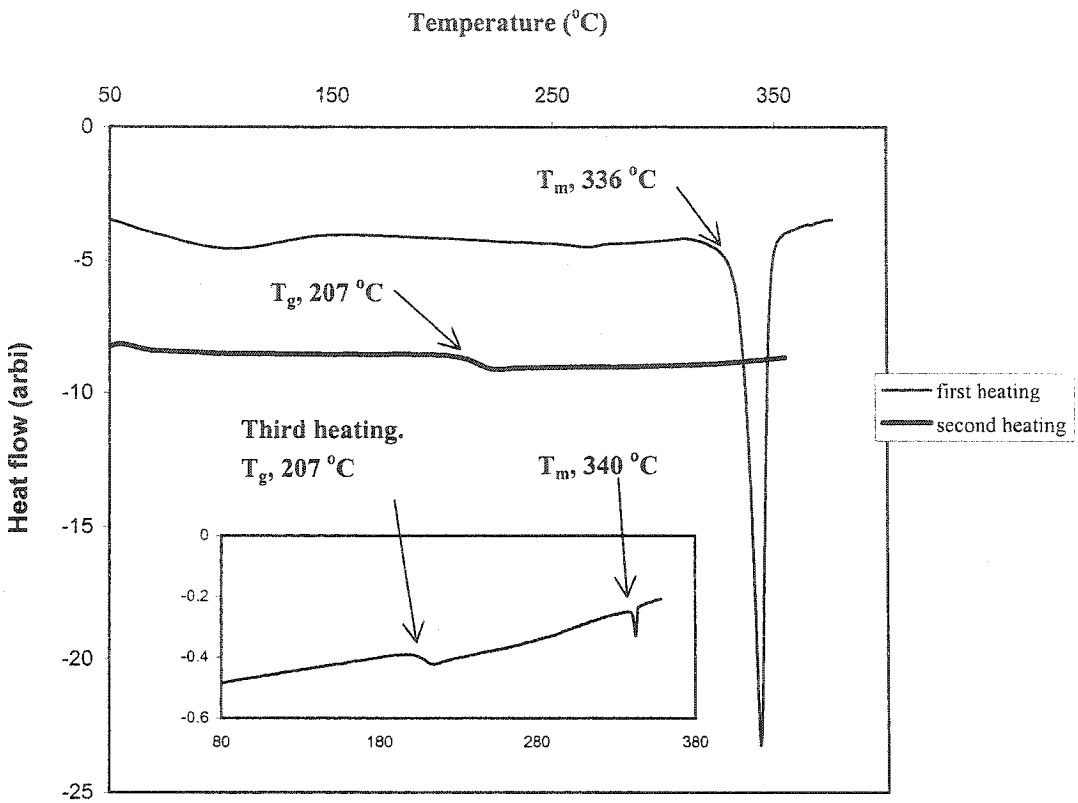

Figure 3.10 DSC traces of $HPAlq_3$ (III-1) at heating rate of 20 °C/min (Outside) and 2 °C/min (inside).

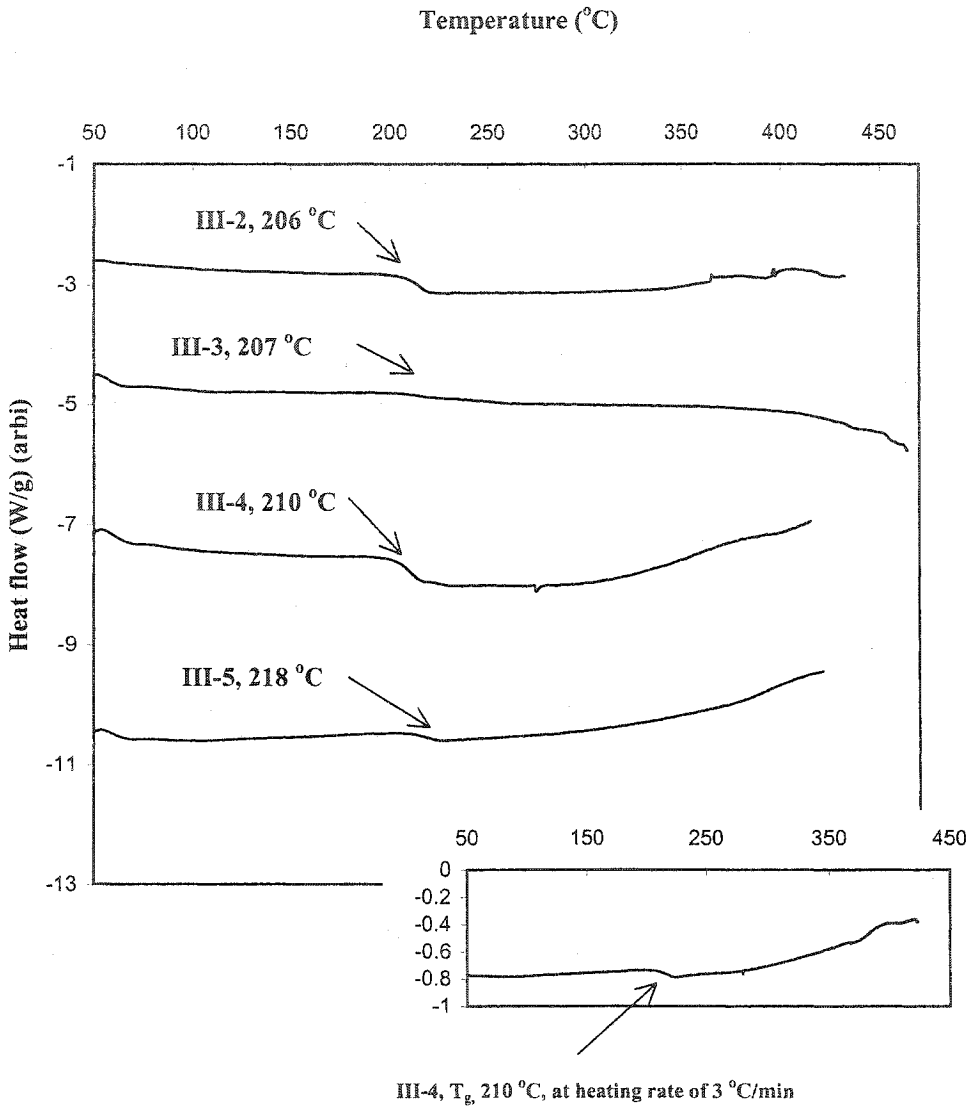

Figure 3.11 T_gs of compounds III 2-5 obtained from the second heating cycle of DSC traces at heating rate of 20 °C/min. Outside window, DSC trace of III-4 at heating rate of 3 °C/min.

One of the first things to note from this data is that only Alq_3 (**Figure 3.6**) and the simplest C-4 substituted analogue of $PAlq_3$ (**III-1**, $HPAlq_3$, R = H, **Figure 3.7**) display clean melting behavior in the TGA/DSC measurements. $HPAlq_{3s}$ shows a lower T_m value (336°C) than the parent Alq_3 which melts at 416°C. The other compounds (**III 2-5**) did not show T_m values from TGA measurements (**Figure 3.8**). The formation of an amorphous phase was anticipated if the melted samples were cooled to room temperature from the melt. The DSC measurements allowed us to observe this phenomenon by first heating the sample to melting, letting it cool to room temperature and then carrying out a second heating cycle. This two-cycle process is shown in **Figures 3.9** and **3.10** for Alq_3 and $HPAlq_3$, respectively. In both cases the first heating cycle showed a characteristic endotherm for melting. In addition, Alq_3 shows a small exothermic phase transition just before melting, which has been ascribed to a polymorph transition.[2f,7e] After these samples were cooled to room temperature, a second heating cycle was commenced. Both Alq_3 and $HPAlq_3$ showed broad thermal events (175 °C and 207 °C respectively) indicative of T_g. For Alq_3, the transition from the amorphous phase to the crystalline phase (T_c) as an exotherm at 208 °C was also observed. After this transition has occurred, the crystalline Alq_3 in the sample pan was heated continuously and thus melting of this material was observed. The absence of melting in $HPAlq_3$ in the second cycle was not unexpected. If the heating rate is faster than transition of the amorphous to crystalline phase transition then we would not observe a T_m. By slowing the cooling rate to 2 °C/min (**Figure 3.10** inset) enough time is allowed for some crystalline material to form which is indicated by the reappearance of T_m (340 °C). The T_m obtained in second heating cycle is

slightly different from the first heating cycle, which is probably due to the slower heating rate.

Regardless of heating rate, the DSC measurements of the remaining C-4 substituted Al compounds (**III 2-5**) do not show any indication of melting or a crystalline phase in DSC measurement in both heating cycles. They do, however, all display glass transition temperature (T_g) values between 206 and 218 °C (the second heating cycles are shown in **Figure 3.11**), which is quite similar to that observed for $HPAlq_3$. Furthermore, these C-4 substituted Alq_3 analogues display DSC data that is reminiscent of that reported for C-4 or C-5 methyl substituted Alq_3.[7e] The second heating cycle of DSC measurements for our compounds indicated that there were no additional transformations. An additional DSC experiment was carried out on $HDAlq_3$ (**III-4**) in which the sample was heated at 3 °C/min in the second heating cycle. The same T_g value was observed, but still no T_m was obtained. This set of observations (no T_ms observed) is ascribed to the bulky C-4 aryl substituents that prevent the alignment of the molecules and therefore retard formation of a crystalline phase. The similar observations on T_ms were also seen for C-5 phenyl substituted Alq_3 derivatives[7j] in which only T_g and decomposition temperature (T_d) were reported.

Upon C-4 substitution of Alq_3, the T_m values of Alq_3, $HPAlq_3$, and $(4Meq)_3Al$ increase in the order $HPAlq_3 < 4Meq_3Al < Alq_3$. It is reasonable to speculate that the angular degree between pyridyl ring and phenyl substituent is around 90°, then it is not unexpected to find that $HPAlq_3$ has the lowest T_m among the three samples, since phenyl substituent will reduce the π-π stacking of pyridyl rings more than that of methyl substituent and thus decrease more of the intermolecular interaction. Since the other

compounds did not exhibit T_m values it is not possible to compare the intermolecular interaction among these C-4 substituted Alq_3 analogues from their melting points.

The literature also reports that Alq_3 exhibits an approximate 15% weight loss that occurs before T_m when it is heated.[7e] The TGA measurement on Alq_3 (see **Figure 3.6**), show a weight loss of ~ 15-20 % before the melting point is observed. In **Table 3.1**, the temperatures that correspond to a 15% weight loss for Alq_3 and the new C-4 substituted derivatives are reported. A comparison of these values indicates that they are higher for the $PAlq_3$ and $DAlq_3$ derivatives than for Alq_3. In addition the trend in these values correlates with the values of T_g obtained for these compounds. Specifically, T_g and T_d values increase in the order $Alq_3 < (4Meq)_3Al << PAlq_3$ derivatives $< DAlq_3$ derivatives.

Overall, the thermal data indicates that the new compounds that were prepared in this chapter have higher thermal stability than Alq_3 and the methyl substituted analogue $4Meq_3Al$. The C-4 substituted compounds readily form amorphous phases and appear to require more energy than Alq_3 to form a crystalline phase. These features suggest that these C-4 substituted species have improved physical properties for OLED applications compared to Alq_3.

3.3.4 Electronic properties

Conventional two layer OLEDs employ the Al chelate complexes as both the ETL and the photoactive emissive component. Therefore any analysis of a new compound must go beyond the physical characterization and examine the photophysical behavior of these species. Typical absorption spectra and photoluminescent spectra for Alq_3, $HPAlq_3$

(**III-1**) and $HDAlq_3$ (**III-4**) are shown in **Figure 3.12**. The excitation energy used in these measurements was the absorption maximum, λ_{max}. **Table 3.2** summarized the spectroscopic data for all the compounds Alq_3, $PAlq_3$, $DAlq_3$, and $4Meq_3Al$.

A $\pi \rightarrow \pi^*$ charge transfer from the electron rich phenoxide ring (HOMO) to the electron deficient pyridyl ring (LUMO) has been demonstrated to be responsible for the optical transition in Alq_3.[3] Thus an electron withdrawing substituent at pyridyl ring will decrease the energy of LUMO, causing a bathochromic (red) shift in absorption as well as emission. Likewise, an electron donating substituent at pyridyl ring will lead to a hypsochromic (blue) shift on absorption and emission spectra. By similar reasoning, the reverse effects should be observed for substitution on the phenoxide ring. This correlation has been clearly demonstrated in the case of methyl substituents.[7e] Substitution of H for methyl on the pyridyl ring to yield $4Meq_3Al$ resulted in a hypsochromic shift both in absorption and emission spectra while $5Meq_3Al$, a phenoxide ring modification, produces the exact the opposite spectral effect.

The photophysical effects of C-4 substituents that have been employed in this thesis are summarized on **Table 3.2**. The aromatic substitutents (**III 1-3**) are electron-withdrawing groups and thus all $PAlq_3$ derivatives exhibit bathochromic shifts in both their absorption (13-14 nm) and emission (17-23 nm) spectra when compared with Alq_3. It was initially expected that the diarylamine substituents should perform like electron-donating groups because of the lone pair at the nitrogen atom, thus hypsochromic shifts (5-6 nm) in absorption and emission were anticipated. In fact, hypsochromic shifts were observed in the emission spectra for $DAlq_3$ derivatives. However, the absorption spectra of the $DAlq_3$ derivatives (**III-4** and **5**) exhibited bathochromic shifts (6-7 nm).

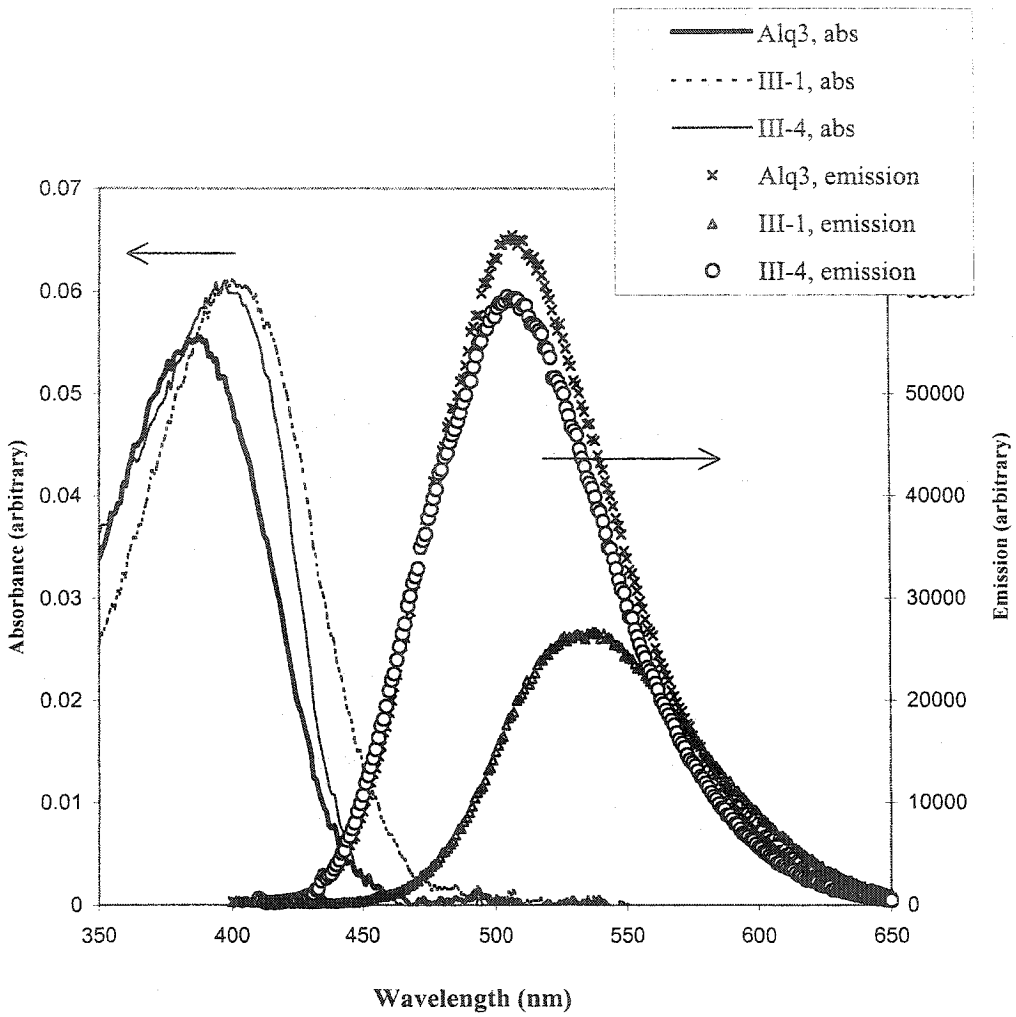

Figure 3.12 UV-vis absorption and emission spectra for Alq_3, III-1 and III-4 in CH_2Cl_2 solution.

Entry	Absorption λ_{max} (nm)	Emission λ_{emi} (nm)	Energy Gap[a] (nm)/(eV)	Stokes shift (nm)	Fwhm (nm)	PL efficiency (vs. Alq_3)	HOMO[b] (eV)	LUMO[b] (eV)
Alq_3	387	511	443/2.80	124	76	100	5.47	2.67
III-1	401	534	469/2.64	133	87	40.1	5.46	2.82
III-2	402	532	467/2.66	130	84	53.0	5.46	2.80
III-3	400	528	466/2.66	128	85	69.5	5.55	2.89
III-4	395	504	445/2.79	109	80	73.0	5.32	2.53
III-5	397	505	444/2.79	108	83	85.0	5.31	2.52

[a] estimated from the intersection of normalized absorption and emission graphs.
[b] HOMO and LUMO energy values were estimated as those shown in Chapter 2.

Table 3.2. Photophysical data obtained in CH_2Cl_2 solution and HOMO/LUMO energy levels estimated from CV.

These apparently conflicting shifts in absorption and emission indicate that the diarylamine substituents were not behaving as simple electron donating groups on the pyridyl ring. The conflicting results were also observed from the Stokes shift and fwhm values of these compounds. Electron-donating group like methyl have both reduced Stokes shift and full-width-at-half-maximum (fwhm) values comparing to Alq_3,[7e] while electron-withdrawing phenyl groups in $PAlq_3$ derivatives in this work show both increased values in Stoke shift (~ 5 nm) and fwhm (~10 nm). Thus, $DAlq_3$ derivatives with electron-donating groups were expected to reduce these values too. However, the experimental results show smaller Stokes shift values (~ 15 nm) but increased fwhm values (~ 5 nm). Therefore, the optical transition in $DAlq_3$ derivatives appear not to be simply ascribed to the $\pi \rightarrow \pi^*$ charge transfer.

Amine substituents provide an alternative $n \rightarrow \pi^*$ electronic transition that might provide an explanation for the observed effects on the absorption and emission spectra of these Al compounds. In **Chapter 2**, an $n \rightarrow \pi^*$ electronic transition involving diarylamine contributed to the optical transition of the naphthalene core diamines. In this work, an $n \rightarrow \pi^*$ electronic transition from nitrogen on the diarylamine group to the pyridyl ring could be used to rationalize the optical transition that have been observed. The electronic transitions for C-4 substituted $PAlq_3$ and $DAlq_3$ derivatives are compared in **Figure 3.13**. As indicated above the trends observed for the $PAlq_3$ derivatives are rationalized as changes to the π-π^* transition. However, the red shifts observed for the $DAlq_3$ derivatives appear to be the result of a different electronic transition from the parent Alq_3. In this case the addition of the non-bonding lone pair localized on the nitrogen center has

introduced an n-π* transition that shifts both the absorption and emission peaks in a bathochromic sense from those of Alq_3.

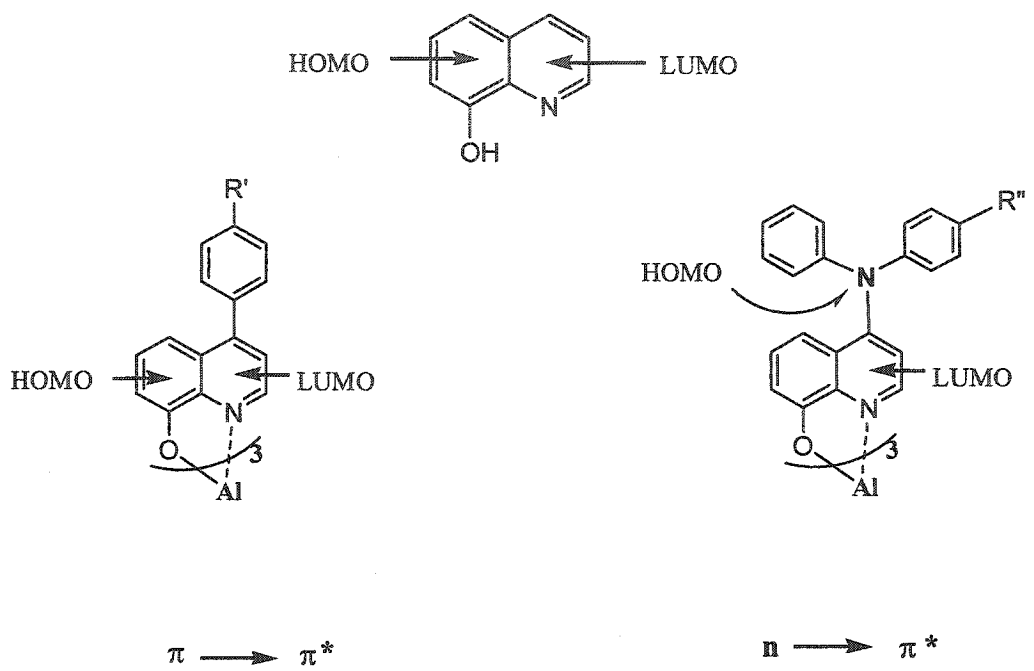

Figure 3.13 Electronic transition for C-4 substituted Alq_3 analogues

The PL efficiency of the compounds **III 1-5** vs. Alq_3 was measured and presented in **Table 3.2**. The lower PL efficiency of the $PAlq_3$ derivatives comparing to Alq_3 are due to the increased energy loss in the excited-state vibrational manifold as indicated from the reduced Stokes shift and fwhm values.[7e] While the PL efficiency of $DAlq_3$ derivatives is larger than those of $PAlq_3$ derivatives, and close to that of Alq_3. The observation for $DAlq_3$ derivatives cannot be explained by simply comparing optical data with those of Alq_3 and $PAlq_3$ derivatives since the types of their electronic transitions are different as discussed in the previous paragraph. However, the results of $DAlq_3$ derivatives indicate

that it would be possible to adjust PL efficiency and orbital energy especially the HOMO level of these $DAlq_3$ derivatives in the same way as discussed in **Chapter 2** by attaching various substituents on the diarylamine as for HT materials. Furthermore, these $DAlq_3$ derivatives bear the electron-rich diamine, which was supposed to improve hole mobility of the new compounds and electron-deficient quinoline core that might be used as bipolar compounds[14] for OLEDs.

It is worth noting that the methyl or fluoro substituents on phenyl or diarylamine have little influence on their optical properties for each group, such as absorption, emission and PL efficiency, and also on T_gs in thermal analysis (**Table 3.1**), however, these substituents have significant influences on their T_ds (decomposition temperatures).

3.3.5 Electrochemistry

Cyclic voltammetry (CV) has been employed to measure the HOMO level of HT materials in solution using ferrocene (Cp_2Fe) as the internal reference.[15,16] This method was more thoroughly discussed in **Section 2.3.7**. The same method has been used to measure the HOMO energies of C-5 aryl substituted Alq_3 in a recent paper.[71] This method for determining the HOMO energies is not as frequently used for ET materials as it is with HT materials, partly due to fact that Ultraviolet Photoelectron Spectroscopy (UPS) and X-ray Photoelectron Spectroscopy (XPS) can be used to directly determine the HOMO levels of ET materials in solid state films.[6, 7c] However, not only does CV offer a simple and inexpensive means to estimate and to compare energy levels of OLED

materials, CV measurements clearly show the electrochemical stability and electrochemical process of an OLED material.

Figure 3.14 shows three CV measurement of Alq_3 in CH_2Cl_2 solution under different conditions. In all three CV experiments two oxidation peaks were observed for Alq_3 in the positive potential region and no reduction peaks were observed. With a scan range of 0 – 2V (**A**), these two oxidation peaks disappear after the first scan cycle. When the potential scan range is increased to –2 V to +2 V (**B**), the two oxidation peaks remain and are quite reproducible from the second scanning cycle. Given that the HOMO is localized on the phenoxide ring we ascribe the first oxidation to removal of an electron from this orbital. The addition of Cp_2Fe to a solution of Alq_3 allows for a reference to estimate the HOMO energy of the Al complex. The results of this experiment are displayed in **Fig. 3.14 (C)**, which shows the oxidation peak but no reduction peak of Cp_2Fe and the oxidation peaks of Alq_3. Moreover, the peak potential differences between Cp_2Fe and first oxidation peak of Alq_3 remain constant for several scan cycles, which indicates the validity of using Cp_2Fe to estimate HOMO of Alq_3. Since there were no reduction peaks of Cp_2Fe and Alq_3 in the CV scan range between –2 to +2V (the reduction between -1 to –2 V was due to the solvent, and it was not discussed in thesis), it was necessary to check the oxidation process of Alq_3 at different scan potential range and whether there was adverse reaction between Cp_2Fe and Alq_3 during and before the CV scan. As shown in **Figure 3.15**, CVs were first scanned between 0 - +2V (**D**); then between 0 - +1.3V, right after the first oxidation (**E**); and after that, adding small amount Cp_2Fe, CV was scanned in the range of redox potential of Cp_2Fe (**F**).

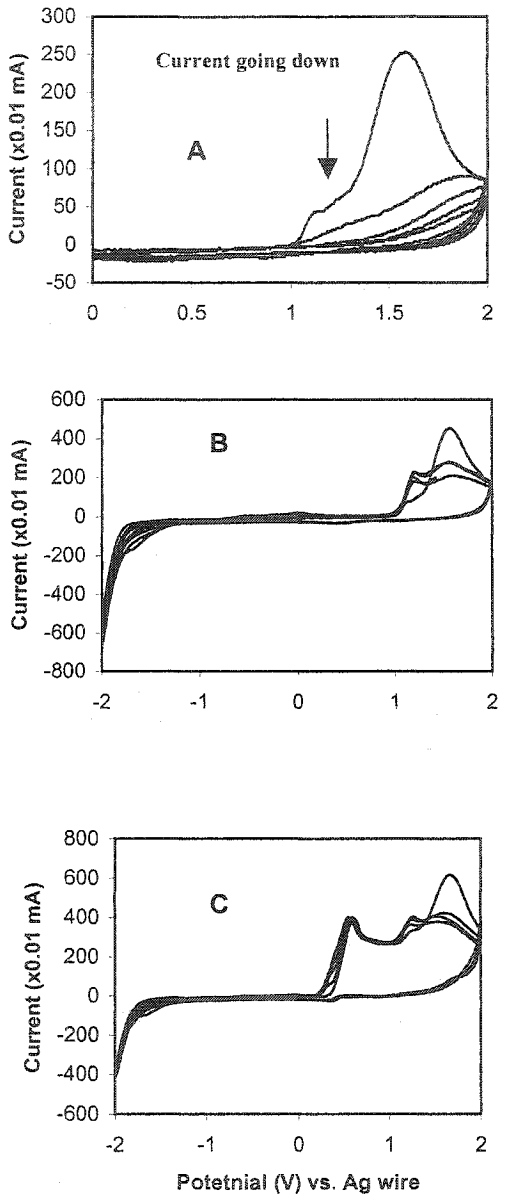

Figure 3.14 CVs at 100 mV/s for Alq_3 in N_2 saturated 0.1M TBAHP CH_2Cl_2 at scan ranges of (A) 0 - +2V; (B) -2 - +2V; and (C) -2 - +2V after adding Cp_2Fe.

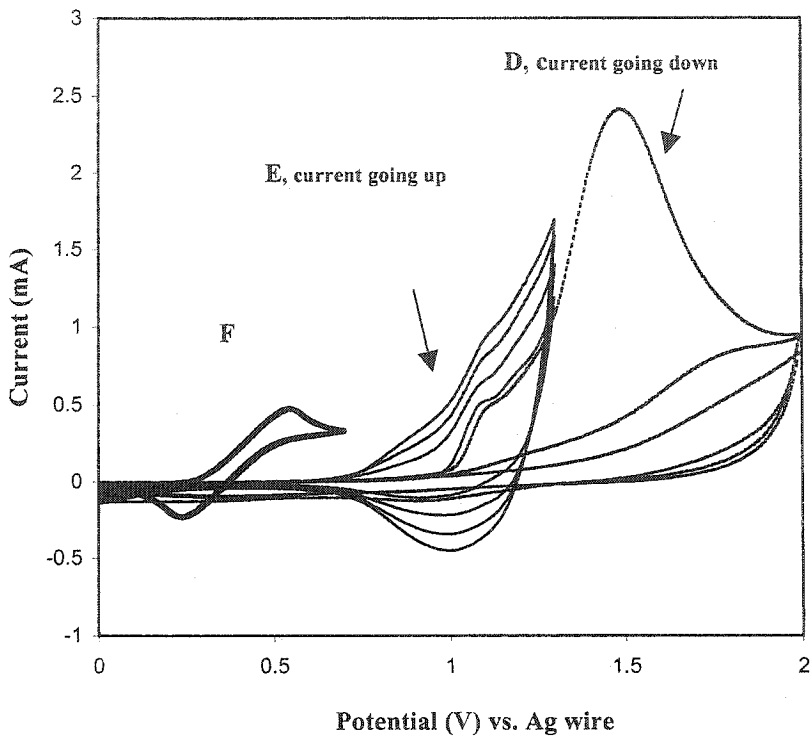

Figure 3.15. CVs at 100 mV/s for Alq_3 in N_2 saturated 0.05 M TBAHP CH_2Cl_2 at scan ranges of (D) 0 - +2V; (E) 0 - +1.3V and (F) 0 - +0.7V after adding Cp_2Fe. At least three cycles were recorded for all CV scans.

From the **Figure 3.15**, it can be seen that non-reversible redox of Alq_3 was mostly correlated to the second oxidation of Alq_3 molecules. From **E**, there was only broad and unstable reduction of Alq_3 showed up, which was probably due to the two oxidation processes proceeded too close. Reversible redox of Cp_2Fe was observed in **F** when the potential scan was stopped before the first oxidation potential of Alq_3. The results excluded the adverse interaction between Cp_2Fe and Alq_3 in CH_2Cl_2 solvent before the CV scan and the produced Cp_2Fe ions would react with oxidants of Alq_3. Further experiments showed that the non-reversible redox of Cp_2Fe was related to oxidation of Alq_3 and its C-4 position, which will be discussed in the final paragraph in this section.

The cyclic voltammetric behavior of the $PAlq_3$ and $DAlq_3$ derivatives is quite similar to what was observed for Alq_3. Sample CV scans for the $PAlq_3$ derivatives (**III 1-3** in **Table 3.2**) are presented in **Figure 3.16**. In all three cases, reproducible CV curves were obtained over a scan range of –2 to +2 V (**Figure 3.16** only displays the region from +0.5 to +2V) with two oxidation peaks at positive potential region being observed for these compounds. The inset in **Fig. 3.16** shows an example of a CV scan of compounds **III-3** over the limited scan range of 0 to +2 V. Again the observed behavior is similar to that of Alq_3 (**Figure 3.14A**).

The CV scans for the diarylamine derivatives (**III 4-5** in **Table 3.2**) over a scan range of –2 to +2V are shown in the **Fig. 3.17** (the figure only displays the region form +0.5 to +2V). While the gross features are reminiscent of Alq_3 and the $PAlq_3$ derivatives, the CV data for the $DAlq_3$ derivatives differs in that there are three broad oxidation peaks in the positive potential region.

In **section 3.3.4**, the absorption spectrum in $DAlq_3$ derivatives was speculated to arise from an $n \rightarrow \pi^*$ electronic transition centered on the nitrogen of the diarylamine group to the pyridyl ring of the quinoline function. If this is indeed the lowest energy electronic transition then it would be expected that the first oxidation peak of $DAlq_3$ derivatives should be different from that of Alq_3 and $PAlq_3$ derivatives. To be clearer, the CV curves before and after addition of Cp_2Fe to samples of $MePAlq_3$ (**III-3**) and $MeDAlq_3$ (**III-5**) derivatives along with Alq_3 are shown in **Fig.3.18**, and HOMO energies estimated from the potential difference between oxidation peak of Cp_2Fe and compounds are listed in **Table 3.2**.

From the HOMO/LUMO results shown in the **Table 3.2**, it can be seen that the HOMO energies of C-4 phenyl substituted $PAlq_3$ derivatives are very close to that of Alq_3, and LUMO energies are smaller than that of Alq_3. This is entirely consistent with the fact that the phenyl group has been introduced on the pyridyl ring, which is the portion of the quinoline framework at which the LUMO is localized. This line of reasoning further suggests that the HOMO energies of $PAlq_3$ derivatives should not be significantly different from that of Alq_3. This is, in fact, what is observed. The $DAlq_3$ derivatives, however, exhibit HOMO energies of 5.32 and 5.31eV. Perhaps not too surprisingly, these HOMO energy values are close to those found for naphthalene core diamines (**Table 2.6**, entry **III-9**, HOMO is 5.31 eV). These facts support the proposition that the HOMO of the $DAlq_3$ derivatives is essentially the non-bonding nitrogen lone pair of the diarylamine group. The LUMO energies of $DAlq_3$ derivatives are lower in energy than that of Alq_3. This observation is consistent with the electron-donating properties of diarylamine which result in less stabilized LUMO energies.

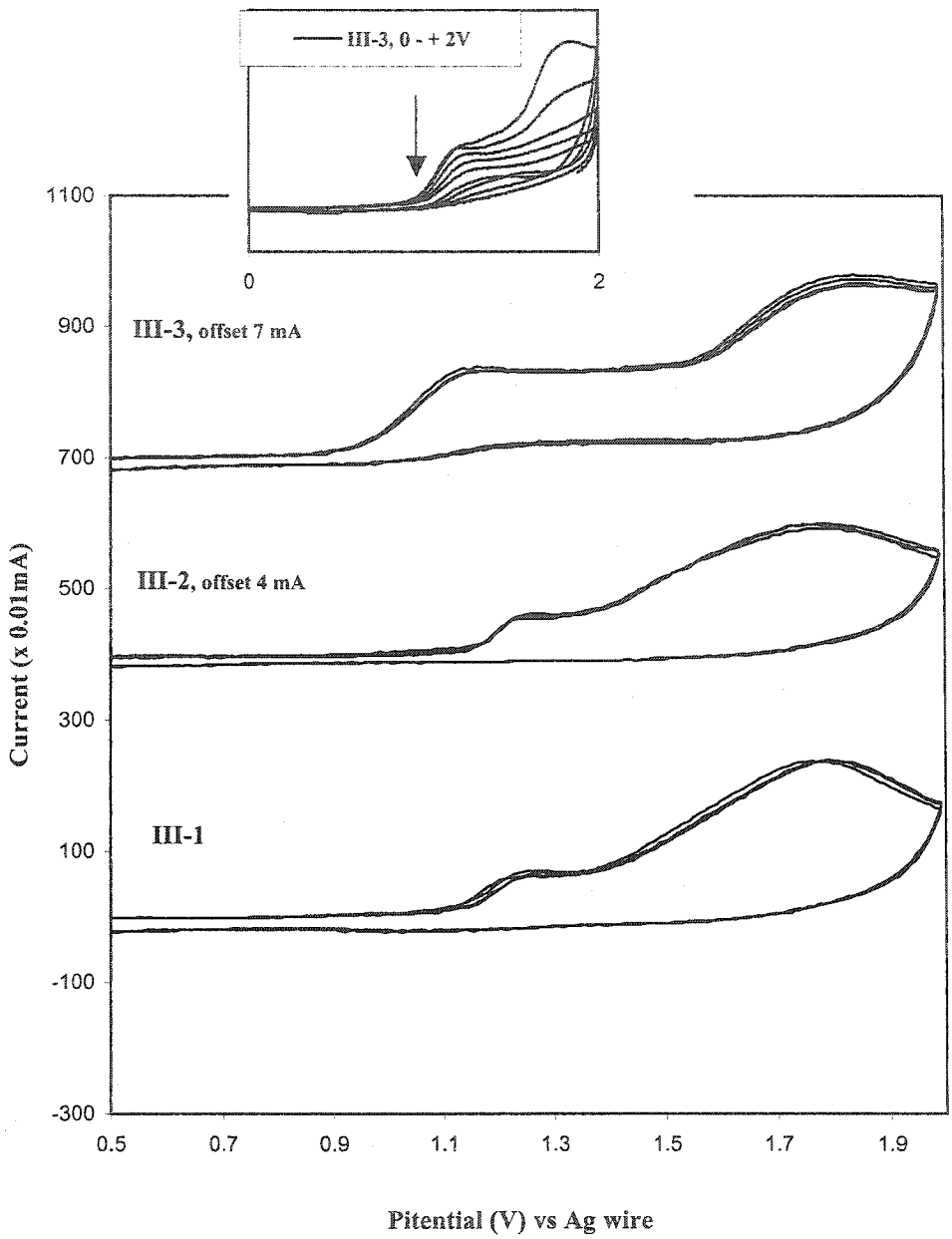

Figure 3.16 CVs at 100 mV/s for $PAlq_3$ derivatives (III 1-3) in N_2 saturated 0.1 M TBAHP CH_2Cl_2 at scan range of -2 V - +2V. Only positive scan is shown and at least three cycles recorded. Up window, CV at 100 mV/s for III-3 at scan range of 0 - +2V.

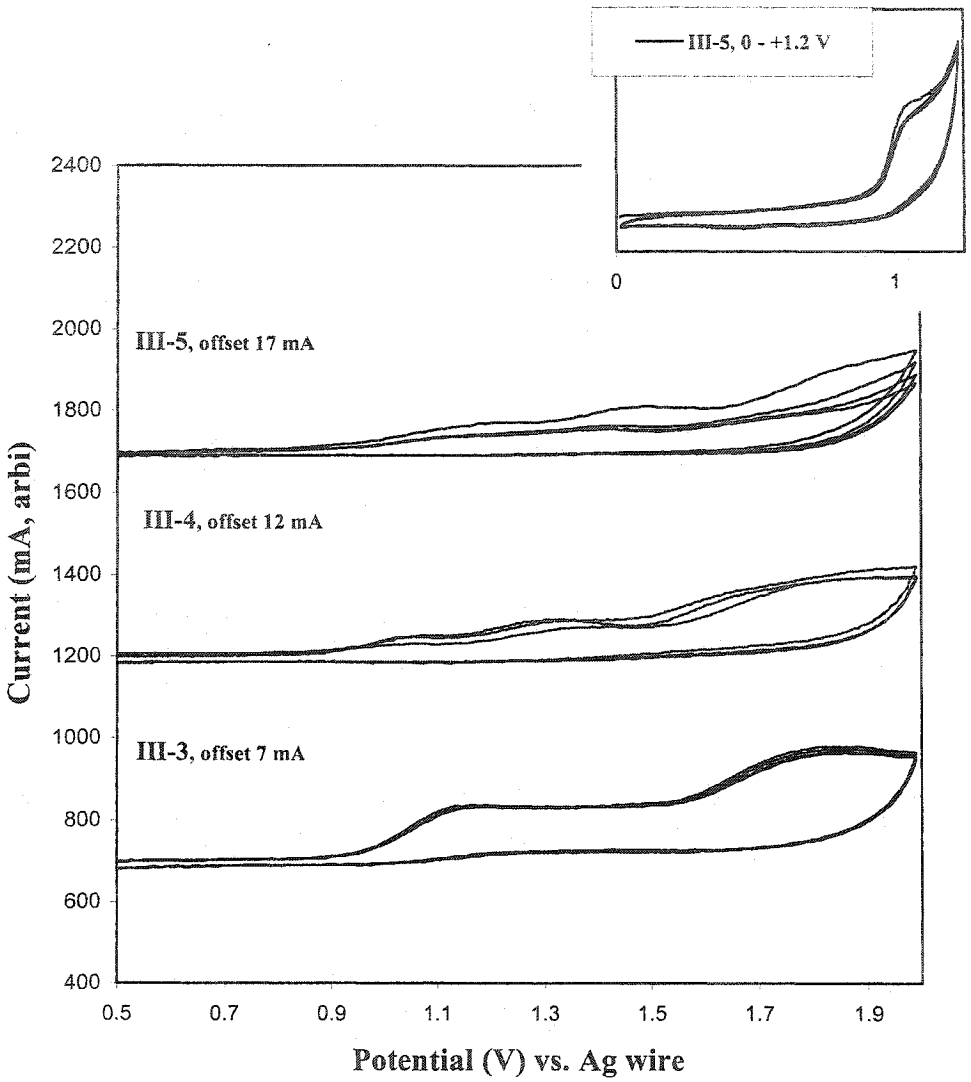

Figure 3.17 CVs at 100 mV/s for $DAlq_3$ derivatives (III 4-5 and III-3 for comparison) in N_2 saturated 0.1 M TBAHP CH_2Cl_2 at scan range of -2 V - +2V. Only positive scan is shown, three cycles recorded. Up window, CV at 100 mV/s for III-5 (0 - +1.2V).

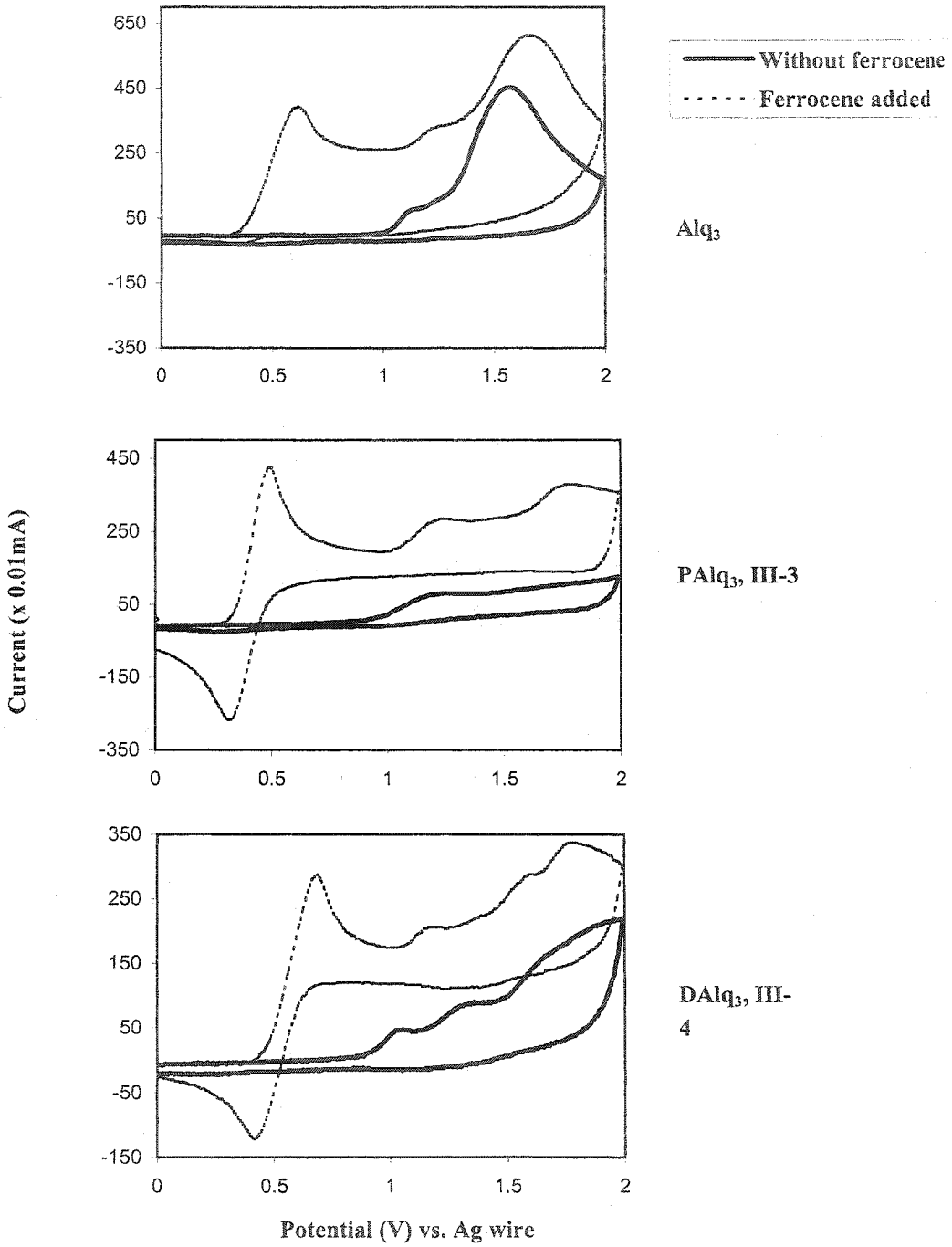

Figure 3.18 CVs at 100 mV/s for C-4 substituted Alq_3 analogues in N_2 saturated 0.1 M TBAHP CH_2Cl_2 before and after adding ferrocene at scan range of -2 V - +2V. Only positive scan and the first cycle are shown.

As discussed previously that non-reversible redox Cp_2Fe in Alq_3 solution was observed at high scan range. In **Figure 3.18**, an interesting phenomenon is that reversible redox peaks of Cp_2Fe in the CVs of $PAlq_3$ and $DAlq_3$ derivatives are observed. This observation indicates that there were adverse reactions between Cp_2Fe^+ and Alq_3 oxidants, and the C-4 position of pyridyl ring was an active center to form radical cation to react with Cp_2Fe^+. The substituents at the C-4 position of Alq_3 analogues, however, appear to have acted like protecting groups, which prevent pyridyl ring to form reactive intermediates to further react with Cp_2Fe^+.

3.4 Conclusions

The C-4 position of the hydroxyquinoline ligand of tris(8-hydroxyquinoline)aluminum (Alq_3) have been derivatized with aromatic groups and diarylamine substituents. Since the pyridyl portion of the quinoline framework is not readily modified by electrophilic substitution the synthetic route to these derivatized species relied on construction of a hydroxyl group protected 4-halo-8-methoxyquinoline followed by Suzuki or Buchwald-Hartwig cross coupling. The tris(chelate) complexes were prepared in a straightforward fashion. A systematic study of the thermal, spectroscopic and electrochemical properties of these C-4 substituted Alq_3 derivatives was carried out with the results directly compared to those of Alq_3. Enhanced T_g values indicate all these compounds have higher thermal stability than Alq_3. The photophysical properties of C-4 aromatic substituted Alq_3 are readily understood in light of the LUMO modulation of π(phenoxy)$\rightarrow\pi^*$(pyridyl) transitions of the parent Alq_3. On the other hand

the C-4 diarylamine substituted Alq_3 derivatives displayed quite different absorption/emission properties. These have been rationalized in terms of a dominant $n \rightarrow \pi^*$ transitions from the diarylamine nitrogen to the pyridyl ring of the quinoline group. This optical transition difference was responsible for the spectroscopic behaviors in their UV-vis absorption, emission and PL efficiency, and also electrochemical properties. The work has provided a new way to modify the most widely used electron-transporting materials Alq_3 with aromatic groups at C-4 position. The characterization data should be good references for the selection of materials to fabricate devices.

References for Chapter 3:

(1) Tang, C. W.; VanSlyke, S. A. *Appl. Phys. Lett.* **1987,** *51*, 913-915.

(2) Selected references: (a) Papadimitrakopoulos, F.; Zhang, X. M.; Thomsen, D. L., III; Higginson, K. A. *Chem. Mater.* **1996**, *8*, 1363-1365. (b) Le, Q. T.; Avendano, F. M.; Forsythe, E. W.; Yan, L.; Gao, Y.; Tang, C. W. *J. Vac. Sci. Technol. A.* **1999**. *17*, 2314. (c) Aziz, H.; Popovic, A. D.; Hu, N.; Hor, A.; Xu, G. *Science*, **1999**, *283*, 1900-1902. (d) Halls, M. D.; Schlegel, B. *Chem. Mater.* **2001,** *13*, 2632. (e) Brinkmann, M.; Gadret, G.; Muccini, M.; Taliani, C.; Masciocchi, N.; Sironi, A. *J. Am. Chem. Soc.* **2000,** *122,* 5147. (e) Cölle, M.; Gmeiner, J.; Milius, W.; Hillebrecht, H.; Brütting, W. *Adv. Funct. Mater.* **2003,** *13,* 108. (f) Utz, M.; Chen, C.; Morton, M.; Papadimitrakopoulos, F. *J. Am. Chem. Soc.* **2003,** *125,* 1371.

(3) Chen, C. H.; Shi, J. *Coord. Chem. Rev.* **1998,** *171,* 161. references therein.

(4) Friend, R. H.; Gymer, R. W.; Holmes, A. B.; Burrouges, J. H.; Marks, R. N.; Taliani, C.; Bradley, D. D. C.; Dos Santos, D. A.; Brédas, J. L.; Lögdlund, M.; Salaneck, W. R. *Nature*, **1999**, *397*, 121-128.

(5) Mitschke, U.; Bäuerle, P. *J. Mater. Chem.* **2000**, *10*, 1471-1507.

(6) Hung, L. S.; Chen, C. H. *Mater. Sci. Engineer.* **2002**, *R 39*, 143-222.

(7) (a) Hopkins, T. A.; Meerholz, K.; Shaheen, S.; Anderson, M. L.; Schmidt, A.; Kippelen, B.; Padias, A. B.; Hall, H. K.; Jr.; Peyghambarian, N.; Armstrong, N. R. *Chem. Mater.* **1996**, *8*, 344-351. (b) Kido, J.; Endo, J. *Chem. Lett.* **1997**, 593-594. (c) Anderson, J. D.; McDonald, E. M.; Lee, P. A.; Anderson, M. L.; Ritchie, E. L.; Hall, H. K.; Hopkins, T.; Mash, E. A.; Wang, J.; Padias, A.; Thayumanavan, S.; Barlow, S.; Marder, S. R.; Jabbour, G. E.; Shaheen, S.; Kippelen, B.; Peyghambarian, N.;

Wightman, R. M.; Armstrong, N. R. *J. Am. Chem. Soc.* **1998,** *120*, 9646. (d) Yu, J.; Chen, Z.; Sakuratani, Y.; Suzuki, H.; Tokita, M.; Miyata, S. Jpn. *J. Appl. Phys.* **1999,** *38*, 6762-6763. (e) Sapochak, L. S.; Padmaperuma, A.; Washton, N.; Endrino, F.; Schmett, G. T.; Marshall, J.; Fogarty, D.; Burrows, P. E.; Forrest, S. R. *J. Am. Chem. Soc.* **2001**, *123*, 6300-6307. (f) Chen, Z.; Yu, J.; Sone, M.; Miyata, S.; Lu, Y.; Watanabe, T. *J. Phys. D: Appl. Phys.* **2001**, *34*, 2679-2682. (g) Yu, J.; Chen, Z.; Miyata, S. *Synth. Met.* **2001**, *123*, 239-243. (h) Han, Y. K.; Lee, S. U. *Chem. Phys. Lett.* **2002**, *366*, 9-16. (i) Ghedini, M.; Deda, M. L.; Aiello, I.; Grisolia, A. *Synth. Met.* **2003**, *10327*, 1-4. (j) Shoji, E.; Miyatake, K.; Hlil, A. R.; Hay, A. S.; Maindron, T.; Jousseaume, V.; Dodelet, J. P.; Tao, Y.; D'iorio, M. *J. Poly. Sci. A: Poly. Chem.* **2003,** *41*, 3006. (k) Pohl, R.; Jr., P. A. *Org. Lett.* **2003**, *5*, 2769-2772. (l) Pohl, R.; Montes, V. A.; Shinar, J.; Anzenbacher Jr., P. *J. Org. Chem.* **2004**, *69*, 1723-1725.

(8) (a) Leung, L.; Lo, W. Y.; So, S. K.; Lee, K. M.; Choi, W. K. *J. Am. Chem. Soc.* **2000**, *122*, 5640. (b) Wang, G.; Liang, F.; Xie, Z.; Su, G.; Wang, L.; Jing, X.; Wang, F. *Synth. Met.* **2002,** *131*, 1-5. (c) Shao, Y.; Qiu, Y.; Hu, W.; Hong, X. *Adv. Mater. Opt. Electron.* **2000**, *10*, 285-288. (d) Liu, S.; Seward, C.; Aziz, H.; Hu, N.; Popović, Z.; Wang, S. *Organometallics* **2000**, *19*, 5709-5714.

(9) Lauer, W. M.; Arnold, R. T.; Tiffany, B.; Tinker, J. *J. Am. Chem. Soc.* **1946,** *68,* 1268.

(10) Gershon, H.; Clarke, D. D. *Monatsh. Für. Chem.* **1991,** *122*, 935.

(11) Schmid, M.; Eberhardt, R.; Klinga, M.; Leskelä, M.; Rieger, B. *Organometallics,* **2001,** *20*, 2321-2330.

(12) Wolfe, J. P.; Buchwald, S. L. *J. Org. Chem.* **2000**, *65*, 1144-1157.

(13) Hartwig, J. F.; Kawatsura, M.; Hauck, S. I.; Shaughnessy, K. H.; Alcazar-Roman, L. M. *J. Org. Chem.* **1999**, *64*, 5575-5580.

(14) (a) Thomas, K. R. J.; Lin, J. Y.; Tao, Y. T.; Chuen, C. H. *J. Mater. Chem.* **2002**, *12*, 3516-3522. (b) Pudzich, R.; Salbeck, J. *Synth. Met.* **2003**, *138*, 21-31.

(15) (a) Pommerehne, J.; Vestweber, H.; Guss, W.; Mahrt, R. F.; Bassler, H.; Porsch, M.; Daub, J. *Adv. Mater*, **1995**, *7*, 551-554. (b) Thelakkat, M.; Schmidt, H. W. *Adv. Mater.* **1998**, *10*, 219-223. (c) Thelakkat, M.; Schmidt, H. W. *Polym. Adv. Technol.* **1998**, *9*, 429-442.

(16) Selected references: (a) Yu, M. X.; Duan, J. P.; Lin, C. H.; Cheng, C. H.; Tao, Y. T. *Chem, Mater.* **2002**, 14, 3958-3963. (b) Thomas, K. R.; Lin, J. T.; Tao, Y. T.; Ko, C. W. *J. Am. Chem. Soc.* **2001**, *123*, 9404-9411.

Chapter 4

Synthesis and Characterization of Substituted Salicylaldimine Diphenyl Boron Complexes

4.1 Introduction

4.1.1 Boron based luminescent complexes

So far, the most widely used and thoroughly studied emission material for organic light-emitting diodes (OLED) is the metal chelate tris(8-hydroxyquinoline)aluminum (Alq_3) due to its good stability, high luminescence and tunable modifications for full color displays,[2-4] which have been discussed in **Chapter 3**. Much progress has been achieved with aluminum based chelate complexes and other groups of emission and electron-transport (ET) materials and this area has been reviewed recently.[4] However, there remain significant needs to further optimize the stability, lifetime, color gamut, and emission efficiencies and this continues to be an active research field. Among these activities, the search for more efficient blue emitters has always been a challenge. In particular, the larger band-gap needed for a blue emitter can lead to inhibited injection of electrons from cathode and result in a lower efficiency. Recently, luminescent boron

complexes have attracted much attention due to their potential applications for OLEDs as blue light emission materials.[5-10]

The blue light-emission properties of boron complexes are believed to be from the special interaction between the ligands and boron center.[2,5-7] Boron, like aluminum, is a member of group 13, but the smaller radius and higher electronegativity of boron leads to stronger covalent bonds with its ligands and to more stable compounds in general. On the other hand, the smaller size of boron relative to aluminum limits the coordination number of boron complexes to predominantly 3 or 4.

The ligands most commonly employed to prepare boron complexes for optoelectronic applications generally have electron donor elements like N or O or both in mixed aromatic rings. For example, 8-quinolinolato that have been used to prepare Alq_3,[6] 2-methyl-8-hydroxyquinoline (q_m)[7,10] pyridine-phenol (dppy),[8] pyridyl-indole series (F-2-PI)[5c,5d] and 2,3-dihydroxynaphthalene (DHN) and their analogues have been used with boron.[9] The boron complexes (**4a-4d**) made from these ligands are shown in **Figure 4.1**. The boron complexes in **Figure 4.1** have exhibited high thermal stability, ease of processability, and most importantly, they exhibit emission in the blue/violet regions of the visible spectrum (except **4a**). It is thus not surprising that many research groups have put significant effort on boron-based complexes for electroluminescent (EL) devices.

The synthetic routes to these boron complexes are generally the one-pot reaction between the ligands and corresponding boron-containing compounds. For example, the boron complexes shown in **Figure 4.1**, **4a**, **4c** and **4d** were prepared by the direct reaction of the ligands with triphenylboron,[5c,5d,6,9] **4b** was obtained from the metathetical reaction of the ligand with BF_3.[8]

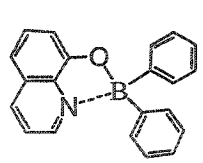

4a

λ_{emi} = 505 nm,
in CH_2CL_2, ref 6.*

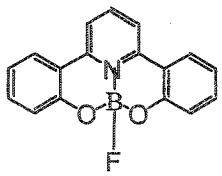

(dppy)BF

4b

λ_{emi} = 445 nm,
in $CHCL_3$, ref 8.

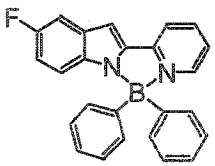

BPh_2(F-2-PI)

4c

λ_{emi} = 490 nm,
in CH_2CL_2, ref 5c,5d.

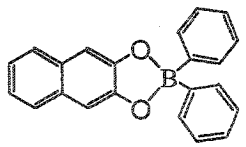

Ph_2B(DHN)

4d

λ_{emi} = 365 nm,
in DMSO, ref 9.

Figure 4.1 Boron complexes used for blue-light emitter

4.1.2 Objectives of this chapter

Boron complexes studied for EL applications as blue-light emitters started just around five years ago.[5a,7] The ligands used for these complexes generally display aromatic structures with nitrogen-based heterocycles as part of the structure. Hohaus has used substituted salicylaldimines, to make boron complexes[11-13] and has measured their photophysical and thermal properties. Importantly, the author discussed the fluorescent properties of these compounds but did not mention any potential application of these complexes in EL devices. It is noteworthy that salicylaldimines have been widely employed to prepare aluminum complexes, but mainly for the purpose of catalysis.[14-20]

To our knowledge there are no reports for the potential OLED applications employing these salicylaldimine-based boron complexes.

The primary objective of the work presented in this chapter is the synthesis of substituted salicylaldimine boron complexes and characterization of these compounds aimed at their potential application of in OLEDs. Salicylaldimines with N-aryl groups possessing various substituents were targeted. In particular, para-substituted phenyl moieties with electron-donating (CH_3O), electron-withdrawing (F, Ph), and an organometallic (ferrocenyl) group have been synthesized and employed in the preparation of salicylaldimine diphenyl boron complexes. An analogous Schiff base ligand derived from N-phenyl-2-(o-hydroxyphenyl)perimidine and its diphenylboron complex were also prepared. The thermal, photophysical and electrochemical properties of these boron complexes have been examined, while the potential application of these species as emission and electron transport materials in OLEDs is discussed.

4.2 Experimental

General information. All reagents, triphenylboron, salicylaldehyde, aniline, 4-fluoroaniline, *p*-anisidine, 4-aminobiphenyl, ferrocene, 5% Pd/C and sodium borohydride were obtained from Aldrich Chemical Company and used without further purification. 1-amino-8-(phenylamino)naphthalene was prepared as described in **Chapter 5**. Toluene and hexane was purified by passage through a column of activated alumina using an apparatus purchased from Anhydrous Engineering. All boron complexes were purified by recrystallization from CH_2Cl_2/hexane mixtures and the structures were characterized by

^{1}H, ^{13}C NMR and HRMS mass spectra. Differential scanning calorimeter (DSC), UV-vis, steady-state fluorescence spectroscopy, XRD, cyclic voltammetry (CV) and other experimental and characterization information are described in **Section 2.2**.

4-Ferrocenylaniline

4-Ferrocenylaniline was synthesized using a modification of the literature preparation[21] (**Eq. 4.2** in **Scheme 4.1**). In a round bottom flask over a ice bath added in 2M HCl and *para*-nitroaniline, sodium nitrite was added slowly to maintain the solution temperature under 5 °C. After that, ferrocene dissolved in ether was added at room temperature and stirred for additional 3 hours. The crude 4-nitrophenylferrocene (**2a**) was separated and extracted by ether into organic layer. After drying and evaporating the solvent, the residue was purified by column chromatography using hexane/ether (4:1) as the eluent. To **2a** in a water/methanol (1:2 volume) solution was added Pd/C (5%) and sodium borohydride and the reaction mixture was stirred for 1 hour. A stream of nitrogen was bubbled through the mixture during the stirring. The reaction mixture was then filtered and acidified with 2M HCl to destroy and remove excess $NaBH_4$ and then neutralized with 2M NaOH. The crude 4-ferrocenylaniline was extracted with ether and purified by column chromatography using hexane/ether (1:3) as the eluent.

General procedure for the synthesis of substituted salicylaldimine ligands

In a Schlenk flask was mixed salicylaldehyde and the corresponding amine in a 1.1:1 molar ratio. Toluene and a small amount of molecular sieves were added to these flasks and the reaction mixtures were refluxed under nitrogen for 12 hours (**Eq. 4.1** in **Scheme**

4.1). On cooling, the crude ligands were filtered and concentrated, then recrystallized from hexane.

N-(*p*-fluorophenyl)-salicylaldimine (2)

^{1}H NMR ($CDCl_3$, δ): 7.00-7.40 (m, 9H), 8.30 (s, 1H), 13.10 (s, 1H). ^{13}C NMR ($CDCl_3$, δ): 116.17 (J_{C-F}, 22.7 Hz), 117.22, 119.02, 119.11, 122.55 (J_{C-F}, 8.4 Hz), 132.26, 133.21, 144.52 (J_{C-F}, 3.0 Hz), 160.98, 161.59 (J_{C-F}, 264.2 Hz), 162.38 (J_{C-F}, 1.4 Hz). m/z, 215 (M^+). HRMS (m/z): Calcd for $C_{13}H_{10}NO$ 215.0746 found 215.0766.

N-(*p*-methoxyphenyl)-salicylaldimine (3)

^{1}H NMR ($CDCl_3$, δ): 3.82 (s, 3H), 6.80-7.03 (m, 4H), 7.25-7.39 (m, 4H), 8.59 (s, 1H), 13.42 (s, 1H). ^{13}C NMR ($CDCl_3$, δ): 55.51, 114.58, 117.14, 118.97, 119.30, 122.26, 131.96, 132.71, 141.21, 158.82, 160.39, 160.97. m/z, 227 (M^+). HRMS (m/z): Calcd for $C_{14}H_{13}NO_2$ 227.0946 found 227.0934.

N-(*p*-biphenyl)-salicylaldimine (4)

^{1}H NMR ($CDCl_3$, δ): 6.91-7.05 (m, 2H), 7.34-7.50 (m, 7H), 7.55-7.70 (m, 4H), 8.68 (s, 1H), 13.28 (s, 1H). ^{13}C NMR ($CDCl_3$, δ): 117.30, 119.13, 121.60, 126.95, 127.46, 128.07, 128.85, 132.31, 133.22, 139.89, 140.24, 147.21, 147.34, 161.21, 162.30. m/z, 273 (M^+). HRMS (m/z): Calcd for $C_{19}H_{15}NO$ 273.1154 found 273.1157.

N-(*p*-ferrocenephenyl)-salicylaldimine (5)

^{1}H NMR ($CDCl_3$, δ): 4.09 (s, 5H), 4.39 (s, 2H), 4.72 (s, 2H), 6.91-7.46 (m, 8H), 8.66 (s, 1H), 13.30 (s, 1H). ^{13}C NMR ($CDCl_3$, δ):66.62, 69.47, 69.99, 84.85, 85.00, 117.22, 119.05, 119.39, 121.20, 126.84, 132.11, 132.82, 138.48, 145.90, 161.23. m/z, 381 (M^+). HRMS (m/z): Calcd for $C_{23}H_{19}FeNO$ 381.0816 found 381.0801.

(1-Phenyl-2-*m*-phenoxy)perimidine

In a Schlenk flask was mixed 1-amino-8-(phenylamino)naphthalene (0.46g, 0.2 mmol), salicylaldehyde (0.27g, 0.24 mmol) and 2 mol% 5% Pd/C and the mixture was heated under reflux overnight (**Eq. 4.3** in **Scheme 4.1**). On cooling, the mixture was filtered, concentrated and recrystallized from hexane. Yield 0.6 g (90 %)

^{1}H NMR ($CDCl_3$, δ): 5.96 (d, 1H), 6.36 (t, 1H), 6.75 (d, 1H), 6.87-7.50 (12H). ^{13}C NMR ($CDCl_3$, δ): 105.39, 114.30, 116.61, 116.71, 117.75, 117.79, 120.57, 121.36, 121.53, 127.30, 128.76, 129.05, 129.13, 129.53, 130.42, 131.48, 134.93, 139.32, 140.49, 155.04, 158.25. m/z, 336 (M^+). HRMS (m/z): Calcd for $C_{23}H_{16}N_2O_1$ 336.1263 found 336.1254.

General procedure for the synthesis of boron complexes

The boron complexes were synthesized from reaction of triphenyl boron with corresponding salicylaldamine ligands at 0.1 mol scale (if not specified) in toluene at reflux under nitrogen for overnight (**Scheme 4.2**). After the solvent was removed, the residue was recrystallized from $CHCl_3$/Hexane. The yields for all the yellow-greenish products are between 50-60 %.

N-Phenyl-salicylaldiminediphenylboron (IV-1)

^{1}H NMR ($CDCl_3$, δ): 6.82 (t, 1m H), 6.9-7.1 (m, 3H), 7.1-7.6(m, 16H), 8.34 (s, 1H). ^{13}C NMR ($CDCl_3$, δ): 118.55, 119.28, 120.59, 124.88, 126.74, 127.31, 128.62, 129.08, 132.58, 134.02, 135.07, 139.18, 145.87, 162.85, 163.22. m/z, 361 (M^+). HRMS (m/z): Calcd for $C_{25}H_{20}BNO$ 361.1438 found 361.1649.

N-(*p*-fluorophenyl)-salicylaldiminediphenylboron (IV-2)

^{1}H NMR ($CDCl_3$, δ): 6.7-6.8 (m, 3H), 6.8-7.1 (m, 3H), 7.1-7.6 (m, 12H), 8.30 (s, 1H). ^{13}C NMR ($CDCl_3$, δ): 115.65 (J_{C-F}, 22.9 Hz), 118.00, 119.00, 120.22, 126.22 (J_{C-F}, 8.6 Hz), 126.49, 127.03, 132.23, 133.57, 134.69, 138.99, 141.54 (J_{C-F}, 3.3 Hz), 161.90 (J_{C-F}, 249.1 Hz), 162.44, 162.90. m/z, 379 (M^+). HRMS (m/z): Calcd for $C_{25}H_{19}BFNO$ 379.1544 found 379.1541.

N-(*p*-methoxyphenyl)-salicylaldiminediphenylboron (IV-3)

^{1}H NMR ($CDCl_3$, δ): 3.08 (s, 3H), 6.2-6.6 (d, 2H), 6.6-6.8 (t, 1H), 6.0-7.1 (m, 3H), 7.1-7.6 (m, 12H), 8.30 (s, 1H). ^{13}C NMR ($CDCl_3$, δ): 55.38, 113.75, 118.24, 118.82, 120.07, 125.56, 126.32, 126.94, 127.92, 132.02, 133.64, 138.44, 138.72, 159.21, 161.96, 162.21. m/z, 391 (M^+). HRMS (m/z): Calcd for $C_{26}H_{22}BNO_2$ 391.1744 found 391.1749.

N-(*p*-biphenyl)-salicylaldiminediphenylboron (IV-4)

^{1}H NMR ($CDCl_3$, δ): 6.80 (t, 1H), 7.0-7.5 (m, 22H), 8.39 (s, 1H). ^{13}C NMR ($CDCl_3$, δ): 118.23, 118.95, 120.20, 124.84, 126.42, 126.97, 126.99, 127.23, 127.81, 127.93, 128.85, 132.24, 133.66, 138.83, 139.49, 141.01, 144.60, 162.50, 162.63. m/z, 437 (M^+). HRMS (m/z): Calcd for $C_{31}H_{24}BNO$ 437.1951 found 437.1958.

N-(*p*-ferrocenylphenyl)-salicylaldiminediphenylboron (IV-5)

^{1}H NMR ($CDCl_3$, δ): 3.83 (s, 5H), 4.08 (t, 2H), 4.34 (t, 2H), 6.40 (t, 1H), 6.6-7.5 (m, 17H), 8.36 (s, 1H). ^{13}C NMR ($CDCl_3$, δ): 72.65, 118.27, 118.87, 120.17, 124.17, 126.02, 126.36, 126.92, 127.92, 128.31, 131.06, 132.14, 133.64, 134.69, 138.60, 139.89, 143.38, 162.12, 162.35. m/z, 545 (M^+). HRMS (m/z): Calcd for $C_{35}H_{28}BFeNO$ 545.1613 found 545.1632.

(1-Phenyl-2-perimidine)-salicylaldiminediphenylboron (IV-6)

^{1}H NMR ($CDCl_3$, δ): 6.0-6.2 (m, 2H), 6.63 (d, 1H), 6.6-7.60 (m, 21H), 7.79 (d, 1H). ^{13}C NMR ($CDCl_3$, δ): 107.22, 116.59, 117.32, 118.02, 120.68, 120.76, 121.81, 122.36, 126.00, 126.51, 127.01, 127.51, 128.07, 128.10, 129.47, 129.71, 130.77, 133.63, 133.78, 134.70, 135.33, 137.73, 139.74, 156.61, 162.89. m/z, 500 (M^+). HRMS (m/z): Calcd for $C_{35}H_{25}BN_2O$ 500.2060 found 500.2031.

4.3 Results and discussion

4.3.1 Synthesis of ligands and boron complexes

The general synthetic routes for the salicylaldimine ligands is presented in **Scheme 4.1**. In all cases the yields of these ligands was excellent and in the range of 90-95 %.

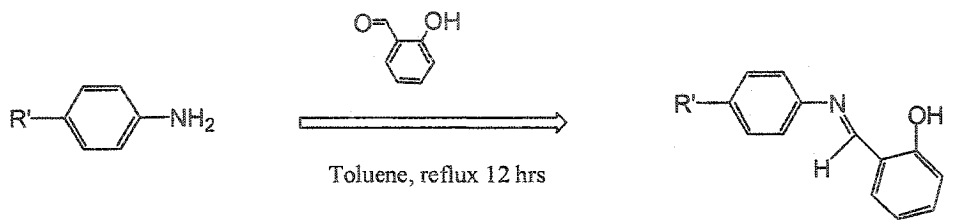

(Eq. 4.1)

R' = H, F (2), CH_3O (3), Ph (4), Cp_2Fe (5)

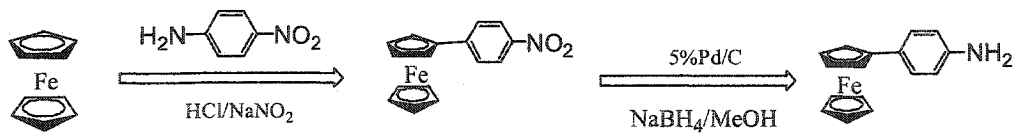

(Eq. 4. 2)

(2a)

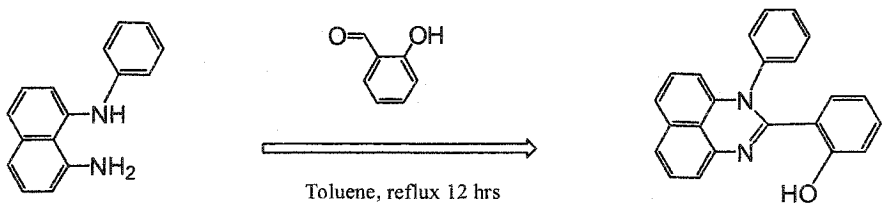

(Eq. 4.3)

Scheme 4.1 Synthesis of phenyl-substituted and perimidine-salicylaldimine ligands

Scheme 4.2 presents the synthetic route and molecular structures for the boron complexes that are reported in this chapter.

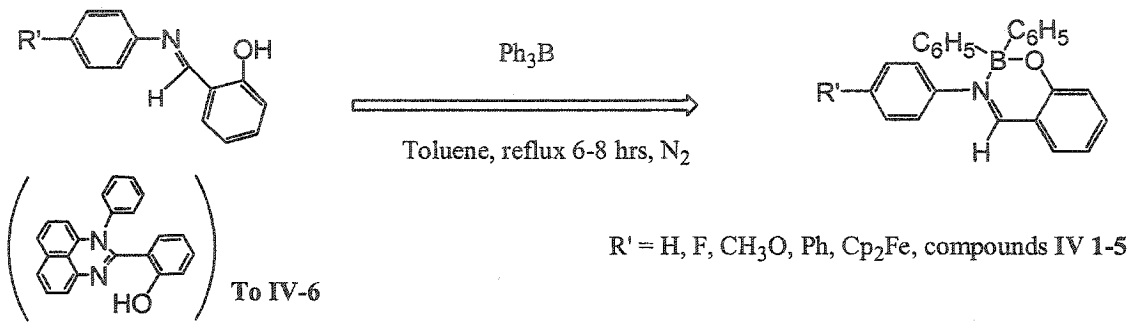

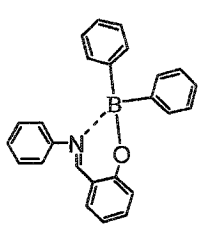

IV-1

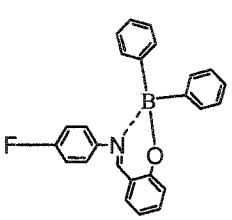

IV-2

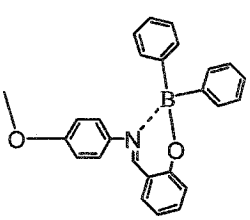

IV-3

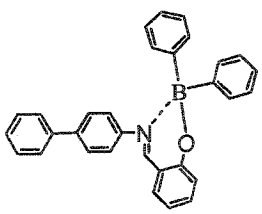

IV-4

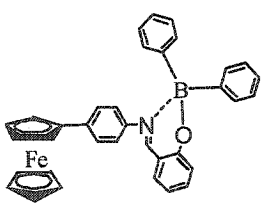

IV-5

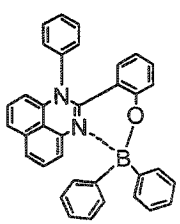

IV-6

Scheme 4.2 Synthetic route and molecular structures for boron complexes

4.3.2 Molecular structures and XRD data

Crystal of boron complex **IV-3** was obtained by dissolving the compound in CH_2Cl_2/Hexane mixture and settled in refrigerator overnight. **Figure 4.2** presents the molecular structure of **IV-3**, and **Table 4.1-2** list some selected XRD data. The XRD data demonstrated the proposed structure of synthesized compounds.

Figure 4.2 Molecular structure and atom numbering scheme for IV-3.

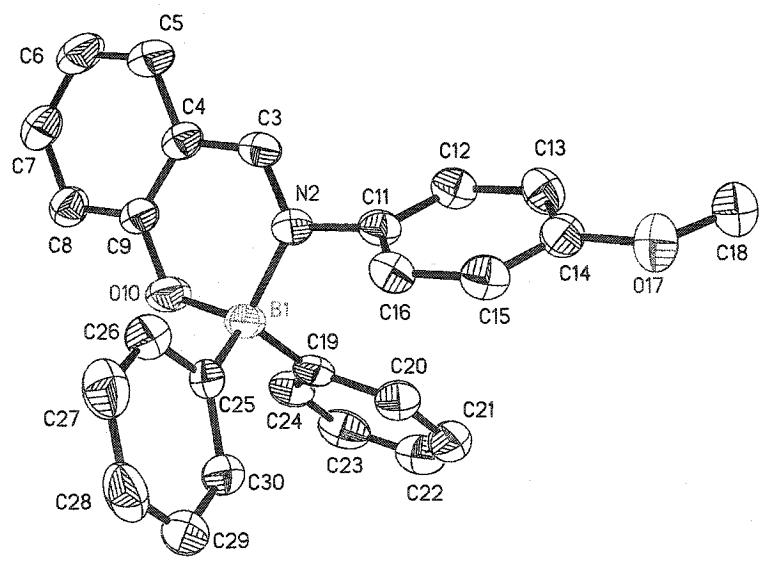

Table 4.1 Selected Crystal Data and Data Collection Parameters for IV-3.

Empirical formula	$C_{26}H_{22}BNO_2$
formula weight	391.26
T (K)	208(2) K
Wavelength (Å)	0.71073
Crystal system	Triclinic
Space group	P-1
a (Å)	8.941(4)
b (Å)	10.568(4)
c (Å)	12.144(5)
α (deg)	72.923(6)
β (deg)	83.943(6)
γ (deg)	71.383(6)
V ($Å^3$)	1039.4(7)
Z, Calculated density mg m^{-3}	2, 1.250
abs coeff (mm^{-1})	0.078
Final R indices	R1 = 0.0634, wR2 = 0.1519

Table 4.2. Selected Bond Distances and Angles for IV-3.

Bond Distances (Å)		Bond Angles (deg)	
B(1)-O(10)	1.505(4)	O(10)-B(1)-C(19)	109.5(2)
B(1)-C(19)	1.621(4)	O(10)-B(1)-C(25)	107.9(2)
B(1)-C(25)	1.622(4)	C(19)-B(1)-C(25)	115.4(2)
B(1)-N(2)	1.657(4)	O(10)-B(1)-N(2)	106.3(2)

4.3.3 Thermal properties

As previously discussed, knowledge of the thermal behavior of potential OLED materials provides information on suitability for amorphous phase formation and details on processability. DSC measurements were obtained for compounds **IV 1-6** and are shown in **Figures 4.3** and **4.4**. A summary of T_ms (obtained from the first heating step) and T_gs (obtained from the second heating step) are presented in **Table 4.3**.

Figure 4.3 presents several DSC measurement of compound **IV-1**. In the top portion of the figure is shown the data for a heating-cooling-reheating cycle employing a heating rate of 20 °C/min. In the first heating step the only observed thermal event is the melting of **IV-1** (T_m) at 154 °C. In the second heating step at 20 °C/min, a typical glass transition is observed at 47 °C (T_g). The fact that no transition is observed at T_m during this second heating step indicates that the heating rate was faster than the rate of crystallization of **1**. By heating at a slower rate of 3 °C/min (bottom portion of **Figure 4.3**), we are able to observe both the T_g at 47°C and T_m at 153 °C. Between T_g and T_m, there are indications of small peaks indicating that molecular reorganization is occurring.

All the other compounds (**IV 2-6**) showed T_ms in the first heating step at rate of 20 °C/min, which are presented in **Table 4.3** and in the second heating step at the same heating rate, compounds **IV-2** and **6** did not show T_ms. The second heating steps for these compounds are presented in **Figure 4.4**. This measurement provides T_g values for these five compounds.

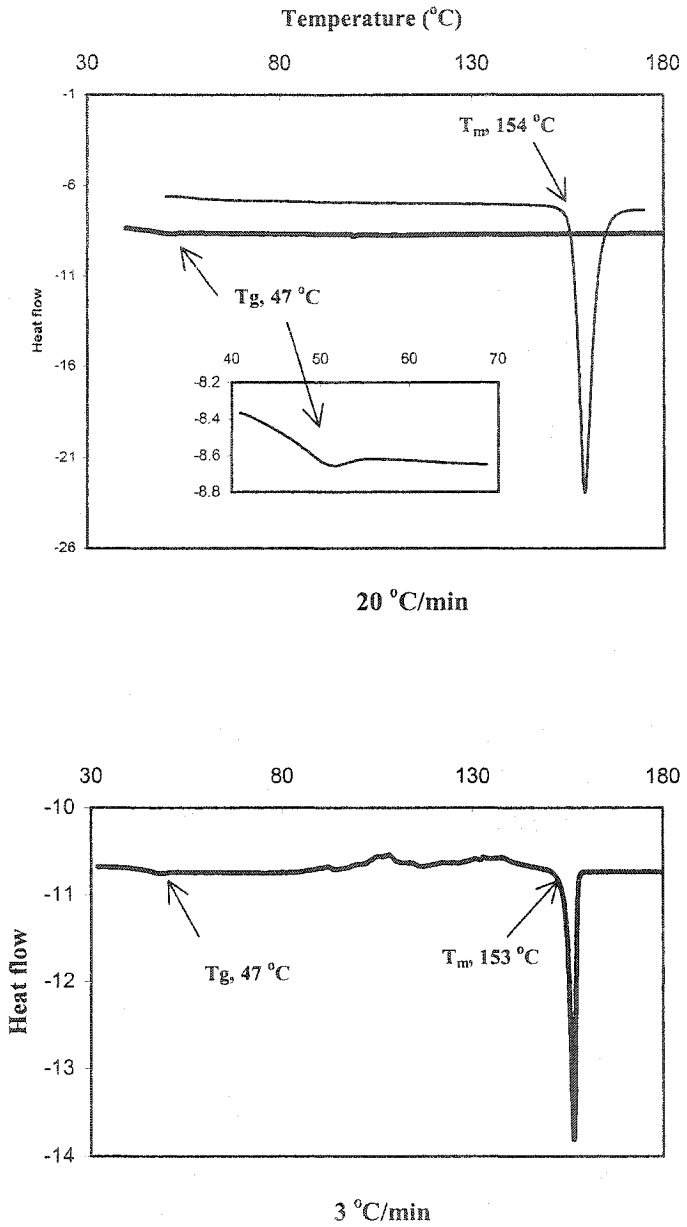

Figure 4.3 DSC traces of compound IV-1.

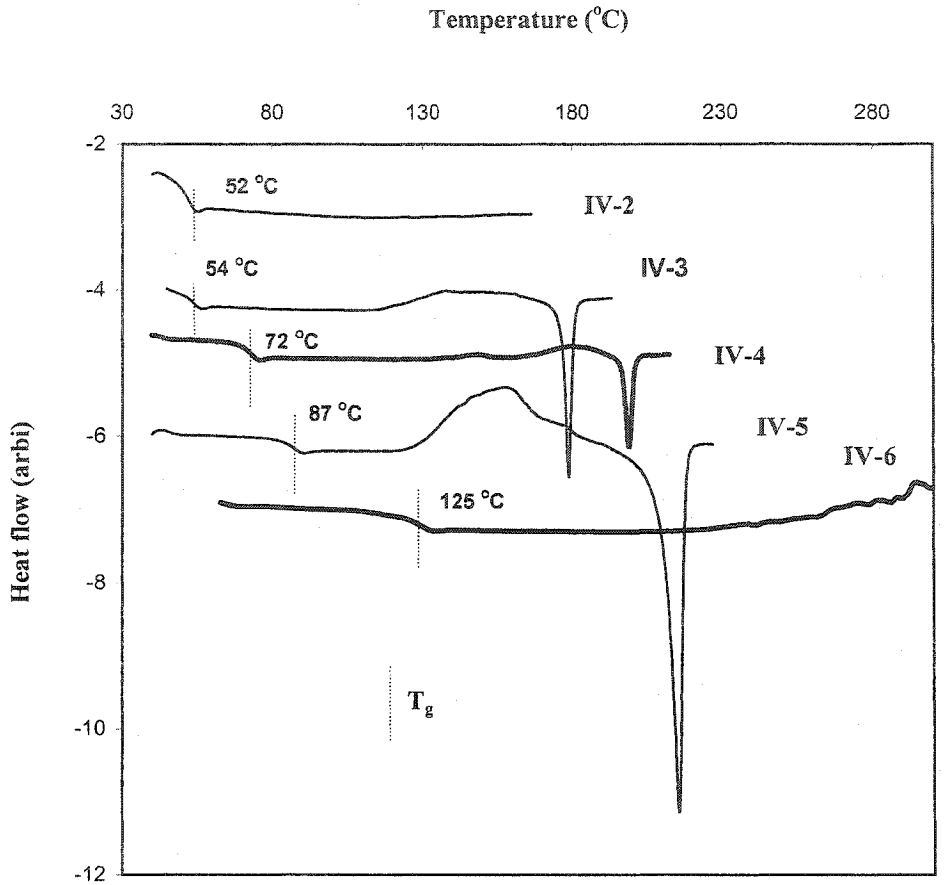

Figure 4.4. DSC traces of the second heating of boron complexes (IV 2-6) at scan rate of 20 °C/min for obtaining T_gs.

Entry	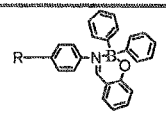 Boron complexes T_g/T_m (^0C)	Absorption λ (nm) CH_2Cl_2/ Toluene	Emission λ (nm) CH_2Cl_2/ Toluene	Energy gap[a] (nm/eV)	Stokes shift (nm)	Relative Φ_{PL} (Alq_3 = 1.00)	HOMO (eV)	LUMO (eV)
IV-1	49/154	400/403	513/518	461/2.69	113	0.37	5.66	2.91
IV-2	52/147	400/403	515/518	466/2.66	115	0.32	5.62	2.92
IV-3	54/174	402/401	514/517	466/2.66	112	0.66	5.58	2.88
IV-4	72/197	405/409	530/528	473/2.62	125	0.69	5.58	2.94
IV-5	87/207	407/NA	No emission	NA	NA	NA	NA	NA
IV-6	125/271	407/NA	No emission	NA	NA	NA	NA	NA

[a] Energy gaps were estimated from the intersection of normalized absorption and emission graph.
NA, not available

Table 4.3. Thermal, Spectroscopic data and HOMO-LUMO energy levels estimated by cyclic voltammetry.

Upon the different substituted phenyl salicylaldimine diphenyl boron complexes, T_ms increase in the order of 2 < 1 < 3 < 4< 5 and T_gs increases in the order of as the entry number 1 < 2 < 3 < 4< 5. The increasing T_ms suggest an increase for intermolecular interactions while the increasing T_gs are consistent with that the bulkier and more rigid structures have higher T_gs.[22] The drop in T_m going from compound **IV-1** to **2** is similar to what have been observed with C-4 substituted Alq_3 compounds reported in **Chapter 3,** in which F-substituted C-4 $PAlq_3$ derivatives exhibited 20 °C less decomposition temperature than the compound with substituents on phenyl. The reason could be in that the high negativity of fluorine will change the dipolar moment of the fluorine-substituted phenyl ring, which result in the decrease of intermolecular interaction. The high T_gs of the compound **IV-4** (74 °C), **IV-5** (90 °C) and **IV-6** (135 °C) suggest that the bulkier aromatic (phenyl) or ferrocene substituents and more rigid ligand will help to improve the thermal stability of the boron complexes. These results are similar to those in **Chapter 2** where the addition of aromatic groups as substituents led to increases in the T_gs.

4.3.4 Photophysical properties

The photophysical properties of boron complexes are the feature that makes them most interesting for OLED applications. It is well known for Alq_3[2, 22(b)] and we saw in **Chapter 3** that the optical transitions centered on the organic ligand played the main role for the photoluminescent of Al complexes. Specifically, in Alq_3 the electronic transition between the electron rich phenoxide ring (HOMO) and the electron deficient pyridyl ring (LUMO) is responsible for the absorption (HOMO (π)→ LUMO (π^*)) and emission

(LUMO (π^*)→HOMO (π)) spectra. In Wang's pyridyl-indole boron complex (BPh_2(2-PI)) (**Figure 4.1**, **4d**)[5d], the electron rich indole moiety has been confirmed by both the experimental results and *ab initio* molecular orbital calculations to be the site where the HOMO is localized, while the LUMO resides mostly on the electron deficient pyridyl ring. Similarly, when considering the salicylaldimine ligand employed in this work, it is reasonable to deduce that the electron rich phenoxide ring can be regarded as the location of HOMO, while phenylimine portion of the ligand is the site of LUMO. This assumption is corresponding to the absorption and emission data in this work, and can be further confirmed by the cyclic voltammetry (CV) experiments that will be discussed in the next section.

In **Fig. 4.5**, the UV-vis absorption spectra of the free ligands (**2-5**) and boron complexes **IV 2-5** are presented. Deprotonation and coordination of the ligand to the diphenyl boron leads to a systematic bathochromic shift of the UV-vis absorption of the ligands.[10] All the compounds have a similar absorption maximum (λ_{max}) between 400-407 nm. Compound **IV-5** with a ferrocenylphenyl substituent displays an additional broad absorption shoulder between 475 – 515 nm, which were ascribed to the electronic transition within Cp_2Fe-Ph group. The appearance of similar absorption maxima values for these compounds indicates that there is little effect of the phenyl substituents (F, OCH_3, Ph) on the electronic transition associated with the absorption (HOMO (π) to LUMO (π^*)). The influence of solvent polarity on the λ_{max} values is shown in **Figure 4.6** where the UV-vis absorption spectra for compounds **IV-1**, **3** and **4** are measured in toluene and in dichloromethane. The small differences between the two solvents indicate that these compounds are not very polar.

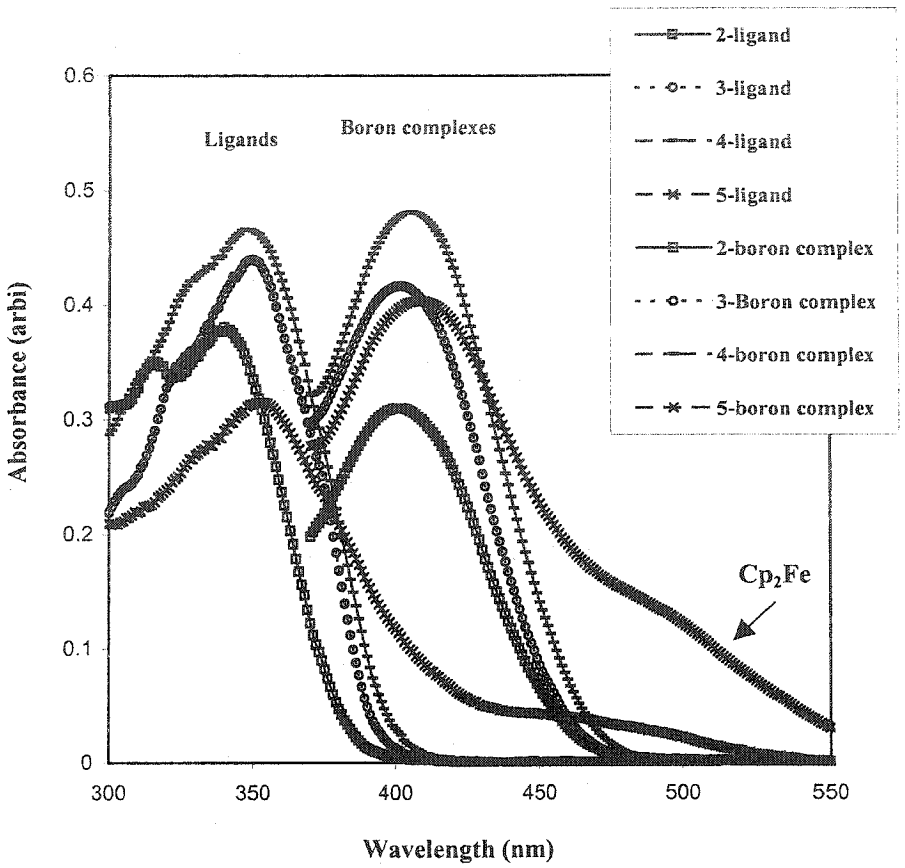

Figure 4.5 UV-absorption spectra for ligands (2-5) and boron complexes (IV 2-5) in CH_2Cl_2. All solutions were prepared in $1x10^{-4}$ M.

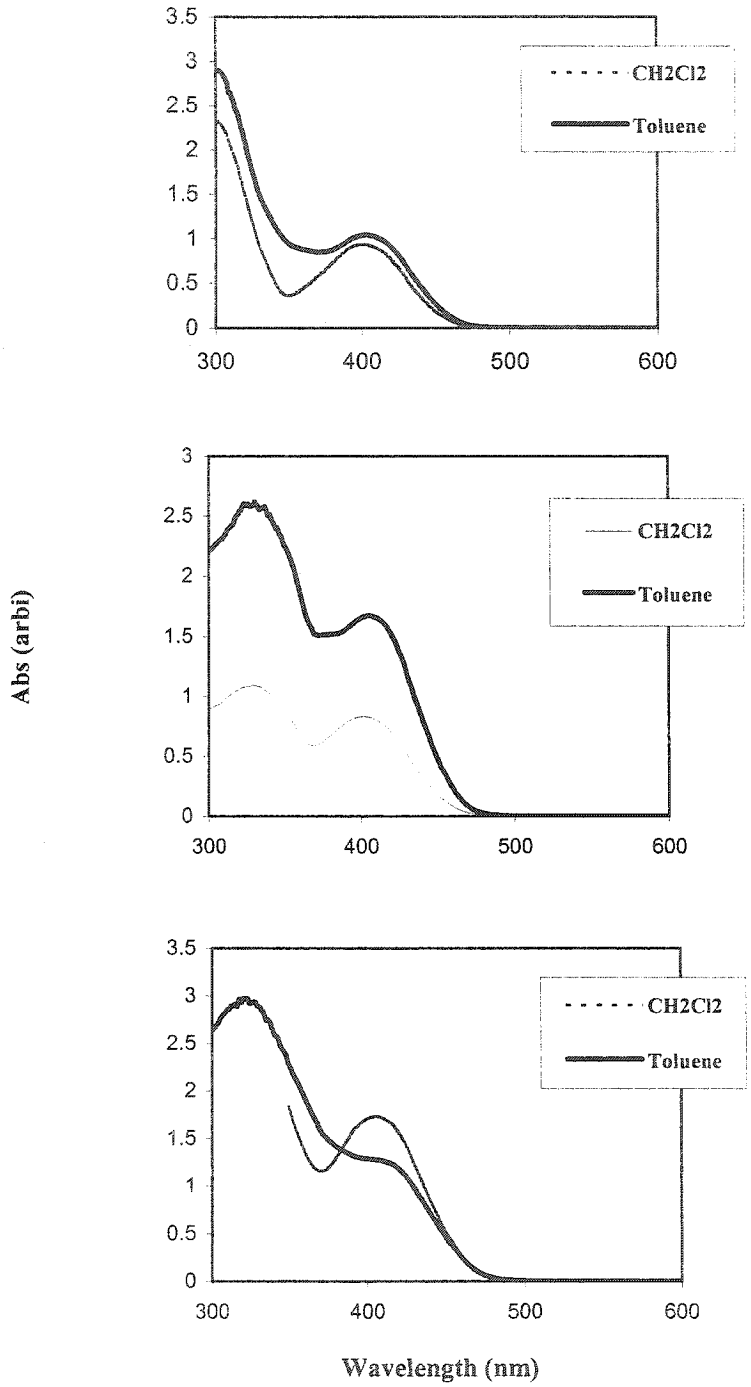

Figure 4.6 UV-absorption spectra for boron complexes (IV-1, up; IV-3, middle; IV-4 bottom) in CH_2Cl_2 and toluene ($1x10^{-4}$M).

The emission and absorption spectra of the boron complexes **IV 1-5** were shown in **Figure 4.7** and summarized in **Table 4.3**. The emission λ_{emi} values for compounds **IV-2** and **3** are also very close to compound **IV-1** (the differences are 2nm and 1nm respectively), while compound **IV-4** shows ca. 15 nm bathochromic-shift comparing to compound **IV-1**. It has been demonstrated that an electron-withdrawing substituent will cause a bathochromic shift when it is directly interacting with the LUMO of a complex and the appearance of this shift in **IV-4** supports the supposition that the LUMO is localized on the imine portion of the ligand.[2] It was also shown in **Chapter 3** that an electron-withdrawing phenyl group on the C-4 position of the pyridyl ring of Alq_3 can lead to a bathochromic shift presumably by stabilizing the LUMO. Thus in the work in this chapter, it is reasonable to deduce that the electron-withdrawing phenyl caused bathochromic-shift. Since a phenyl group bridged between (C=N) imine and substituents, this bathochromic-shift value is very small. This phenyl separation may be the reason that compounds **IV 1-3** have the close λ_{emi} values. When it comes to the non-aromatic substituents (F and OCH_3) that were supposed to cause hypsochromic-shift because of their electron-donating properties in my initial synthetic design, the electronic-effect have come very faint after a phenyl bridge.

The PL efficiencies (Φ_{PL}) for the compounds **IV 1-6** were measured in both the dichloromethane and toluene and compared with Alq_3 in dichloromethane. Higher quantum yields were observed for compounds **IV-3** and **4** than for compounds **IV-1** and **2**. The results show that the bulkier and more rigid structures of compounds **IV-3** and **4** relative to **IV-1** and **2** will increase Φ_{PL} of the compounds and this should be helpful for the future synthetic effort when a boron complex with better performance is desired.

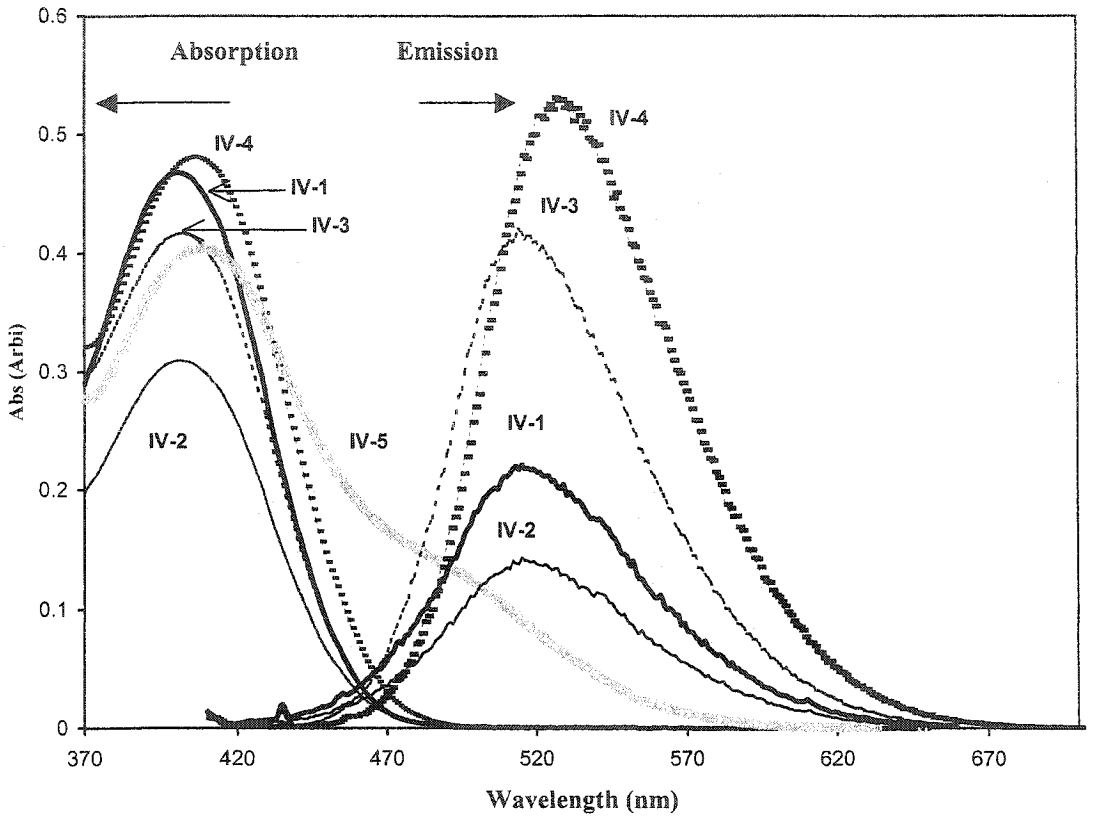

Figure 4.7 Absorption (IV 1-5) and emission (IV 1-4) spectra of boron complexes in CH_2Cl_2. Absorption spectra were collected in $1x10^{-4}$M solution and emission spectra were measured in diluted solution by controlling the absorbance between 0.03 to 0.1.

It was not unexpected that compound **IV-5** did not show detectable quantum yield since the ferrocene is known to be an efficient quencher of triplet states. The lack of emission for compound **IV-6** is apparently correlated to the parent perimidine structure of the ligand. More discussion on this point is presented in **Chapter 5**. Overall, the reasonable Φ_{PL}, especially for compounds **IV-3** and **4** indicates the promising candidates of these salicylaldimine diphenyl boron complexes as potential EL materials.

4.3.5 Electrochemistry

Unlike Alq_3 that is used as both an electron transport and an emitting material in OLEDs, so far, most boron complexes have only been reported to function as emitting materials.[5b,6-11] Devices that employ boron emission materials must have an ET layer that interfaces with the boron emitting layer. As a result, suitable matching of the HOMO/LUMO energy levels between these two material materials is required for efficient device operation (see **Figure. 1.2).** Since Alq_3 has been the most frequently used ET material with boron emitting layers, in this work the HOMO/LUMO of salicylaldimine diphenyl boron complexes will be compared with those of Alq_3.

Again the HOMO energy levels were estimated using the electrochemical method that we have previously described and that has been reported in the literature.[24-27] CV measurements of the boron complexes **IV 1-6** were carried out as pure materials and then repeated with Cp_2Fe as an internal standard.

For complexes **IV 1-5**, two irreversible oxidation peaks in CH_2Cl_2 solution were observed as shown in **Figure 4.8-4.10**. As can be seen from the CVs of these compounds,

they had quite similar behavior to Alq_3 and the Alq_3 analogues reported in **Chapter 3** in that there were no reduction peaks at positive scan range. Unlike Alq_3, they presented more reproducible CVs and there were no adverse interaction/reaction between Cp_2Fe at different scan potential range. For example CVs of the compound **IV-1** in **Figure 4.8**, two oxidation peaks of boron complex at positive scan region remained the same at three different conditions: (**A**) 0 - +1.8 V; (**B**) –1.8 V - +1.8 V and (**C**) after adding Cp_2Fe. The CVs of other compounds (**IV 2-4**) presented the similar behaviors and CVs of compound **IV-2** and **3** are shown in **Figure 4.9**. Since compound **IV-5** already has ferrocenyl group in the structure, its CV was carried with adding internal reference (Cp_2Fe) and shown in **Figure 4.10**. This compound exhibited unstable CV compared to compounds **IV 1-4**. With the potential scan continued, the oxidation peaks boron complex and reduction peak of ferrocenyl were disappeared (**D**). However, when potential scan was controlled at redox region of Cp_2Fe, reversible redox peaks of Cp_2Fe stayed (**E**). This observation suggests that there were intramolecular interactions occurring in the case of compound **IV-5** at high potential scan. The CVs at different conditions of compound **IV-6** shown in **Figure 4.11** suggested that this perimidine-containing boron complex had the similar electrochemical properties to those of compounds **IV 1-4**.

The results from these electrochemical studies are summarized in the HOMO values reported in **Table 4.3.** Since there were no emission spectra obtained for compound **IV-5** and **6**, the energy levels of these two compounds were not included the discussion. The values for the LUMO energy levels in **Table 4.1** were calculated by subtracting the energy gap obtained from the UV-vis measurements from this HOMO value.

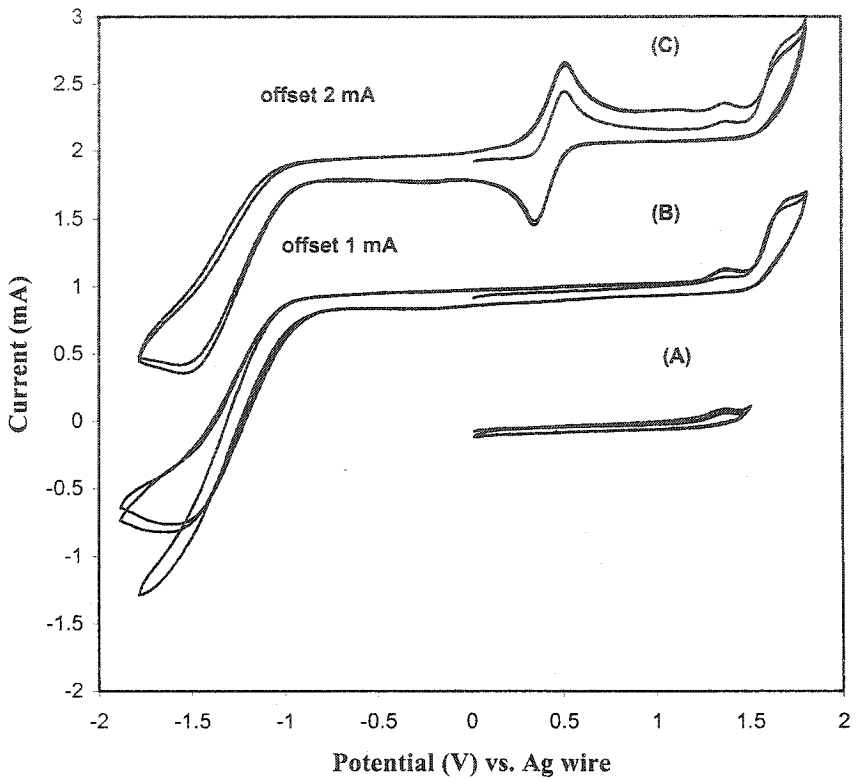

Figure 4.8 CVs of compound IV-1 at 100 mV/s in 0.1 M TBAHP CH_2Cl_2. Three cycles recorded. (A) 0 - +1.8 V; (B) –1.8 V - +1.8 V and (C) after adding Cp_2Fe.

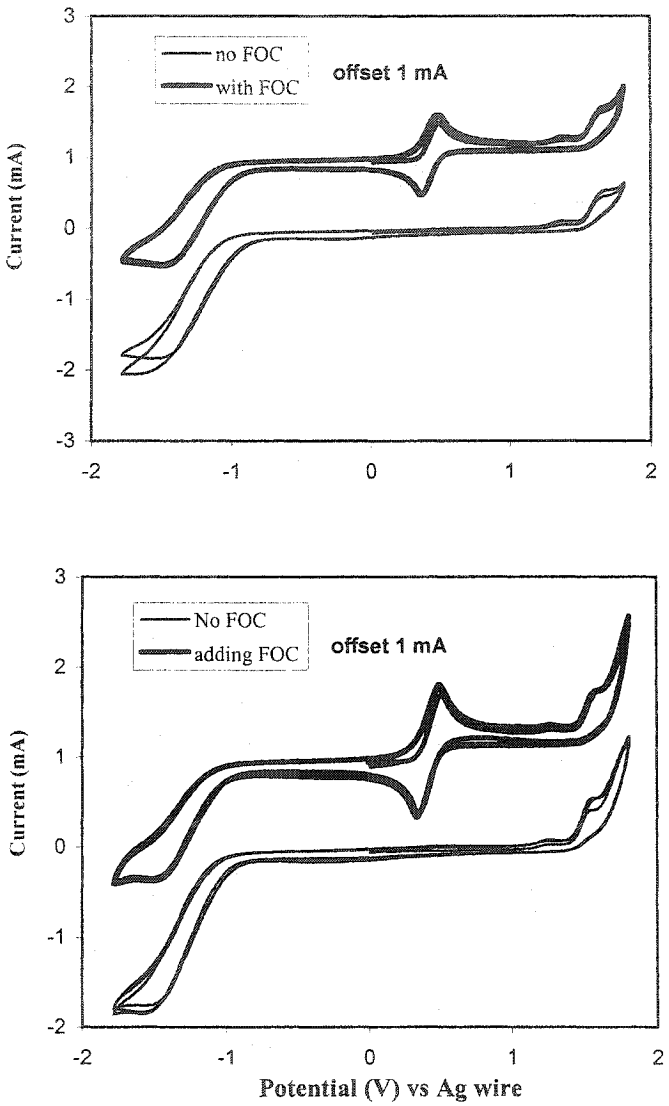

Figure 4.9 CVs of compounds IV-2 and 3 at 100 mV/s in 0.1 M TBAHP CH_2Cl_2. Three cycles recorded.

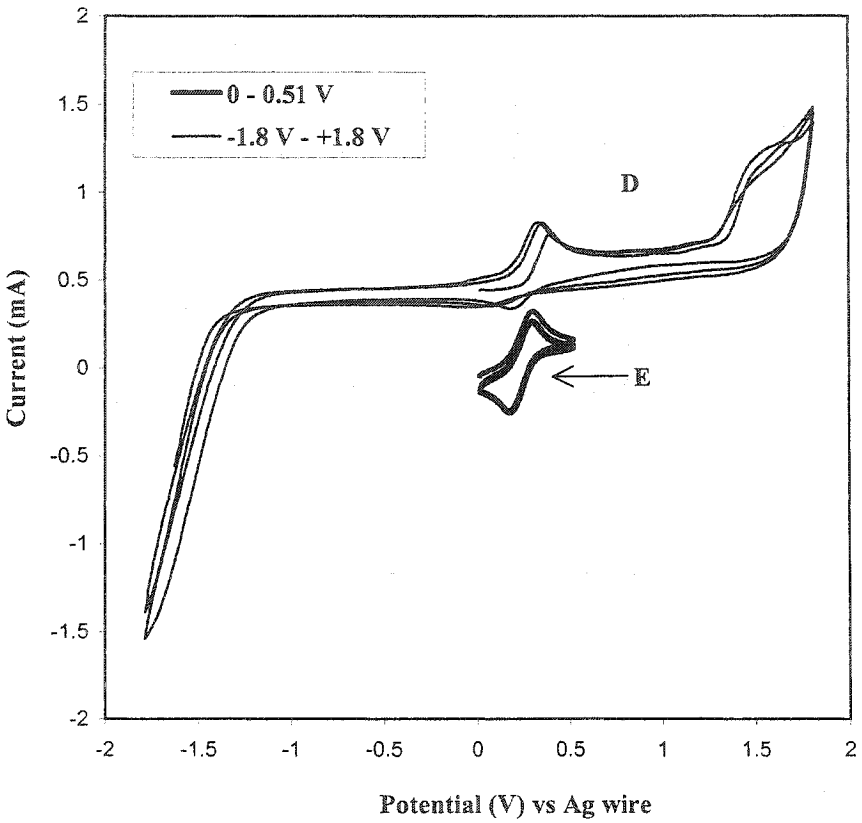

Figure 4.10 CVs of compound IV-5 at 100 mV/s in 0.1 M TBAHP CH_2Cl_2. Three cycles recorded.

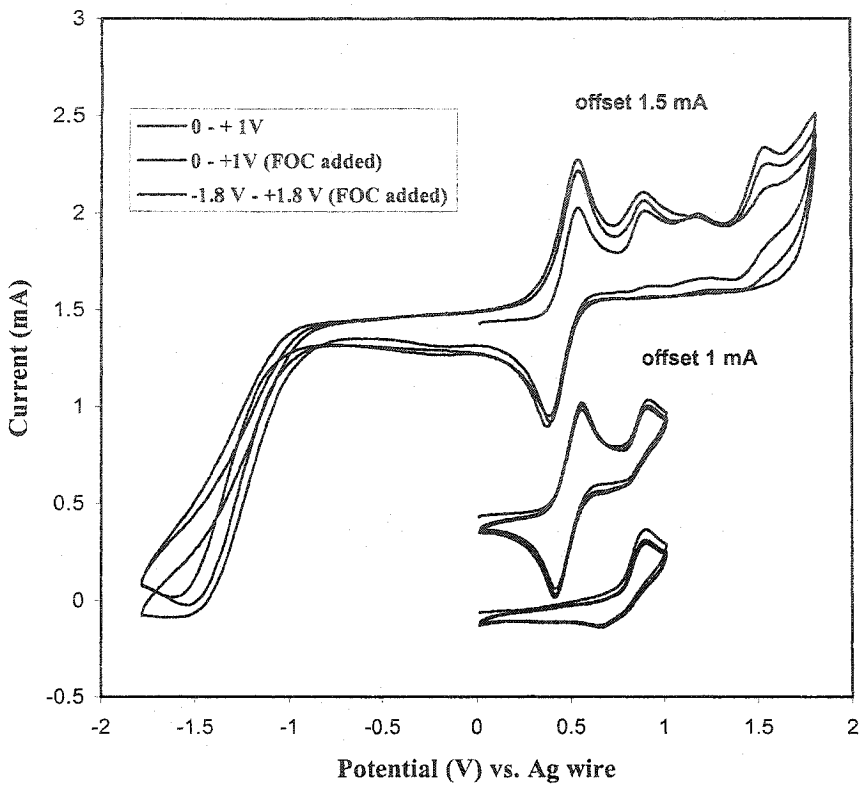

Figure 4.11 CVs of compound IV-6 at 100 mV/s in 0.1 M TBAHP CH_2Cl_2. Three cycles recorded.

Overall the energy gaps observed for boron complexes **IV 1-4** are quite similar and suggest that there are only minor effects for substitutions on the N-phenyl group. Like Alq_3, the boron compounds **IV 1-4** are green light emitters. For comparison the HOMO and LUMO values of Alq_3 obtained by this same method in **Chapter 3** were 5.47 eV and 2.67 eV respectively. The fact that the boron compounds possess higher HOMO and LUMO energies than Alq_3 means that a multilayer device that would employ compounds **IV 1-4** as EM and ET layer would block holes more efficient from HT layer and have less energy barrier for charge injection from cathode to into this layer.

4.4. Conclusions

Salicylaldimine diphenyl boron complexes derivatized at para-position position of phenyl with F, OCH_3, phenyl and ferrocenyl, and a structure of perimidine-containing boron complex have been prepared and characterized. Thermal analysis indicates that the bulkier substituents and incorporate the imine function in the ring-structured ligand will improve the T_gs of these boron complexes. All these compounds show absorption λ_{max} at *ca.* 400 nm and emission λ_{emi} (for compounds **IV 1-4** only) in green light region (515 nm). Phenyl substituted compound (**IV-4**) had a slightly bathochromic-shift (15 nm) in emission spectra compared to other compounds (**IV 1-3**). The PL efficiency comparing to Alq_3 suggest that these boron complexes are good candidates for EL application and the high HOMO and LUMO energy levels will give good instruction to fabricate a device in the future work.

References for Chapter 4:

(1) Tang, C. W.; VanSlyke, S. A. *Appl. Phys. Lett.* **1987**, *51*, 913-915.

(2) Chen, C. H.; Shi, J. *Coord. Chem. Rev.* **1998**, *171*, 161. references therein.

(3) Pohl, R.; Montes, V. A.; Shinar, J.; Anzenbacher Jr., P. *J. Org. Chem.* **2004**, *69*, 1723-1725.

(4) Hung, L. S.; Chen, C. H. *Mater. Sci. Engineer.* **2002**, *R 39*, 143-222. References therein.

(5) References selected from Wang's group: (a) Wu, Q.; Esteghamatian, Hu, N.; Popovic, Z.; Enright, G.; Breeze, S. R.; Wang, S. *Angew. Chem. Int. Ed. Engl.* **1999**, *38*, 985-988. (b) Wu, Q.; Esteghamatian, M.; Hu, N.; Popovic, Z.; Enright, G.; Tao, Y.; D'Iorio, M.; Wang, S. *Chem. Mater.* **2000**, *12*, 79-83. (c) Liu, S.; Wu, Q.; Schmider, H. L.; Aziz, H.; Hu, N.; Popovic, A.; Wang, S. *J. Am. Chem. Soc.* **2000**, *122*, 3671-3678. (d) Liu, Q.; Mudadu, M. S.; Schmider, H.; Thummel, R.; Tao, Y.; Wang, S. *Organometallics* **2002**, *21*, 4743-4749.

(6) Anderson, S.; Weaver, M. S.; Hudson, A. J. *Synth. Met.* **2000**, *111-112*, 459-463.

(7) (a) Tao, X. T.; Suzuki, H.; Wada, T.; Miyata, S.; Sasabe, H. *J. Am. Chem. Soc.* **1999**, *121*, 9447-9448. (b) Tao, X. T.; Suzuki, H.; Wada, T.; Sasabe, H.; Miyata, S. Appl. Phys. Lett. **1999**, *75*, 1655-1657.

(8) Li, Y.; Liu, Y.; Bu, W.; Guo, J.; Wang, Y. *Chem. Commun.* **2000**, 1551.

(9) Lim, H. J.; Kim, S. M.; Lee, S.; Jung, S.; Kim, Y. K.; Ha, Y. *Optical Materials* **2002**, *21*, 211.

(10) Middleton, A. J.; Marshall, W. J.; Radu, N. S.; *J. Am. Chem. Soc.* **2003**, *125*, 880.

(11) Hohaus, E.; *Monatsh. Chem.* **1980**, *111*, 863.

(12) Hohaus, E.; *Z. anorg. Allg. Chem.* **1982**, *484*, 41.

(13) Hohaus, E.; *Z. anorg. Allg. Chem.* **1983**, *506*, 185.

(14) Berg, E. W.; Herrera, N. M. *Anal. Chim. Acta.* **1972**, *60*, 117.

(15) Prasad, R. N.; Tandon, J. P. *Z. Naturforsch.* **1973**, *28*, 153.

(16) Chaturvedi, K. K.; Singh, R. V.; Tandon, J. P.; *Indian. J. Chem.* **1986**, *25A*, 774.

(17) Goyal, M.; Mishra, S.; Singh, A.; *Main Group Metal Chemistry* **2001**, *24*, 829.

(18) Redshaw, C.; Elsegood, M. R. J. *Chem. Commun.* **2001**, 2016.

(19) Cameron, P. A.; Gibson, V. C.; Redshaw, C.; Segal, J. A.; Solan, G. A.; White, A. J. P.; Williams, D. J.; *J. Chem. Soc., Dalton Trans.*, **2001**, 1472.

(20) Wei, P.; Atwood, D.; *Chem. Commun.* **1997**, 1427.

(21) Lanez, T.; Pauson, P. L. *J. Chem. Soc. Perkin. Trans.* **1990**, *1*, 2437-2442.

(22) (a) Naito, K.; Miura, A. *J. Phys. Chem.* **1993**, *97*, 6240-6248. (b) Sapochak, L. S.; Padmaperuma, A.; Washton, N.; Endrino, F.; Schmett, G. T.; Marshall, J.; Fogarty, D.; Burrows, P. E.; Forrest, S. R. *J. Am. Chem. Soc.* **2001**, *123*, 6300-6307.

(23) Lees, A. J. *Chem. Rev.* **1987**, *87*, 711-743.

(24) Bridgleb, G.; *Angew. Chem., Int. Ed. Engl.* **1964**, *3*, 617.

(25) Kuder, J. E.; Gibson, H. W.; Wychick, D. *J. Org. Chem.* **1975**, *40*, 875.

(26) Pommerehne, J.; Vestweber, H.; Guss, W.; Mahrt, R. F.; Bassler, H.; Porsch, M.; Daub, J. *Adv. Mater*, **1995**, *7*, 551-554.

(27) Thelakkat, M.; Schmidt, H. W. *Adv. Mater.* **1998**, *10*, 219-223.

Chapter 5

Heterocycles Based on 1-Phenyl-Perimidine Chromophores. Thermal, Photophysical and Electrochemical Studies

5.1 Introduction

5.1.1 Heterocycles in organic light-emitting diodes

As was pointed out in **section 1.2,** in a typical two-layer OLED hole mobility in the hole transport (HT) layer is much faster than electron mobility in the ET layer, so the recombination of holes and electrons will usually occur in the ET layer. When the ET layer is also the emission layer, this difference in mobility leads to an accumulation of holes within the ET layer. This can result in quenching in the ET layer and electron trapping near the cathode which will in turn decrease the operational stability and device efficiency. This has been demonstrated when using Alq_3 as both ET and EM materials in OLED.[1] One method to address this issue has been to employ low molecular weight heterocycles in multilayer OLEDs with the aim of providing additional electron injection/transport and a hole-blocking layers. **Figure 5.1** presents two examples of typical π-electron deficient heterocycles (TPBI and PBD) that have been used for this

purpose and some examples of basic π-electron deficient aromatic rings that could be incorporated into heterocycles with for the same goals.[2]

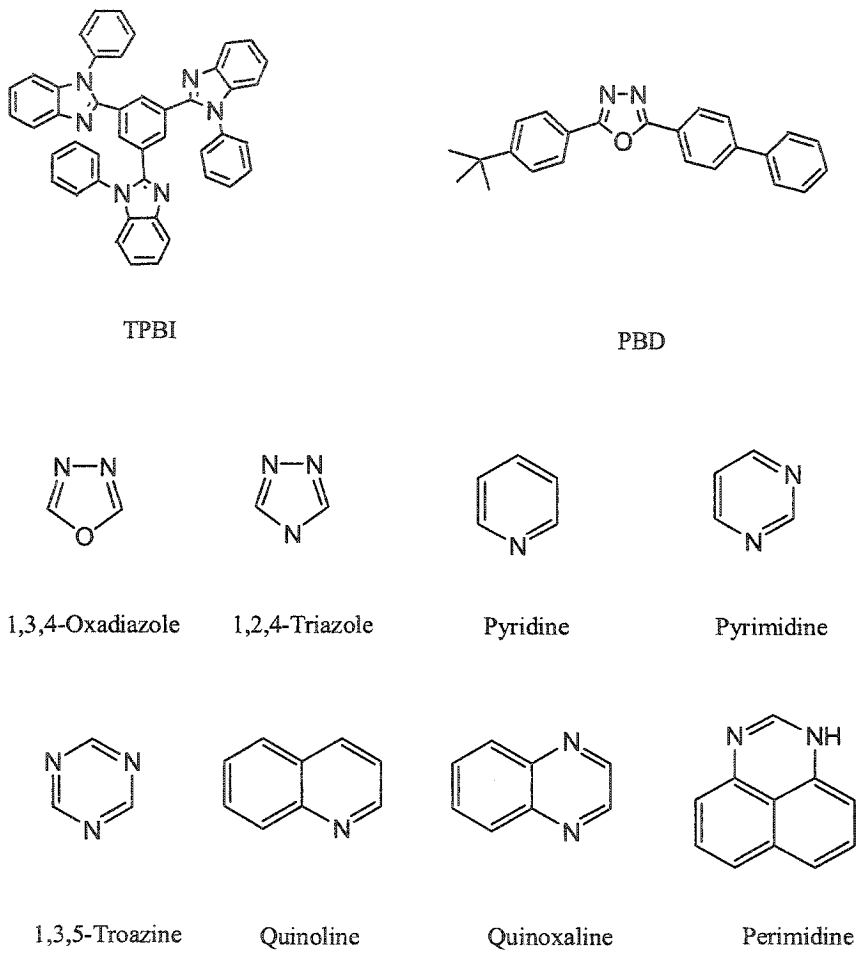

Figure 5.1. Examples of π-electron deficient aromatic rings incorporated into heterocycles

Specifically, 2-(4-biphenyl)-5-(4-*t*-butylphenyl)-1,3,4-oxadiazole (PBD) has a 1,3,4-oxadiazole unit and 2,2′,2″-(benzene-1,3,5-triyl)-tris(1-phenyl-1H-benzimidazole) (TPBI) has the benzimidazole moiety. These two species are probably the most widely employed heterocyclic compounds in OLEDs. Each of them possesses a nitrogen/oxygen

containing π-electron deficient aromatic ring. Adachi *et al.* were the first research group to use oxadiazoles in OLEDs.[3] In their work, PBD was used as ET and hole blocking layer, and an additional emission material deposited between HT and ET layer was used as the emission layer. TPBI was developed by the group in Kodak in the later 90s[4] and has been used in OLEDs mainly in two ways. One way is to use TPBI as the ET layer and the host for fluorescent dopants which provide the source of emission[5] and the other way is to use TPBI as the ET layer and employing an HT layer or an additional layer for emission.[6]

Since PBD is a crystalline material, it lacks stability in an OLED operation, especially at higher temperature. To overcome this problem, many attempts have been tried to synthesize spiro[7], dimer[8], starburst[9] derivatives of PBD or to incorporate the oxadiazole moiety in a polymer as either a side group[10] or in the main chain.[11] The key step in the synthesis of oxadiazole containing materials is a ring closure dehydration reaction of bishydrazides using strong acids such as $POCl_3$. For example the PBD can be synthesized starting from the commercial available reagents, 4-butylbenzoic acid and 4-biphenylcarbonyl chloride and the route is depicted in **Scheme 5.1 (Route 1)**.[2, 7-11]

Compared to the variety of oxadiazole-containing heterocyclics that have been examined, only the parent TPBI has been examined for use in OLEDs.[4,5,11] The synthetic route to TPBI according to the patent is generalized in **Scheme 5.1 (Route 2)**.[4]

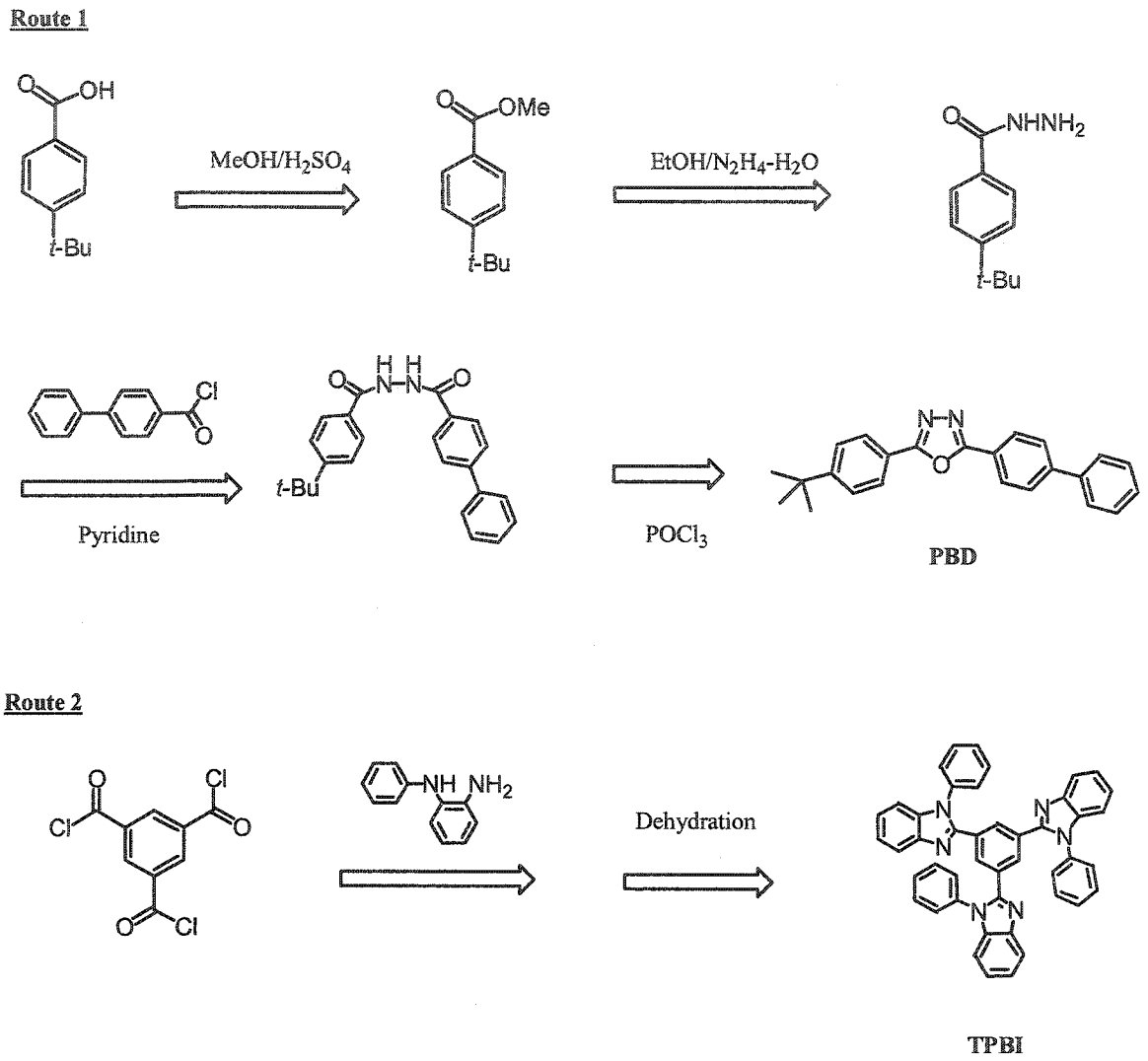

Scheme 5.1 Synthetic routes to PBD and TPBI

In addition to the oxadiazole-containing heterocyclic species and TPBI, triazole, triazine and quinoxaline-containing compounds have been used for OLEDs, and further references to these materials can be found in reference 2. It appears that heterocyclic compounds will continue contributing for OLED development and will provide additional balance and flexibility for the materials with various electronic properties.

5.1.2 Objectives of this chapter

Given the effort that has been focused on heterocyclic species, and oxadiazole in particular, in OLED technology it is a bit surprising that there are so few reports for the application of TPBI and its analogues in this regard. Furthermore, there has been little reported on the basic thermal, photophysical and electrochemical characterization of TPBI. Part of the reason for this apparent omission may be due to the fact that the patent on TPBI is still valid. On the other hand, some related species, 1,4-di(phenyl-2-benzimidazoly)-benzene (DPBI1) and 4,4'-di(phenyl-2-benzimidazoly)-bi-phenyl (DPBI2) have been reported.[12,13] One interesting piece of reported information on TPBI is that it emits blue light at 458 nm (HOMO-LUMO = 6.2 – 2.7 eV).[12] The use of TPBI as hole-blocking material is based on its high HOMO stability. This yields a large barrier (almost 1 eV compared to most HT materials) that will prevent holes from moving into the ET layer. As a result recombination of electrons and hole can be localized in an emission layer other than ET layer.

This chapter reports the synthesis and characterization of a new heterocyclic set of compounds that take their inspiration from the TPBI type heterocycles. Our group has been developing the chemistry of perimidine-based systems and we have noted the analogy of these species with benzimidazoles. This chapter begins with the proposal that replacing the benzimidazole moieties in TPBI and analogues with perimidines might lead to novel materials with application to OLEDs. Therefore, compounds with one, two and three perimidine groups on a phenyl ring were targeted and prepared. Furthermore, the phenyl core has been replaced by other heterocyclic aromatics such a pyridine and

thiophene. The thermal, photophysical and electrochemical properties of these compounds were then investigated and are reported.

5.2 Experimental

General information. All reagents, 1,8-diaminonaphthalene, iodobenzene, benzaldehyde, terephthalaldehyde, isophthalaldehyde, 2,6-pyridinedimethanol, 2,5-thiophenedicarboxaldehyde, 1,3,5-benzenetricarboxylic acid, lithium aluminum hydride, manganese(IV) oxide, pyridinum chlorochromate, copper powder, potassium carbonate and 5% Pd/C were obtained from Aldrich Chemical Company and used without further purification. THF, toluene and ether were purified by passage through a column of activated alumina using an apparatus purchased from Anhydrous Engineering. All other solvents, diphenyl ether, xylenes, ethylene dichloride, dichloromethane, ethylacetate and chloroform were used without further purification. Differential scanning calorimeter (DSC), UV-vis, steady-state fluorescence spectroscopy, cyclic voltammetry (CV) and other experimental and characterization information are described in **Section 2.2**. The detailed synthetic procedures are described in the following sections.

Synthesis of 1-Amino-8-(phenylamino)naphthalene

The known compound was synthesized according to the ref. 17 with the following minor modifications. 1,8-Diaminonaphthalene (5g) and iodobenzene (15g) in molar ratio around 1:3, 2g copper, 2g potassium carbonate, a trace of iodine and 20 ml phenyl ether were added successively in a 100 ml flask. The mixture was heated at reflux under

nitrogen for 2 days. On cooling, the diphenyl ether was removed by distillation. The solid residue was collected by filtration and washed with dichloromethane (*ca.* 300 mL) to remove the copper and potassium salts till the filtrate became the colorless. After vacuum evaporation of the solvent, the solid crude product was washed with cooled hexane and cooled ethanol, and purified by column chromatograph with an eluent of 3:1 CH_2Cl_2/Hexane. A pale pink product was obtained (yield 50%).

General procedure for the synthesis of mono-perimidine (V-1) and di-perimidine compounds (V-2)

Scheme 5.2 and **5.3** summarize the synthetic routes to **V-1** and **V 2-5**. **V-1** can be synthesized through either **Route 1** or **Route 2** in **Scheme 5.2**. **V 2-5** were synthesized according to the **Route 4** shown in **Scheme 5.2** by reacting 1-amino-8-(phenylamino)naphthalene with corresponding dialdehydes. 1-Amino-8-(phenylamino)naphthalene and corresponding dialdehyde (2.2:1), 10% weight of 5% Pd/C were added in Schlenk flask and the mixture was refluxed in xylene under nitrogen overnight. On cooling and filtration, the crude product was purified by chromatrography using CH_2Cl_2 as the eluent.

1,2-Diphenyl-perimidine (V-1)

Route 1. In a 250 mL Schlenk flask diaminonaphthalene and benzaldehyde were added in a molar ratio of 1/1.2. To this mixture, 5%Pd/C was added in 10% weight of reagents and the mixture was refluxed in xylene under nitrogen overnight. On cooling

and filtration, the crude product 2-phenyl-perimidine was washed with hexane and dried and used directly in the next step. 2-Phenyl-perimidine and bromobenzene in a molar ratio of 1/1.2 were added to an oven dried Schlenk flask and nitrogen was bubbled through the solution. To this mixture was added the toluene, Na-*t*-O-Bu, and Pd/BINAP catalysts (note: this procedure is similar to that described in **Section 2.2**). The mixture was heated to reflux overnight. The reaction was cooled to room temperature, filtered and concentrated by vacuum evaporator. This crude product was purified by column chromatograph using an eluent of CH_2Cl_2/EtOAC (4:1). (yield ~ 70%).

Route 2. 1-Amino-8-(phenylamino)naphthalene and benzaldehyde (1.2:1) along with 10 weight percent of 5% Pd/C were mixed in a Schlenk flask and the mixture was heated to reflux in xylene under nitrogen overnight. The reaction was cooled to room temperature, filtered and the crude product was purified by column chromatrography using an eluent of CH_2Cl_2/EtOAC (4:1). A green product was obtained (yield ~ 50%). One hidden ^{13}C was found overlapped with 128.48 by $^1H^{13}C$ HMQC.

^1H NMR ($CDCl_3$, δ): 5.75 (d, 1H), 6.9-7.1 (m, 2H), 7.1-7.4 (m, 13H), ^{13}C NMR ($CDCl_3$, δ): 103.71 (CH), 115.65 (CH), 119.53 (CH), 120.72 (CH), 121.83(C), 127.19 (CH), 127.88 (CH), 128.48 (2 CH), 128.75(CH), 128.91 (CH), 129.91 (CH), 130.20 (CH), 135.16 (C), 135.89(C), 139.23, 141.29, 142.90 (C), 155.90 (C). m/z, 320 (M^+). HRMS (m/z): Calcd for $C_{23}H_{16}N_2$ 320.1313, found 320.1310.

1,4-Di(1-phenyl-2-perimidine)-benzene (V-2)

V-2 was synthesized from 1-amino-8-(phenylamino)naphthalene and terephthalaldehyde A yellow product was obtained (yield ~ 50%). ^1H NMR ($CDCl_3$, δ):

5.69 (d, 2H), 7.03-7.10 (m, 4H), 7.10-7.4 (m, 20H). ^{13}C NMR ($CDCl_3$, δ): 103.93 (CH), 115.64 (CH), 119.65 (CH), 120.97 (CH), 121.70, 127.17 (CH), 128.36 (CH), 128.69 (CH), 128.86 (CH), 129.75 (CH), 130.44 (CH), 135.07, 136.05, 138.99, 141.19, 150.49, 154.88. m/z, 562 (M^+). HRMS (m/z): Calcd for $C_{40}H_{26}N_4$ 562.2157, found 562.2134.

1,5-Di(1-phenyl-2-perimidine)-benzene (V-3)

V-3 was synthesized from 1-amino-8-(phenylamino)naphthalene and isophthalaldehyde. A yellow product was obtained (yield ~ 60%). ^1H NMR ($CDCl_3$, δ): 5.73 (d, 2H), 6.8-7.5 (24H). ^{13}C NMR ($CDCl_3$, δ): 103.74, 115.70, 119.62, 120.91, 121.72, 127.18, 127.27, 128.11, 128.55, 128.90, 129.13, 129.88, 130.42, 135.10, 135.46, 139.13, 141.16, 142.70, 154.71. m/z, 562 (M^+). HRMS (m/z): Calcd for $C_{40}H_{26}N_4$ 562.2157, found 562.2159.

2,6-Di(1-phenyl-2-perimidine)-pyridine (V-4)

V-4 was synthesized from 1-amino-8-(phenylamino)naphthalene and 2,6-dialdehydepyridine. 2,6-Dialdehydepyridine was synthesized according the ref. 17 (**Scheme 5.3, Eq. 5.3**) in which 2,6-pyridinedimethanol in chloroform was refluxed with manganese dioxide for 5 hours. On cooling, the mixture was filtrated and extracted with ethyl acetate and concentrated. The crude product was purified by flash chromatography using ethyl acetate as eluent. A bright yellow **5d** was obtained (yield ~ 60%). ^1H NMR ($CDCl_3$, δ): 5.73 (d, 2H), 6.8-7.0 (m, 4H), 6.94 (d, 6H), 7.12-7.5 (m, 13H), ^{13}C NMR ($CDCl_3$, δ): 103.74 (CH), 115.74 (CH), 119.45 (CH), 121.04 (CH), 122.08 (C), 123.74

(CH), 127.27 (CH), 128.53 (CH), 128.80 (CH), 129.78 (CH), 129.95 (CH), 135.14 (C), 136.99 (CH), 138.85 (C), 141.35 (C), 142.73 (C), 152.19 (C), 153.01 (C). m/z, 563 (M^+). HRMS (m/z): Calcd for $C_{39}H_{25}N_5$ 563.2110, found 563.2098.

2,5-Di(1-phenyl-2-perimidine)-thiophene (V-5)

V-5 was synthesized from 1-amino-8-(phenylamino)naphthalene and 2,5-thiophenedicarboxaldehyde. A deep red product was obtained (yield 70%). ^{1}H NMR ($CDCl_3$, δ): 5.62 (d, 2H), 6.04 (s, 2H), 6.8-7.6 (m, 20H). ^{13}C NMR ($CDCl_3$, δ): 103.81, 115.67, 119.63, 120.75, 121.46, 126.44, 127.14, 128.93, 129.52, 129.64, 130.01, 130.91, 134.99, 138.88, 141.51, 142.50, 148.52. m/z, 568 (M^+). HRMS (m/z): Calcd for $C_{38}H_{24}N_4S$ 568.1722, found 568.1723.

1,3,5-Tri(1-phenyl-2-perimidine)-benzene (V-6), TPPI

TPPI was synthesized from the reaction of the 1,3,5-triformylbenzene and 1-amino-8-(phenylamino)naphthalene in molar ratio 1:3.3.1,3,5-Triformylbenzene was synthesized following the exact same procedures from the reference 19, and each step was presented in **Scheme 5.4**. In the last **step 4**, 1,3,5-triformylbenzene and 1-amino-8-(phenylamino)naphthalene (1: 3.3), 10% weight of 5% Pd/C were added in Schlenk flask and the mixture was refluxed in diphenyl ether under nitrogen more than 12 hours. Before cooling the mixture to room temperature, the diphenylether solvent was removed under 150 - 160 °C under vacuum distillation. The mixture was then cooled to room temperature and filtered. The crude product was purified using column chromatography with ethyl acetate as the eluent. The green-yellow product was obtained in 40 % yield. ^{1}H

NMR ($CDCl_3$, δ): 5.73 (d, 3H), 6.7-7.5 (m, 33H). ^{13}C NMR ($CDCl_3$, δ): 103.43, 115.67, 115.97, 119.64, 120.92, 121.71, 127.19, 128.57, 128.90, 129.11, 129.87, 130.44, 135.09, 135.29, 139.19, 141.19, 154.73. Anal. Calcd for $C_{57}H_{36}N_6$: C, 85.05; H, 4.51; N, 10.44. Found C, 84.97; H, 4.46; N, 10.10.

5.3 Results and discussion

5.3.1 Synthetic methods for perimidine compounds

Scheme 5.2 presents some synthetic avenues to obtain, 1,2-diphenyl-perimidine (**V-1**) and the di-perimidine compound, 1,4-di(1-phenyl-2-perimidine)-benzene (**5b**). **Route 1** was initially chosen over **Route 2** due to the fact that it employed simpler reaction conditions and provided a superior yield of product. The yield in the first step of **Route 1** was more than 90% according to reference 15. The second step in the C-N coupling reaction between bromobenzene and 2-phenyl-perimidine provided a 75% yield. **Route 2** was modified from the reference 16 by replacing the dehydrogenation agents to Pd/C. Comparing to **Route 1**, the **Route 2** toward the **V-1** gave relatively low yield (50%), however when considering lower price of catalysts, it was also a reasonable way to obtain monomer.

When two different methods were applied to synthesize the di-perimidine compound **V-2**, the opposite results were observed. In **Route 3**, there was no desired product obtained through the Pd-catalyzed reaction, while in **Route 4**, *ca.* 50% **V-2** was obtained after chromatographic purification. Therefore, this route, the reaction between 1-amino-8-

(phenylamino)naphthalene and correspond dialdehydes, was employed for the synthesis of the other di-perimidine species **5c-e** as shown in **Scheme 5.3**.

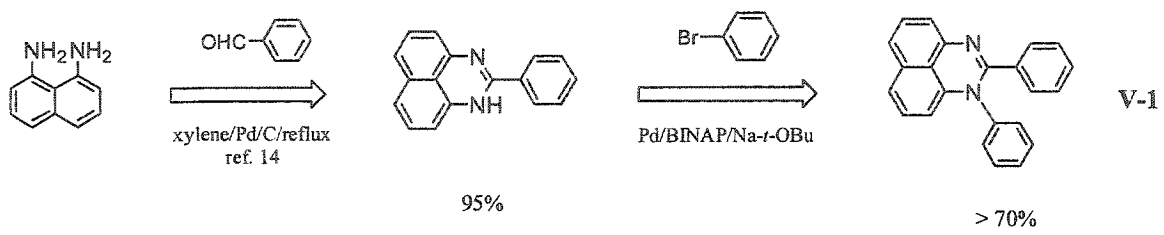

Route 1

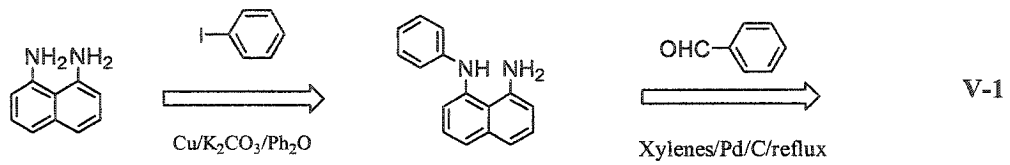

Route 2

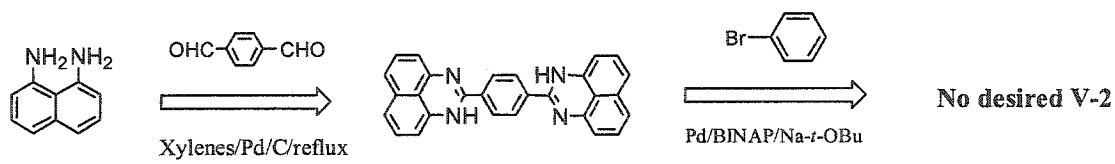

Route 3

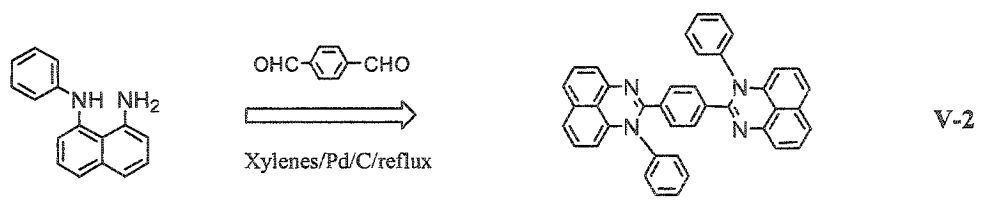

Route 4

Scheme 5.2 Synthetic routes to mono-perimidine (V-1) and di-perimidine (V-2).

Eq. 5.3

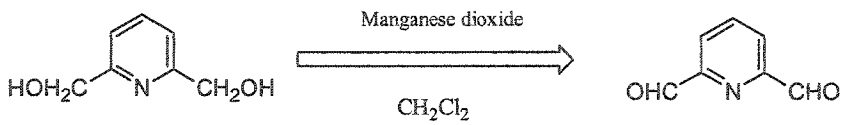

Eq. 5.4

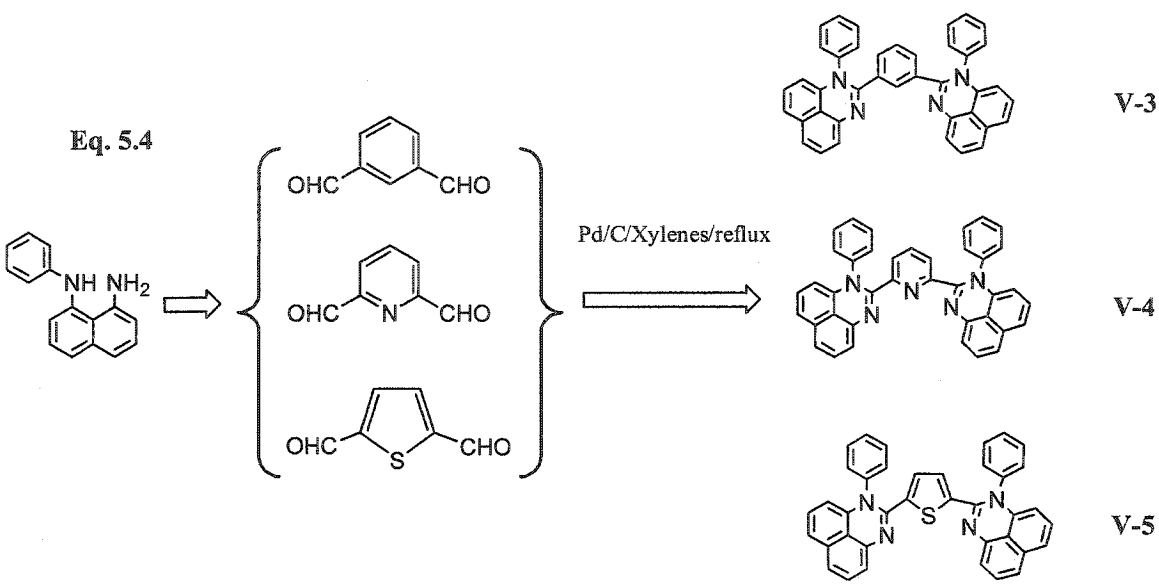

Scheme 5.3 Synthetic routes to di-perimidine V 3-5.

The synthetic route to the tri-perimidine species **V-6** (TPPI) is shown in **Scheme 5.4**, which followed the similar procedure as di-perimidine compounds except using diphenyl ether solvent in step 4 instead of xylenes.

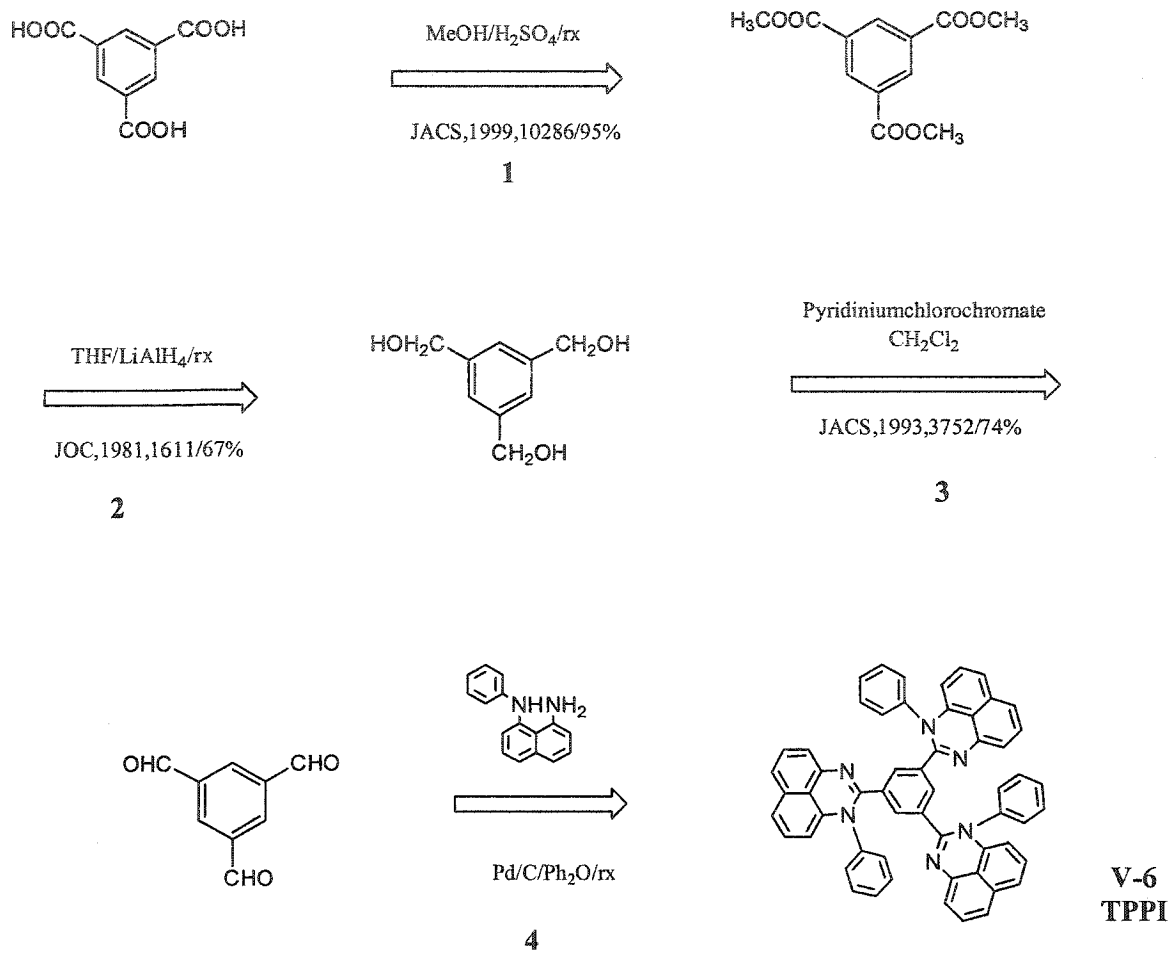

Scheme 5.4 Synthetic routes to TPPI, V-6.

5.3.2 Thermal properties

The thermal properties of the new 1-phenyl-perimidine based heterocyclic species were determined by DSC. The DSC heating cycles of **V 1-6** are shown from **Fig. 5.2-4** and summary of the $T_g/T_c/T_m$ data can be found in **Table 5.1.**

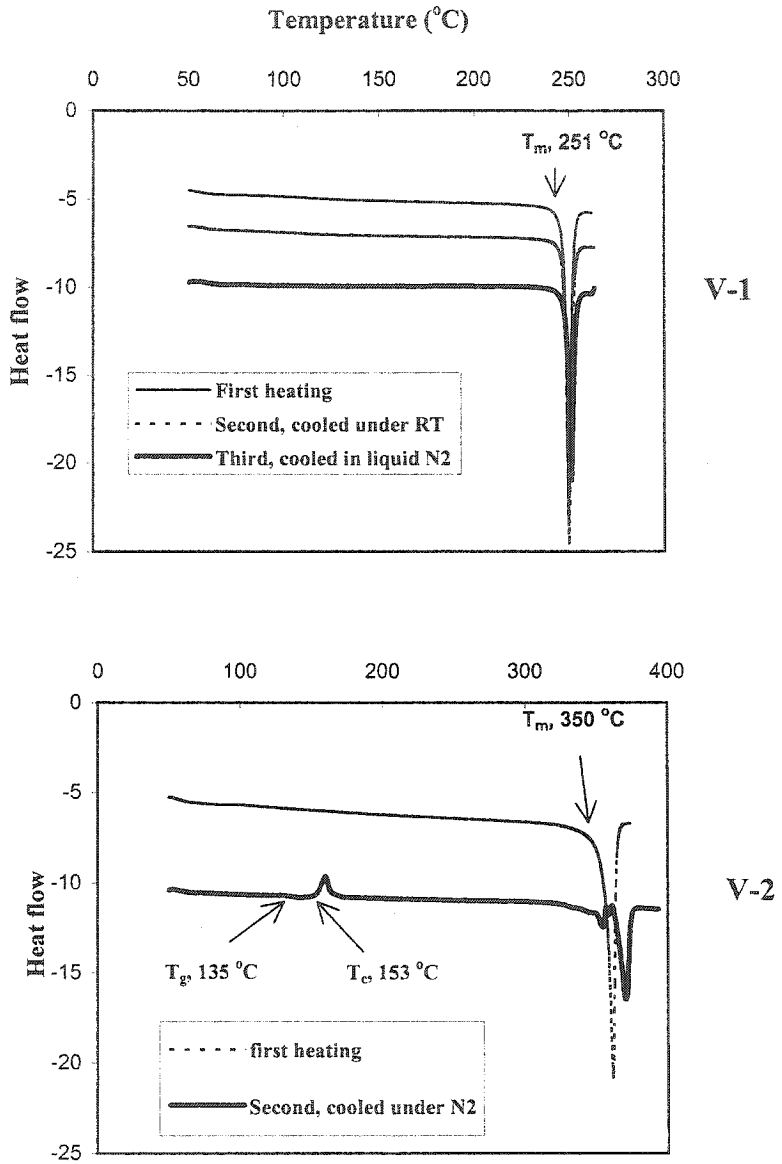

Figure 5.2 DSC traces of compounds V-1 and V-2 at the heating rate of 20 °C/min.

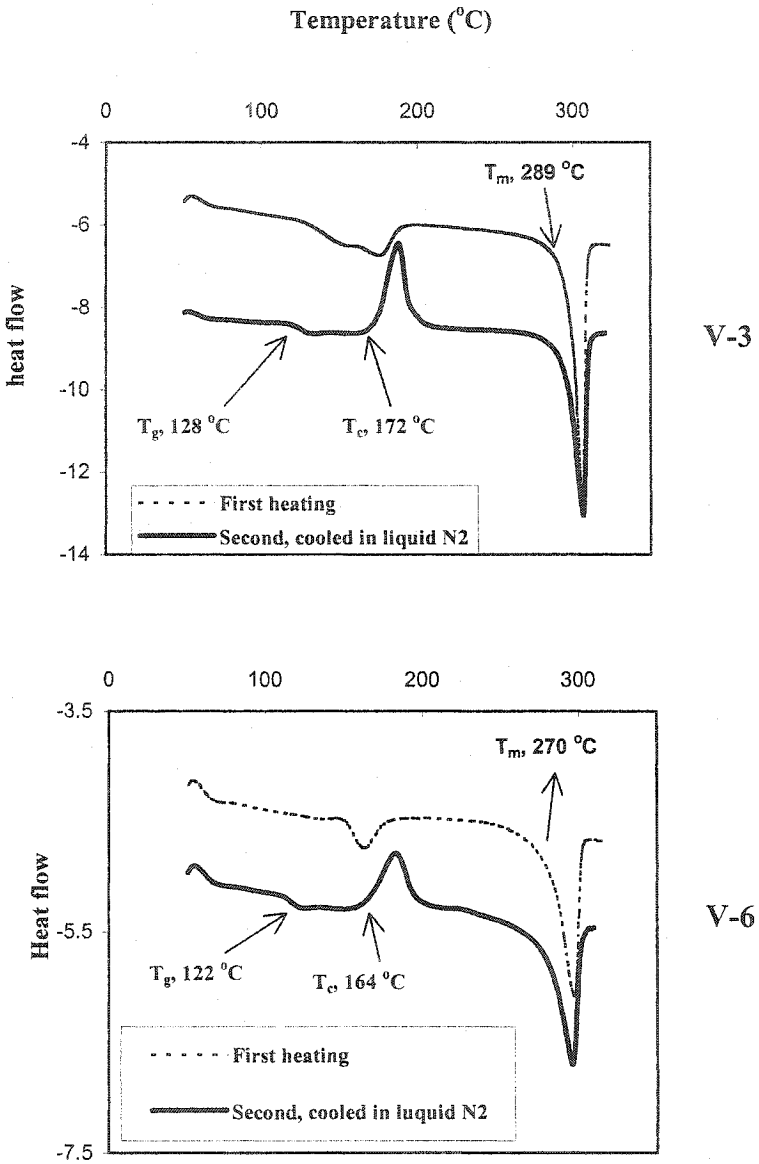

Figure 5.3 DSC traces of compounds V-3 and V-6 at the heating rate of 20 °C/min

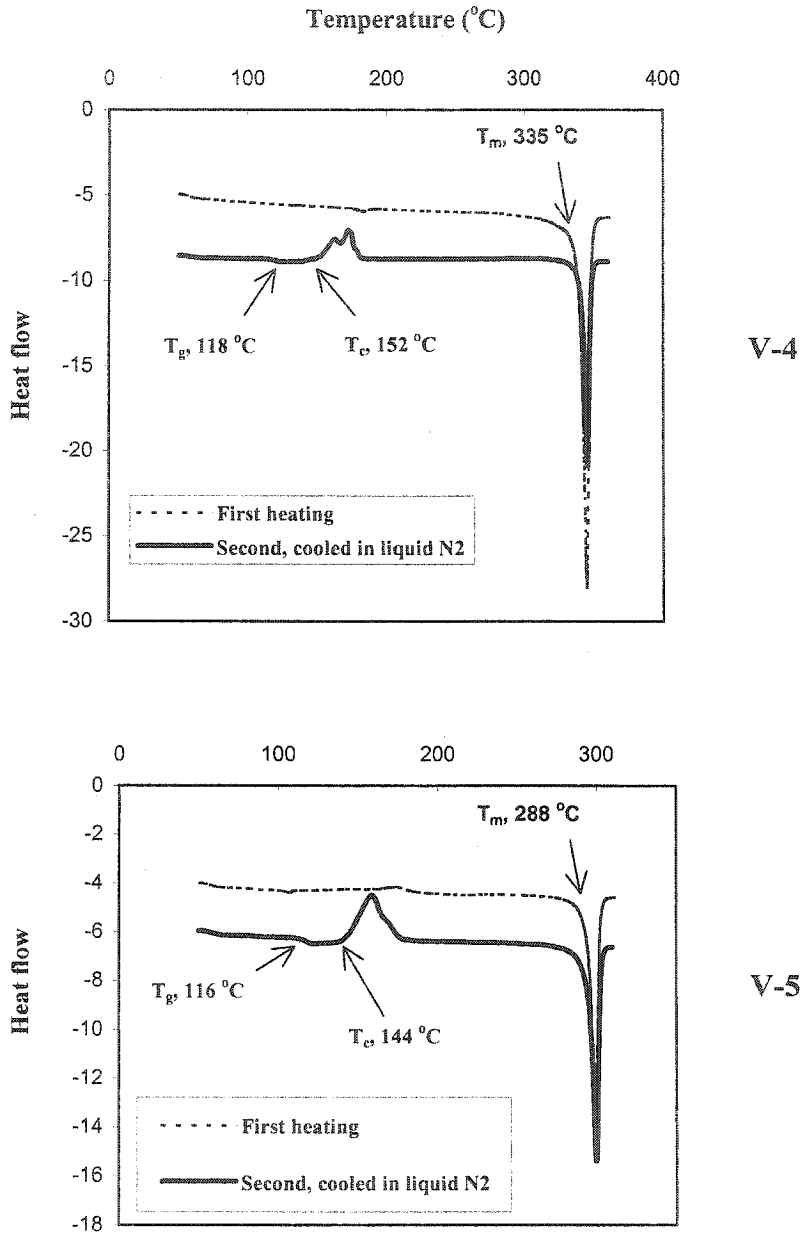

Figure 5.4 DSC traces of compounds V-4 and V-5 at the heating rate of 20 °C/min

Entry	$T_g/T_c/T_m$ (^{0}C)	Onset abs. λ (nm)/eV	abs. at short wavelength λ_{max} (nm)	ΔV[a]	HOMO[b]/ LUMO[c] (eV)
V-1	NO/NO/251	481/2.58	336	0.276	5.08/2.50
V-2	135/153/350	486/2.55	336	0.299	5.10/2.55
V-3	128/172/289	489/2.54	338	0.306	5.11/2.57
V-4	118/152/335	515/2.41	339	0.280	5.08/2.67
V-5	116/144/288	590/2.10	336	0.261	5.06/2.96
V-6	112/164/270	490/2.53	339	0.325	5.13/2.60

NO, not observed

[a] Calculated from the oxidation potential difference between the compounds and ferrocene.

[b] HOMO = (4.8 + ΔV) eV

[c] LUMO = (HOMO – Onset) eV

Table 5.1 Thermal, photophysical and electrochemical data of 1-phenyl-perimidine based compounds.

The first heating cycle for compounds **V 1-6** clearly displayed the melting and in the case of **V-3** and **V-6** there were indications of other thermal events that occurred prior to melting. Cooling of these materials and observing a second heating cycle revealed the T_g and T_c for all of the compounds except **V-1**. The T_gs that were obtained fall in the range from 112 to 135 °C. Compound **V-1** only showed T_m at 251 °C and did not exhibit T_g and T_c even when rapid quench cooling conditions were employed. It is interesting to note

that T_gs values are in order of **V-2>V-3>V-4>V-5>V-6**. As was pointed out in the reference 20 that $T_g = a\text{-}b\Sigma\Delta S_{tr,m}/N$, where is $\Sigma\Delta S_{tr,m}$ is the sum of the entropies of fusion and of phase transitions between T_g and T_m, N is the number of heavy atoms per molecules except hydrogen and a and b are constants. So, large molecule with small $\Sigma\Delta S_{tr,m}$ will usually give higher T_g. Since the largest molecule **V-6** has the smallest T_g, it is reasonable to deduce that **V-2** or **V-3**, where **V-2**, **V-3** and **V-6** have the similar structures, have more dense, rigid and symmetric structures, which are corresponding to the smaller $\Delta S_{tr,m}$. The same trend in T_ms of these three compounds also indicate **V-2** has the strongest intermolecular interaction while that of **V-6** is the weakest among three compounds.

Overall, the thermal results show that 1-phenyl-perimidine based TPBI analogues are quite stable. The compounds can be stored under atmosphere in long period without losing their chemical properties.

5.3.4 Optical properties

The UV-vis absorption spectra of compounds **V 1-6** measured in CH_2Cl_2 are shown in **Fig. 5.5** and are summarized in **Table 5.1**. All the compounds have an absorbance maximum (λ_{abs}) at short wavelength (336-339 nm) with a second, smaller, absorbance peak at long wavelength between 370 – 500 nm (370 –570 nm for **V-5**). The absorption reflects the nature of π-excess naphthalene ring and different cores (benzene, pyridine and thiophene) in these compounds.

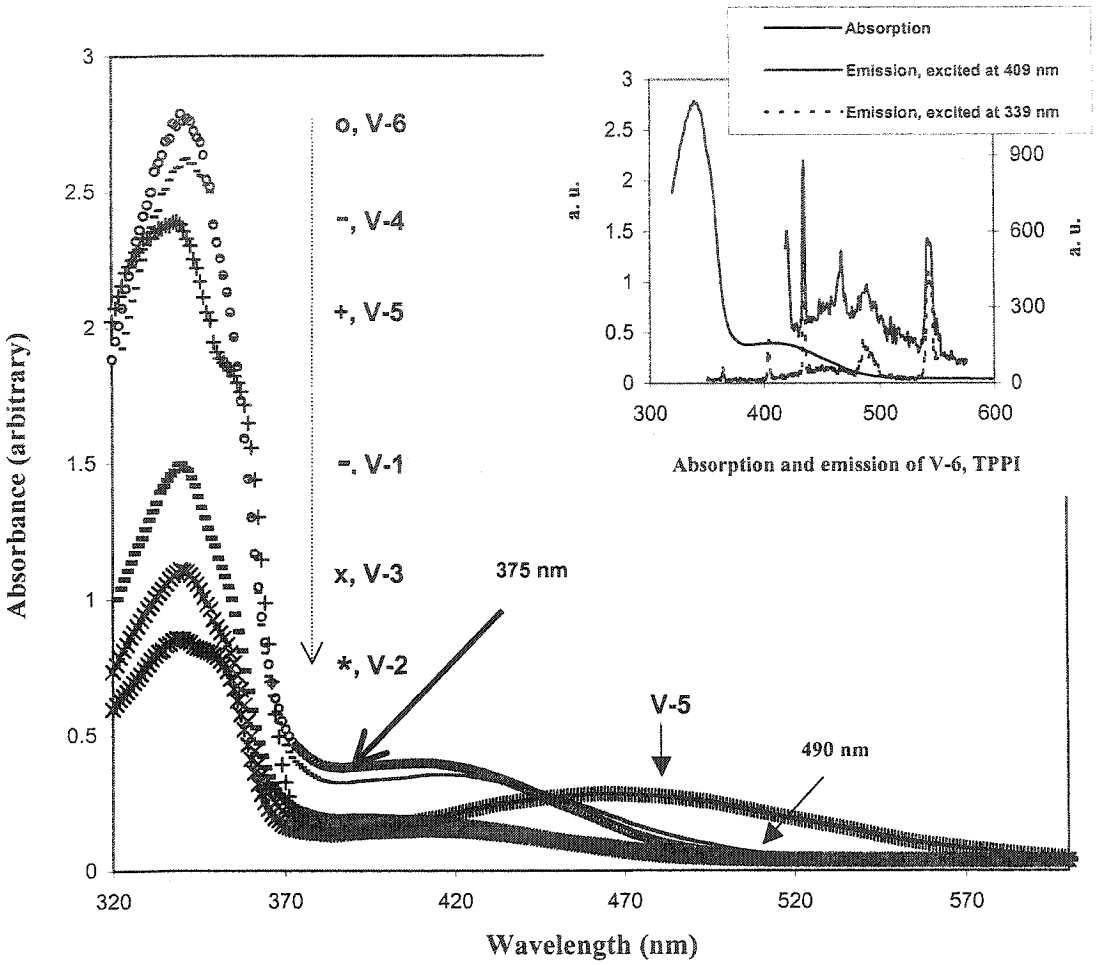

Figure 5.5. UV-absorption of 1-phenyl-perimidine based compounds in CH_2Cl_2, 10^{-4}M. Up right figure, the emission measured in CH_2Cl_2 controlling the absorbance value ca. 0.05.

Since all the compounds have only one electron-deficient center, imine, thus the imine site can be regarded as the LUMO site. There are two electron-rich sites, naphthalene ring and cores; therefore two different absorption regions can be attributed to the electronic transition happening between the two electron-rich sites and imine. Fluorescence measurements on these compounds were carried out in both CH_2Cl_2 and toluene and with excitation of both absorption bands. All of the compounds exhibited very small fluorescence intensity and quantum yield could not be evaluated. One example of the emission spectrum of compound **V-6** in CH_2Cl_2 is presented as an insert in **Figure. 5.5**. Again there was no overwhelming emission peak.

To confirm the involvement and roles of electron-rich naphthalene and electron-deficient imine in the electronic transition and investigate the overall low quantum efficiency of these perimidine-based heterocycles, ab initio molecular calculations for the parent perimidine structure were then performed. The DFT/B3LYP calculations were carried out using the Gaussian 03 program[21] and employed a 6-311G++(d,p) basis set. Some of the results of these calculations are summarized in the **Figure 5.6**. The upper portion of this figure displays the perimidine skeleton and numbering scheme as well as the calculated Mulliken atomic charges. The bottom portion of the figure provides graphical depictions of some of the frontier molecular orbitals for perimidine.

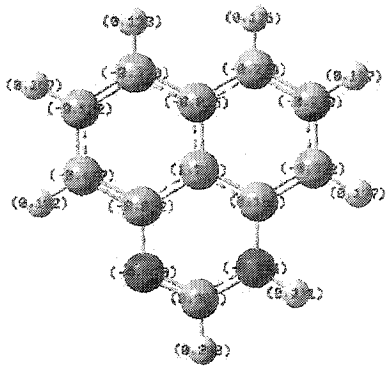

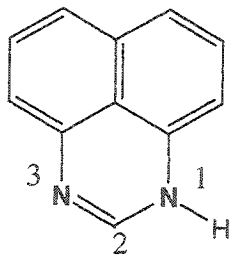

1H-perimidine

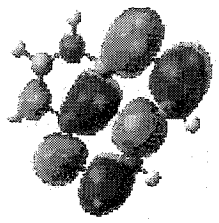

-0.042

LUMO

E (Hartee)

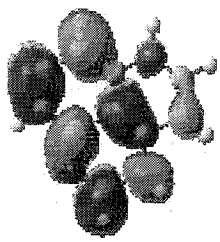

-0.031

LUMO + 1

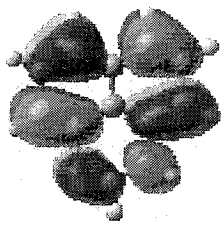

-0.191

HOMO

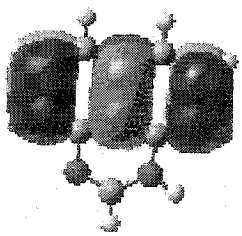

-0.255

HOMO - 1

Figure 5.6 Charge distribution, HOMO, second HOMO, LUMO, and second LUMO of 1H-perimidine

As shown in **Figure 5.6**, the HOMO and HOMO-1 for the perimidine are dominated by the π orbitals of the naphthalene ring. The HOMO does have π orbital contributions from the N=CN(H) portion of the molecule. Specifically, there is a bonding contribution between positions C2 and N3 which is countered by a π* interaction between C2 and N1. The net interaction in the NCN group is thus nonbonding. The LUMO and LUMO+1 are π* orbitals with significant contributions from the antibonding interactions within the N=CN(H) group. Both of these orbitals are strongly antibonding for the imine function represented by C2=N1. This orbital analysis leads to the reasonable assumption that the absorption around 339 nm for all the compounds is due to the electronic transition between the naphthalene ring and imine site in this work. On the other hand, the low quantum efficiency of these perimidine-based compounds could be explained by their electron distribution compared with that of beznimidazole chromophore in TPBI shown in **Scheme 5.5**.

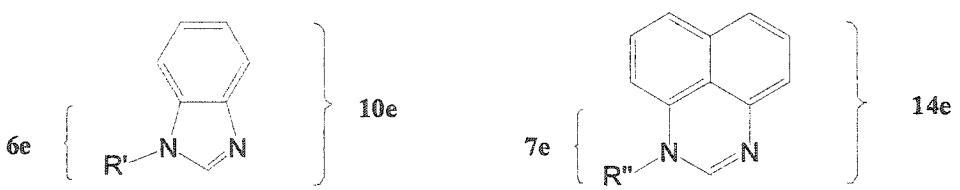

R', R'' = H or aromatic groups

Scheme 5.5 Electronic distribution of benzimidazole and perimidine chromophore.

Both chromophores obey Hüchel's rule, containing 4n+2 π electrons when the lone pair from nitrogen was considered to be delocalized. However, when counting the electrons involving in the imine ring only, benzimidazole and perimidine have 6e and 7e

structure respectively. The non-aromatic properties of the latter could be the reason for the non-emission behavior of perimidine-based compounds. The examples of these two structures can be compared with the reported compounds, 2-phenylbenzimidine[22] and 1-methyl-2-phenyl-perimidine.[23] Low quantum efficiency was also observed for perimidine-containing compounds. Further experimental demonstration is required before a more definite rationale can be provided. In any case, the low quantum efficiencies for these perimidine-based compounds indicate that these compounds cannot be used as fluorescent materials in OLEDs. They might have potential as hosts for fluorescent dopants or as charge transport materials which will be discussed in the next section.

5.3.5 Electrochemical properties

Using the same three-electrode electrochemical system as described in the previous chapters, the electrochemical behavior of compounds **V 1-6** was measured. These cyclic voltammetry (CV) experiments were carried out in CH_2Cl_2 solvent under nitrogen with TBAHP as supporting electrolyte. Ferrocene was used as both a reference material and as a means of calculating the HOMO energy as described previously.

For all the compounds, only **V-1** exhibited reproducibility and electrochemical stability under different scanning potential range. All other compounds showed pseudo-reversible single oxidations under short CV scanning range. CVs of **V-1** were presented in **Fig. 5.7**.

It can be see from the figure that there is no reduction peaks for **V-1** and the oxidation potential peaks are almost unchanged when potential scanning continues. The

CV after adding Cp_2Fe shows that there is no interaction between Cp_2Fe and the compound.

These electro-reproducibility and stability were not observed for other compounds. When all the other compounds were subjected to CV potential scan at high range, the CVs in the second cycle will be different from the first run, either the oxidation peaks moved or reduction peaks totally disappeared, thus only the first CV scanning cycles for all the compounds were shown in the **Fig. 8-10**. The scanning potentials were then stopped for each compound (except for **V-5**) right after the first oxidation peak and CVs were recorded. It can be seen that for all the compounds, the redox potentials will keep going up when CV scanning continued. The reason for this could be in that cation ions (or radical ions) produced in dimer and trimer were not as stable as those produced in **V-1**, the monomer. The imine nitrogens in dimer and trimer will communicate through the core and increase the activity. On the other hand, all these compounds have shown two oxidation peaks in the whole scanning range with specialty of **V-5** whose two oxidation peaks were close to each other and both at relatively low potentials. After adding Cp_2Fe, CVs were scanned again. It was found the redox peaks for Cp_2Fe almost no change at small scanning range (examples see **Figure. 5.7, V-1** and **Figure 5.8, V-2**), therefore the potential difference between the compounds and Cp_2Fe were calculated again and the HOMO energy level were estimated by adding 4.8 to the difference. The energy gap that was estimate from the onset UV-absorption spectra was subtracted from the HOMO and LUMO were obtained. The HOMO/LUMO results were presented in **Table 5.1**.

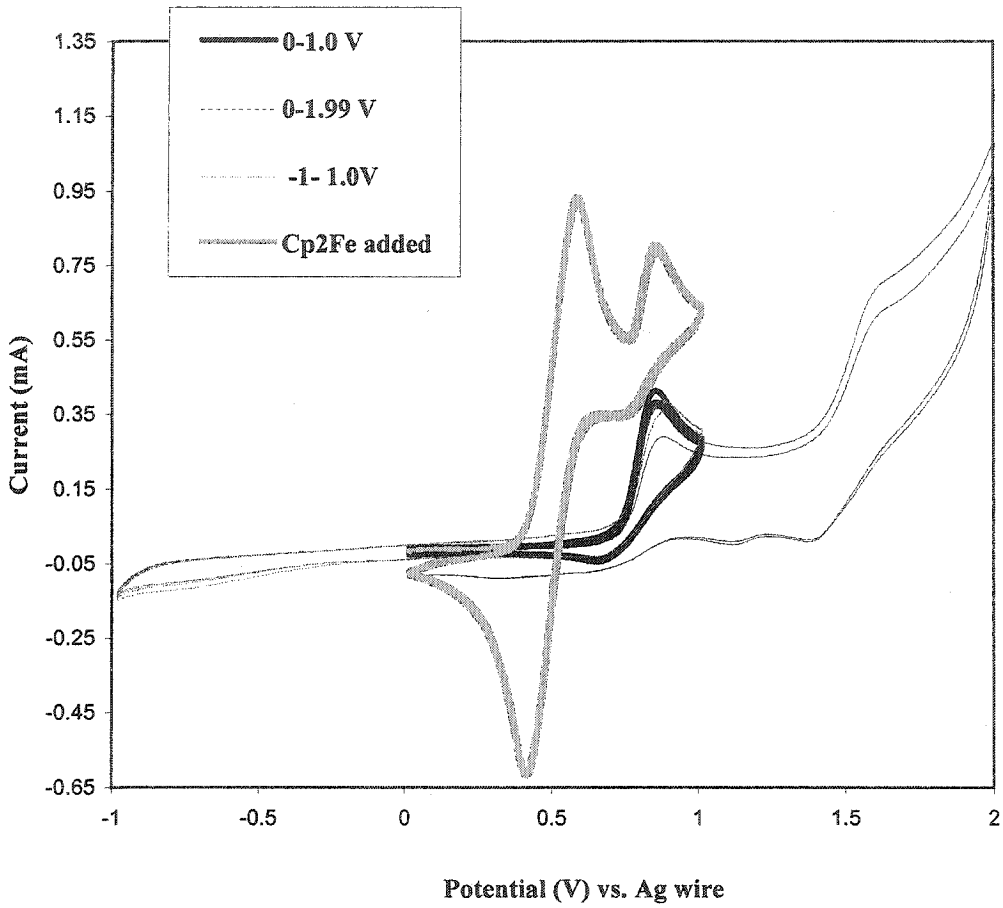

Figure 5.7 CVs of compound V-1 at 100 mV/s in N_2 saturated 0.05 M TBAHP CH_2Cl_2, $1x10^{-3}$ M solution at different scan ranges. At least three cycles recorded.

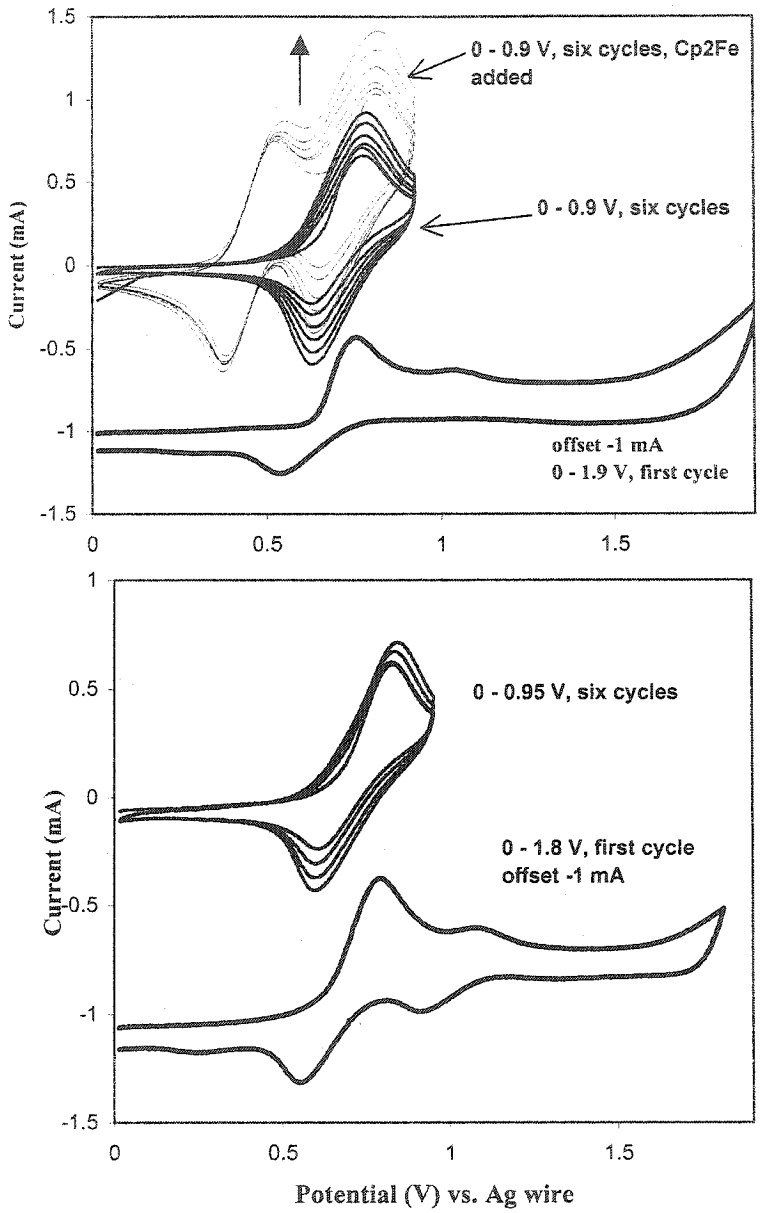

Figure 5.8 CVs of compounds V-2 and V-3 at 100 mV/s in N_2 saturated 0.05 M TBAHP CH_2Cl_2, $1x10^{-3}$ M solution.

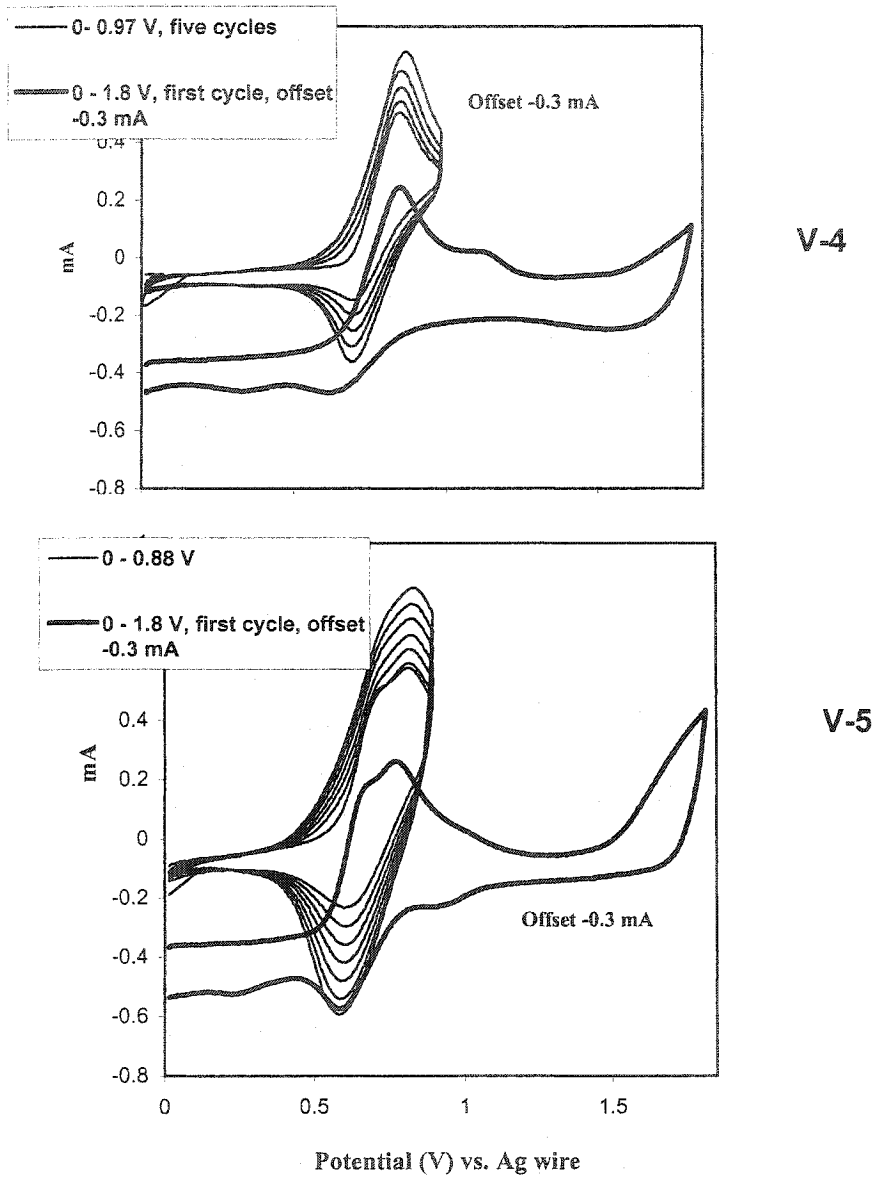

Figure 5.9 CVs of compounds V-4 and V-5 at 100 mV/s in N_2 saturated 0.05 M TBAHP CH_2Cl_2, $1x10^{-3}$ M solution at different scanning ranges.

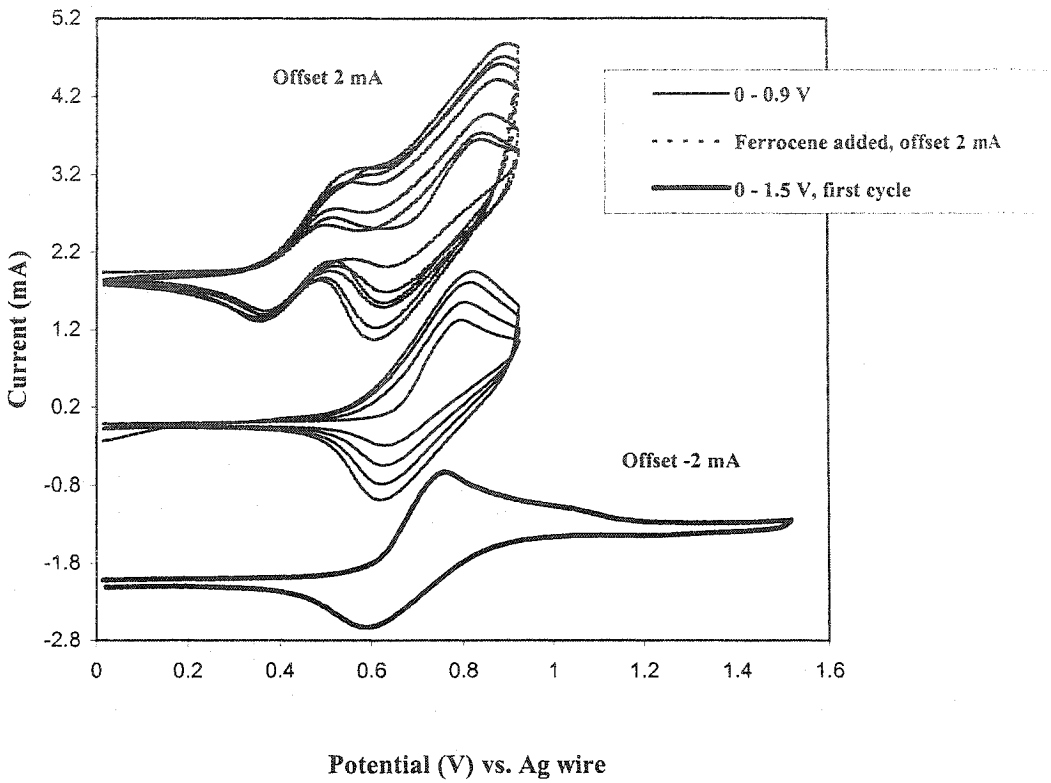

Figure 5.10 CVs of compound V-6 at 100 mV/s in N_2 saturated 0.05 M TBAHP CH_2Cl_2, $1x10^{-3}$ M solution at different scan ranges.

Compounds **V 1-6** all exhibited smaller HOMO energy values, which could be related to the electron-rich 7e imine-containing structure, than that of TPBI (6.20 eV). This might be expected with the replacement of benzimidazole by the electron-rich perimidine group. However, the HOMO energies of these imine-containing compounds (5.06 – 5.13 eV) were closer to those of naphthalene core diamine (~ 5.1 eV), the HT materials that have been reported in **Chapter 2**. The small energy gaps show these compound have large LUMO levels (2.50 – 2.96 eV) and the smallest energy gap for **V-5** is obviously related to the most electro-rich thiophene core.

The HOMO/LUMO results obtained for **V 1-6** indicate that these 1-phenyl-perimidine-based compounds are best suited as HT materials or host materials at HT layer. This contrasts with the initial aim of this work to prepare TPBI analogues for use as ET materials.

5.4 Conclusions

This chapter presents synthetic efforts at preparing perimidine-based materials that were targeted as potential TPBI analogues. Success was achieved with the preparation of mono-, di- and tri(perimidine) substituted benzenes (**V 1-3** and **V-6**) and in the preparation of analogues with pyridine (**V-4**) and thiophene (**V-5**) cores. The thermal characterization showed these compounds have high T_g values. These compounds presented small HOMO/LUMO energy gaps as determined by UV-vis absorption and fluorescence measurements indicated that they had very poor emission intensities. The HOMO energy levels were obtained from an electrochemical measurement that indicated

a rather small energy. The emission and HOMO energy results implying that these compounds are not suitable for emission materials, however, they are suitable for HT or host materials in OLEDs.

References for Chapter 5

(1) Aziz, H.; Popovic, A. D.; Hu, N.; Hor, A.; Xu, G. *Science*, **1999**, *283*, 1900-1902.

(2) Thelakkat, M.; Schmidt, H. W. *Polym. Adv. Technol.* **1998**, *9*, 429-442.

(3) (a) Adachi, C.; Tsutsui, T.; Saito, S. *Appl. Phys. Lett.* **1989**, *55*, 1489-1491. (b) Adachi, C.; Tsutsui, T.; Saito, S. *Appl. Phys. Lett.* **1990**, *56*, 799-801. (c) Adachi, C.; Tsutsui, T.; Saito, S. *Appl. Phys. Lett.* **1990**, *57*, 531-533.

(4) (a) Shi, J.; Tang, C. W.; Chen, C. H. U.S. *Patent No. 5,646,948*, **1997**.

(5) Selected references: (a) Gao, Z.; Lee, C. S.; Bello, I.; Lee, S. T.; Chen, R.; Luh, T.; Shi, J.; Tang, C. W. *Appl. Phys. Lett.* **1999**, *74*, 865-867. (b) Gao, Z.; Lee, C. S.; Bello, I.; Lee, S. T.; Wu, S. K.; Yan, Z. L.; Zhang, X. H. *Synth. Met.* **1999**, *105*, 141-144. (c) Zhang, X. H.; Lai, W. Y.; Wong, T. C.; Gao, Z.; Jiang, T. C.; Wu, S. K.; Kwong, H. L.; Lee, C. S.; Lee, S. T. *Synth. Met.* **2000**, *114*, 115-117. (d) Zhang, X. H.; Lai, W. Y.; Gao, Z.; Wong, T. C.; Lee, C. S.; Kwong, H. L.; Lee, S. T.; Wu, S. K. *Chem. Phys. Lett.* **2000**, *320*, 77-80.

(6) Selected references: (a) Balasubramaniam, E.; Tao, Y. T.; Danel, A.; Tomasik, P. *Chem. Mater.* **2000**, *12*, 2788-2793. (b) Thomas, K. R.; Lin, J. T.; Tao, Y. T.; Ko, C. W. *J. Am. Chem. Soc.* **2001**, *123*, 9404-9411. (c) Danel, K.; Huang, T. H.; Lin, J.

T.; Tao, Y. T.; Chuen, C. H. *Chem. Mater.* **2002**, *14*, 3860-3865. (d) Yu, M. X.; Duan, J. P.; Lin, C. H.; Cheng, C. H.; Tao, Y. T. *Chem, Mater.* **2002**, 14, 3958-3963.

(7) Johansson, N.; Salbeck, J.; Bauer, J.; Weissortel, F.; Broms, P.; Andersson, A.; Salaneck, W. R. *Adv. Mater.* **1998**, *10*, 1136.

(8) (a) Ueda, H.; Kitahora, T.; Furukawa, K.; Terasaka, Y. *Synth. Met.* **1997**, *91*, 257. (b) Wang, C.; Jung, G.; Hua, Y.; Pearson, C.; Bryce, M. R.; Petty, M. C.; Batsanov, A. S.; Goeta, A. E.; Howard, J. A. K. *Chem. Mater.* **2001**, *13*, 1167-1173.

(9) Bettenhausen, J.; Greczmiel, M.; Jandke, M.; Strohriegl, P. *Synth. Met.* **1997**, *91*, 223.

(10) Lee, Y. Z.; Chen, X.; Chen, S. A.; Wei, P. K.; Fann, W. S. *J. Am. Chem. Soc.* **2001**, *123*, 2296-2307.

(11) (a) Pei, Q.; Yang, Y. *Adv. Mater.* **1995**, *7*, 559. (b) Yang, Y.; Pei, Q. *J. Appl. Phys.* **1995**, *77*, 4807.

(12) Cheng, L. F.; Hung, L. M.; Ding, X. M.; Gao, Z. Q.; Lee, C. S.; Lee, S. T. *Displays*, **2000**, *21*, 51-54.

(13) Wong, T. C.; Kovac, J.; Lee, C. S.; Hung, L. S.; Lee, S. T. *Chem. Phys. Lett.* **2001**, *334*, 61-64.

(14) Zhang, X. H.; Wong, Q. Y.; Gao, Z. Q.; Lee, C. S.; Kwong, H. L.; Lee, S. T.; Wu, S. K. *Mater. Sci. Engineer.* **2001**, *B85*, 182-185.

(15) Paragamian, V.; Baker, M. B.; Puma, B. M.; Jr., J. R. *J. Heterocyclics. Chem.* **1968**, *5*, 591-597.

(16) (a) Starshikov, N. M.; Pozharskii, A. F. *Khimiya Geterotsiklicheskikh Soedinenii* **1978**, *10*, 1413-1417. (b) Starshikov, N. M.; Pozharskii, A. F. *Khimiya Geterotsiklicheskikh Soedinenii* **1980**, *1*, 96-100.

(17) Rimmler, G.; Krieger, C.; Neugebauer, F. A. *Chem. Ber.* **1992**, *125*, 723-728.

(18) Papadopoulos, E. P.; Jarrar, A.; Issidorides, C. H. *J. Org. Chem.* **1965**, *31*, 615-616.

(19) (a) Dimick, S. M.; powell, S. C.; McMahon, S. A.; Moothoo, D. N.; Naismith, J. H.; Toone, E. J. *J. Am. Chem. Soc.* **1999**, *121*, 10286-10296. (b) Nakazaki, M.; Yamamoto, K.; Toya, T. *J. Org. Chem.* **1981**, *46*, 1611-1615. (c) Fourmigué, M.; Johannsen, I.; Boubekeur, K.; Nelson, C.; Batail, P. *J. Am. Soc. Chem.* **1993**, *115*, 3752-3759.

(20) (a) Naito, K.; Miura, A. *J. Phys. Chem.* **1993**, *97*, 6240-6248. (b) Sapochak, L. S.; Padmaperuma, A.; Washton, N.; Endrino, F.; Schmett, G. T.; Marshall, J.; Fogarty, D.; Burrows, P. E.; Forrest, S. R. *J. Am. Chem. Soc.* **2001**, *123*, 6300-6307.

(21) Gaussian 03, Revision A.1, Frisch, M. J.; Trucks, G. W.; Schlegel, H. B.; Scuseria, G. E.; Robb, M. A.; Cheeseman, J. R.; Montgomery, Jr., J. A.; Vreven, T.; Kudin, K. N.; Burant, J. C.; Millam, J. M.; Iyengar, S. S.; Tomasi, J.; Barone, V.; Mennucci, B.; Cossi, M.; Scalmani, G.; Rega, N.; Petersson, G. A.; Nakatsuji, H.; Hada, M.; Ehara, M.; Toyota, K.; Fukuda, R.; Hasegawa, J.; Ishida, M.; Nakajima, T.; Honda, Y.; Kitao, O.; Nakai, H.; Klene, M.; Li, X.; Knox, J. E.; Hratchian, H. P.; Cross, J. B.; Adamo, C.; Jaramillo, J.; Gomperts, R.; Stratmann, R. E.; Yazyev, O.; Austin, A. J.; Cammi, R.; Pomelli, C.; Ochterski, J. W.; Ayala, P. Y.; Morokuma, K.; Voth, G. A.; Salvador, P.; Dannenberg, J. J.; Zakrzewski, V. G.; Dapprich, S.; Daniels, A. D.; Strain, M. C.; Farkas, O.; Malick, D. K.; Rabuck, A.

D.; Raghavachari, K.; Foresman, J. B.; Ortiz, J. V.; Cui, Q.; Baboul, A. G.; Clifford, S.; Cioslowski, J.; Stefanov, B. B.; Liu, G.; Liashenko, A.; Piskorz, P.; Komaromi, I.; Martin, R. L.; Fox, D. J.; Keith, T.; Al-Laham, M. A.; Peng, C. Y.; Nanayakkara, A.; Challacombe, M.; Gill, P. M. W.; Johnson, B.; Chen, W.; Wong, M. W.; Gonzalez, C.; and Pople, J. A.; Gaussian, Inc., Pittsburgh PA, 2003

(22) Catalan, J.; Mena, E.; Fabero, F. *J. Chem. Phys.* **1992**, *96*, 2005-2016.

(23) Valle, J. C. D.; Catalán, J.; Foces-Foces, C.; Llamas-Saiz, A. L.; Elguero, J.; Sanz, D.; Dotor, J.; Claramunt, R. *J. Luminescence*, **1997**, *75*, 17-26.

Chapter 6

Summary of Contributions and Prospective Efforts

6.1 Summary of contributions

The work presented here began in the early 2001 with the desire to employ Buchwald-Hartwig coupling reactions to synthesize a group of new hole transport materials designed around naphthalene core diamines. Along with the successful synthetic efforts and rationalized conditions, we found that various diarylamines have a decisive influence on the thermal, photophysical and electrochemical properties of these materials. The work in **Chapter 2** provides a reference to synthesize naphthalene core diamines for future OLED application as hole transport (HT) materials. Our work focuses on Pd-catalysts that were first pioneered by the Marder (triarylamines) and Thompson (biphenyl core diamines) groups for synthesis of HT OLED materials.[1,2] It is worth noting here that during the period 2002 to 2003, Tao's group has reported a series of the different core center diamines employing the similar Pd catalyst system as ours, and has successfully fabricated them into OLEDs.[3] It can be envisioned that the Pd-catalyst will continue playing important role in this field and more new hole transport materials will be developed to meet the property and fabrication requirements for OLEDs.

In addition to our initial examination of naphthalene-core diamines, new C-4 substituted Alq_3 derivatives for emission and electron transport OLED materials have also been prepared. Electrochemical characterization of these C-4 substituted Alq_3 analogues revealed them to be more stable to oxidation than the parent Alq_3. This data has provided direct experimental evidence suggesting a possible origin of unstable Alq_3 cations in an OLED operation. Furthermore, C-4 diarylamine substituted Alq_3 analogues were proposed to be potential dipolar OLED materials combining amine and Alq_3, which could be used in fabricating single-layer OLED.[4]

Two new research directions were also initiated. The first focused on developing boron complexes for emission materials and built on some of the ideas from the latest work from Wang's group.[5] The second was the design and development of perimidine-based compounds for electron transport materials. In fact, the properties of these species suggest that they are better suited to be hole transport compounds.

6.2 Summary of work and prospective efforts

The previous chapters were focused on materials synthesis for different functions in multilayer OLEDs and chemical characterization has been carried out separately in each chapter. Since one of the efforts in this work is aimed at employing one, two or more new compounds for an OLED device, it would be appropriate and perhaps useful to discuss their properties in an integrated fashion. On the other hand, no device performance of these materials is provided. In this discussion, I will present the potential roles of these compounds for OLEDs and some topics on engineering will be briefly introduced.

6.2.1 T_gs and T_ms

As pointed out in **Chapter 1** that operational stability of OLEDs is one of the most critical issues that needs improvement in order to compete with inorganic LEDs. In **section 1.3**, some common requirements of organic EL materials have also been listed and thermal stability has been the first consideration for characterization of these OLED materials in this thesis. A high T_g is always needed for a potential OLED material. In this thesis, most of compounds we prepared have high T_gs. Since we have conducted DSC measurements on a number of compounds that would form the different components of OLEDs and there is a general rule that compounds that form glassy phases have a relationship for the ratio $T_g/T_m = 2/3$,[6] it would be interesting to compare T_g/T_m values of the new compounds when both are available. It can be seen in **Figure 6.1** that except for **PAlq$_3$** and **II-7** which deviate from the line, all other compounds exhibit nearly linear relationship of T_g and T_ms with $T_g/T_m = 0.71$. In summary, the investigations on thermal properties, namely, T_g, T_m, T_c and T_d in this work have provided important physical information of the new compounds synthesized in this thesis, which will benefit future research as well the potential application in fabricating OLEDs.

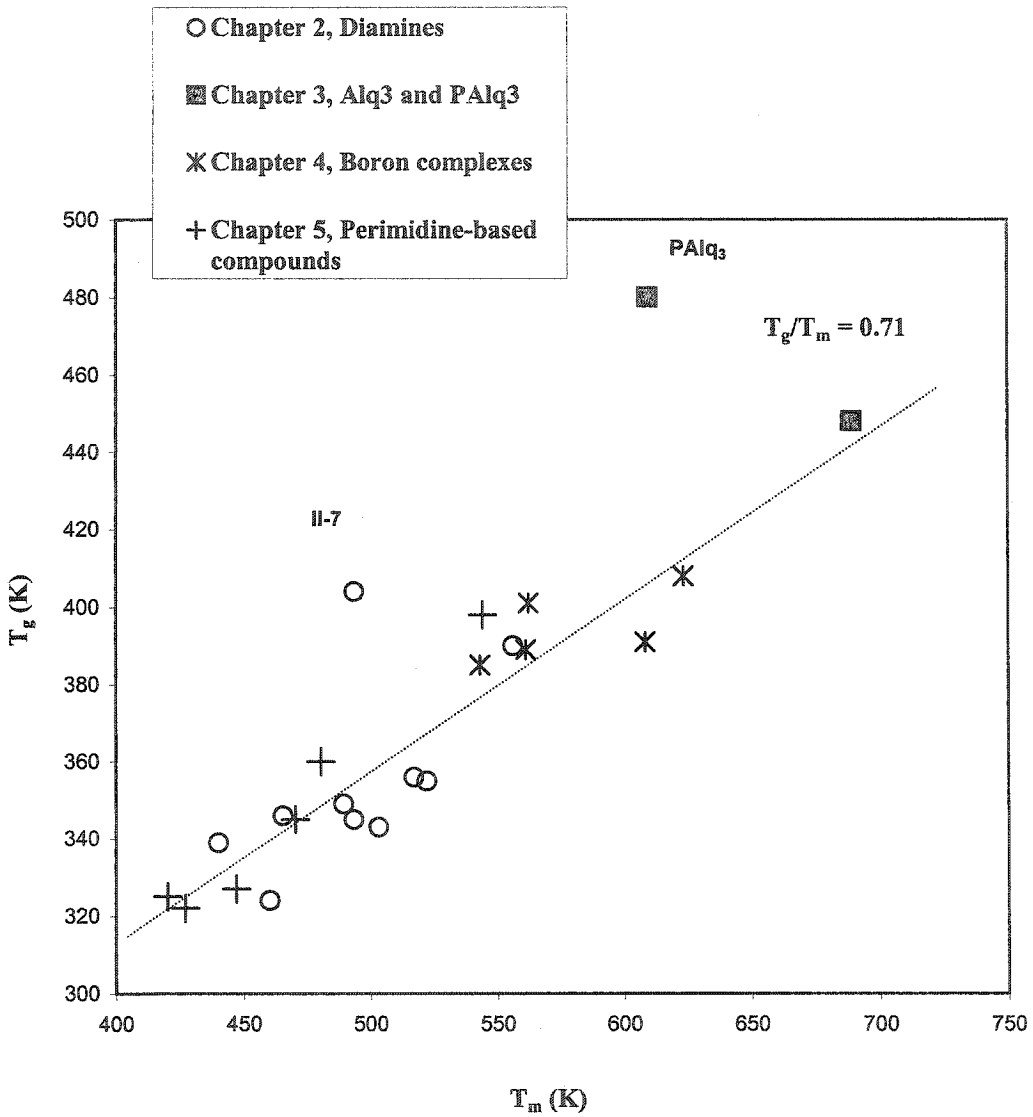

Figure 6.1. Relation between glass transition temperature (T_g) and melting point (T_m) for the compounds synthesized in this thesis.

6.2.2 Emission color and quantum efficiency

The photophysical properties of these materials are important and their measurement represent a significant effort in this thesis. If these new compounds are to be used as EM materials for an OLED, it would be interesting to measure their emission color in addition to their quantum efficiency. Most of the compounds reported in this thesis emit in the color range of blue to green. In **Figure 6.2**, emission spectra of some compounds from each group are selected and displayed here. The emission color of these compounds when excited by a UV lamp is presented at the bottom of this figure. In order to obtain a full-color RGB display, the work presented in this thesis is deficient in red emission materials. The deficiency could be addressed by adding stronger electron-withdrawing groups at C-4 position of Alq_3. Alternatively, a similar approach could be applied to the boron complexes. Besides emission color, quantum efficiency should also be in a consideration when synthesizing new compounds.

6.2.3 HOMO/LUMO and potential roles

The third key property of the compounds presented in this thesis is the estimate of the HOMO/LUMO energy levels of these compounds. As pointed out earlier, OLED materials should have suitable HOMO/LUMO energy levels for charge injection from the electrodes and charge transport within the different layers. The efficient charge injection and transport are the intrinsic factors which influence the operational stability of OLEDs. In **Figure 6.3**, the energy levels of some compounds from each group obtained in this

thesis are presented. Their potential roles in an OLED are then indicated from the relative positions of each compound. The HOMO/LUMO energy levels of TPD and Alq_3 were shown in the figure as a comparison.

The HOMO energy levels of **II-1** as well as **II 2-7** (energy levels not shown) and **TPPI** are very close to that of TPD. Thus, these compounds are good candidates for HT materials. Compounds **II-8** and **9** have higher HOMOs, indicating they would require a hole-injection material in order to be efficiently applied in an OLED device. Compared to Alq_3, $DAlq_3$ has both smaller HOMO and LUMO energy values. This species could be used to fabricate single-layer OLED, however, it may need additional layers for charge injections from both electrodes. $PAlq_3$, on the other hand, has smaller LUMO and similar HOMO as that of Alq_3. The smaller LUMO suggests that the electron transport will be increased in this layer. Since electron transport is usually slow in OLEDs this may lead to an improvement in operation. As pointed in the **Chapter 3** that more stable cationic ions of both $DAlq_3$ and $PAlq_3$ would improve the reliability of an OLED compared with Alq_3 as the ET layer. Boron complex (**IV-4**) exhibits much higher HOMO and LUMO energies than that of Alq_3, which has dual applications. As EM materials, these compounds would need HT materials possessing high HOMO levels for hole injection and low LUMO levels to block electron within the EM layer. Alternatively, the large HOMO energy level indicates this compound could also be used as ET materials which would then require low HOMO and high LUMO HT materials.

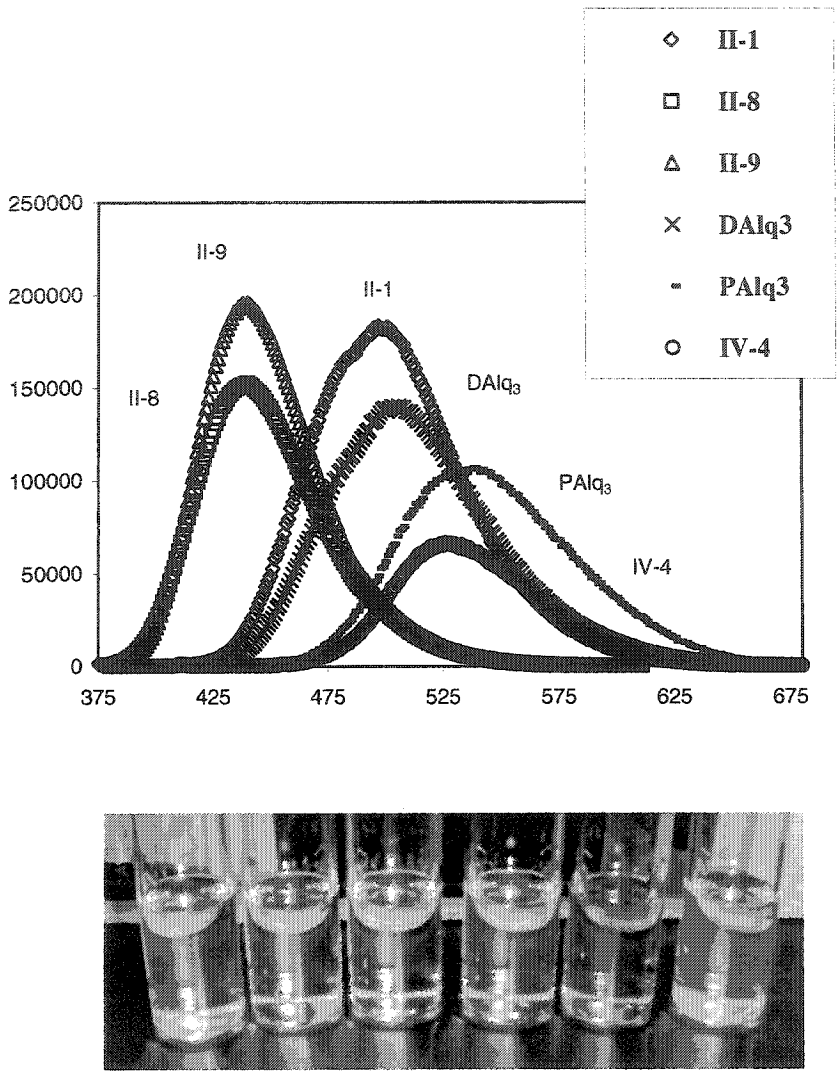

Figure 6.2. Photoluminescent emission spectra and emission color in front of a UV lamp of compounds II-1, II-8, II-9, $DAlq_3$, $PAlq_3$ and IV-4 (from left to right) in CH_2Cl_2 solution. Intensity has been adjusted for clearance.

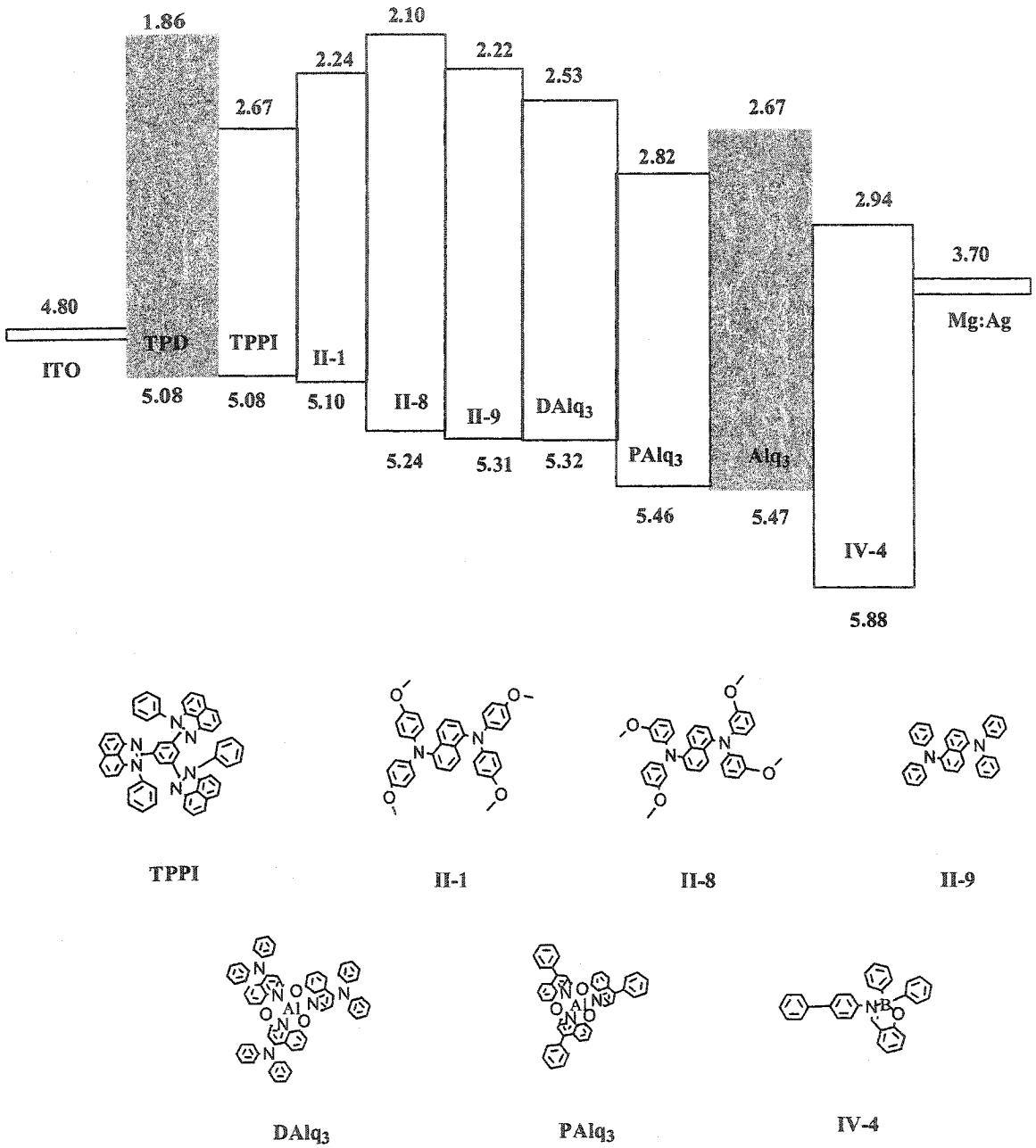

Figure 6.3 Configuration of relative HOMO/LUMO energy levels of some compounds synthesized in this thesis and their molecular structures. Unit: eV.

6.3 Epilogue

This thesis has discussed a number of new compounds including their properties and potential applications from a chemist's perspective. The engineering-based fabrication processes such as pre-processing the electrodes, controlling the thickness of layers, the order of deposition and building alternative layers, encapsulation and finally incorporating an OLED in active-matrix represent important fields both in academic and industrial units.[7] These topics, while beyond the efforts of this thesis, nevertheless will be the main prospective efforts of this thesis in the future.

References for Chapter 6:

(1) Thayumanavan, S.; Barlow, S.; Grubbs, R. H.; Marder, S. R. *Chem. Mater.* **1997**, *9*, 3231-3235. (b) Bellmann, E.; Shaheen, S. E.; Thayumanavan, S.; Barlow, S.; Grubbs, R. H.; Marder, S. R.; Kippelen, B.; Peyghambarian. *Chem. Mater.* **1998**, *10*, 1668-1676.

(2) Koene, B. E.; Loy, D. E.; Thompson, M. E. *Chem. Mater.* **1998**, *10*, 2235-2250.

(3) (a) Thomas, K. R.; Lin, J. T.; Tao, Y. T.; Ko, C. W.; *J. Am. Chem. Soc.* **2001**, *123*, 9404-9411. (b) Yu, M. X.; Duan, J. P.; Lin, C. H.; Cheng, C. H.; Tao, Y. T. *Chem. Mater.* **2002**, 14, 3958-3963. (c) Danel, K.; Huang, T. H.; Lin, J. T.; Tao, Y. T.; Chuen, C. H. *Chem. Mater.* **2002**, *14*, 3860-3865.

(4) (a) Thomas, K. R. J.; Lin, J.; Tao, Y, T.; Chuen, C. H. *Chem. Mater.* **2002**, *14*, 2796-2802. (b) Thomas, K. R. J.; Lin, J. Y.; Tao, Y. T.; Chuen, C. H. *J. Mater. Chem.* **2002**, *12*, 3516-3522. (c) Thomas, K. R. J.; Lin, J.; Tao, Y, T.; Chuen, C. H. *Chem. Mater.* **2002**, *14*, 3852-3859. (d) Patra, A.; Pan, M.; Friend, C. S.; Lin, T. C.; Cartwright, A. N.; Prasad, P. N. (e) Pudzich, R.; Salbeck, J. *Synth. Met.* **2003**, *138*, 21-31.

(5) Selected references: (a) Wu, Q.; Esteghamatian, Hu, N.; Popovic, Z.; Enright, G.; Breeze, S. R.; Wang, S. *Angew. Chem. Int. Ed. Engl.* **1999**, *38*, 985-988. (b) Liu, Q.; Mudadu, M. S.; Schmider, H.; Thummel, R.; Tao, Y.; Wang, S. *Organometallics* **2002**, *21*, 4743-4749.

(6) Naito, K.; Miura, A. *J. Phys. Chem.* **1993**, *97*, 6240-6248. References therein.

(7) Hung, L. S.; Chen, C. H. *Mater. Sci. Engineer.* **2002**, *R 39*, 143-222.